PROTON EXCHANGE MEMBRANES BASED ON COLUMNAR SIDE-CHAIN LIQUID CRYSTALLINE POLYETHERS AND POLYAMINES

Xavier Montané Montané

Department of Analytical Chemistry and Organic Chemistry

Proton exchange membranes based on columnar side-chain liquid crystalline polyethers and polyamines

By

Xavier Montané Montané

Doctoral Thesis

Supervisors:

Dr. José Antonio Reina

Dr. Marta Giamberini

UNIVERSITAT ROVIRA I VIRGILI

Tarragona

2016

UNIVERSITAT ROVIRA I VIRGILI

Department of Analytical Chemistry and Organic Chemistry
C/ Marcel·lí Domingo, s/n
Campus Sescelades
43007, Tarragona
Tel: 977 559 769
Fax: 977 558 446

José Antonio Reina, Associate Professor at the University Rovira i Virgili, Department of Analytical Chemistry and Organic Chemistry and Marta Giamberini, Associate Professor at the University Rovira i Virgili, Department of Chemical Engineering,

We state that the present study, entitled “Proton exchange membranes based on columnar side-chain liquid crystalline polyethers and polyamines”, presented by Xavier Montané Montané for the award of the degree of Doctor, has been carried out under our supervision at the Department of Analytical Chemistry and Organic Chemistry at the University Rovira i Virgili, and that it fulfils all the requirements to be eligible for the Doctor European Mention.

Tarragona, 02 September 2016

Supervisor of the doctoral thesis Co-supervisor of the doctoral thesis

Dra. José Antonio Reina Dr. Marta Giamberini

Agraïments

Durant aquests 3 anys, han sigut moltes les persones que han contribuït al treball realitzat en aquesta tesis.

En primer lloc vull donar les gràcies als que han estat els meus directors de la tesis doctoral: al Dr. José Antonio Reina per donar-me l'oportunitat de poder realitzar la tesis en aquest grup. Li estic especialment agraït per la confiança transmesa i per preocupar-se en tot moment per la meva formació. El mateix puc dir de la Dra. Marta Giamberini, co-directora de la tesis, gràcies per estar sempre disponible per resoldre qualsevol dubte, confiar en mi i pels ànims rebuts.

També vull agrair a la Prof. Àngels Serra el seu interès per la química i la recerca. Durant aquests anys, les converses que hem tingut sempre han estat molt profitoses per ampliar els meus coneixements.

M'agradaria també donar les gràcies a la resta dels professors de l'Àrea de Química Orgànica: Dr. Gerard Lligadas, Prof. Marina Galià, Prof. Joan Carles Ronda, Prof. Virginia Cádiz, Dr. Yolanda Díaz, Prof. Sergio Castillón i Prof. Maribel Matheu.

Agrair per la seva paciència als tècnics de laboratori (Juan Luis i Tere), així com a la Dúnia i l'Avelina per la seva ajuda en tots els tràmits administratius.

Als tècnics del Servei de Recursos Científics. Especialment, al Ramón Guerrero i al Francesc Gispert per estar sempre disponibles, per la seva ajuda i per solucionar els dubtes en qualsevol moment.

I am very grateful to Dr. Robert Graf for his incredible help and valuable advices during my research stay in the Max Planck Institute for Polymer Research in Mainz. I would like to thank all the kind people, whom I met in the Department of Molecular Electronics. Among them, especially Roland Rohloff and Naresh Kotadiya for their help and funny talks in the office. I

would also like to show my gratitude to Petra Pausch for her kindness and help during my stay in Germany.

Als meus companys de laboratori, amb els quals hem compartit estones de feina, de sobretaula i de gresca durant aquests 3 anys. A la Cristina, per acollir-me al seu costat des del primer dia. A més, tu sempre m'has explicat tot tipus d'aventures o històries amb les quals passàvem bones estones. Trobaré a faltar la música que escoltàvem al laboratori... A la Dailyn, por su amabilidad, aparte de enriquecer la biblioteca musical del laboratorio. Y que voy a decir de Alberto? Creo que tanto sentados en la mesa como en la poyata hemos tenido conversaciones muy interesantes de química, física, y sobre muchos otros temas con los que nos hemos reído. Gracias a ti Rubén por poder hablar con alguien de fútbol y de deporte en general, mientras el "Barça" siga ganando. Tú también terminarás tu "Tour" de la tesis. Al David Santiago, que sempre ens ve a fer "companyia". Encara que hem coincidit poc, vull agrair al Blai i a l'Isaac pels moments que hem rigut al laboratori.

Agradecer también a todos aquellas personas que han pasado por el laboratorio 330: Asta, Surya, Adrian, Marjorie, Vincenzo, Oleksandra, Rita y Yvonne. Y como no, al "equipo italiano", formado por Mario, Claudio, Mimmo, Gianmarco. Con vosotros pasé momentos muy divertidos tanto dentro como fuera del laboratorio.

Voldria agrair també a la resta de companys de l'Àrea de Química Orgànica pels divertits moments que hem passat a l'hora del cafè, sopars, ... Als companys de SusPol: Marc, Carmen, Lorena, Adrià i Iván. Als "Suspoleros" que ja no hi són: Camilo, Alev, Cristina Lluch. I als veïns del grup de sucres: Jordi, David, Macarena, Adrià, Irene por la seva simpatia.

Gràcies al membres del grup METEOR per la seva ajuda y la disponibilitat mostrada: Dr. Ricard Garcia Valls, Dra. Tània Gumí, Dr. Bartosz Tylkowski, Pepa, Kamila, Ada, Cristina Quintas, Judit i Claude. Especialmente, agradecer a Dr. Krzysztof Artur Bodganowicz, un gran amigo con el que he compartido ideas y también buenos momentos durante este tiempo.

Als companys que sempre, des de que vaig començar a estudiar a la universitat, han estat al meu costat i amb els que he passat un munt d'aventures: Joan i Sergi. Encara recordo el primer dia que ens vam trobar a la residència, Sergi. D'ençà d'aquell dia, sempre has estat al meu costat, ajudant-me en tot. Joan, tu també has estat un company inseparable. Tots tres tenim camí per recórrer juntament amb la resta de "químics": Lorena, David, Pau.

Gràcies als companys del poble per compartir rutes a peu per la muntanya, sopars i algun partidet de pàdel!

Quiero agradecer también a la Zeynep por haber estado a mi lado durante la realización de esta tesis, por su hospitalidad y apoyo.

I per fi, ha arribat el teu torn d'agrair a les persones més importants de la meva vida. Als meus pares gràcies per tot. Gràcies per l'educació que m'heu donat i per estimar-me com ho esteu fent. En tot moment heu estat al meu costat. I a l'Eva, la meva germana, gràcies per ser tant pacient i compartir moltes de les teves aventures amb mi.

Moltes gràcies!!

Als meus pares i germana

LIST OF ABBREVIATIONS

^{1}H NMR	Proton nuclear magnetic resonance
^{13}C NMR	Carbon nuclear magnetic resonance
ρ	Density
AAO	Anodized aluminium oxide
AFC	Alkaline fuel cell
BAM	Ballard Advanced Materials
CA	Contact angle
$CHCl_3$	Chloroform
CP-MAS	Cross-polarization magic angle-spinning
DCC	*N,N'*-dicyclohexylcarbodiimide
DMAP	4-dimethylaminopyridine
DMF	*N,N*-dimethylformamide
DMFCs	Direct methanol fuel cells
DMSO	Dimethyl sulfoxide
DP	Polymerization degree
DSC	Differential scanning calorimetry
EEGE	1-ethoxyethyl glycidyl ether
FEP	Fluorinated ethylene propylene
FT-IR	Fourier-transformed infrared spectroscopy
FWHM	Full width at half maximum
GADDS	General Area Detector Diffraction System
I_{lim}	Limiting current density

INEPT MAS	Intensive Nuclei Enhanced by Polarization Transfer Experiment
LCP	Liquid-crystalline polymer
LPG	Linear polyglycidol
LS	Light scattering
LSV	Linear sweep voltammetry
MAS	Magi angle-spinning
MCLCPs	Main-chain liquid-crystalline polymers
MCFC	Molten carbonate fuel cell
M_n	Number average molecular weight
M_w	Weight average molecular weight
NMP	*N*-methyl-2-pyrrolidone
PAFC	Phosphoric acid fuel cell
PAZE	Poly[2-(aziridine-1-yl)ethanol]
PBI	Polybenzimidazole
PECH	Poly(epichlorohydrin)
P(ECH-co-EO)	Poly(epichlorohydrin-co-ethylene oxide)
PEFC	Polymer electrolyte fuel cell
PEM	Polymer electrolyte membrane
PG	Polyglycidol
POM	Polarized optical microscopy
SOFC	Solid oxide fuel cell
RNA	Ribonucleic acid
R_{ohm}	Ohmic resistance density
RT	Room temperature

SAXS	Small-angle X-ray scattering
SCLCPs	Side-chain liquid-crystalline polymers
SEC	Size-exclusion chromatography
SEM	Scanning electron microscopy
TAP	3,4,5-tris[4-(n-dodecan-1-yloxy)benzyloxy]benzoic acid
T_c	Clearing temperature
TEM	Transmission electron microscopy
T_g	Glass transition temperature
TGA	Thermogravimetric analysis
THF	Tetrahydrofuran
T_m	Melting temperature
TMS	Tetramethylsilane
TMV	Tobacco Mosaic Virus
VT	Variable temperature
XRD	X-ray diffraction

TABLE OF CONTENTS

Chapter 1

General introduction and objectives

1.1. Artificial photosynthesis and fuel cells: an overview

Since the industrial revolution took place in the second half of the XVIII century, the world population has been increasing in an exponential manner. Nowadays, the production of enough energy to maintain human life and development on earth is an important and at the same time required topic. During the last three centuries, most of the energy needs have been provided by the combustion of fossil fuels like carbon, petroleum or natural gas. The use of fossil fuels leads to the emission of polluting gases in the atmosphere which are toxic for life. Another important drawback of fossil fuels is that they are found in limited quantities in nature. The disadvantages of fossil energy differs from the clean and sustainable energy sources, which are unlimited in nature.

In recent years, the use of artificial photosynthesis, fuel cells and batteries to produce alternative energy is a topic of growing interest because these systems use green energy. For instance, **Figure 1.1** illustrates the increment of the number of journal articles published on fuel cells from 1991 to 2015.

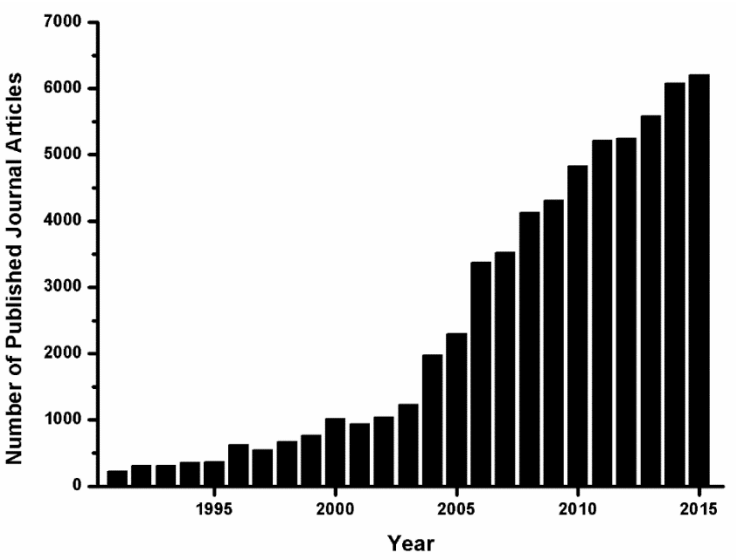

Figure 1.1. Number of journal articles on fuel cells based on a search using Scopus. [1]

Artificial photosynthesis is a chemical process that mimics a natural action that plants do: photosynthesis. The final goal of this process is to convert water and carbon dioxide into hydrogen or simple organic compounds using light or other renewable energy sources (**Figure 1.2**). The obtained hydrogen, which has a higher energy density than any other fuel, can be used as a fuel or stored for electricity production. [2, 3]

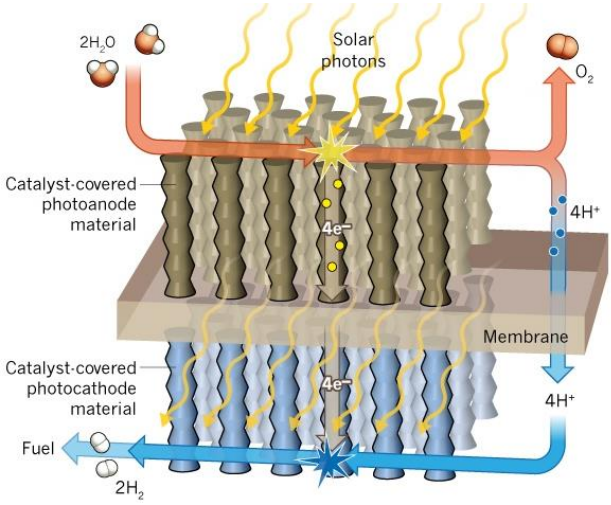

Figure 1.2. General scheme of artificial photosynthesis system.

On the other hand, a fuel cell is an electrochemical device that continuously converts chemical energy directly into electric energy as long as fuel and oxidant are supplied. Indeed, the electrochemical process that takes place in a fuel cell is free from any thermal or mechanical intermediate process; for this reason, these devices achieve higher efficiencies than thermal machines, which are limited by the Carnot cycle efficiency. Hence, fuel cells have a high energy efficiency, between 40-60%, and can reach up to >90% in cogeneration, if the waste heat is captured for use. [4-6] There are several types of fuel cells under development. They can be classified in many ways, but the most common classification of fuel cells is by the type of electrolyte used in the cells:

- Polymer electrolyte fuel cell (PEFC), which includes direct methanol fuel cell (DMFC)
- Alkalyne fuel cell (AFC)
- Phosphoric acid fuel cell (PAFC)
- Molten carbonate fuel cell (MCFC)
- Solid oxide fuel cell (SOFC)

The used electrolyte in every type of fuel cell dictates its operating temperature range and useful life, and indirectly determines the physicochemical and thermomechanical properties of the materials used in the cell components (i.e., electrodes, electrolyte, current collector, etc.). Consequently, the five fuel cells found in this classification contain different materials, work at different temperatures and also vary in their performance characteristics.

PEFCs play an important role in both artificial photosynthesis and fuel cell systems in terms of the mode of operation and applications. In both systems, PEFCs produce energy in a constant fashion if fuel is supplied continuously to the system, allowing uninterrupted power generation. In addition, the versatile conditions referring to operation temperature at which PEFCs work and the usage of “green” raw materials make preferable these systems for their use in artificial photosynthesis and fuel cell systems. Additionally, these systems are clean, silent and efficient. A PEFC consists of two electrodes and a solid polymer membrane, which acts as an electrolyte. [7] DMFCs are a type of PEFC which produce electricity by direct conversion of liquid methanol (**Figure 1.3**). During the last decades, a considerable amount of work dealing with DMFCs has been published. [8, 9]

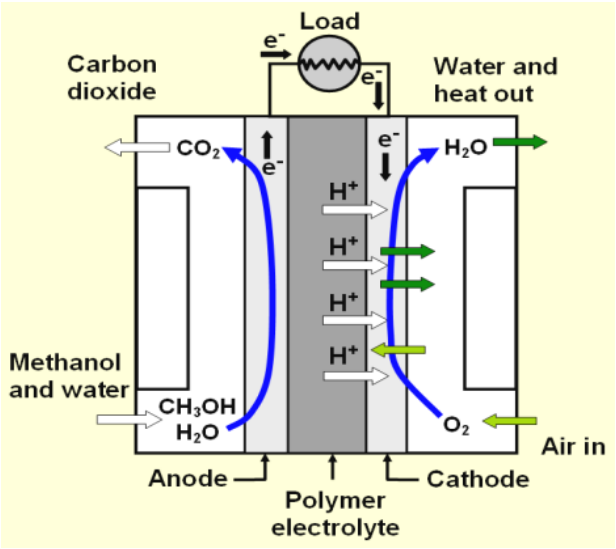

Figure 1.3. General scheme of Direct Methanol Fuel Cell.

The processes that occur in the different compartments of the DMFCs are explained further on. In a DMFC, liquid methanol is introduced to the anode, where it is split into protons and free electrons and gives out carbon dioxide. The produced protons move through the polymer electrolyte membrane (PEM) to the cathode compartment. At the cathode, where air or oxygen is introduced, the protons are bonded with oxygen to form water. As a consequence, the passing of protons across the polymer membrane generates a current that can be used to generate electrical energy. A scheme of the separated reactions which take place in the anode and cathode compartments and the overall reaction process occurring in a DMFC equipped with a proton-conducting electrolyte are outlined below:

Anode reaction:

$$CH_3OH + H_2O \rightarrow CO_2 + 6H^+ + 6e^-$$

Cathode reaction:

$$\frac{3}{2}O_2 + 6H^+ + 6e^- \rightarrow 3H_20$$

Overall reaction:

$$CH_3\mathrm{OH} + \frac{3}{2}O_2 \rightarrow CO_2 + 2H_20$$

In DMFCs, the solid polymer membrane displays an important role. Inside the fuel cell, PEM have two different functions: the membrane acts as separator between the fuel and oxidant to prevent their mixing; on the other hand, it drives the protons through the membrane in a selective manner from anode to cathode. Different polymers can be used as polymer electrolyte membrane.

The first commercial polymer membranes applied in a fuel cell were polystyrene-sulfonic acid (PSSA) membranes, which were developed in 1959 by the researcher Willard T. Grubb. [10] Since that time, the synthesis of different polymers with sulfonated groups at different extents were developed. As an example, the structure of some sulfonated polymers used as PEM are depicted in **Figure 1.4**: sulfonated poly(ether ether ketone) (SPEEK), [11, 12] sulfonated poly(arylene ether sulfone)s (SPAES), [13, 14] sulfonated poly(phenyleneoxide)s (SPPO), [15, 16] sulfonated poly(styrene) (SPS), [17] sulfonated polyimide (SPI), [18, 19] and sulfonated poly(phosphazene) (SPOP). [20, 21] These families of polymers have been largely studied as promising PEM due to easy tuning of molecule architecture and relatively non expensive cost.

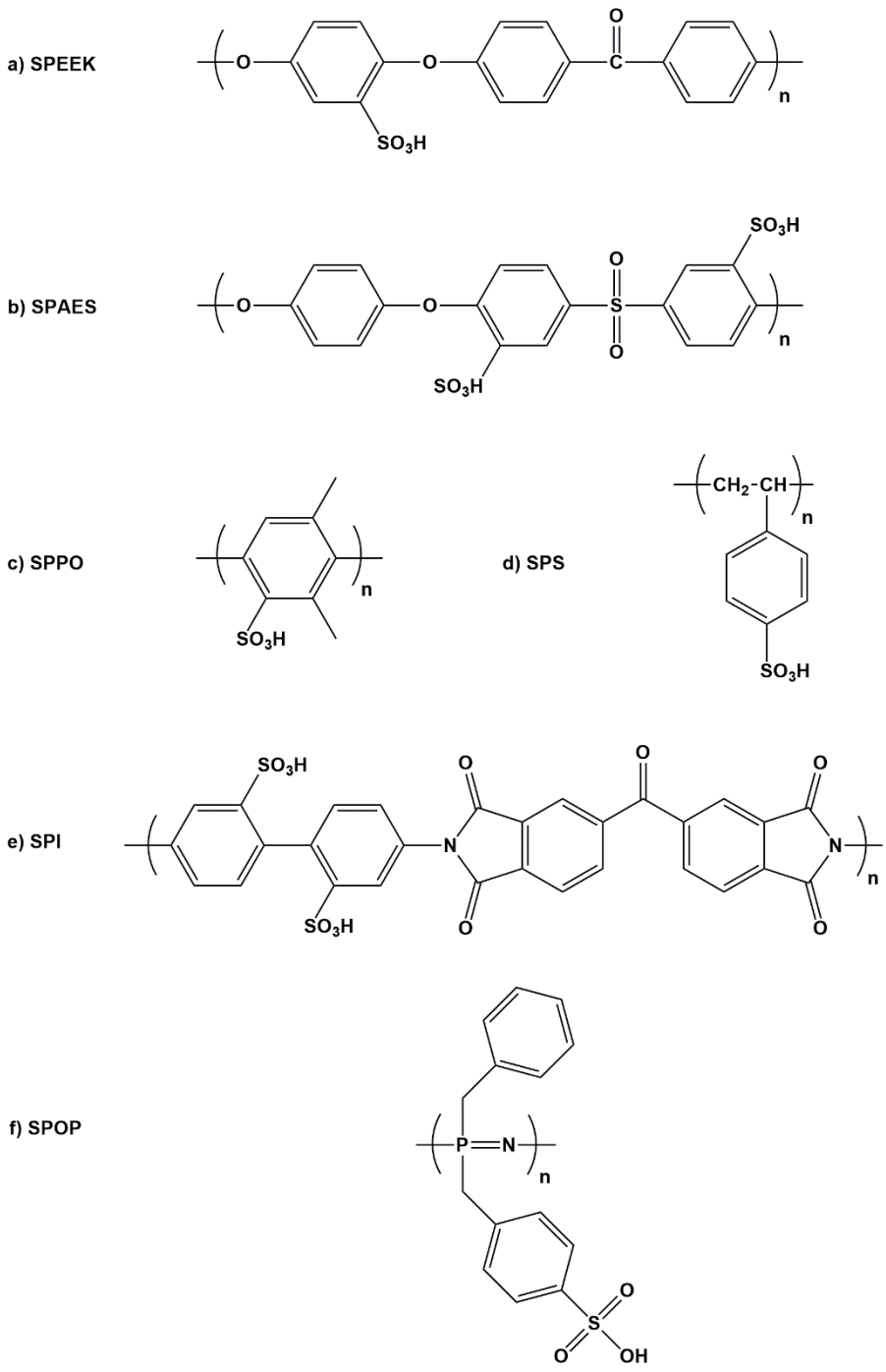

Figure 1.4. Schematic illustration of different sulfonated polymers.

Despite the improvements that partially and completely sulfonated polymers show when they are used as polymer electrolyte, they present low conductivity at low water contents and relatively low molecular strength at higher temperature. [20]

Another group of polymers used in the synthesis of membranes are perfluorinated ones. At the present time, perfluorosulfonic acid (PFSA)-based membranes such as Nafion®, produced by DuPont, have been extensively used as polymer electrolyte membranes for DMFC. Nafion® 117 chemical structure and other commercial polymers used as polymer electrolyte membranes are displayed in **Figure 1.5** in its anhydrous form (-SO_3H). The membranes obtained by using these polymers exhibit a high proton conductivity which is attributed to the presence of sulfonic groups. Other benefits of the usage of Nafion® membranes are the good mechanical strength and thermal and chemical stability conferred by the fluorinated groups in the polymer backbone. However, these materials present some drawbacks like high methanol crossover, especially when the concentration of methanol is too high, and high cost due to the expensive fluorination step. [22, 23] Furthermore, systems like Nafion® should be kept fully hydrated during the permeation process to promote proton/ion transport. This water-dependence conductivity limits the operation temperature below 100˚C to obtain a good efficiency. Despite of water stimulating effect on the ionization of sulfonic groups, it causes also swelling of the ionomeric polymer membrane. This lack of dimensional stability caused by water uptake negatively affects Nafion® membrane properties. [24]

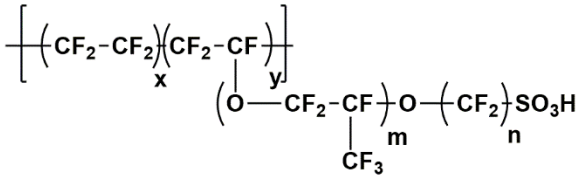

Nafion® 117	**$m \geq 1$, n = 2, x = 5-13.5, y = 1000**
Flemion®	**m = 0,1; n = 1-5**
Aciplex®	**m = 0,3; n = 2-5, x = 1.5-14**
Dow membrane	**m = 0, n = 2, x = 3.6-10**

Figure 1.5. Chemical structures of perfluorinated polymers used as polymer electrolyte membranes.

The observed poor selectivity for proton is another shortcoming of Nafion® membranes. Thus, other undesired cations or even small molecules, which could damage the electrodes or provoke undesired reactions, can be conducted through Nafion®. The comprehension of the conductivity mechanisms at a molecular level in hydrated polymeric matrices is a useful tool to understand the reasons for low selectivity against proton exhibited by Nafion systems.

For proton transport, there are two different mechanisms:

a) Proton "hopping" mechanism (or also Grotthus mechanism): This mechanism of proton transport was proposed by Theodor Grotthus in 1806 to explain water conductivity. In this mechanism, protons hop from one hydrolysed ionic site (SO_3^- H_3O^+) to another, through a hydrogen bond network.
b) Vehicular mechanism (or also diffusive mechanism): In this mechanism, protons bound to one or more water molecules ($H^+(H_2O)_x$) previously; then water itself drag them across the membrane.

Figure 1.6 display a scheme of both kinds of proton transport. On increasing the hydration level of the membrane, the vehicular mechanism is more favoured than "hopping" mechanism, which results in a less selective proton transport through the membrane. Therefore, considering all the disadvantages of Nafion®, it is important to achieve a balance of water in the electrolyte to obtain a good proton conductivity.

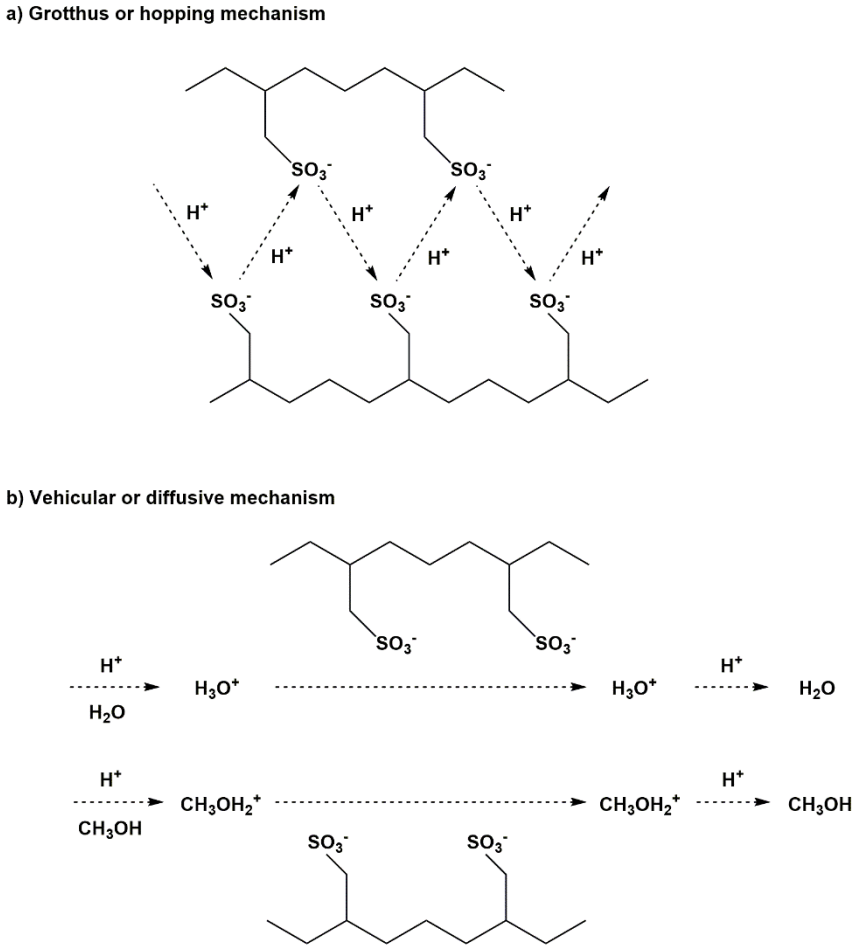

Figure 1.6. Schematic representation of: a) Grotthus or hopping mechanism and b) vehicular or diffusive mechanism.

Besides, different transition metal complexes of platinum, ruthenium, rhodium, titanium, manganese and other transition metals are efficient catalysts for their use in artificial photosynthesis. Nevertheless, on increasing the hydration level, the vehicular mechanism might involves the migration of these metal ions across Nafion®, causing the contamination of the feed and stripping solutions or also the polymer membrane. In addition, catalyst fragments can be trapped in the ion channels of the membrane, which results in the formation of less efficient catalyst clusters and smaller pore sizes of ion channels. [25] All these reasons confirm that Nafion® membranes are not the most appropriate candidates for their use in artificial photosynthesis.

In order to gather the properties of Nafion® with the advantages of other sulfonated membranes derived from styrene, the preparation of polymers which combine a perfluorinated backbone with aromatic groups was reported. BAM membranes, produced by Ballard Advanced Materials Corporation are a representative example (**Figure 1.7**). [20] In the resulting polymers, aromatic groups are laterally grafted to the fluorinated main chain.

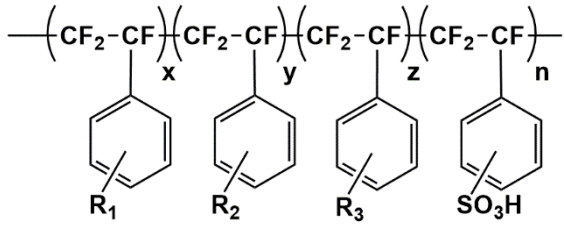

R_1, R_2, R_3 = alkyls, halogens, OR, $CF=CF_2$, CN, NO_2, OH

Figure 1.7. Chemical structure of perfluorinated BAM polymer electrolyte membranes.

Sulfonated block copolymers are interesting materials as fuel cell membranes because the combination of ionic and non-ionic blocks provides the potential for highly ordered morphologies where transport properties can be tailored in a reliable manner. [26, 27]

One more option could be the use of acid-base systems. The most common example is the phosphoric acid-doped polybenzimidazole (PBI/H_3PO_4) based systems. [28] **Figure 1.8** shows the structure of a PBI and PBI salt obtained after doping PBI with H_3PO_4. In these systems, the doping with phosphoric acid at different extents of previously sulfonated polymers ameliorate the proton conductivity: a higher doping level could lead to higher proton conductivity but conversely a deterioration of the mechanical properties and chemical stability were found. [29, 30] Additionally, phosphoric acid also tends to be easy detached and may corrode the electrodes and bipolar plates of the fuel cell. [31]

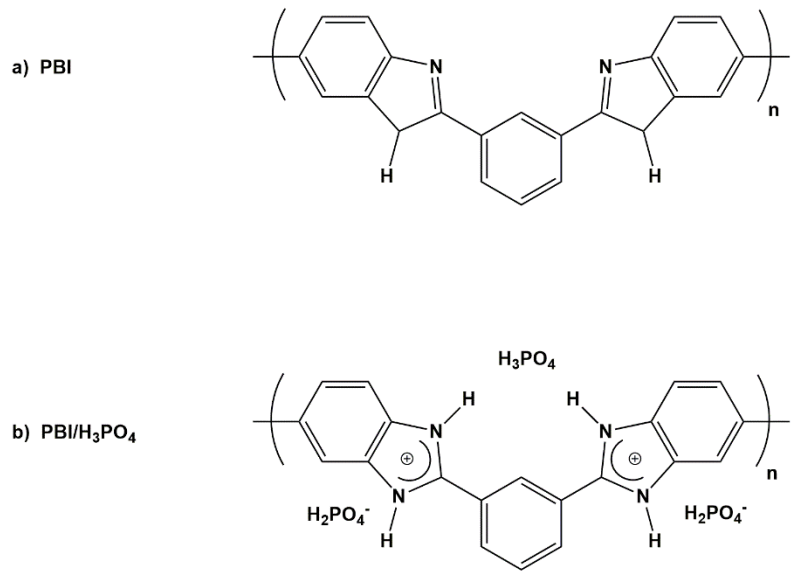

Figure 1.8. Structure example of: a) polybenzimidazole compound (PBI) and b) poly-salt formed by phosphoric acid doping of the same PBI. [32]

To date, there has been continuous extensive research on developing a membrane which can fulfil all the essential characteristics to yield the desired performance in DMFCs. In the course of this research, a useful tool to develop new PEM is the building of hybrid membranes by combining the original materials to produce new membranes with variously enhanced properties. [33, 34] Thus, the preparation of blends of different polymers, [35] and composites [36, 37] where a polymer matrix is reinforced with different organic or inorganic compounds are techniques used nowadays to prepare materials which could act as electrolyte membrane in DMFCs.

The development of completely new polymeric structures with enhanced proton conductivity as well as excellent fuel cell performance can be a further alternative. To achieve this goal, the design of materials containing ion transport channels by self-assembling, in which the channels localize the permeation path and simultaneously protect the transport process against the environment, like an ion-transporting molecular cable, can be an intriguing option. Under this hypothesis, membrane hydration is not necessary for ionic transport and, therefore, the problems related to methanol crossover and polymer swelling can be avoided.

1.2. Biomimetic ion transport

Nature behaviour has always been a source of inspiration for humans. In research, scientists try to extract guiding principles from nature in order to provide technological devices which allow us to live in a better and more sustainable society. [38, 39]

During the last decades, one natural phenomenon that has been studied extensively is proton transport, because it occurs with high selectivity and efficiency in natural systems like in the photosynthesis of green plants.

In biological systems, transport mainly occurs by means of three different mechanisms:

- Carriers: molecules that transport specific substances through intracellular compartments, or across the cell membrane into the extracellular fluid.

- Channels: they act as a tunnel across the cell membrane to facilitate the movement of ions through the membrane according to their electrochemical gradient.

- Doors: they are a moving structure used to block off or allow access of ions/molecules to the cell membrane or an intracellular compartment.

For instance, **Figure 1.9** displays in what manner ion carriers and ion channels allow ion transport in biological systems across the cell membrane.

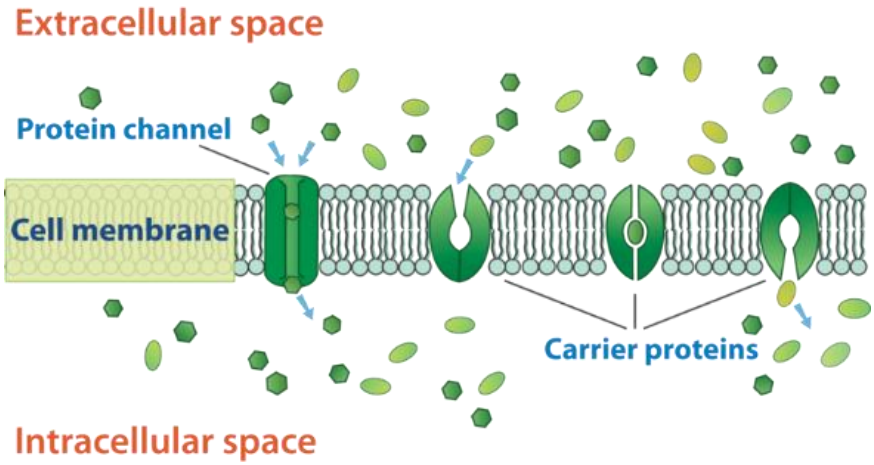

Figure 1.9. Example of ion transport through protein channels and carriers across cell membrane.

Among all these systems, ion channels based on proteins are the most commonly used systems to transport ions through the membranes in the cells. However, these proteins exhibit some drawbacks which limit their utility for technological applications. First of all, transmembrane proteins are difficult to isolate in their pure and functional form and they tend to denature easily. Furthermore, their chemical modification into more elaborated molecular systems is almost impossible due to their complex multidomain structure. [40] To diminish these disadvantages, various studies to develop artificial supramolecular assemblies capable of transporting ions across membranes by the channel mechanism have been the subject of increasing interest.

In the 1980s, Dulyea and coworkers prepared polymers that incorporate a crown ether-carboxylic acid along the backbone. In the resulting structure, which is able to act as an ion channel, the crown ether molecules were packed as a cylinder. [41] In the 1990s, Voyer reported some studies of artificial ion channels constructed using peptides which have linked crown ethers in the outer part (**Figure 1.10**). [42-44] Nonetheless, the attraction of a cation within one crown ether unit inside the cylinder is relatively strong and therefore, the energy barrier needed for the proton to jump to the following crown ether molecule is too high. One attempt carried out to eliminate this energy barrier was reported by Koert and coworkers in 1994. Koert described the building of oligo(tetrahydrofuran)s which tend to adopt a helical conformation. [45] Despite this, the synthetic route involves multiple and complex steps, a fact that makes this route of limited interest.

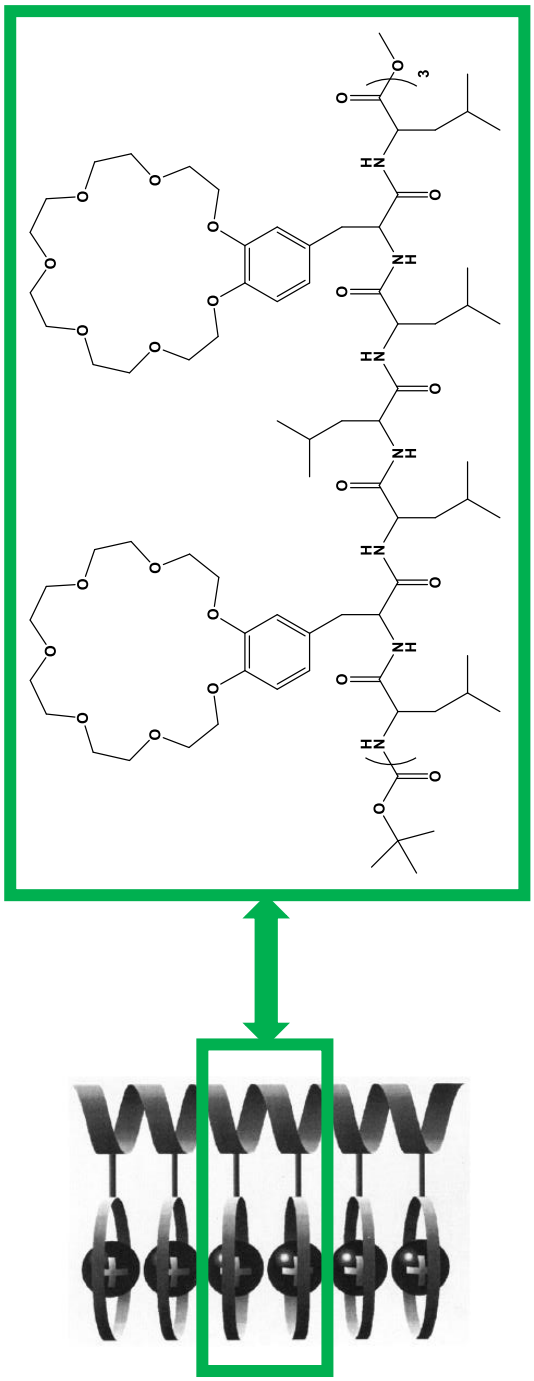

Figure 1.10. Ion channels formed by cylindrical packing of crown ether molecules.

In general, polyethers adopt a random coil conformation: for this reason, the synthesis of polyethers that can adopt cylindrical structures, acting as ion channels, is not obvious.

Another strategy that prompts the generation of cylindrical polymers capable to adopt a helical conformation could be supramolecular chemistry. Supramolecular chemistry may be defined as “chemistry beyond the molecule”, bearing on the organised entities of higher complexity that result from the association of two or more chemical species held together by non-covalent interactions. [46] There are different types of non-covalent interactions: hydrogen bonds, Van der Waals forces, electrostatic interactions, etc. Furthermore, the processes that involve the formation of discrete and subsequently well-organised supramolecular objects like micelles, liquid crystals, colloids, etc. are called self-assembly, followed eventually by self-organisation. [47]

Examples of self-assembly can be found in nature. The Tobacco Mosaic Virus (TMV) consists of 2130 units of a single type of protein molecule and a chain of ribonucleic acid (RNA). This protein molecule presents a tapered shape. When the proteins and the ribonucleic acid chain are mixed, the TMV self-assembles into a helical structure, in which the proteins organise themselves in a regular helical pattern and force the RNA to adopt a helical conformation in the inner part of the structure (**Figure 1.11**). [48]

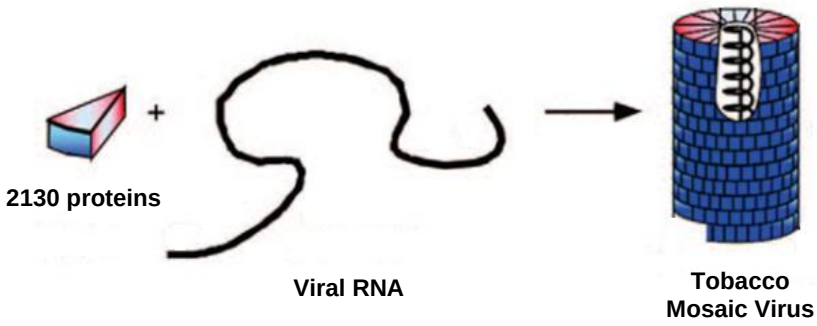

Figure 1.11. Supramolecular self-assembly of Tobacco Mosaic Virus into a helical conformation. [49]

The proteins in TMV act as exo-receptor due to the large enough contact area and similar size and geometry (tapered shape), which make easy to start the exo-recognition process between them along the RNA chain. In the exo-recognition process, non-bonding intermolecular forces occur between the external proteins of the self-assembled molecular architecture of TMV.

Recently, the use of peptides with helical structure obtained by self-assembling combined with crown ethers has been used to prepare artificial ion channels. [50]

In the same way as observed in TMV, one can expect that the addition of moieties with a tapered shape to a polymer chain will probably lead to a cylindrical supramolecular structure, where the polymer chain lies in the inner part of the generated column surrounded by the tapered moieties. Moreover, this tapered units grafted to the polymer could force the polymer chain to adopt a helical conformation. Hence, the use of self-assembled polymers could be an interesting tool to construct biomimetic ion channels for ion conducting materials. Thus, this approximation could be achieved by using columnar liquid-crystalline polymers.

1.3. Liquid-crystalline polymers

Materials in nature can exhibit different states of matter, depending on the order and mobility of the individual atoms or molecules. The most common states of matter are the solid, the liquid and the gaseous state. Although this three states seem very well defined, the borders between them are not always clear. Apart from the three classical states of matter, other intermediate states may exist. One of these intermediate states is the liquid-crystalline state (also called mesophase from the greek word "*mésos*", between). In the liquid-crystalline state, molecules present an intermediate behaviour between the high order and rigidity characteristic of solid materials and the mobility of a liquid. In **Figure 1.12**, the order at molecular level in the three traditional states of matter and also the liquid-crystalline state are presented. [51] Since the observation of the first liquid crystal (LC) by the Austrian botanist Friedrich Reinetzer in 1888, different liquid-crystalline mesophases were discovered. Furthermore, the particular properties of LCs make them unique for their applications in technology.

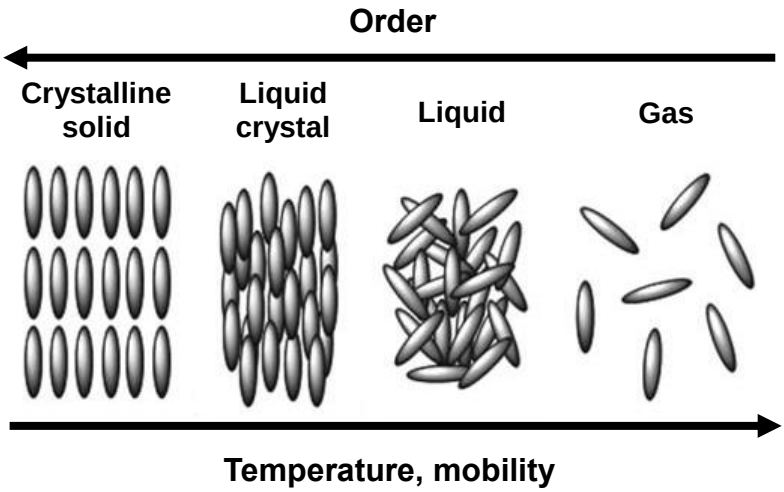

Figure 1.12. Schematic representation of the molecular ordering in different states of matter: crystalline solid, liquid crystal, isotropic liquid and gas.

A great variety of organic molecules can form liquid-crystalline mesophases. These molecules are called mesogens or mesogenic molecules. They are generally characterized by relative rigidity, anisotropic shape and anisotropy of molecular polarizability.

LCs can be classified following different criteria. The most used classification is based on how the liquid-crystalline phase can be observed. [51] According to this, there are two types of LCs:

- Thermotropic LCs: The liquid-crystalline behaviour exhibits only a temperature dependence.
- Lyotropic LCs: The liquid-crystalline properties appear induced by the presence of a suitable solvent under appropriate conditions of concentration and temperature, with mesophases depending on solvent concentration, as well as temperature.

Additionally, thermotropic LCs are divided into two different subgroups:

- Enantiotropic LCs: These materials exhibit a thermodynamically stable LC mesophase which can be detected either by heating a solid or by cooling an isotropic liquid.
- Monotropic LCs: These materials exhibit the liquid-crystalline mesophase only when the temperature changes in one direction, usually by cooling the isotropic liquid, because the liquid crystal mesophase is thermodynamically metastable.

Related to their shape, thermotropic LC can be classified into two main types:

- Calamitic (rod-shaped) liquid crystals
- Discotic (Disk-like shaped) liquid crystals

Figure 1.13 shows an example of different types of LC related to their shape. [52] Calamitic mesogens have an elongated geometry which allows for preferential alignment along one spatial direction. Conversely, discotic LC are plane disk-like molecules generally consisting of a core of adjacent aromatic rings.

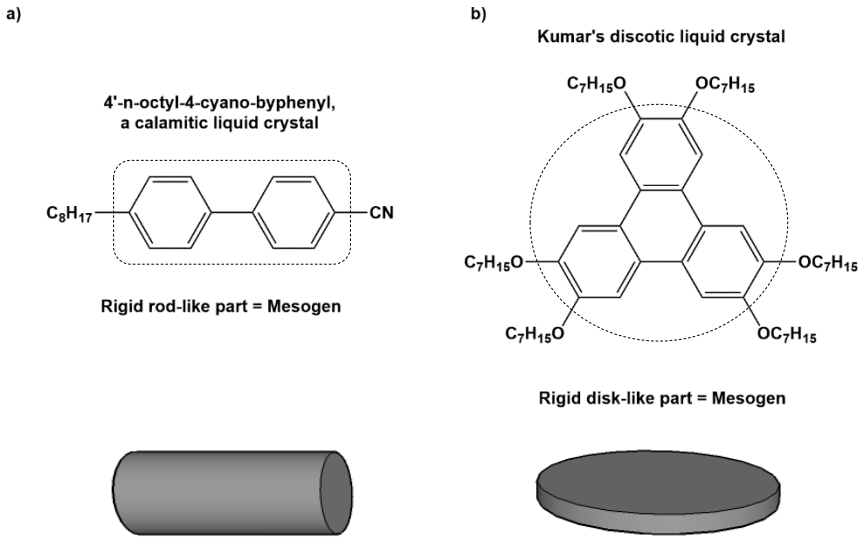

Figure 1.13. Schematic representation of: a) calamitic liquid crystal mesogen and b) discotic liquid crystal mesogen.

Usually, the disk-shaped structure promotes the stacking effect of discs into columns in discotic liquid crystals. Predominantly, the generated columns tend to array into nematic discotic or different columnar mesophases depending on the degree of order in the final structure. (**Figure 1.14**). From this possible mesophases, nematic discotic mesophase (N_D) is the less ordered mesophase because the disks only possess some long-range orientational order, but no long-range positional order. On the other hand, when the disk-like molecules stack in columns the mesophases are columnar

(ranging from lamellar to hexagonal columnar mesophase). Columnar mesophases (*Col*) exhibit both long-range orientational and 2-dimensional positional order. Columnar nematic (N_{col}) mesophase is a particular case because it does not form 2-dimensional lattice structures although it display a positional short-range order and orientational long-range order. [51]

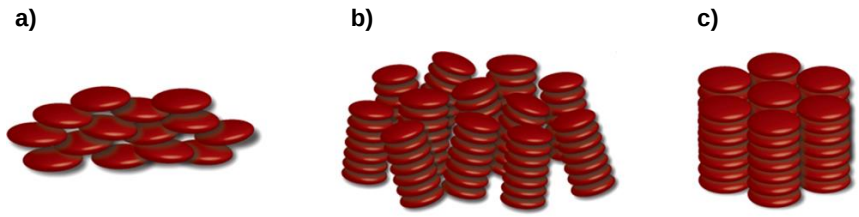

Figure 1.14. Schematic representation of: a) nematic discotic mesophase (N_D), b) columnar nematic (N_{col}) and c) columnar mesophases (*Col*). [53]

Liquid-crystalline polymers (LCPs) are a kind of polymers which contain mesogenic units. Hence, LCPs combine the properties of polymers with the properties of liquid crystals. This combination of properties make LCPs interesting materials which are used for electrical, mechanical or optical applications. This thesis focuses on discotic liquid crystal polymers.

There are different types of LCPs. Depending on the position of the mesogenic group inside the polymer, there are two types of LCP:

- Main-chain liquid-crystalline polymers (MCLCPs)
- Side-chain liquid-crystalline polymers (SCLCPs)

Schematic representation of both possible structures can be observed in **Figure 1.15**. MCLCPs are formed when the mesogenic cores are

themselves a part of the main chain or backbone of the polymer. On the contrary, SCLCPs are formed when the mesogens are connected as side chains to the polymer backbone by a flexible spacer.

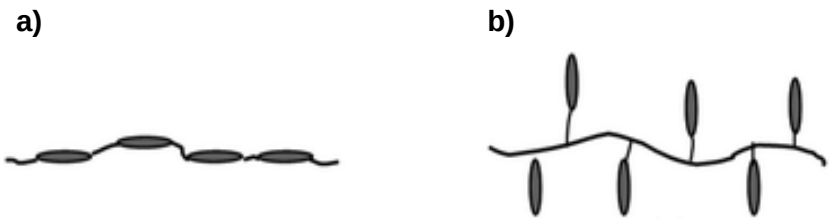

Figure 1.15. Schematic representation of: a) MCLCPs and b) SCLCPs.

Different factors such as the nature of the mesogen group introduced, the polymer molecular weight, the structure and the length of the spacer can affect the resulting molecular organisation and degree of order. Therefore, several mesophases can be formed depending on the degree of order generated in the material.

In this thesis, SCLCPs which shows different columnar mesophases are studied.

1.4. Supramolecular self-assembling structures

The combination of liquid crystal mesogens with tapered shape grafted to a polymeric chain allow, via supramolecular chemistry, the generation of systems that could act as ion channels. In the resulting supramolecular systems, the presence of these tapered moieties facilitate the self-assembly process of polymers into a columnar structure able for cation transport for example in fuel cells. As an example, the self-assembly process

of a dendronised polymer into a hexagonal columnar structure is depicted in **Figure 1.16**.

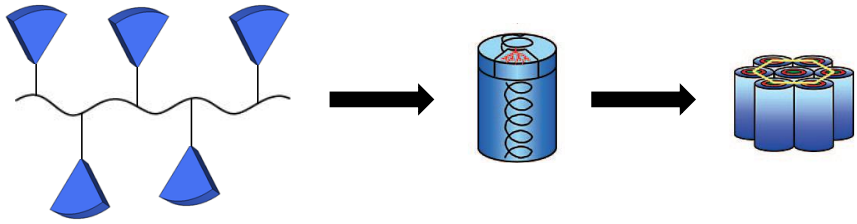

Figure 1.16. Schematic representation of the self-assembly of dendronised polymers into a hexagonal columnar structure.

The first studies conducted on this topic were carried by the group of Percec. In 1991, they reported the first examples of polymers containing tapered minidendritic side groups that self-assembled intramolecularly in cylindrical macromolecules, which subsequently self-organised in hexagonal columnar lattices. [54] Since then, this group conducted a wide investigation on the self-assembly and subsequent self-organisation of supramolecular dendrons, dendrimers and dendronised polymers into liquid-crystalline phases. This approach could be used in the design of ion-active nanostructured supramolecular systems. [55]

In the last decade, our group reported the synthesis and characterization of side chain liquid-crystalline polyamines and polyethers which self-assemble into a columnar structure. [56, 57] In this way, poly[2-(aziridin-1-yl)-ethanol] (PAZE), poly(epichlorohydrin) (PECH) and poly(epichlorohydrin-co-ethylene oxide) [P(ECH-co-EO)] were modified with the dendron 3,4,5-tris[4-(n-dodecan-1-yloxy)benzyloxy]benzoic acid. Depending on the amount of tapered grafted to the polymer, different types of columnar mesophases were obtained. In the resulting supramolecular

systems, the presence of oxygen and nitrogen atoms in the polymer main chain, which act as an ion channel, facilitates the interaction with proton and other cations.

Afterwards, the SCLCPs have been studied as possible ion channels candidates for their application in membrane technology. Tylkowski and coworkers prepare oriented membranes based on modified PECH which exhibit proton transport comparable to Nafion® N117 and no water uptake. [58] Continuing this research, Bogdanowicz et al. performed a deep study about the preparation, characterization and assessment of different oriented membranes based on modified polyamines and polyethers. [59-61]

1.5. Objectives

The objectives of this thesis can be summarized as follows:

- Synthesis of novel self-assembling side-chain columnar liquid-crystalline polyamines and polyethers containing tapered side groups. These synthesis will be carried out both by the polymerisation and the chemical modification of the previously synthesised poly[2-(aziridn-1-yl)ethanol] and linear polyglycidol respectively.

- Preparation, characterization and assessment of novel ion conductive membranes derived from the synthesised side-chain columnar liquid-crystalline polyamines and polyethers.

- Determination of the structure and dynamics of some of these functional supramolecular materials in order to understand the behaviour of these systems in the solid state.

- Improvement of the polymerisation of glycidol, in order to obtain linear polyglycidol (LPG) with higher molecular weight than previously reported.

The main hypothesis which reinforce the objectives are:

- The preparation of polyamines or polyethers with tapered side-groups will lead to liquid-crystalline columnar mesophases. In the resulting structures, the polymer main chain forms a channel in the inner part of the columns, while the hydrophobic side-chain dendrons lie in the outer part.

- The presence of electro-donor atoms like nitrogen or oxygen atoms in the inner channel favours the interaction with proton and other cations.

- Solid state NMR techniques can provide information about the local structure and local molecular dynamics of dendritic polymers. Furthermore, solid state NMR can help to understand the self-assembly process of the resulting supramolecular systems.

- The preparation of linear polyglycidol with high degree of polymerisation could lead to a polymer chain which can be modified with tapered groups in order to obtain LC polymers. These LC polymers could be used to prepare oriented membranes with improved mechanical properties.

1.6. References

1. www.scopus.com, 2016.

2. Edwards PP, Kuznetsov VL, David WIF, and Brandon NP. Energy Policy 2008;36(12):4356-4362.

3. Sharma S and Ghoshal SK. Renewable Sustainable Energy Rev. 2015;43:1151-1158.

4. Steele BCH and Heinzel A. Nature 2001;414(6861):345-352.

5. Wang Y, Chen KS, Mishler J, Cho SC, and Adroher XC. Appl. Energy 2011;88(4):981-1007.

6. Maharana T, Sutar AK, Nath N, Routaray A, Negi YS, and Mohanty B. Polyetheretherketone (PEEK) Membrane for Fuel Cell Applications, in Advanced Energy Materials. Hoboken, NJ: John Wiley & Sons, 2014. pp. 433-464.

7. Rikukawa M and Sanui K. Prog. Polym. Sci. 2000;25(10):1463-1502.

8. DeLuca NW and Elabd YA. J. Polym. Sci., Part B: Polym. Phys. 2006;44(16):2201-2225.

9. Zhang H and Shen PK. Chem. Rev. 2012;112(5):2780-2832.

10. Grubb WT. J. Electrochem. Soc. 1959;106(4):275-278.

11. Gil M, Ji X, Li X, Na H, Eric Hampsey J, and Lu Y. J. Membr. Sci. 2004;234(1–2):75-81.

12. Xing P, Robertson GP, Guiver MD, Mikhailenko SD, Wang K, and Kaliaguine S. J. Membr. Sci. 2004;229(1–2):95-106.

13. Pang J, Zhang H, Li X, Wang L, Liu B, and Jiang Z. J. Membr. Sci. 2008;318(1–2):271-279.

14. Kim DS, Robertson GP, and Guiver MD. Macromolecules 2008;41(6):2126-2134.

15. Guan R, Gong C, Lu D, Zou H, and Lu W. J. Appl. Polym. Sci. 2005;98(3):1244-1250.

16. Yang S, Gong C, Guan R, Zou H, and Dai H. Polym. Adv. Technol. 2006;17(5):360-365.

17. Carretta N, Tricoli V, and Picchioni F. J. Membr. Sci. 2000;166(2):189-197.

18. Asano N, Aoki M, Suzuki S, Miyatake K, Uchida H, and Watanabe M. J. Am. Chem. Soc. 2006;128(5):1762-1769.

19. Saito J, Miyatake K, and Watanabe M. Macromolecules 2008;41(7):2415-2420.

20. Hickner MA, Ghassemi H, Kim YS, Einsla BR, and McGrath JE. Chem. Rev. 2004;104(10):4587-4612.

21. Wycisk R and Pintauro PN. Polyphosphazene Membranes for Fuel Cells, in Fuel Cells II, vol. 216. Heidelberg: Springer, 2008. pp. 157-183.

22. Yildirim MH, Stamatialis D, and Wessling M. J. Membr. Sci. 2008;321(2):364-372.

23. Kim DS, Guiver MD, and Kim YS. Proton Exchange Membranes for Direct Methanol Fuel Cells, in Electrocatalysis of Direct Methanol Fuel Cells. Weinheim: Wiley-VCH Verlag GmbH & Co. KGaA, 2009. pp. 379-416.

24. Gebel G and Lambard J. Macromolecules 1997;30(25):7914-7920.

25. Piela P, Eickes C, Brosha E, Garzon F, and Zelenay P. J. Electrochem. Soc. 2004;151(12):A2053-A2059.

26. Higa M, Feng S, Endo N, and Kakihana Y. Electrochim. Acta 2015;153:83-89.

27. Elabd YA, Napadensky E, Sloan JM, Crawford DM, and Walker CW. J. Membr. Sci. 2003;217(1–2):227-242.

28. Mader J, Xiao L, Schmidt TJ, and Benicewicz BC. Polybenzimidazole/Acid Complexes as High-Temperature Membranes, in Fuel Cells II, vol. 216. Heidelberg: Springer, 2008. pp. 63-124.

29. Schuster MFH and Meyer WH. Annu. Rev. Mater. Res. 2003;33(1):233-261.

30. Yue Z, Cai Y-B, and Xu S. J. Membr. Sci. 2016;501:220-227.

31. Matar S, Higier A, and Liu H. J. Power Sources 2010;195(1):181-184.

32. Asensio JA, Sanchez EM, and Gomez-Romero P. Chem. Soc. Rev. 2010;39(8):3210-3239.

33. Ahmad H, Kamarudin SK, Hasran UA, and Daud WRW. Int. J. Hydrogen Energy 2010;35(5):2160-2175.

34. Kim DJ, Jo MJ, and Nam SY. J. Ind. Eng. Chem. 2015;21:36-52.

35. Ngamsantivongsa P, Lin H-L, and Leon Yu T. J. Membr. Sci. 2015;491:10-21.

36. Wehkamp N, Breitwieser M, Buchler A, Klingele M, Zengerle R, and Thiele S. RSC Adv. 2016;6(29):24261-24266.

37. Kim DJ, Choi DH, Park CH, and Nam SY. Int. J. Hydrogen Energy 2016;41(13):5793-5802.

38. Nielsen CH. Anal. Bioanal. Chem. 2009;395(3):697-718.

39. Wegst UGK, Bai H, Saiz E, Tomsia AP, and Ritchie RO. Nat. Mater. 2015;14(1):23-36.

40. Biron E, Otis F, Meillon J-C, Robitaille M, Lamothe J, Van Hove P, Cormier M-E, and Voyer N. Biorg. Med. Chem. 2004;12(6):1279-1290.

41. Dulyea LM, Fyles TM, and David Robertson G. J. Membr. Sci. 1987;34(1):87-108.

42. Voyer N. J. Am. Chem. Soc. 1991;113(5):1818-1821.

43. Voyer N and Robitaille M. J. Am. Chem. Soc. 1995;117(24):6599-6600.

44. Meillon JC and Voyer N. Angew. Chem., Int. Ed. Engl. 1997;36(9):967-969.

45. Koert U, Stein M, and Harms K. Angew. Chem., Int. Ed. Engl. 1994;33(11):1180-1182.

46. Lehn J-M. Proc. Natl. Acad. Sci. U. S. A. 2002;99(8):4763-4768.

47. Rosen BM, Wilson CJ, Wilson DA, Peterca M, Imam MR, and Percec V. Chem. Rev. 2009;109(11):6275-6540.

48. Klug A. Angew. Chem., Int. Ed. Engl. 1983;22(8):565-582.

49. Rudick JG and Percec V. Acc. Chem. Res. 2008;41(12):1641-1652.

50. Otis F, Auger M, and Voyer N. Acc. Chem. Res. 2013;46(12):2934-2943.

51. Kumar S. Introduction, in Chemistry of Discotic Liquid Crystals: From Monomers to Polymers. Boca Raton, FL: Taylor & Francis Group, 2011. pp. 1-48.

52. Wolf JR. Liq. Cryst. Rev. 2014;2(1):28-46.

53. Goossens K, Lava K, Bielawski CW, and Binnemans K. Chem. Rev. 2016;116(8):4643-4807.

54. Percec V and Heck J. J. Polym. Sci., Part A: Polym. Chem. 1991;29(4):591-597.

55. Sun H-J, Zhang S, and Percec V. Chem. Soc. Rev. 2015;44(12):3900-3923.

56. Šakalytė A, Reina JA, and Giamberini M. Polymer 2013;54(19):5133-5140.

57. Bhosale SV, Rasool MA, Reina JA, and Giamberini M. Polym. Eng. Sci. 2013;53(1):159-167.

58. Tylkowski B, Castelao N, Giamberini M, Garcia-Valls R, Reina JA, and Gumí T. Mater. Sci. Eng. C 2012;32(2):105-111.

59. Bogdanowicz KA, Rapsilber GA, Reina JA, and Giamberini M. Polymer 2016;92:50-57.

60. Bogdanowicz KA, Sistat P, Reina JA, and Giamberini M. Polymer 2016;92:58-65.

61. Bogdanowicz KA, Bhosale SV, Li Y, Vankelecom IFJ, Garcia-Valls R, Reina JA, and Giamberini M. J. Membr. Sci. 2016;509:10-18.

Chapter 2

Advances in the design of self-supported ion-conducting membranes- new family of columnar liquid-crystalline polyamines. Part 1: copolymer synthesis and membrane preparation

Xavier Montané, Krzysztof Artur Bogdanowicz, Gianmarco Colace, José Antonio Reina, Pierfrancesco Cerruti, Marta Giamberini*

*- Polymer, submitted.

2.1. Introduction

In natural systems proton transport conductivity occurs with high selectivity and efficiency. For this reason, in the last thirty years, most research in the field of proton conductivity has been devoted by the materials science community mainly for the development of new proton-conducting materials to be used in electrochemical cells (e. g. fuel cells, batteries, sensors). [1, 2]

Liquid crystals (LCs) are interesting materials because of their unique properties: they combine molecular order and mobility. This unique combination leads to the formation of chemical entities that present a well-ordered internal structures. [3] Thus, the design of LCs as new functional materials can be an attractive option for various applications such as ion [4, 5] or charge [6, 7] transport, separation membranes, [8, 9] and catalysis. [10, 11]

Up to now, Percec group carried out an extensive investigation on the synthesis and posterior self-assembly process of supramolecular dendrons, dendrimers and dendronised polymers into liquid-crystalline mesophases. [12]

In our group we design dendronised polyethers and polyamines that forms ion transport channels by self-assembling, in which the channels localise the permeation path and simultaneously protect the transport process against the environment, like an ion-transporting molecular cable. [13-16]

As it was described previously, we tackled the chemical modification of polymer poly[2-(aziridin-1-yl)ethanol] (PAZE) with the mesogenic group 3,4,5-tris[4-(n-dodecan-1-yloxy)benzyloxy]benzoic acid (TAP) in order to obtain side-chain liquid-crystalline polyamines. [16] In that study we prepared a family of copolyamines with different degrees of modification of TAP groups. These copolymers can be used to prepare oriented membranes for

small cation transport, in agreement with the results that we obtained on oriented membranes based on poly(epichlorohydrin) (PECH) modified with the same dendron, where proton permeability comparable to Nafion® 117 was found. [17] As we reported before, these polymers self-assemble into a columnar structure, due to an exo-recognition of the side-chain dendrons. In the resulting structure, the polyamine main chain forms a channel in the inner part of the columns, while the hydrophobic side-chain dendrons lie in the outer part. The presence of the polar linkages in the inner channel favours the interaction with proton and other cations, in the same way as crown ethers would do. [18] For this reason, the inner polyamine main chain could work as an ion channel, while the hydrophobic side-chain dendrons lie on the outer part. However, the resulting copolyamines evidenced a strong tendency to crystallise.

In this work, to suppress the crystallisation process of the obtained copolymers and give more stability to the LC mesophases, we successfully modified PAZE using different amounts of both TAP and benzoyl chloride units. The presence of the TAP group induces self-assembling into a columnar structure, due to an exo-recognition of the side-chain dendrons, while the benzoyl group is expected to inhibit polymer crystallinity.

Finally, we prepared oriented and stable membranes based on selected copolymers, having two different modification degrees. Membrane orientation was achieved by means of a simple and reproducible thermal treatment on fluorinated ethylene propylene (FEP) sheet support.

2.2. Experimental

2.2.1. Materials

1-(2-hydroxyethyl)aziridine (95%) and benzoyl chloride (99%) were supplied by Sigma Aldrich. 4-dimethylaminopyridine (DMAP, ≥98.0%) and

N,N'-dicyclohexylcarbodiimide (DCC, ≥99.0%) were supplied by Fluka. Pyridine (99.99%) was supplied by Fisher Scientific and *N*-methyl-2-pyrrolidone (NMP, 99%) was supplied by Scharlab. All the solvents were purchased from Scharlab. Benzoyl chloride, DMAP and DCC were used as received. NMP and pyridine were purified prior to use. NMP was first dried by removing water as benzene azeotrope (Dean-Stark apparatus) and then fractionally distilled, collecting the desired fraction (78-79˚C/12 mmHg) over Linde type 4 Å molecular sieves. Pyridine was first predried over KOH pellets and then fractionally distilled from sodium hydride over Linde type 5 Å molecular sieves. [19] Linde type 4 Å and 5 Å molecular sieves were previously activated by heating them in an oven at 220˚C for 48 h, and then left to cool and kept under argon atmosphere in a well-dried flask.

3,4,5-tris[4-(n-dodecan-1-yloxy)benzyloxy]benzoic acid (TAP) was synthesised as previously reported. [16] Yield: 93%.

Synthesis of the poly[2-(aziridin-1-yl)ethanol] (PAZE)

The synthesis of the PAZE polymer was reported in our previous study. [20] The polymer used for modification reactions was obtained with 1 mol% boron trifluoride ethylamine ($BF_3 \cdot EtNH_2$) in the absence of solvent at 45˚C: in this case, a polymerization degree of about 44 monomeric units was found.

Chemical modification of PAZE using benzoyl chloride (Synthesis of copolymers PA-Bn)

In a round-bottomed flask 1.74 g (20.0 mmol) of PAZE was dissolved in 10 mL of dry NMP by stirring for 30 min at 0˚C and then the stoichiometric amount of dry pyridine to benzoyl chloride and 0.122 g (1.00 mmol) of DMAP were added giving a pale green solution. After additional 15 min, the required

amount of benzoyl chloride was added dropwise and the solution colour changed to a bright yellow. The mixture was magnetically stirred under argon atmosphere at room temperature (**Scheme 2.1**). After 3 days the reaction mixture was precipitated in THF according to Saucă et al. [21] The precipitated product was dissolved in methanol and reprecipitated in THF twice. Finally, the modified polymer was collected and dried at 40˚C *in vacuo* for 48 hours.

Chemical modification of PAZE-Bn with TAP

In a round-bottomed flask 0.751 g (1.66 mmol) of PAZE-Bn and the stoichiometric amount of DMAP to TAP were dissolved in 10 mL of NMP (or in $CHCl_3$ in case of PA1.1) by stirring for 30 min at 0˚C. Subsequently, the stoichiometric amount of DCC to TAP was added. After additional 15 min, the necessary amount of TAP dissolved in 6 mL of THF was added dropwise and the mixture was magnetically stirred for 10 days at room temperature according to Šakalytė et al. (**Scheme 2.2**). [16] The reaction mixture was filtered in order to eliminate undesirable *N,N'*-dicyclohexylurea and precipitated into cold ethanol. The precipitated product was dissolved in chloroform and precipitated twice in methanol or cold ethanol, depending on the modification degree. Finally, the modified polymer was collected and dried at 40˚C *in vacuo* for 48 hours.

Membranes preparation

Membranes were prepared by immersion precipitation process, in which a homogeneous polymer solution in THF (30% w/w) was cast on a FEP (fluorinated ethylene propylene) sheet support and immersed in a bath of Milli-Q water. The solvent diffused into the precipitation bath, while the non-solvent (water) diffused into the cast film. After a time, in which the solvent

and the non-solvent were exchanged, the polymer solution (wet film) became thermodynamically unstable and demixing took place. Finally, a solid polymer membrane was formed with an asymmetric structure. Afterward, the membrane was dried overnight at room temperature and subsequently used for baking process. The polymer membrane along with FEP sheet was mounted on a hot stage (Linkam TP92) and it was heated above the clearing temperature; then it was allowed to cool slowly (0.5˚C/min) to room temperature, including an isothermal step at temperature characteristic for each polymer. The same thermal procedure was repeated on a bigger scale using a Hewlett Packard 5890 Series II Gas Chromatograph oven. After the baking process, the membrane was kept at room temperature for approximately 1 h and then it was separated from the FEP sheet and obtained as an intact, uniform membrane with thickness between 120-330 μm. The thickness of the membranes was measured using a micrometer with a sensitivity of 2 μm. The measurements were carried out at various points, and the membranes were found to have constant thickness.

2.2.2. Characterisation and measurements

Nuclear magnetic resonance (NMR) spectroscopy

^{1}H NMR and ^{13}C NMR spectra were recorded at 400 and 100.4 MHz, respectively, on a Varian Gemini 400 spectrometer with proton noise decoupling for ^{13}C NMR. The chemical shifts were given in parts per million from TMS (Tetramethylsilane) in ^{1}H NMR spectra, while the central peak of the solvent was taken as the reference in the case of ^{13}C NMR spectra. The ^{13}C NMR spectra of the polymers were recorded at 30˚C, with a flip angle of 45˚, and the number of transients ranged from 20,000 to 40,000 with 10-20% (w/v) sample solutions in deuterated chloroform ($CDCl_3$) or deuterated dimethyl sulfoxide (DMSO-d_6). A pulse delay time of 5 s for the ^{1}H NMR spectrum was used.

Quantitative ^{13}C NMR spectra were performed using deuterated chloroform ($CHCl_3$) or deuterated dimethyl sulfoxide (DMSO-d_6) at 30˚C with a pulse delay time of 5 s. Delay time was selected on the basis of the relaxation times determined for the monomer 1-(2-hydroxyethyl)aziridine.

Fourier-transformed infrared spectroscopy (FT-IR)

Fourier-transformed infrared spectra were recorded on an FTIR-ATR 680 PLUS spectrophotometer from JASCO with a resolution of 4 cm^{-1} in the absorbance mode. This device is equipped with an attenuated total reflection accessory (ATR) with thermal control and a diamond crystal (Golden Gate heated single reflection diamond ATR from Specac-Teknokroma). The spectra were recorded at room temperature and at 150˚C for pure compounds.

Differential scanning calorimetry (DSC)

Calorimetric studies were performed in aluminium standard 40 µL crucibles without pin (ME-26763) with a Mettler DSC822e thermal analyser at the heating rate of 10˚C/min using about 5 mg of sample, nitrogen as a purge gas (100 mL/min) and liquid nitrogen for the cooling system. The equipment was previously calibrated with indium (156.6˚C) and zinc (418.6˚C) pearls.

Polarised optical microscopy (POM)

Clearing temperatures and LC mesophases were investigated by polarised optical microscopy (POM); textures of the samples were observed

with an Axiolab Zeiss optical microscope equipped with a Linkam TP92 hot stage.

Thermogravimetric analysis (TGA)

Thermal stability studies were carried out in ALU OXIDE crucibles of 70 µL (ME-24123) with a Mettler TGA/SDTA851e/LF/1100 device at temperatures ranging from 30 to 600˚C with a heating rate of 10˚C/min using around 10 mg of sample in a nitrogen atmosphere (100 mL/min). The equipment was previously calibrated with indium (156.6˚C) and aluminium (660.3˚C) pearls.

X-ray diffraction (XRD)

For X-ray experiments, two different diffractometers were used depending on the 2θ range investigated:

For low 2θ range, XRD measurements were performed with a Bruker-AXS D8-Discover diffractometer equipped with parallel incident beam (Göbel mirror), vertical θ-θ goniometer, XYZ motorized stage and with a GADDS (General Area Detector Diffraction System). Samples were placed directly on to a low background Si(510) sample holder for reflection analysis. An X-ray collimator system close-to-the-sample allows to analyse areas of 500 µm. The X-ray diffractometer was operated at 40 kV and 40 mA to generate $Cu_{K\alpha}$ radiation. The GADDS detector was a HI-STAR (multiwire proportional counter of 30x30 cm with a 1024x1024 pixel) placed at 30 cm from the sample. The X-ray beam hit the sample at 0.5˚ of incidence. The collected frame (2D XRD pattern) covers a 2θ range from 0.9 up to 9.2˚. The diffracted X-ray beam travels through a He beam path (SAXS attachment) to reduce the air scattering at low angles. The direct X-ray beam is stopped by a beam stop placed directly on the detector face. The exposition time was of 300 s

per frame. The resulting frames were both gamma integrated to obtain a 2θ diffractogram and 2θ integrated to obtain an azimuthal intensity plot. In the case of membranes, XRD experiments were performed on both sides and no differences could be detected.

For medium 2θ range, XRD measurements were performed with a Siemens D5000 diffractometer (Bragg-Brentano parafocusing geometry and vertical θ-θ goniometer) fitted with a curved graphite diffracted-beam monochromator, incident and diffracted-beam Soller slits, a 0.06˚ receiving slit and scintillation counter as a detector. Samples were placed directly on to a low background Si(510) sample holder for reflection analysis. The X-ray diffractometer was operated at 40 kV and 30 mA to generate $Cu_{K\alpha}$ radiation. The angular 2θ diffraction range was between 1 and 40˚. The data were collected with an angular step of 0.03˚ at 6 s per step.

Scanning electron microscopy (SEM)

SEM analysis was performed using a FEI Quanta 200 FEG (Eindhoven, The Netherlands) in high vacuum mode, using a secondary electron detector and an accelerating voltage ranging between 15 and 20 kV. The samples were fractured by impact after cooling them with liquid nitrogen. In the resulting specimens a brittle fracture was obtained. Before the analysis, samples were coated with a gold-palladium layer (about 15 nm thick) by means of an Emitech K575X sputter coater.

2.3. Results and discussion

In a previous paper our group reported the chemical modification of PAZE with a dendritic group in order to induce the formation of columnar mesophases and to get a material which could be used in the preparation of proton transport membranes. [16] However, the obtained LC side-chain

polyamines evidenced a strong tendency to crystallise, to the detriment of columnar phase stability and the mechanical properties of final membranes. To explain the crystallisation process, considering the low molecular weight of the starting polymer, the regularity of the structure increases on increasing the modification degree with TAP; in the same way, the presence of free hydroxyl groups can contribute to the crystallinity through hydrogen bonds formation. In order to overcome this drawback, another side group could be grafted in addition to TAP to suppress some of the free hydroxyl groups of PAZE: thus, some irregularities in the structure are introduced. The chosen group was a benzoyl because it is a small group that should not affect the self-assembling process of the resulting polymer. The first way that we chose to introduce the benzoyl units was by the reaction with benzoic acid. Thus, the reaction of PAZE polymer with both dendritic group and benzoic acid was tested in one pot using the same conditions as in previous studies performed with TAP only. [16] However, this attempt was unsuccessful, probably due to the poor solubility of benzoic acid in chloroform. Therefore, we tackled the reaction in two steps, the former by nucleophilic substitution with benzoyl chloride and the second by Steglich esterification with TAP, respectively.

2.3.1. Chemical modification of PAZE using benzoyl chloride (Synthesis of PAZE-Bn copolymers)

Scheme 2.1 shows the first step of the chosen pathway to modify the PAZE polymer. Chemical modification conditions, the resulting degrees of modification and product yields are reported in **Table 2.1**.

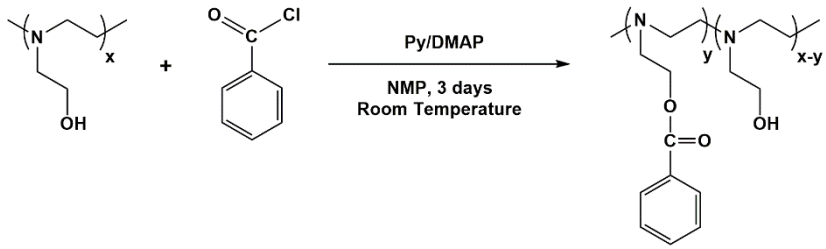

Scheme 2.1. Chemical modification of PAZE with benzoyl chloride.

Table 2.1. Chemical modification conditions, modification degrees, resulting yields and thermal characterization of PAZE-Bn copolymers.

Polymer	T (˚C)	Polymer/ COCl molar ratio	Modification degree (%) [a]	Yield (%) [b]	T_g (˚C)	Onset TGA curve (5% mass loss) (˚C)
PAZE	RT [c]	-	0	75	-35	217
PAZE-B1	RT	1:0.1	9	54	-16	185
PAZE-B2	RT	1:0.20	19	48	-1	171
PAZE-B3	RT	1:0.25	25	56	4	173
PAZE-B4	RT	1:0.35	33	73	20	222
PAZE-B5	RT	1:0.5	48	74	29	220
PAZE-B6	RT	1:0.75	75	50	43	228

[a] Modification degree determined by using ^{13}C NMR.
[b] Calculated from the degree of modification.
[c] RT = 25 ± 5˚C.

The structure of the copolymers was characterized by NMR spectroscopy. As we can see in **Table 2.1**, benzoyl moieties always are grafted to PAZE quantitatively. **Table 2.2** reports ^1H NMR spectrum data in DMSO-d_6 of modified PAZE-B5 as an example.

Table 2.2. NMR data and structure of the PAZE-B5 copolymer in DMSO-d_6.

^{1}H-NMR		^{13}C-NMR	
Signal (ppm)	**Assignment**	**Signal (ppm)**	**Assignment**
b, b'	3.2-3.4	**a, a'**	47.9-48.3; 56.0
c'	3.5	**b, b'**	54.8
a, a'	3.6-3.9	**c'**	58.5
c	4.5	**c**	61.3
d'	5.3	**I-III**	128.1-129.4
f, g	7.4-7.6	**IV**	133.1
e	8.0	**COO**	165.5

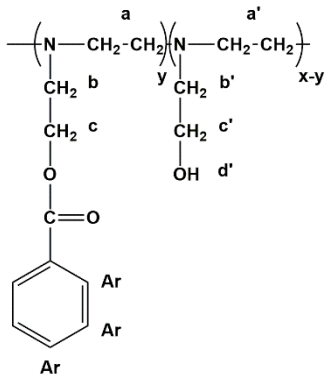

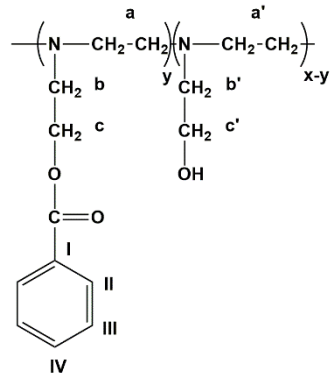

All ^{1}H NMR spectra are characterized by broad signals in two regions. The aromatic region shows 4 partially overlapped signals at 8.0, 7.6, 7.5 and 7.4 ppm. Considering the relative integration, the signal at 8.0 ppm was assigned to the protons of the benzoyl group plus the benzyl aromatic protons *ortho* to the carbonyl group. The signals between 7.6 and 7.4 ppm (2H + 1H) correspond to the benzyl aromatic protons *meta* and *para* to the carbonyl group, respectively. The protons of the main chain and the protons assigned to the signals *b*, *b'* and *c'* appear overlapped between 3 and 4 ppm. The signal

at 4.5 ppm corresponds to the methylenic protons *c* in the modified unit and a broad signal at 5.3 ppm corresponds to the –OH group.

Table 2.2 shows the ^{13}C NMR data of the polyamine PAZE-B5 with the corresponding assignments. The aromatic and carbonyl carbons of the moiety introduced appear between 165.5 and 128.1 ppm. The carbons of the main chain are observed between 47.9-48.3 and 56.0 ppm, while the signals assigned as *b, b'* appear at 54.8 ppm. The methylenic carbons *c'* and *c* of the unmodified and modified units appear resolved at 58.5 and 61.3 ppm, respectively.

The structures of copolymers were also characterised and confirmed by FT-IR technique. In the FT-IR spectrum, we could observe the decrease of the –OH vibration band around 3290 cm^{-1}, coming from PAZE. Furthermore, the ester carbonyl group characteristic band around 1715 cm^{-1} (C=O) appears, which confirms that polymer chemical modification occurred.

The results of thermal characterisations shown in **Table 2.1** indicate that the T_g of the resulting copolymers increased on increasing the modification degree as expected on the basis of the higher amount of side bulky aromatic groups contained: for the same reason, thermal stability was generally improved as shown by higher values of temperature of 5 wt% mass loss.

2.3.2. Chemical modification of PAZE-Bn with TAP

The second step of the modification of PAZE polymer consists of the modification of the PAZE-Bn copolymers with TAP by Steglich esterification (**Scheme 2.2**).

The use of *N,N'*-dicyclohexylcarbodiimide (DCC) as a promoter represents one of the most versatile esterification methods. [22] Although stoichiometric dosage of this reagent or even a small excess is necessary,

this procedure demonstrates its various advantages over other esterification reactions. The reaction usually proceeds at room temperature, and the conditions are mild. Unfortunately, this procedure has some drawbacks: yields are not always high, and undesirable *N*-acylureas are occasionally formed. These drawbacks can be overcome by addition of a catalytic amount of *p*-aminopyridines. [23, 24]

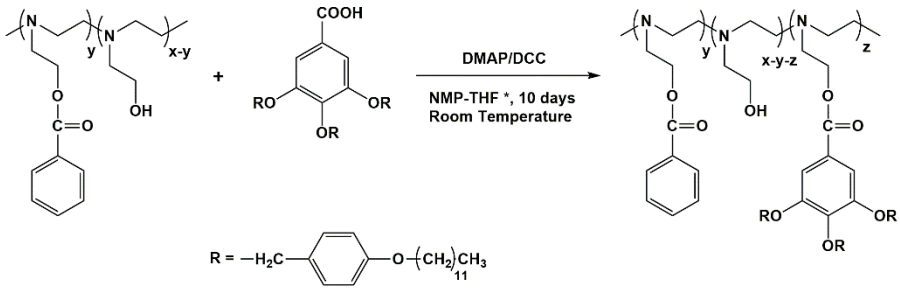

*** $CHCl_3$ as a solvent in the case of PA1.1 copolymer.**

Scheme 2.2. Modification reaction of copolymers PAZE-Bn with 3,4,5-tris[4-(n-dodecan-1-yloxy)benzyloxy]benzoic acid (TAP) using esterification method with DMAP/DCC.

In the case of the previously synthesized PAZE-Bn copolymers, we studied this chemical modification under different reaction conditions, which are given in **Table 2.3** with their corresponding degree of modification and product yields.

In all cases this esterification was carried out at room temperature, since the side product *N*-acylurea formation is less likely at lower temperatures; in other words, high temperatures favour the formation of side products and are therefore expected to reduce modification degrees correspondingly. In these conditions, the FT-IR spectrum of the resulting

copolymers showed the decrease of the –OH vibration band around 3290 cm^{-1}, attributed to the remaining hydroxyl groups.

Table 2.3. Chemical modification conditions, modification degrees and resulting yields of PA1-PA6 copolymers.

Copolymer	Solvent	PAZE-Bn/ COOH molar ratio	Benzoyl modification degree (%) [a]	TAP modification degree (%) [a]	Total modification degree (%) [a]	Yield (%) [b]
PA1	THF/NMP	1:1	9	29	38	56
PA1.1	$CHCl_3$	1:1	9	85	94	28
PA2	THF/NMP	1:1	19	55	74	40
PA3	THF/NMP	1:1	25	75	100	39
PA3.1	THF/NMP	1:1	25	62	87	34
PA3.2	THF/NMP	1:1	25	55	80	71
PA4	THF/NMP	1:1	33	43	76	79
PA5	THF/NMP	1:1	48	21	69	27
PA5.1	THF/NMP	1:1.2	48	31	79	51
PA6	THF/NMP	1:1	75	-	75	-

[a] Modification degree determined by using ^{13}C NMR.
[b] Calculated from the degree of modification.

As we can see in **Table 2.3**, when we increase the modification degree with benzoyl chloride, the expected modification with the TAP dendron decreases probably due to conformational inaccessibility of the remaining free hydroxyl groups of the copolymers PAZE-Bn. As a matter of fact, of the entire family of copolyamines, only in one case, i.e. polymer PA3, we succeeded in quantitatively modifying free hydroxyl groups of the starting PAZE polymer. Furthermore, in the case of samples PA1.1 and PA3.1 a total modification degree around 90% was reached. On the opposite side, when the degree of modification with benzoyl units was 75%, the reaction with TAP groups did not occur.

Surprisingly, we found an exception that breaks the observed tendency. PAZE-B1 had the highest amount of free hydroxyl groups before carrying the Steglich esterification. When the second step was performed, the grafted amount of TAP into the copolymer structure was smaller than expected (only 29% of the 91% possible amount of the dendron was introduced). To enhance this reaction, the behaviour of PAZE-B1 copolymer was deepened, especially in terms of solubility. It was observed that this copolymer, which was modified only with 9% of benzoyl, showed a similar behaviour to the starting PAZE polymer. For this reason, as we did in previous studies when we modified the PAZE polymer with only the dendron, [16] we replaced the mixture of solvents (*N*-methyl-2-pyrrolidone and THF) by chloroform and the chemical modification with TAP was improved considerably from 29 to 85%.

For the sample PA5, the modification degree with TAP was not quantitative. To improve the modification of this step, we change the molar ratio between the free hydroxyl groups of the polymer and the acid groups of the dendron. Nevertheless, as we could observe in the case of copolymer PA5.1, an excess of 20% mol of the mesogen only increases the TAP modification from 21 to 31%, still far away from the maximum 50% expected.

The structure of the copolymers was characterized by NMR spectroscopy. **Table 2.4** reports the ^{1}H NMR spectrum data in $CDCl_3$ of modified PA4 as an example (**Figure S2.1**).

All ^{1}H NMR spectra are characterized by broad signals in three regions. The aromatic region shows 4 partially overlapped signals at 7.9, 7.2, 6.7 and 6.6 ppm. Considering the relative areas, the signal at 7.9 ppm can be assigned to the protons of the benzoyl unit in *ortho* to the carbonyl group. In comparison with the spectrum of 3,4,5-tris[4-(n-dodecan-1-yloxy)benzyloxy]benzoic acid, the signals between 7.0 and 7.4 ppm can be assigned to the protons of TAP group in *ortho* to the –CH_2OPh–. Also the two protons in *ortho* position to the carbonyl group of the inner aromatic ring of TAP can be found between 7.0 and 7.4 ppm. The rest of the signals of the protons of the benzoyl units added previously appear overlapped with the signals between 7.0 and 7.4 ppm. The signals at 6.7 and 6.6 ppm (4H + 2H) correspond to the benzyl aromatic protons *meta* to the –CH_2OPh– of the lateral and central alkyloxybenzyloxy substituents of TAP, respectively. The characteristic signals of the protons which correspond to the long alkyl chains in TAP can be observed in the upfield region at 1.7, 1.3, 1.1 and 0.8 ppm. The most interesting region lies between 5 and 2 ppm in which 4 signals can be observed. First of all, a signal at 4.7 ppm can be assigned to the benzylic methylenes of the dodecyloxybenzyloxy substituent. The signal at 4.3 ppm corresponds to the methylenic protons c, c'' in the modified monomeric units with benzoyl and TAP, whereas the signal at 3.8 ppm corresponds to the methylene attached to the oxygen in the long alkyl chains. Hidden behind the last peak and centred at 3.6 ppm, the signal of the methylenic protons c' of the unmodified units appears. Finally, a broad signal centred at 2.7 ppm is observed, which corresponds to the carbons a, a', a'', b, b', b'' of the modified and unmodified units.

Table 2.4. NMR data and structure of the PA4 copolymer in $CDCl_3$.

^{1}H NMR		^{13}C NMR	
Signal (ppm)	**Assignment**	**Signal (ppm)**	**Assignment**
12	0-8	**12**	14.0
3-11	1.2-1.4	**11**	22.6
2	1.7	**3**	26.0
a, a', a'', b, b', b''	2.5-2.8	**2, 4-9**	29.1-29.6
c'	3.6	**10**	31.8
1	3.8	**a, a', a'', b, b', b''**	52.0-57.0
c, c''	4.3	**c'**	59.3
e''	4.8	**c, c''**	62.3
Ar	6.5-7.9	**1**	67.8
		e'' lateral	70.8
		e'' central	74.6
		II'	108.8
		VII'	114.0
		I'	124.8
		I-IV, V', VI'	128.3-133.0
		IV'	142.4
		III'	152.5
		VIII'	158.6
		COO	165.9-166.2

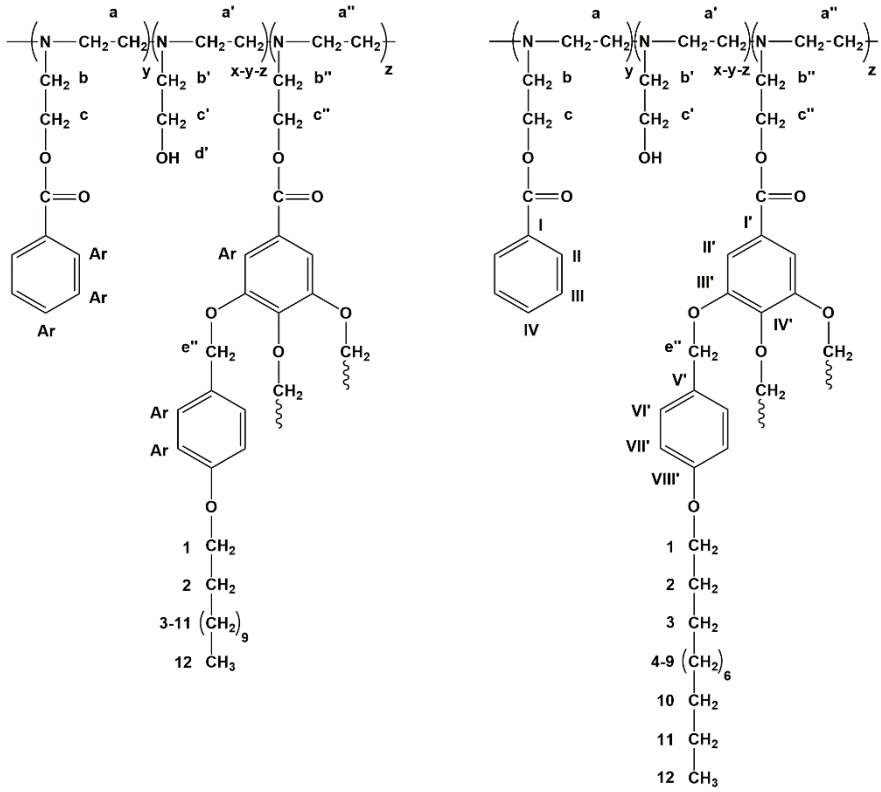

Table 2.4 shows the ^{13}C NMR data of the polyamine PA4 with the corresponding assignments (**Figure S2.2**). The carbonyl carbons of benzoyl group and TAP introduced appear between 165.9 and 166.2 ppm. The aromatic carbons appear between 108.8 and 158.6 ppm, whereas carbons 2-12 of the long alkyl chains appear in the expected region at 14.0-31.8 ppm. The carbon assigned as 1 of the alkyl chains appears at 67.8 ppm. The chemical shifts of the benzylic methylenes depend on their relative position in the aromatic ring: the ones in position 3 and 5 appear at 70.8 ppm, whereas the one in position 4 appears downfield at 74.6 ppm. The carbons of the main chain appear in the range within 52.0 and 57.0 ppm. By last, the methylenic units assigned as c' of the non-modified monomeric units appear resolved at 59.3 ppm and the methylenic carbons c, c'' of the modified units appear upfield at 62.3 ppm.

2.3.3. Mesomorphic characterisation of modified LC polyamines

The mesomorphic characterization was performed on the basis of differential scanning calorimetry (DSC), optical microscopy between crossed polars (POM) and X-ray diffraction experiments (XRD). **Table 2.5** shows calorimetric data of the whole PAn copolymers while **Table 2.6** presents the obtained XRD results of this family of copolyamines.

In all cases, the DSC analysis reveals the presence of two endotherms. For the samples PA1 and PA2 to PA5.1, the first endotherm could be related to the melting and the second one to the clearing point. On increasing the modification degree with the mesogenic group, the clearing points and enthalpies of the copolymers also increased, similarly to what was reported for columnar copolyethers and copolyamines modified only with TAP. [13, 16] Besides, the clearing enthalpy values were of a similar order like in the case of the previously mentioned copolyethers. In addition, another tendency regarding enthalpy and benzoyl content can be observed: on increasing the modification degree with benzoyl units, the polymers exhibit a decrease of the clearing enthalpy values. An exception could be also found in the less modified copolymer (PA1), which demonstrates different behaviour as a consequence of low modification degree, as expected.

In the obtained family of copolyamines, except for PA1.1, benzoyl small side group was introduced in order to enhance the stability of the LC mesophase with respect to the previously reported columnar copolyamines modified only with TAP. [16] Considering PA2 to PA5.1 copolymers, as we can observe in **Table 2.5**, the highest clearing temperatures were found when the introduced amount of benzoyl is 25% and also the dendron content is higher than 62%. (PA3 and PA3.1 copolymers). For these two copolymers the amount of free hydroxyl groups, which unfavourably affects the LC mesophase, is the smallest found in the whole group of copolymers (except for PA1.1). On the other hand, a decrease in the TAP content leads to a decrease of the clearing temperature as we expected. Related to the benzoyl,

a higher amount than 25% of this side group induces a diminution of the clearing temperature.

On the contrary, the sample PA1.1 has a similar behaviour to the previously reported copolyamines modified only with TAP. [16] For this sample, two endotherms appear overlapped in the second calorimetric analysis: the first one showed a sharp and big endotherm at 46˚C and a second one broader and smaller with maximum at 61˚C. This suggested that this sample, due to its quite regular structure and relatively low molecular weight, tended to crystallise partially. To confirm the hypothesis and to have better visualisation of both endotherms, prior to DSC analysis the sample was annealed for 2 hours at temperature slightly below the first peak maximum (39-42˚C) and cooled to -100˚C. Due to the pre-treatment, two sharp endotherms were obtained, one at 48˚C and another at 62˚C. The first transition could be related to the melting of crystalline part, whereas the second one can be attributed to the clearing of a monotropic LC mesophase that grew during the annealing.

Table 2.5. Calorimetric features of modified copolyamines.

Copolymer	Total modification degree (%)	T_m (˚C) [a]	T_c (˚C) [a]	Onset TGA curve (5% mass loss) (˚C)	ΔH_c (kJ/mol) [b]
PA1	38	-14	92-96	272	1.1
PA1.1	94	62	48 [c]	291	-
PA2	74	-7	82-86	273	1.6
PA3	100	-13	100-104	285	1.7
PA3.1	87	-14	102-105	276	1.5
PA3.2	80	-10	93-97	278	1.4
PA4	76	-14	81-86	266	0.9
PA5	69	-17	88-91	235	0.5
PA5.1	79	-19	86-89	261	0.8

[a] Determined by DSC second heating scan and POM.
[b] Expressed per mol of TAP group.
[c] Monotropic liquid crystal.

Liquid-crystalline mesophase of PA1.1 was observed under POM microscope between crossed polars and exemplary micrographs are shown in **Figure 2.1**. The liquid-crystalline texture was obtained after performing the annealing at 40˚C, evident as a typical dendritic aggregates growth. After subsequent cooling the same sample to 30˚C, the appearance of crystals, combined with the remaining small domains of the LC mesophase was noticed, thus confirming the monotropic nature of the columnar mesophase.

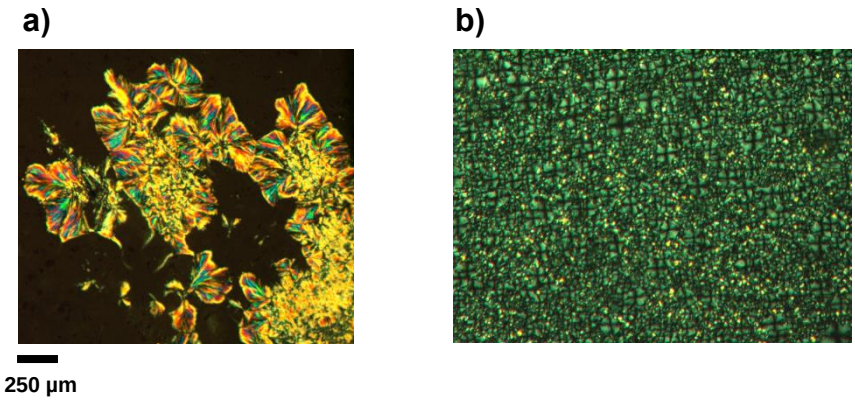

Figure 2.1. Optical micrographics between crossed polars on cooling from the isotropic phase of PA1.1 at: a) 40˚C; b) 30˚C.

The liquid-crystalline textures of other LC polyamines were observed by POM after annealing samples between 2 and 16 hours at a temperature slightly lower than their respective clearing temperatures, in order to favour the growth of the liquid-crystalline domains.

POM images in **Figure 2.2** revealed a broken fan-shaped texture in case of PA3 and PA3.1 sample, whose modification degree of benzoyl is 25% and the degree of modification with TAP is 75 and 61% respectively. Differently, PA4 exhibited a texture which resembled smectic bâtonnets.

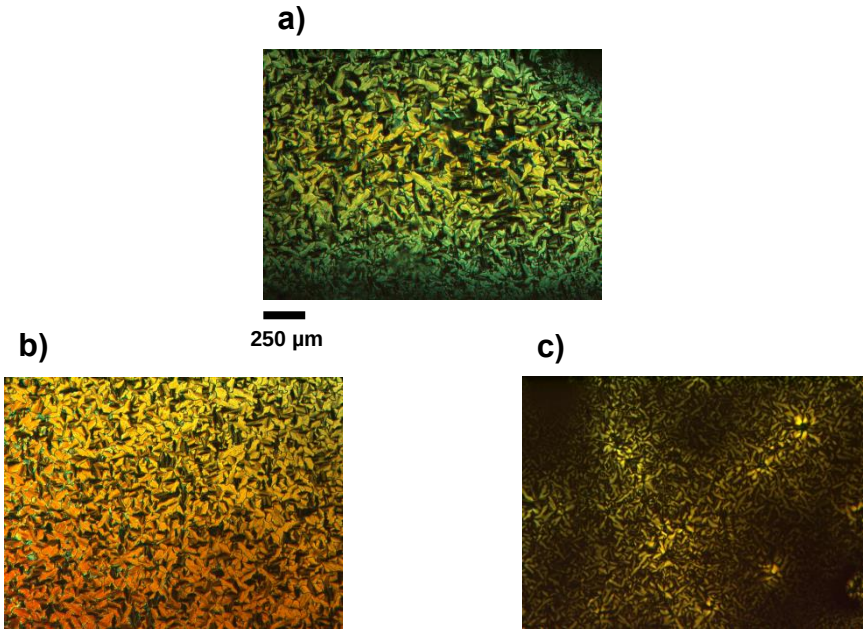

Figure 2.2. Optical micrographics between crossed polars on cooling from the isotropic phase of: (sample, test temperature) a) PA3, 80˚C; b) PA3.1, 80˚C; c) PA4, 80˚C.

In order to confirm assignation of their mesophases, the synthesized LC polyamines were studied by XRD. The analysis was performed at different temperatures in order to confirm calorimetric features and to identify the copolymers mesophase.

For all copolymers except PA1.1, the XRD analysis below T_c showed three quite sharp reflections located in ranges of 2θ angles 1.8˚ – 2.1˚, 2.9˚ – 3.6˚ and 3.1˚ – 4.2˚, corresponding to d-spacings between d = 41.9 Å – 49.6 Å, 24.3 Å – 30.6 Å and 21.3 Å – 25.0 Å, respectively; also a presence of a broad halo centred around 2θ = 19.4˚ – 20.1˚, giving d = 4.4 – 4.6 Å was identified (**Figure S2.3** and **Figure S2.4** show the XRD pattern of PA3 and PA4). This diffraction pattern, which exhibited d-spacings of the sharper reflections in the ratio 1:1/√3:1/2 and a diffuse halo at higher angles,

confirmed the presence of a hexagonal columnar mesophase (Col_h), where the first three sharp reflections correspond to the planes (100), (110) and (200), respectively, while the broad halo is related to the plane (001).

Differently, the X-ray diffraction pattern of polymer PA1.1 suggested a rectangular columnar crystalline phase (Col_r^k), as evident from the high number of sharp reflections (**Figure S2.5**). As a matter of fact, the reflections located at 2θ = 2.1˚ and 3.1˚, corresponding to d = 41.3 Å and 28.8 Å, exhibited d-spacings in the ratio 1:1/√2 and could be assigned to (100) and (110) planes, respectively. Unfortunately, due to the insufficient number of indexed signals, we could not univocally assign the spatial group for this copolymer.

Table 2.6. X-ray diffraction data of modified copolyamines at room temperature.

Copolymer	Total modification degree (%)	d_{100} (Å)	d_{110} (Å)	d_{200} (Å)	d_{001} (Å)	a (Å) [a]	Mesophase [b]
PA1	38	45.1	26.9	23.0	4.4	52.1	Col_h
PA1.1	94	41.3	28.8	-	-	41.3	Col_r^k
PA2	74	45.1	26.7	23.1	4.4	52.1	Col_h
PA3	100	41.9	24.3	21.3	4.5	48.4	Col_h
PA3.1	87	42.5	24.7	21.6	4.5	49.1	Col_h
PA3.2	80	46.5	26.9	23.5	4.5	53.7	Col_h
PA4	76	45.8	27.0	23.3	4.6	52.9	Col_h
PA5	69	43.1	25.5	-	4.5	49.8	Col_h
PA5.1	79	49.6	28.8	25.1	4.5	57.3	Col_h

[a] Dimension of the hexagonal unit cell.
[b] Col_r^k: crystalline rectangular columnar, Col_h: hexagonal columnar mesophase.

In all cases, the organisation of the copolymers into columns can indicate a possible formation of biomimetic ion channels, where the polyamine main chain arranges in the inner part of the column.

The thermal stability of the polymers was studied using TGA. As an example, TGA scans of selected samples are reported in **Figure 2.3**. The onset of thermal decomposition (determined as the temperature corresponding to 5% mass loss) ranged between 235 and 291˚C. The onset of thermal decomposition increased on increasing the copolymers modification degree with TAP, probably due to higher amount of mesogenic groups introduced in the structure. Copolymer PA1.1 behaved the best in this respect, exhibiting a mass loss onset temperature of 291˚C. Moreover, as far as char yield is concerned, the obtained copolymers have a similar behaviour to the copolymers modified with the mesogenic TAP group only. [16] In this case, the char yield at 600˚C ranged from 9 to 14%.

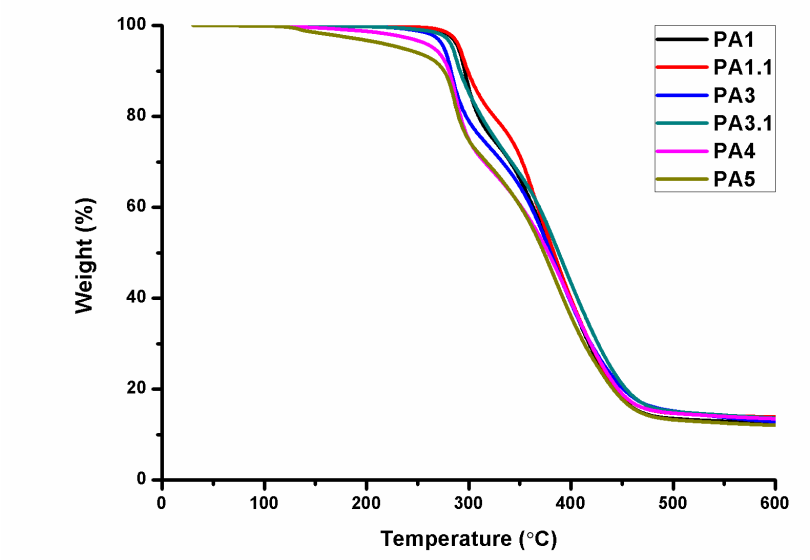

Figure 2.3. TGA thermograms of selected copolymers recorded at a heating rate of 10˚C/min.

2.3.4. Membrane preparation and characterisation

As described in the experimental part, all membranes were prepared by immersion precipitation process. In previous studies, we proved the positive influence of the thermal treatment on the improvement of the homeotropical alignment of columns formed by liquid crystal polyglycidols, polyethers and polyamines containing TAP groups as side dendrons. [15, 25, 26] In these cases, to obtain the required alignment of the columns, the membrane was heated above the clearing temperature; next, it was kept at a temperature slightly below the clearing point for a proper time and then cooled slowly to room temperature. This process is characteristic for each polymer and allows orientation of the columns in the expected direction for the observed columnar mesophases.

With the described baking process we obtained homeotropically oriented membranes. To ensure the growth of the columnar mesophase for these kind of LC copolymers, the baking process was carried out during overnight at their respective temperatures. PA3 and PA4 were selected as two representative examples because they present different modification degrees of benzoyl, TAP mesogenic groups and free hydroxyl groups in the resulting copolymer structure. As shown in **Figure 2.4**, homogeneous and mechanically stable membranes were obtained with a thickness between 120-330 µm.

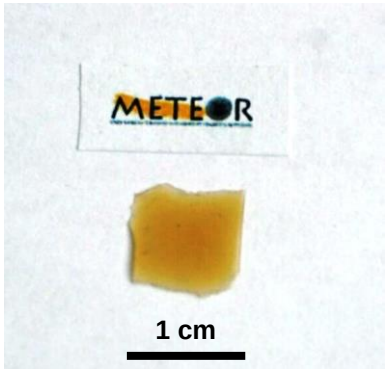

Figure 2.4. Oriented membrane of polymer PA4 obtained after the baking process.

To assess the orientation of the columns, the membranes were analysed by X-ray diffraction. As an example, **Figure 2.5** shows the XRD diffractogram of two membranes, one prepared with the copolyamine PA3 and another one using the copolyamine PA4.

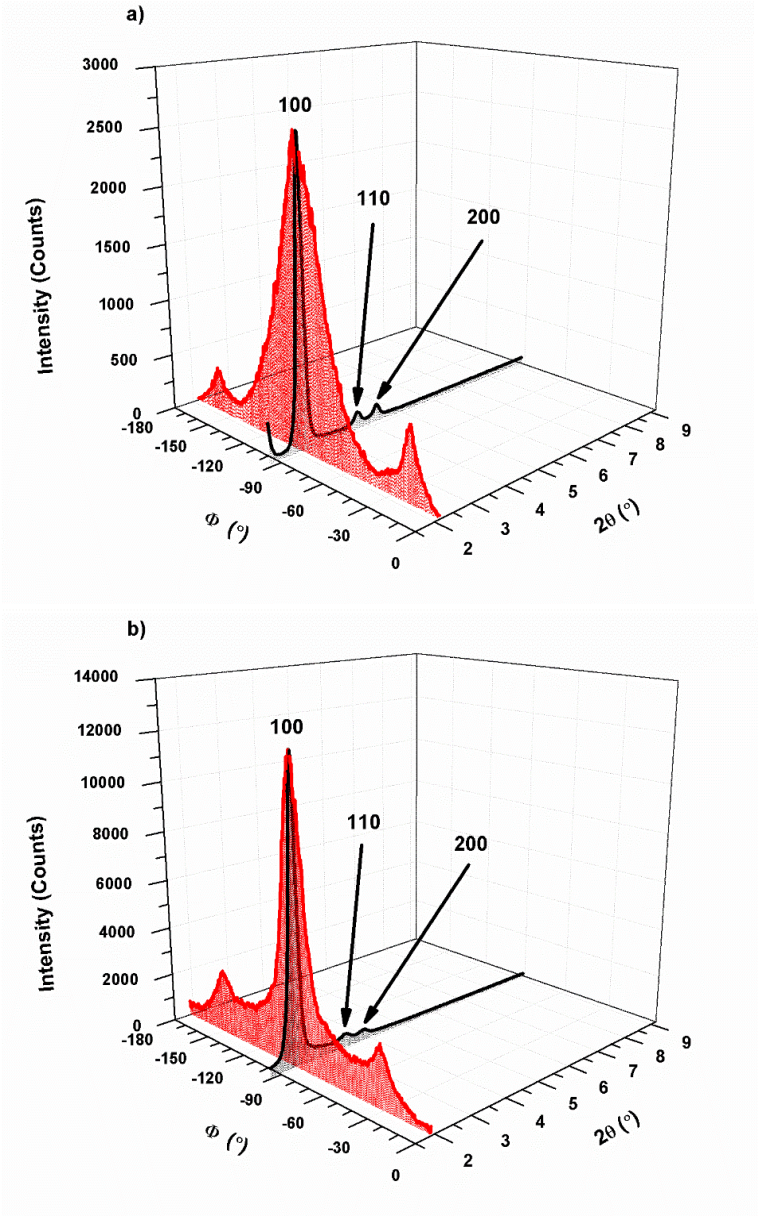

Figure 2.5. Comparison of 2-theta in the range 1.5˚ – 9.0˚ and azimuthal scan at room temperature of baked membranes obtained from different copolymers after annealing: a) PA3, at 99˚C and b) PA4 at 75˚C, respectively.

In the case of the membrane obtained with the copolymer PA3, at low 2θ angles three sharp reflections can be observed at 2.1˚, 3.7˚ and 4.3˚, corresponding to d = 41.1 Å, 23.9 Å and 20.7 Å respectively (**Figure 2.5a**). These d-spacings give the ratio 1:1/√3:1/2, which is characteristic for hexagonal columnar mesophase (*Col*$_h$), and thus confirm its presence in the tested material. Moreover, a narrowing of the signal at ϕ = 92˚ in the azimuthal scan for the reflection d_{100} demonstrates orientation of the columns in the equatorial plane with calculated full width at half maximum (FWHM) of the peak equal to 35.8˚. This confirms that in this membrane most of the columns are quite uniformly oriented perpendicularly to the membrane surface.

Similar to PA3, the XRD diffractogram of the membrane prepared with the copolyamine PA4 shows three sharp reflections corresponding to d = 45.9 Å, 26.7 Å and 23.0 Å respectively (**Figure 2.5b**). The d-spacings correspond also to the (100), (110) and (200) planes of the hexagonal columnar mesophase. Referring to the alignment of the columns, for this membrane the azimuthal scan shows a narrowing of the signal centred at ϕ =91˚ for the reflection attributed to the spacing d_{100}, which confirms that also in this membrane most of the columns are homeotropically oriented. Moreover, the full width at half maximum (FWHM) of the peak is 15.2˚.

Figure 2.6 and **Figure 2.7** present some micrographs of membranes prepared with PA3 and PA4 copolymers, respectively obtained by SEM microscopy. In **Figure 2.6a** we can observe the cross-section of an unoriented membrane of PA3 copolymer while the surface of an unoriented membrane prepared with the PA4 copolymer is appreciated in **Figure 2.7a**. In both pictures, we can observe the presence of pores in the material resulting from the fast precipitation of the copolymer during the phase inversion process. On the other hand, **Figure 2.6b** and **Figure 2.7b** show a micrograph of the same membranes after applying the thermal treatment. It is possible to observe that, after this treatment, the homogeneity of the membranes was clearly improved. Two changes were detected, which

evidenced this fact: the removal of the membrane pores and the presence of a smoother fracture surface in the case of the unoriented membranes.

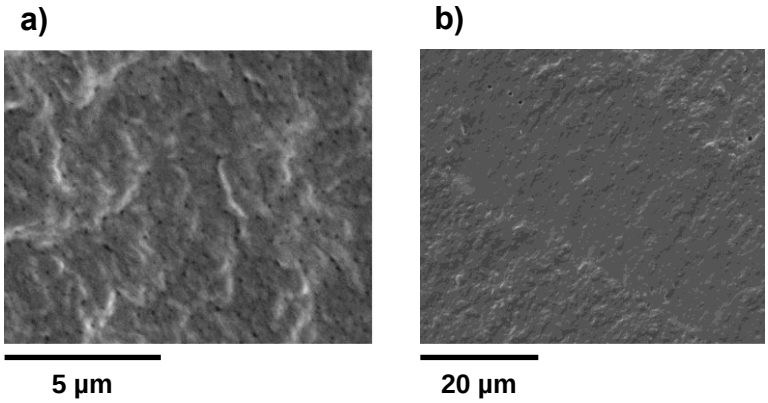

Figure 2.6. SEM micrographs showing the morphology of the cryofractured cross-section of a membrane prepared with the PA3 copolymer: a) unoriented and b) oriented membrane.

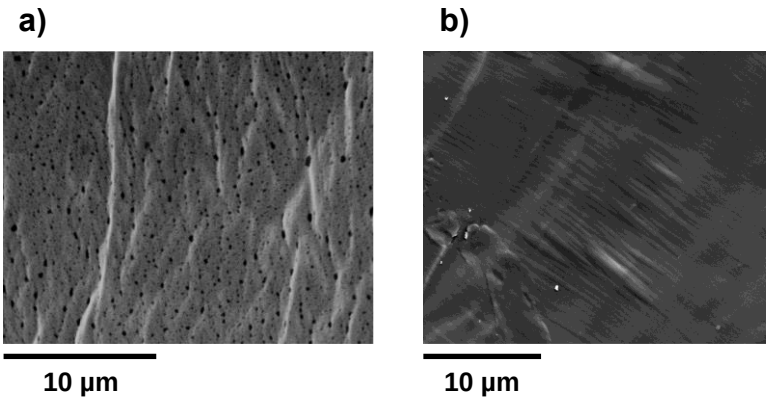

Figure 2.7. SEM micrographs showing the morphology of the cryofractured surface of a membrane prepared with the PA4 copolymer: a) unoriented and b) oriented membrane.

Thus, the introduction of a small side group to the PAZE polymer before modifying with TAP allows to obtain LC copolymers with a higher range of the LC mesophase, as predicted. Furthermore, a successful preparation of homeotropically oriented self-supported membranes based on these side-chain liquid-crystalline polymers (SCLCP) shows a great potential in terms of further applications.

2.4. Conclusions

We prepared a family of self-assembling LC polyamines by chemical modification of PAZE with different amounts of benzoyl chloride and the dendron 3,4,5-tris[4-(n-dodecan-1-yloxy)benzyloxy]benzoic acid (TAP). To achieve this goal, PAZE was first modified with benzoyl chloride by using a nucleophilic substitution and afterwards the resulting polymer was modified with the dendritic group by using carbodiimide mediated Steglich esterification. In all cases, the modification of PAZE polymer with benzoyl chloride took place quantitatively. On the other hand, the quantity of introduced TAP depends on the amount of remaining free hydroxyl groups and also of the amount of benzoyl units introduced in the first step, causing additional steric effect reducing in some cases the possibility of complete modification. In the case of modification degree with benzoyl chloride higher than 25%, the modification with TAP groups was not quantitative, probably due to conformational inaccessibility of free hydroxyl groups. Despite of this, in all cases the obtained copolymers exhibited a LC columnar mesophase. Moreover, they are not crystalline at room temperature and exhibit higher clearing temperatures (T_c), when compared to the LC polyamines obtained by modification of PAZE with TAP only, reported in previous studies.

Finally, oriented membranes based on selected LC polyamines were prepared. An orientation of the copolymer columns perpendicular to the membrane surface was accomplished using a thermal treatment and confirmed by XRD.

Furthermore, ionic transport across the oriented membranes will be the subject of extensive studies presented in the next chapter.

2.5. Acknowledgements

Financial support from CTQ2013-46825-R (Ministerio de Economía y Competitividad) is gratefully acknowledged. The authors are grateful to Dr. Cinta Bladé, Santiago Moreno and Rosa Pastor for help with the centrifugation experiments and also to Dr. Francesc Gispert for help with the XRD experiments.

2.6. Supporting information

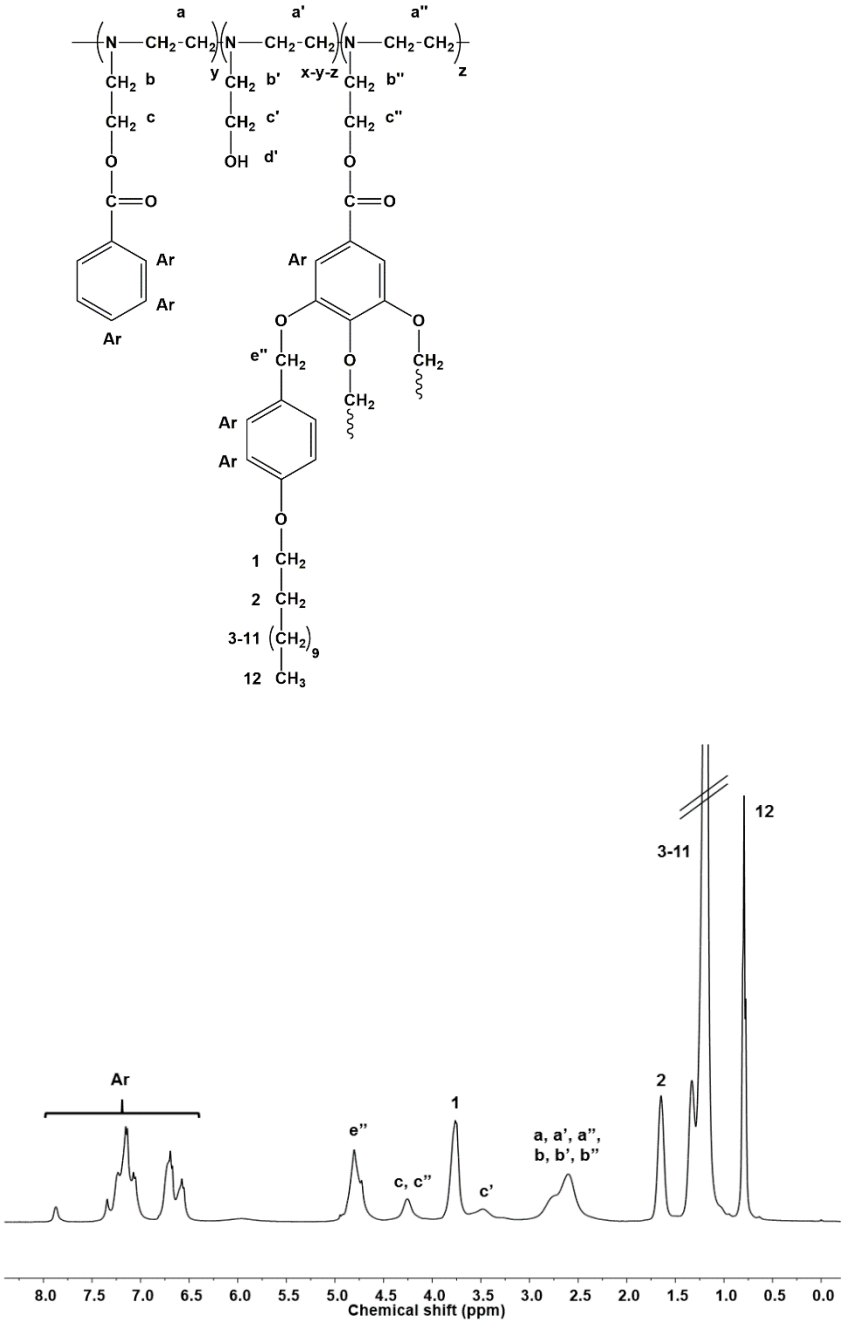

Figure S2.1. ^{1}H NMR spectrum of PA4 in $CDCl_3$.

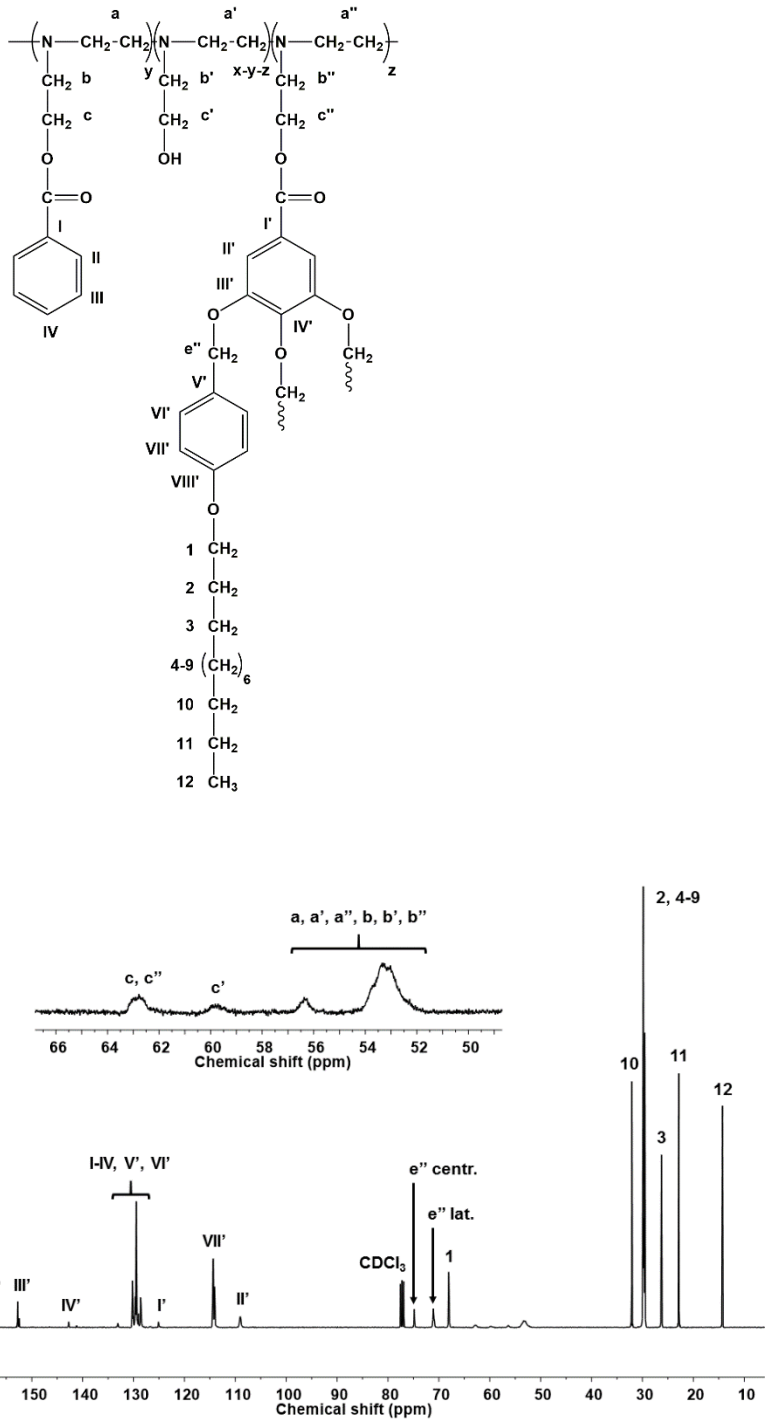

Figure S2.2. ^{13}C NMR spectrum of PA4 in $CDCl_3$.

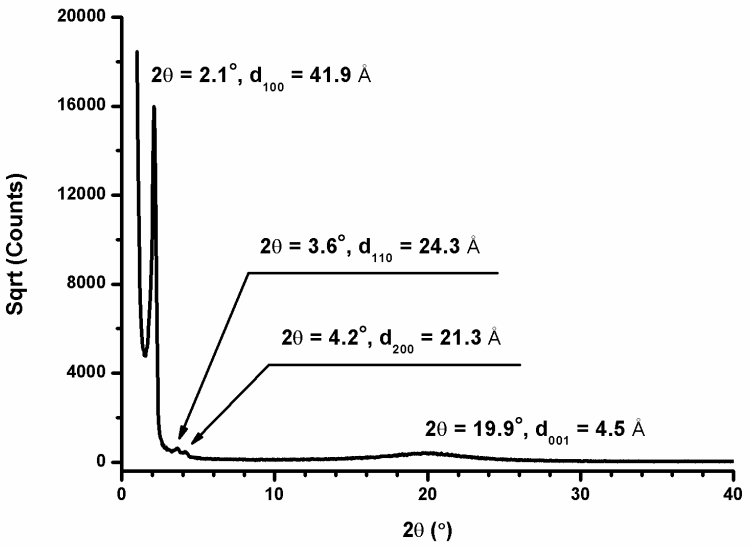

Figure S2.3. XRD pattern of PA3 at room temperature.

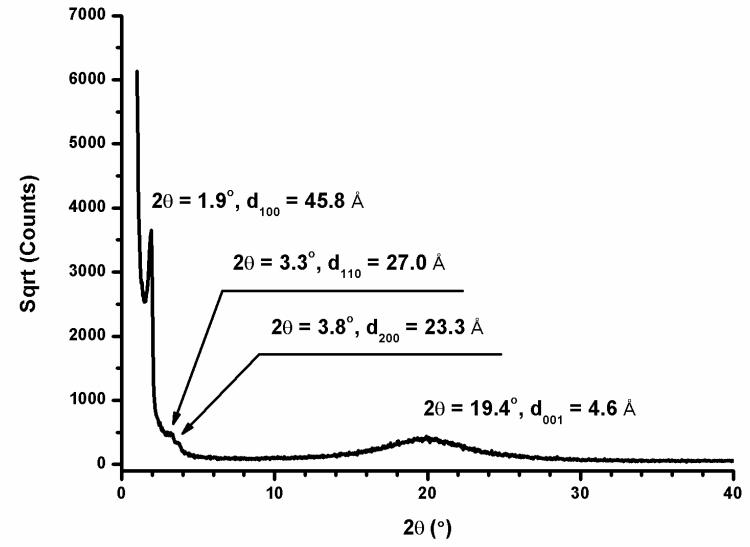

Figure S2.4. XRD pattern of PA4 at room temperature.

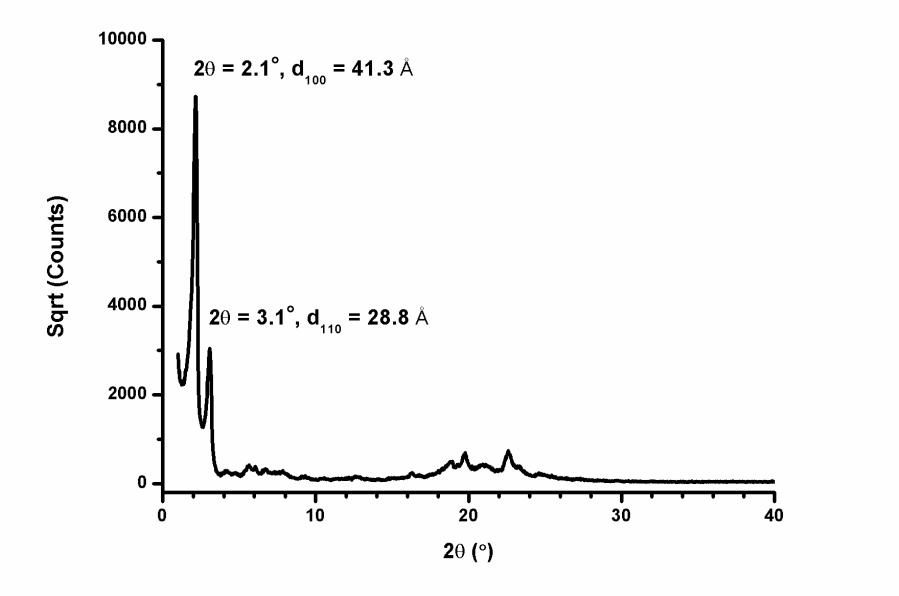

Figure S2.5. XRD pattern of PA1.1 at room temperature.

2.7. References

1. Listorti A, Durrant J, and Barber J. Nat. Mater. 2009;8(12):929-U922.

2. Armand M, Endres F, MacFarlane DR, Ohno H, and Scrosati B. Nat. Mater. 2009;8(8):621-629.

3. Pasechnik S, Chigrinov V, and DV; S. Physical Backgrounds for Practical Applications of Liquid Crystals, in Liquid Crystals: Viscous and Elastic Properties. Weinheim: Wiley-VCH Verlag GmbH & Co. KGaA, 2009. pp. 7-43.

4. Cho B-K. RSC Adv. 2014;4(1):395-405.

5. Sakuda J, Hosono E, Yoshio M, Ichikawa T, Matsumoto T, Ohno H, Zhou H, and Kato T. Adv. Funct. Mater. 2015;25(8):1206-1212.

6. Sergeyev S, Pisula W, and Geerts YH. Chem. Soc. Rev. 2007;36(12):1902-1929.

7. Funahashi M. Polym. J 2009;41(6):459-469.

8. Gin DL and Noble RD. Science 2011;332(6030):674-676.

9. Zhou M, Nemade PR, Lu X, Zeng X, Hatakeyama ES, Noble RD, and Gin DL. J. Am. Chem. Soc. 2007;129(31):9574-9575.

10. Gin DL, Gu W, Pindzola BA, and Zhou W-J. Acc. Chem. Res. 2001;34(12):973-980.

11. Ishida Y, Kai Y, Kato S-y, Misawa A, Amano S, Matsuoka Y, and Saigo K. Angew. Chem., Int. Ed. 2008;47(43):8241-8245.

12. Sun H-J, Zhang S, and Percec V. Chem. Soc. Rev. 2015;44(12):3900-3923.

13. Ronda JC, Reina JA, and Giamberini M. J. Polym. Sci., Part A: Polym. Chem. 2004;42(2):326-340.

14. Bhosale SV, Rasool MA, Reina JA, and Giamberini M. Polym. Eng. Sci. 2013;53(1):159-167.

15. Montané X, Bhosale SV, Reina JA, and Giamberini M. Polymer 2015;66:100-109.

16. Šakalytė A, Reina JA, and Giamberini M. Polymer 2013;54(19):5133-5140.

17. Tylkowski B, Castelao N, Giamberini M, Garcia-Valls R, Reina JA, and Gumí T. Mater. Sci. Eng. C 2012;32(2):105-111.

18. Dulyea LM, Fyles TM, and David Robertson G. J. Membr. Sci. 1987;34(1):87-108.

19. Perrin DD and Armarego WLF. Purification of Laboratory Chemicals, 6th ed. Oxford: Pergamon Press, 2009. pp. 412, 425-426.

20. Šakalytė A, Reina JA, Giamberini M, and Lederer A. Polym. Eng. Sci. 2014;54(3):579-591.

21. Saucă S, Giamberini M, and Reina JA. Polym. Degrad. Stab. 2013;98(1):453-463.

22. Otera J. Reaction of Alcohols with Carboxylic Acids and their Derivatives, in Esterification: Methods, Reactions, and Applications. Weinheim: Wiley-VCH GmbH & Co. KGaA, 2003. pp. 21-24.

23. Hassner A and Alexanian V. Tetrahedron Lett. 1978(46):4475-4478.

24. Ivanov VT and Mikhaleva II. Main-Chain-Modified Peptides, in Methods of Organic Chemistry (Houben - Weyl): Synthesis of Peptides and Peptidomimetics, vol. E 22 c. Stuttgart: Thieme Publishers, 2003. pp. 277-280.

25. Bogdanowicz KA, Rapsilber GA, Reina JA, and Giamberini M. Polymer 2016;92:50-57.

26. Bogdanowicz KA, Bhosale SV, Li Y, Vankelecom IFJ, Garcia-Valls R, Reina JA, and Giamberini M. J. Membr. Sci. 2016;509:10-18.

Chapter 3

Advances in the design of self-supported ion-conducting membranes- new family of columnar liquid-crystalline polyamines. Part 2: ion transport characterisation and comparison to hybrid membranes

Xavier Montané, Krzysztof Artur Bogdanowicz, Judit Prats-Reig, Gianmarco Colace, José Antonio Reina, Marta Giamberini*

*- Polymer, submitted.

3.1. Introduction

The interest in finding more sustainable methods of power generation has been increasing due to the awareness-raising about the climate change and the increasing demand for fossil fuels. Recently, artificial photosynthesis is one of the most studied systems, which is based on sunlight conversion into liquid hydrocarbons, which are further used to power the existing energy infrastructure. [1] Another green technology under development is fuel cells, which are able to transform chemical energy of a fuel into electrical energy. [2]

Proton-conducting membranes are the element which contributes to the efficiency of artificial photosynthesis and fuel cells; [3] they have different functions like: charge carrier for protons, separation of the two compartments and electronic insulator since they do not let electrons pass through the membrane. [4] The efficiency of proton-exchange membranes depends mainly on their ability of rapid and selective transfer of proton ions; therefore, the study of these materials is essential for further development of green technologies. [5, 6]

Several materials have been developed in the last few decades in order to meet these requirements, while trying to reduce the cost of membranes. [4] One of under development and very promising approach is the bio-mimicking one. The general idea is to develop artificial materials with exceptional properties similar to the ones observed in the natural systems. Biomimetics, studying the phenomena of ion transport in biological membranes, focuses on achieving high efficiency and selective systems for instance by incorporating biomolecules [7, 8] or by implementing self-assembly technique as a tool. [9, 10]

In the literature many examples of promising materials that use self-assembly strategy can be found, like families of modified poly(epichlorohydrin) (PECH), polyglycidol (PG) and poly[2-(aziridin-1-yl)ethanol] (PAZE) with 3,4,5-tris[4-(n-dodecan-1-yloxy)benzyloxy]benzoic

acid (TAP) groups. The presence of dendritic groups allows their exo-recognition and forces the copolymer to adopt a columnar structure; the main chain forms a channel in the inner part of the columns, while the hydrophobic side-chain dendrons lie in the outer part. [11] These copolymers were synthesised for the first time with the objective to be used as non-ionomeric electrolyte membranes; this approach resulted successful in the case of self-supported PECH and PG-based membranes. [11-13] As for family of modified PAZE, all copolymers exhibit tendency to crystallise, which prevented preparation of self-supported membranes; hence, selected copolymers were used to prepare hybrid membranes containing anodised aluminium oxide (AAO) as support material. [14] It was reported that the inorganic support improves the mechanical properties; moreover, it induces formation of polymeric wires inside the pores. These wires, consisted of polymeric columns oriented in a homeotropical-like fashion, create conducting pathways. First in-depth studies of ion transport through biomimetic membranes were described for such hybrid membranes by means of current-voltage curves and impedance measurements. The results of those experiments put into evidence that, in the case of non-ionomeric membranes, more accurate characterisation can be obtained by linear sweep voltammetry. [15]

To address the crystallisation issue and to enable the evaluation of ion transport properties of self-supported membranes based on dendronised polyamines, a two-step modification of PAZE was employed. The modification included grafting with dendritic TAP group and benzoyl units; the addition of benzoyl modifier aimed at disturbing mainly the regularity of the structure and reducing number of free hydroxyl groups that can form hydrogen bonds. As reported in chapter 2, [16] this approach successfully yielded a new family of liquid-crystalline copolyamines and in most cases extended the liquid-crystalline behaviour over a wider range of temperatures, as expected. Furthermore, those copolymers self-assembles into columnar structures. Ionic channels are formed by columns, consisting of the main chain as the central part, and the tapered side groups as the outer part. The

presence of electron-donor atoms in main chain is expected to facilitate the cation transport through these channels; however, a homeotropical-like orientation of columns is essential for the transport and can be achieved by applying a thermal treatment at optimum conditions for each type of copolymer. [16]

This work describes the evaluation of ion transport through biomimetic ionic channels in membranes prepared out of two selected liquid-crystalline polyamines (**Figure 3.1**), modified both with benzoyl groups and TAP in proportion 0.25 : 0.75 and 0.33 : 0.43 (PA3 and PA4 copolymers, respectively). Current-voltage curves were used to study membrane selectivity as well as membrane resistance to the passing cations. In order to evaluate the performance of these new ion-conducting systems, a comparison with the hybrid systems based on PAZE modified with TAP only was done.

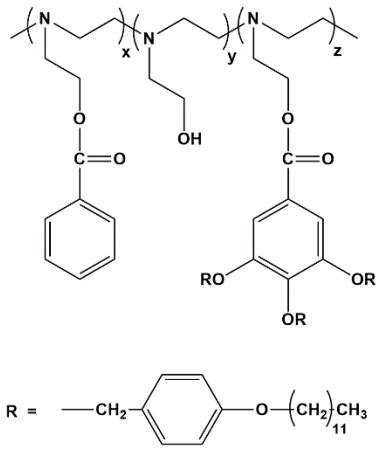

PAZE-40	**x = 0, y = 0.60, z = 0.40**
PAZE-72	**x = 0, y = 0.28, z = 0.72**
PA3	**x = 0.25, y = 0, z = 0.75**
PA4	**x = 0.33, y = 0.24, z = 0.43**

Figure 3.1. General structure of the two polymeric families based on modified poly[2-(aziridin-1-yl)ethanol].

3.2. Experimental

3.2.1. Materials

1-(2-hydroxyethyl)aziridine (95%) and benzoyl chloride (99%) were supplied by Sigma Aldrich. 4-dimethylaminopyridine (DMAP, ≥98.0%) and *N,N'*-dicyclohexylcarbodiimide (DCC, ≥99.0%) were supplied by Fluka. Pyridine (99.99%) was supplied by Fisher Scientific and *N*-methyl-2-pyrrolidone (NMP, 99%) was supplied by Scharlab. All the solvents were purchased from Scharlab. Benzoyl chloride, DMAP and DCC were used as received. NMP and pyridine were purified prior to use. Anodised aluminum oxide (AAO) from Whatman™ with pore size 0.2 µm in a disc form and a dimeter of 13 mm were used as received. The thickness of AAO rings is 60 µm. All the acids (HCl and HNO_3) and all the salts (LiCl, NaCl, KCl, $NaNO_3$, KNO_3, $AgNO_3$) used in linear sweep voltammetry experiments were purchased from Sigma Aldrich (Purity ≥99.0%).

Synthesis of copolymers

The copolymers were obtained in two step reaction by grafting first with benzoyl chloride and then with the dendron 3,4,5-tris[4-(n-dodecan-1-yloxy)benzyloxy]benzoic acid (TAP) according to the procedure described in chapter 2. [16]

Membranes preparation

PA-based membranes were prepared according to the procedure described in chapter 2, [16] while the hybrid membranes were prepared following procedure reported by Bogdanowicz et. al. [15]

3.2.2. Characterisation and measurements

Nuclear magnetic resonance (NMR) spectroscopy

^{1}H NMR spectra were recorded at 400 MHz on a Varian Gemini 400 spectrometer. The central peak of the solvent was taken as the reference, and the chemical shifts were given in parts per million from TMS (Tetramethylsilane). The spectra were recorded at room temperature with pulse delay time of 5 s.

X-ray diffraction (XRD)

For low 2θ range, XRD measurements were performed with a Bruker-AXS D8-Discover diffractometer equipped with parallel incident beam (Göbel mirror), vertical θ-θ goniometer, XYZ motorized stage and with a GADDS (General Area Detector Diffraction System). Samples were placed directly on to a low background Si(510) sample holder for reflection analysis. An X-ray collimator system close-to-the-sample allows to analyse areas of 500 μm. The X-ray diffractometer was operated at 40 kV and 40 mA to generate $Cu_{k\alpha}$ radiation. The GADDS detector was a HI-STAR (multiwire proportional counter of 30x30 cm with a 1024x1024 pixel) placed at 30 cm from the sample. The X-ray beam hit the sample at 0.5˚ of incidence. The collected frame (2D XRD pattern) covers a 2θ range from 0.9 up to 9.2˚. The diffracted X-ray beam travels through a He beam path (SAXS attachment) to reduce the air scattering at low angles. The direct X-ray beam is stopped by a beam stop placed directly on the detector face. The exposition time was of 300 s per frame. The resulting frames were both gamma integrated to obtain a 2θ diffractogram and 2θ integrated to obtain an azimuthal intensity plot. XRD experiments were performed on both sides of the membranes and no differences could be detected.

Linear sweep voltammetry (LSV)

Linear sweep voltammetry was performed using Autolab PGstat204 in potentiostatic mode with current ranging (automatic) from 100 mA to 100 µA, potential range from 0 V to 5 V, step 0.01 V and scan rate 0.01 $V \cdot s^{-1}$. The experimental set-up is presented in **Figure 3.2**. The distance between the reference electrodes (Ag/AgCl) and membrane was 1 cm. The solution volume in each compartment was 200 mL. The measurements were performed at room temperature. Samples for these measurements were placed in Teflon frame with a window giving a total membrane area equal to 0.5 cm^2. The membranes were placed between two sheets of Teflon and pressed.

Hydrochloric acid and nitric acid both in concentrations of 0.1 M and 0.025 M were used to study the proton transport. Besides, a series of measurements with salts were performed in two concentrations, 0.025 M and 0.1 M, in order to study the selectivity. Specifically, the following series of solutions were used: HCl, LiCl, NaCl and KCl; HNO_3, $NaNO_3$ $AgNO_3$ and KNO_3. Silver nitrate was used only in series at 0.025M electrolyte concentration. One series of measurements was applied to one membrane in the increasing order of cationic radius. Experiment for specific cation includes five consecutive current-voltage measurements at different times: 0, 10, 20, 45 and 60 minutes. From one set of measurements, the last obtained curve (60 minutes) was used to calculate the ohmic resistance (R_{ohm}) and limiting current densities (I_{lim}) for each cation.

The values of voltage for samples were calculated by subtracting the solution resistance without the membrane. Compensation was calculated according to equation:

$$U_{comp} = U_m - R_{sol} \cdot I_m \quad (1)$$

where U is the voltage, R is the resistance, I the current and the subscripts comp, m and sol refer to compensated value, measured value and solution alone, respectively.

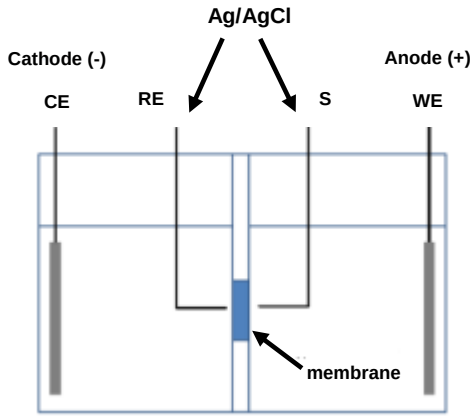

Figure 3.2. The experimental set-up for lineal sweep voltammetry measurements. WE is working electrode, CE is counter electrode, RE is reference electrode and S is sensitive electrode.

Chronoamperometry

Chronoamperometry experiment was carried out using Autolab PGstat204 with constant potential of 4 V during 6 hours in 0.1 M hydrochloric acid solution with two electrodes in cell similar to one used for linear sweep voltammetry.

Scanning electron microscopy (SEM)

SEM analysis was performed using a FEI Quanta 200 FEG (Eindhoven, The Netherlands) in high vacuum mode, using a secondary electron detector and an accelerating voltage ranging between 15 and 20 kV. The samples were cooled down with liquid nitrogen, and a brittle fracture was obtained. Before the analysis, samples were coated with a gold-palladium layer (about 15 nm thick) by means of an Emitech K575X sputter coater.

Transmission electron microscopy (TEM)

Samples of polymer membranes were embedded in a waterborne acrylic latex paint. Ultrathin membrane cross-section specimens (100 nm thick) were obtained using a Leica UC7 ultramicrotome system operating at 60˚C. The sections were placed on copper grids and stained by immersion in an aqueous 1% phosphotungstic acid solution for 10 s, then observed in bright field mode on a FEI Tecnai G12 Spirit Twin TEM operating at 120 kV acceleration voltage.

Solution uptake test

Weighted membranes were immersed in Milli-Q water or methanol solutions (1 M, 2 M, 6 M and 12 M) at room temperature every 15 minutes during first 2 hours and finally for 24 h to ensure the membranes were saturated. The liquid on the surface of the wet membranes was quickly removed with filter paper, and then the mass was measured. The mass of the dry membranes was obtained after the wet membranes were dried in air for 4 days at room temperature, until constant mass was reached. The water or methanol uptake can be calculated as follows:

$$Water\ uptake\ (\%) = \frac{(Wwet - Wdry)}{Wdry} \cdot 100 \qquad (2)$$

where W_{wet} and W_{dry} are the mass of wet and dry membrane samples, respectively.

3.3. Results and discussion

Chapter 2 [16] presents an extensive description of synthesis and characterisation of a new family of liquid-crystalline polyamines modified with both benzoyl and dendritic group 3,4,5-tris[4-(n-dodecan-1-yloxy)benzyloxy]benzoic acid (TAP) in different molar ratios. Thanks to the dendritic moiety, copolymers tend to self-assemble forming columns, as confirmed by XRD analysis. Two of them, PA3 and PA4, were selected and used to successfully prepare self-supported membranes, which is a promising advantage over hybrid systems based on dendronised PAZE copolymer. A comparison between these systems will be done, presenting a number of strong and weak points of both of them in terms of future application as proton-conducting membranes.

3.3.1. Hybrid membranes vs. self-supported membranes: structural and morphological comparison

Bogdanowicz et al. described the development of liquid-crystalline polymeric wires in anodised aluminium oxide (AAO) support by columnar mesophase growth of homeotropically-like oriented columns, inside the pores. As polymeric materials, two dendronised PAZEs with 40% (PAZE-40) and 72% (PAZE-72) modification degree were used. From the structural and the morphological point of view, both PAZE copolymers show almost identical features and behaviour in all studied aspects. The presence of the inorganic support does not affect the thermal properties of the polymer; furthermore, it strengthened the organisation of the columns in the satisfactory orientation and contributes to preserving the dimensional firmness of the membrane. [14]

As described in chapter 2, [16] the preparation of self-sustaining polyamine membranes was performed using two selected copolymers i.e. PA3 and PA4. The characteristics of the copolymers discussed in this paper are shown in **Table 3.1**.

Table 3.1. Total modification degree, TAP content and clearing temperatures in tested systems.

Copolymer	Total modification degree (%)	TAP modification degree (%)	T_c (˚C)
PA3	100	75	100-104
PA4	76	43	81-86
PAZE-40	40	40	43
PAZE-72	72	72	44

Additional modification with benzoyl unit in PAn copolymers has a significant impact on the stability of the LC phase, displacing the clearing temperature towards higher values. This fact is an important point in terms of future application. As a matter of fact, it is desirable to use the membranes based on both copolymer families as polymer electrolyte membrane (PEM), for instance in direct methanol fuel cell (DMFC) devices, where the operating temperature usually may range between 23˚C and 80˚C. [17] If we compare, for instance, copolymers with very similar total modification degree, such as PAZE-72 and PA4 with clearing temperature at 44˚C and between 81-86˚C, respectively, it is evident that the replacement of approximately 30% of TAP by benzoyl units leads to an increase of mesophase stability. Therefore, PA4 could exhibit columnar organisation up to higher temperatures than PAZE-72, maintaining the alignment of columns, which is critical for ion-conductive properties; hence, it meets better the expectations set for PEM materials.

The study of columns orientation of these materials is very important, since it affects the correct formation of ion-conducting pathways. As indicators of columns orientation, we considered the position of the maximum of the signal in the azimuthal scan on the reflection corresponding to d_{100} from XRD analysis, and its full width at half maximum (FWHM). The first one represents the average angle of columns alignment with respect to membrane surface, while FWHM gives information about the distribution of column orientation; it is desirable that the maximum is centred at 90˚ with distribution as sharp as possible. In general, membranes made of both polyamine families showed approximately perpendicular orientation of the columns to the membrane surface, although better results were observed in the case of non-supported PAn materials. As an example, in the hybrid system based on PAZE-72, the maximum intensity of d_{100} was centred at around 70˚ with FWHM of 76˚, [14] while for PA4-based membrane the reflection d_{100} had a maximum centred at around 91˚ and FWHM equal to 15˚, [16] as it can be observed in **Figure 3.3**. This put into evidence that self-supported membranes achieve much better results in terms of homeotropical alignment and narrow orientation distribution. The arrangement of the columns in required fashion could be explained by increased mobility of polymeric columns in non-supported membrane during the thermal treatment, necessary for orientation.

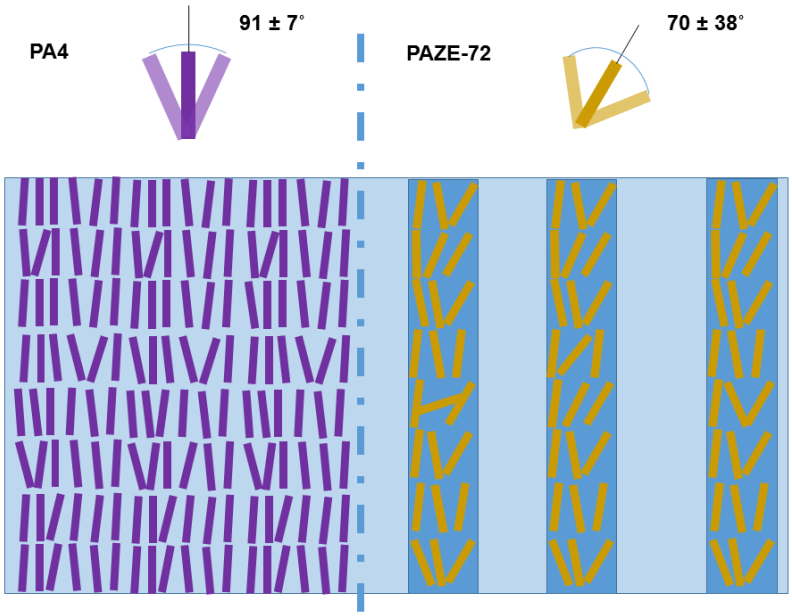

Figure 3.3. Visualisation of polymeric column orientation inside a PA4 membrane (left) and PAZE-72 inside AAO support (right).

Water uptake tests revealed low absorption, equal to 2.5 ± 0.5%, reaching the saturation point after 20 minutes of immersion time, as it is presented in **Figure 3.4a**. In the case of methanol uptake in 1 M solution, the test showed the same value as water. In concentrations above 1 M, low resistance of the copolymer to methanol was observed as negative values were noted during the experiment and mass decline of dry membrane after the experiment (**Figure 3.4b**). The reason for such behaviour can be explained as a result of increased copolymer solubility with the increment of methanol concentration, as it could be reasonably expected. In case of supported membranes, the uptake values were found around 10 ± 3% both for water and methanol solutions, without noticing any mass loss after the experiments; in this case low solubility in methanol can be attributed to smaller copolymer-methanol contact area and inability to swell inside the rigid structure of AAO support.

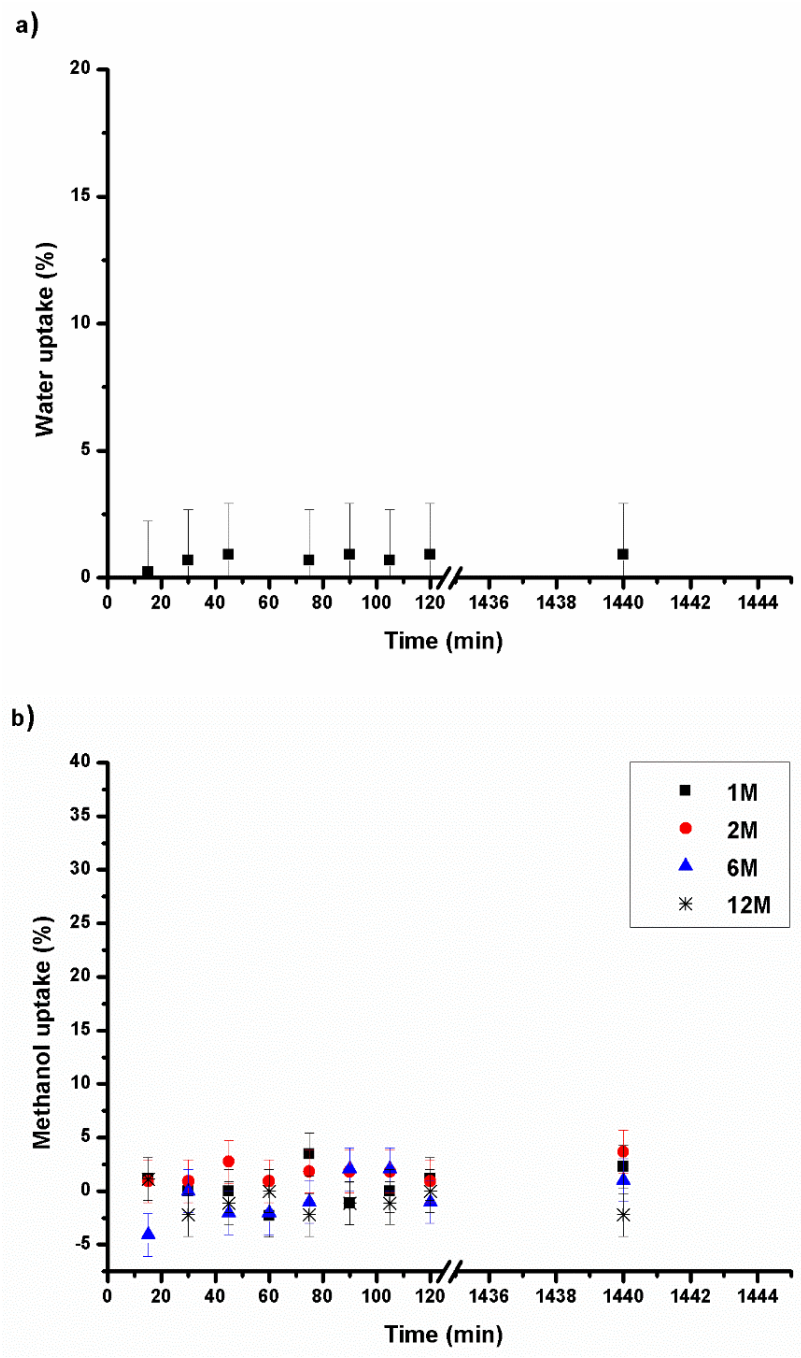

Figure 3.4. Water (a) and methanol solutions (b) absorption for oriented PA4 membrane.

3.3.2. Ionic transport

To characterise the ion transport, current-voltage measurements were performed using the proper set-up and applying the parameters described in the experimental section. A typical current-voltage curve can be generally divided into three regions. The first one, called ohmic region, gives information about resistance density of ion passing through the membrane. The following region can be presented as a *pseudo-plateau* characterised by a very slow variation of the current. From this region the limiting current density can be evaluated, that gives information about permselectivity, thickness of the diffusion boundary layer, diffusion coefficient and cation transport number in the membrane. Finally, a third region with increasing slope is called overlimiting current, which presence could be explained by electroconvection theory. [12, 13, 18, 19]

As it was presented by Bogdanowicz et al., linear sweep voltammetry is the most suitable technique to describe transport through non-ionomeric membranes. The experimental procedure includes set of measurements for different solutions using one membrane. The purpose of such design is to register ion transport in conditions where, in consecutive experiments, a membrane is exposed to more than one species passing through. This procedure could also give information about the stability of membrane after suffering several experiments. For sake of comparison, hybrid membranes were tested in the same conditions.

For membranes based on PA3 and PA4, it was impossible to perform a complete set of experiments using hydrochloric acid and its salts without damaging the membrane. At higher concentration (0.1 M), the current-voltage curves obtained for acid solution had linear trend, with the slope rising sharply, indicating consequently low resistance values, similar to the ones found in blank experiment performed for solution alone. For lower concentration (0.025 M) ion transport could be measured just for the hydrochloric acid solution: the resistance density values were in the range of

10^{-6} ($\Omega \cdot cm^2$) and the limiting current density was $4.9 \cdot 10^{-7}$ $A \cdot cm^{-2}$. When the experiment was subsequently performed with 0.025 M lithium chloride solution on the same membrane, rapidly increasing slope for consecutive measurements, that is, decreasing resistance values, was found.

This is the opposite of expected behaviour, which might suggest physical damage of the membrane during the experiments with hydrochloric acid and chloride salts. It must be taken into account that throughout linear sweep voltammetry experiments electrolysis occurs; in the case of chloride anion, gaseous chlorine is formed in the anode side as a consequence of oxidation reactions. Chlorine is a strong oxidizing agent, [20, 21] which could interact with polymer structure at membrane surface, thus causing its degradation. To confirm this hypothesis further analyses were performed and are described in the following section. As for hybrid systems, no damages of the membrane were detected for experiments performed for different chloride solutions, as it was previously reported. [15]

Therefore, in order to characterise the transport through PAn-based membranes, nitric acid and its salts were chosen to perform the experiments in two concentrations, 0.025 M and 0.1 M. No limiting current region was observed in any of the cases; only the difference between ohmic and overlimiting regions was distinguishable, as it can be seen in **Figure 3.5** for PA4. The resistance for proton was generally lower than for the other cations, which implies that proton passes easier through the channels. For all experiments with nitrates, the limiting current was not observed, probably due to inadequate setup configuration and experimental conditions (**Table 3.2** and **Table 3.3**). However, the cation permselective behaviour was confirmed in the experiments with hydrochloric acid at 0.025 M concentration, where limiting current was observed (**Figure 3.6**).

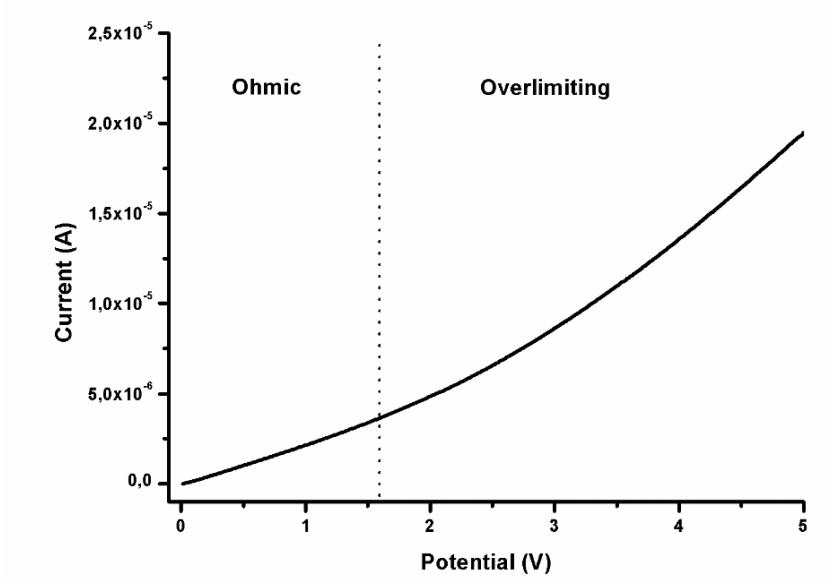

Figure 3.5. PA4 current-voltage curve from the first scan in 0.1 M nitric acid.

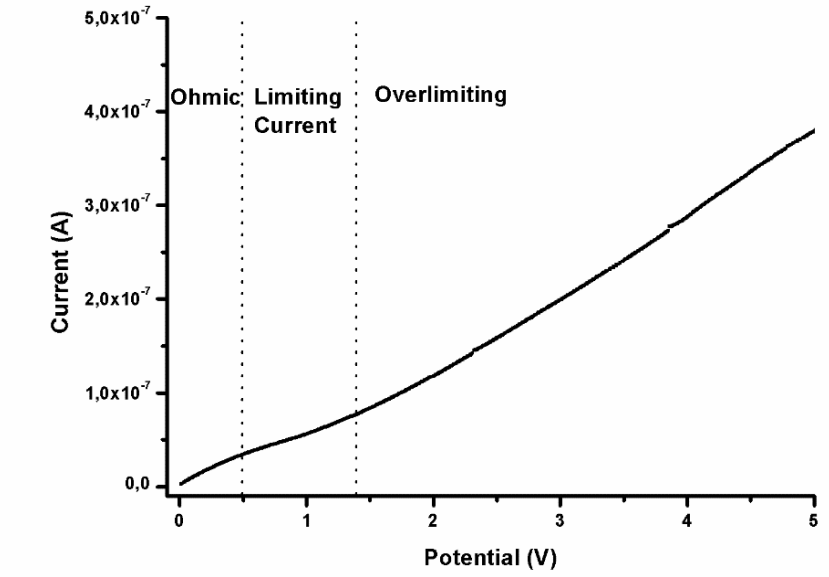

Figure 3.6. Current-voltage curve obtained in 0.025 M hydrochloric acid for PA4.

In order to reproduce the exact conditions of ion transport and evaluate the performance similarly to PAn-based membranes, experiments for hybrid systems were performed in the same conditions of concentration and with the same type of electrolyte. Only current-voltage curves for PAZE-40 at concentrations 0.1 M did not evidence the limiting current region and displayed linear trend. In all other experiments on hybrid systems, it was possible to observe the limiting current region and the values of limiting current densities that are reported in **Table 3.2** and **Table 3.3** along with specific ohmic resistance densities. As it was previously reported, hybrid membranes showed low resistance density values for proton in comparison to other tested monovalent cations when experiments were performed separately for each cation. Consecutive experiments performed on a single membrane revealed similar tendency, that is proton transport was favoured over other monovalent cations. [15]

A direct comparison of resistances between hybrid system and PAn-based membranes cannot be done directly, due to the difference in the membrane thickness (**Table 3.2** and **Table 3.3**). However, some tendencies were observed, for instance: the cation resistance values increase with membrane thickness, as expected, and in the experiments performed with proton, resistance values decreased with progressive number of performed experiments. This latter evidence could be associated to the reorganisation of the ionic pathways, that adapt their conformation after proton passage. An improvement of ion transport in subsequent experiments was also detected in permeability tests for other biomimetic membranes based on modified linear polyglycidol. [22] On the other hand, when subsequent experiments were performed with different cations, in order of increasing size, increasing resistance values were found (**Table 3.2** and **Table 3.3**).

Table 3.2. Resistance density and limiting current density values for the experiments carried out with $AgNO_3$ and KNO_3 water solutions.

Copolymer	Thickness (μm)	HNO_3 (0.012 Å) [a]				$NaNO_3$ (1.02 Å) [a]			
		0.025 M		0.1 M		0.025 M		0.1 M	
		R_{ohm} x10^{-2} (Ω·cm^2)	I_{lim} x10^3 (A·cm^{-2})	R_{ohm} x10^{-2} (Ω·cm^2)	I_{lim} x10^3 (A·cm^{-2})	R_{ohm} x10^{-2} (Ω·cm^2)	I_{lim} x10^3 (A·cm^{-2})	R_{ohm} x10^{-2} (Ω·cm^2)	I_{lim} x10^3 (A·cm^{-2})
PA3	120-140	1215.9	-	181.2	-	1824.9	-	258.0	-
PA4	240-330	1697.4	-	851.9	-	2848.2	-	1201.9	-
PAZE-40	70-90	4.5	0.6	417.3	-	12.4	0.8	1365.7	-
PAZE-72	70-90	4.2	1.5	0.8	11.1	8.2	1.4	3.3	1.6

[a] cationic radius

Table 3.3. Resistance density and limiting current density values for the experiments carried out with $AgNO_3$ and KNO_3 water solutions.

Copolymer	Thickness (μm)	$AgNO_3$ (1.26 Å) [a]				KNO_3 (1.38 Å) [a]			
		0.025 M		0.1 M		0.025 M		0.1 M	
		R_{ohm} x10^{-2} ($\Omega \cdot cm^2$)	I_{lim} x10^{3} ($A \cdot cm^{-2}$)	R_{ohm} x10^{-2} ($\Omega \cdot cm^2$)	I_{lim} x10^{3} ($A \cdot cm^{-2}$)	R_{ohm} x10^{-2} ($\Omega \cdot cm^2$)	I_{lim} x10^{3} ($A \cdot cm^{-2}$)	R_{ohm} x10^{-2} ($\Omega \cdot cm^2$)	I_{lim} x10^{3} ($A \cdot cm^{-2}$)
PA3	120-140	3005.0	-	-	-	4045.9	-	364.5	-
PA4	240-330	5033.1	-	-	-	5466.1	-	2112.9	-
PAZE-40	70-90	13.6	0.5	-	-	21.9	0.8	1607.2	-
PAZE-72	70-90	5.8	2.6	-	-	20.8	0.1	9.2	3.9

[a] cationic radius

As an example, **Figure 3.7** shows the case of PAZE-40. The significant curve variation suggests a change in type of transported cations through the membrane. Further comparison of the last curve of one series, i.e. Na^+, with the first curve of the new one, i.e. Ag^+, showed relatively similar values of the resistance in spite of the difference in cationic radius (1.02 Å and 1.26 Å for sodium and silver, respectively). This suggests that the former test refers to a "mixed cations" transport: that is, at the beginning, current values are due to the passage of smaller cations, remaining in the membrane after the previous experiments; as experiments proceed further, these smaller cations are replaced in the structure by bigger ones, currently under analysis. Under this hypothesis, the first recorded curves therefore represent a mixed transport of cations remaining inside the membrane and of new ones provided by the new solution. Moreover, the concentration gradient phenomenon that is created between the cathode and anode compartments has its impact on ion transport. Cations in the anode side are forced to pass to cathode side by the applied potential; on the other hand, cations are accumulated in the cathode side in each measurement with the exception of proton that is reduced to hydrogen. As a result, during each subsequent measurement, cations need to overcome an increasing cation concentration gradient caused by previous experiments.

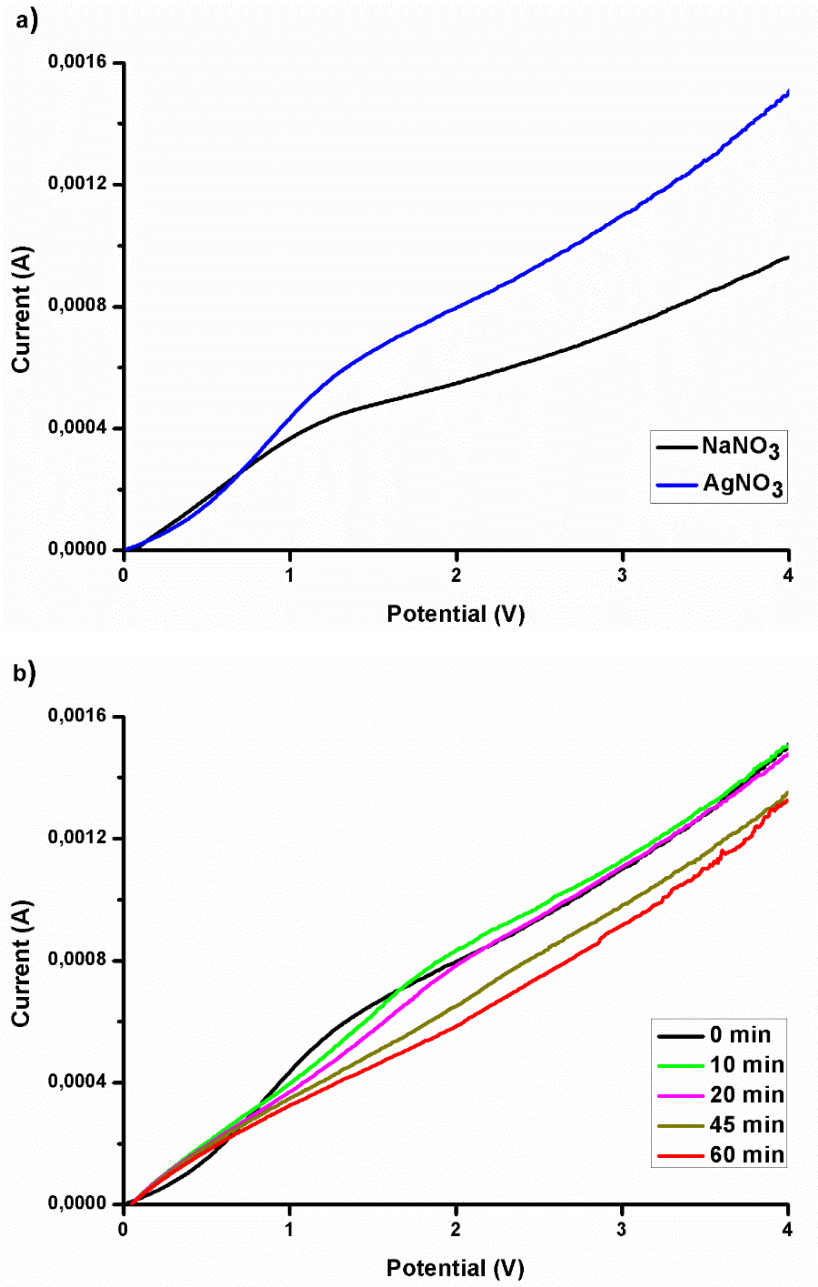

Figure 3.7. Current-voltage curves for PAZE-40 at 0.025 M concentration: (a) last curve for Na^+ and first of Ag^+; (b) All five consecutive experiments for Ag^+ at different time.

To express the membrane preferential selectivity, a ratio of conductance ($G_i=1/R_i$) of alkali ion value over proton value (G_{ion}/G_{H+}) was calculated and it is reported in **Table 3.4**. A direct comparison of conductance values between these two systems cannot be done due to the difference in the diffusion boundary layers and membrane thickness. However, it was possible to observe that membrane thickness generally improves selectivity. Besides, the tendency of preferential ion transport for most membranes, in decreasing order, was: proton, sodium, silver and potassium. PAn-based membranes revealed very similar performances despite different modification degrees and distinct ratios of benzoyl to TAP moieties. When compared with hybrid systems, non-supported membranes displayed lower selectivity. This could be explained by increased polymer mobility compared to supported membranes. In most cases size dependent transport was registered: the smaller the cation radius, the easier it passes through the membrane. Regarding the result for PAZE-72, surprisingly the higher achieved preferential selectivity was observed for silver ion. This phenomenon can be explained in terms of the different channel size and well-known affinity of silver to nitrogen atoms. [23]

Table 3.4. Preferential selectivity of tested membranes for nitrate solutions.

Copolymer	$G_{Na+/H+}$		$G_{Ag+/H+}$		$G_{K+/H+}$	
	0.025 M	**0.1 M**	**0.025 M**	**0.1 M**	**0.025 M**	**0.1 M**
PA3	67%	70%	40%	-	30%	50%
PA4	60%	71%	34%	-	31%	40%
PAZE-40	36%	31%	33%	-	21%	26%
PAZE-72	51%	24%	73%	-	20%	8%

3.3.3. Degradation of PAn copolymers

In order to evaluate the extent of membrane degradation after LSV experiments in the presence of chloride anions, an electron scanning microscopy analysis was performed on the samples after applying linear sweep voltammetry (**Figure 3.8**). The micrographs of PA4 membrane surface revealed a scaly-like texture (**Figure 3.8a**), whereas the analysis of cross-section showed the presence of pores (**Figure 3.8b**). These images put into evidence a physical damage caused by the oxidising conditions created during the ion transport experiment.

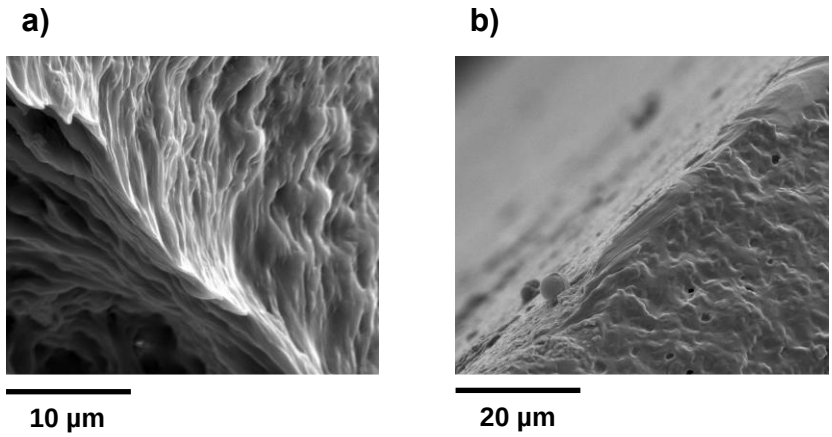

Figure 3.8. SEM micrographs of surface (a) and cross-section (b) of membrane made of PA4.

TEM analysis was performed on stained cross-section of PA4 membrane before and after LSV experiment in chloride solutions (**Figure 3.9**). The analysis for sample before the LSV experiment demonstrated a striped-like cross-section surface. Measurement of the width of a single stripe gave approx. 60 nm and could correspond to columns agglomerates forming

ionic pathways. The TEM image after LSV experiments disclosed morphological changes, presenting numerous dark lines and spots. This fact put into evidence that the oxidising conditions during LSV experiment could cause chemical degradation of polymer.

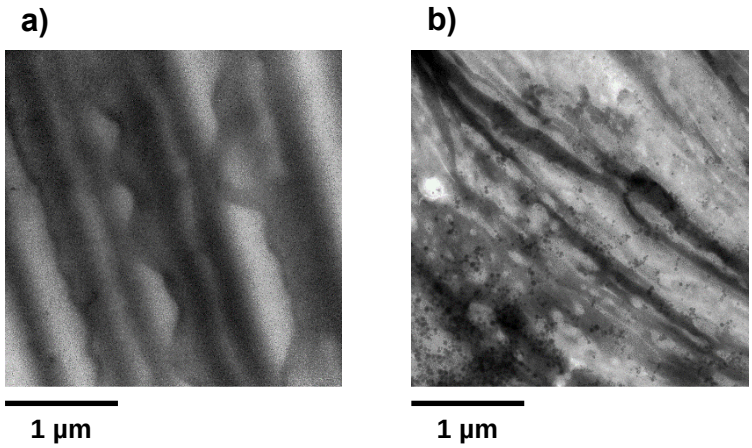

Figure 3.9. TEM images of PA4 membrane cross-section before (a) and after (b) LSV experiment.

In order to demonstrate chemical degradation of PAn-based membranes, NMR analysis were performed. Prior to nuclear resonance analysis, in order to increase the extent of degradation, the membrane was exposed to long term oxidising conditions similar to those for LSV, according to the procedure described for chronamperometry in the Experimental section. ^{1}H NMR quantitative spectra of the copolymer from the damaged membrane unveiled structural changes in the amount of modified lateral groups (**Figure 3.10**). Generally, the spectra had qualitatively identical aspect to the starting polymeric material, showing all characteristic signals. From the integrated areas corresponding to benzoyl and TAP protons in the ranges: 0.8-2.0 ppm (aliphatic chains of TAP, 75 protons), 6.5-7.7 ppm (aromatic

14 protons of TAP and 3 protons of benzoyl) and 7.8-8.2 ppm (aromatic 2 protons of benzoyl) it was detected that the proportion of groups had changed from 0.33 : 0.43 to 0.20 : 0.43, for benzoyl and TAP respectively. The ratio of the integrals of TAP and main chain of copolymer maintained its starting proportion within the experimental error. These results evidenced that the most vulnerable part of the copolymer structure is the benzoyl group that can be detached in oxidising environment.

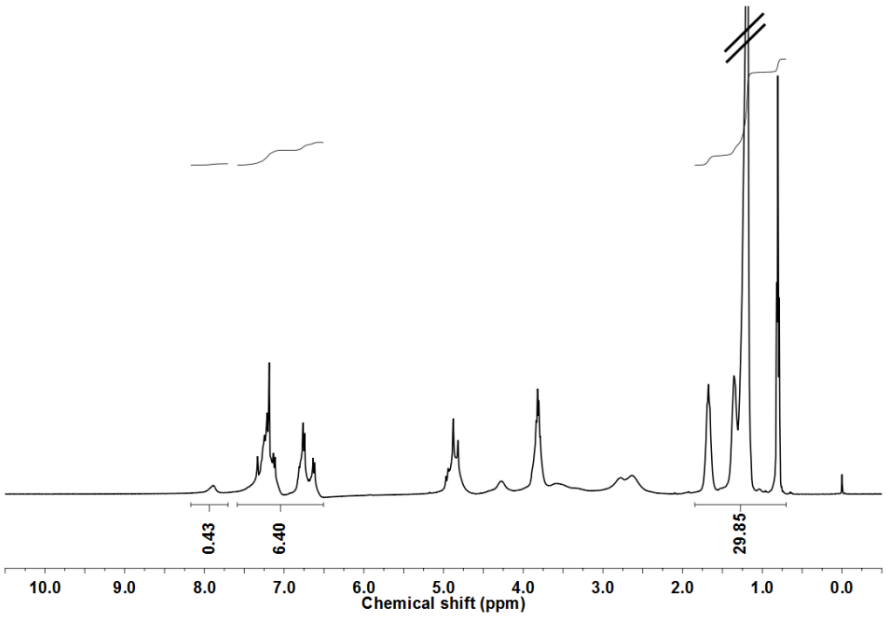

Figure 3.10. Quantitative ^{1}H NMR spectra of PA4 copolymer after the chronoamperometry experiment.

3.4. Conclusions

Self-supported biomimetic membranes based on liquid-crystalline poly[2-(aziridin-1-yl)ethanol] modified both with benzoyl and TAP units in different proportion were prepared. Both copolymers self-assembled into homeotropically oriented columns, forming ionic channels. Evaluation of ion transport through the membrane confirmed cation permselective nature for all biomimetic membranes. Linear sweep voltammetry experiments in chloride solution revealed damage probably caused by the presence of gaseous chlorine, as confirmed by SEM, TEM and ^{1}H NMR analyses. A comparison of PAn-based membranes with their analogue hybrid systems put into evidence better homeotropical orientation, higher values of clearing temperature and improved mechanical properties. However, some disadvantages like sensitivity to gaseous chlorine and lower selectivity were found. These novel biomimetic systems can be considered complementary to the hybrid membranes previously reported, since they exhibit worse performances as far as selectivity is concerned; on the other hand, membranes can be more easily prepared, are cheaper, possess higher thermal stability and are not brittle. Therefore, they could be used, for instance, in applications where higher temperature regimes are required.

3.5. Acknowledgements

Financial support from CTQ2013-46825-R (Ministerio de Economía y Competitividad) is gratefully acknowledged.

3.6. References

1. Concepcion JJ, House RL, Papanikolas JM, and Meyer TJ. Proc. Natl. Acad. Sci. U. S. A. 2012;109(39):15560-15564.

2. Li X. Thermodynamic Performance of Fuel Cells and Comparison with Heat Engines, in Advances in Fuel Cells, vol. 1. Oxford: Elsevier Science, 2007. pp. 1-46.

3. Smitha B, Sridhar S, and Khan AA. J. Membr. Sci. 2005;259(1–2):10-26.

4. Peighambardoust SJ, Rowshanzamir S, and Amjadi M. Int. J. Hydrogen Energy 2010;35(17):9349-9384.

5. Edwards PP, Kuznetsov VL, David WIF, and Brandon NP. Energy Policy 2008;36(12):4356-4362.

6. Wang Y, Chen KS, Mishler J, Cho SC, and Adroher XC. Appl. Energy 2011;88(4):981-1007.

7. Xiao K, Wen L, and Jiang L. Small 2016;12(21):2810-2831.

8. Zhou T, Zhu Y, Li X, Liu X, Yeung KWK, Wu S, Wang X, Cui Z, Yang X, and Chu PK. Prog. Mater. Sci. 2016;83:191-235.

9. Wu M, Cao Z, Zhao Y, Zeng R, Tu M, and Zhao J. Mater. Sci. Eng. C 2016;64:346-353.

10. Huang BJ, Hu JC, and Athanasiou KA. Biomaterials 2016;98:1-22.

11. Tylkowski B, Castelao N, Giamberini M, Garcia-Valls R, Reina JA, and Gumí T. Mater. Sci. Eng. C 2012;32(2):105-111.

12. Choi J-H, Lee H-J, and Moon S-H. J. Colloid Interface Sci. 2001;238(1):188-195.

13. Chamoulaud G and Bélanger D. J. Colloid Interface Sci. 2005;281(1):179-187.

14. Bogdanowicz KA, Rapsilber GA, Reina JA, and Giamberini M. Polymer 2016;92:50-57.

15. Bogdanowicz KA, Sistat P, Reina JA, and Giamberini M. Polymer 2016;92:58-65.

16. Montané X, Bogdanowicz KA, Colace G, Reina JA, Cerruti P, and Giamberini M. In preparation.

17. Aricò AS, Baglio V, and Antonucci V. Direct Methanol Fuel Cells: History, Status and Perspectives, in Electrocatalysis of Direct Methanol Fuel Cells. Weinheim: Wiley-VCH Verlag GmbH & Co. KGaA, 2009. pp. 1-78.

18. Choi J-H, Park J-S, and Moon S-H. J. Colloid Interface Sci. 2002;251(2):311-317.

19. Pawlowski S, Sistat P, Crespo JG, and Velizarov S. J. Membr. Sci. 2014;471:72-83.

20. Lee Y and von Gunten U. Water Res. 2010;44(2):555-566.

21. Deborde M and von Gunten U. Water Res. 2008;42(1–2):13-51.

22. Montané X, Bhosale SV, Reina JA, and Giamberini M. Polymer 2015;66:100-109.

23. Aslan K, Leonenko Z, Lakowicz JR, and Geddes CD. J. Fluoresc. 2005;15(5):643-654.

Chapter 4

Structure and dynamics of liquid-crystalline copolyamines with benzoyl and TAP side groups

4.1. Introduction

The macroscopic properties of synthetic polymers depend on their molecular structure and on their organisation, i.e. morphology, molecular order and molecular dynamics. Functional supramolecular materials have great importance due to their numerous important applications. To determine the structure and identify the structure-driving and structure-directing features of the supramolecular systems represent an important challenge for modern characterization techniques in the rapidly developing field of supramolecular chemistry. [1-4]

Nuclear magnetic resonance (NMR) spectroscopy is a powerful tool in different fields like organic chemistry, analytical chemistry, solid-state physics or structural biology. [5] Today, solution state NMR is one of the most important tools for structural characterization in synthetic chemistry. [6, 7]

Furthermore, there is a considerable interest in studying the solid-state properties of polymers because the majority of these systems are used as solid materials. [8, 9] Advanced solid-state NMR methods like fast magic-angle spinning (MAS) performed at variable temperatures or multidimensional analysis can provide detailed information on local molecular structure and mobility in the samples. [10-14]

Rapp and coworkers studied the local structure of supramolecular systems by using solid-state NMR techniques. [15] The investigated polymers, which were formed by polymethacrylate (PMA) or polystyrene (PS) as a polymer backbone with large dendritic side groups grafted to the polymer backbone, self-assemble into columnar structures. The attached dendrons contain aromatic moieties and flexible ethylene oxide linkers. In the supramolecular assembly a mobility gradient was detected from the interior of the dendritic branches to the periphery. Thus, it was deduced from this study that the inner backbone has little influence on structure and properties for the resulting self-assembled polymers.

In recent times, our group reported the synthesis and characterization of liquid-crystalline dendronised polymers based on poly(epichlorydrin) (PECH), poly(epichlorydrin-co-ethylene oxide) [P(ECH-co-EO)], poly[2-(aziridin-1-yl)ethanol] (PAZE) and polyglycidol (LPG) modified at different extent with 3,4,5-tris[4-(n-dodecan-1-yloxy)benzyloxy]benzoic acid (TAP) as a dendron. [16-19] Due to their columnar structure, these materials were proposed as biomimetic ion channels. Using these liquid-crystalline copolymers, oriented membranes could be prepared. The obtained membranes exhibit promising proton permeability and conductivity, comparable to Nafion®, which is the reference material in the field of proton exchange membranes (PEM). Nevertheless, understanding and comprehension of the relation structure-property and dynamics of these systems is a fundamental requirement if their use as PEM materials will be enhanced.

The objective of this work is to understand the structure and dynamics of a family of liquid-crystalline copolyamines previously synthesised by chemical modification of PAZE with benzoyl chloride and the TAP dendron. [20] The general structure of these copolyamines is presented in **Figure 4.1**.

The following related copolymers were investigated:

a) PAZE with modification degree of 94 %, henceforth referred to as PA1.1.
b) PAZE with modification degree of 100 %, henceforth referred to as PA3.
c) PAZE with modification degree of 76 %, henceforth referred to as PA4.

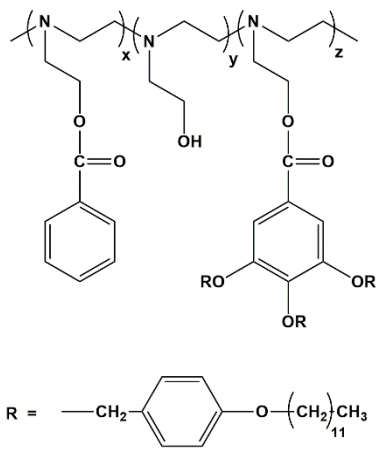

PA1.1	**x = 0.09, y = 0.06, z = 0.85**
PA3	**x = 0.25, y = 0, z = 0.75**
PA4	**x = 0.33, y = 0.24, z = 0.43**

Figure 4.1. General structure of the studied copolymers.

Studies of the molecular organisation of this family of copolyamines were carried out over a representative selection of systems which contain different amounts of benzoyl and TAP. The benzoyl units and the dendrons are attached to a copolymer backbone by a short and flexible –$COOCH_2CH_2$– linking unit. The behaviour of these copolymers was investigated by Differential Scanning Calorimetry (DSC), Polarised Optical Microscope (POM) and solid state NMR techniques.

4.2. Experimental

4.2.1. Materials

PAZE was synthesised as described in a previous paper. [21] Chemical modification of PAZE was performed as described in a previous study. [20]

4.2.2. Characterisation and measurements

Nuclear magnetic resonance (NMR) spectroscopy

a) Solution-state NMR

^{1}H NMR and ^{13}C NMR spectra were recorded at 400 and 100.4 MHz, respectively, on a Varian Gemini 400 spectrometer with proton noise decoupling for ^{13}C NMR. The central peak of the solvent was taken as the reference, and the chemical shifts were given in parts per million from TMS (Tetramethylsilane). The ^{13}C NMR spectra of the polymers were recorded at 303.2 K, with a flip angle of 45˚, and the number of transients ranged from 20,000 to 40,000 with 10-20% (w/v) sample solutions in deuterated chloroform ($CDCl_3$) or deuterated dimethyl sulfoxide (DMSO-d_6). A pulse delay time of 5 s for the ^{1}H NMR spectrum was used.

Quantitative ^{13}C NMR spectra were performed using deuterated chloroform ($CHCl_3$) or deuterated dimethyl sulfoxide (DMSO-d_6) at 30˚C with a pulse delay time of 5 s. Delay time was selected on the basis of the relaxation times determined for the monomer 1-(2-hydroxyethyl)aziridine.

b) Solid-state NMR

Solid-state NMR experiments were performed using two different Bruker Avance III NMR spectrometers equipped with different superconducting magnets: 11.7 T wide bore (500.22 MHz for ^{1}H and 125.8 MHz for ^{13}C) and 19.9 T standard bore (850.27 MHz for ^{1}H and 213.8 MHz for ^{13}C). Commercial double resonance MAS probes supporting zirconia rotors with 2.5 mm and 4.0 mm outer diameter allowed the experiments to be performed at MAS spinning frequencies of 25 and 10 kHz, respectively. The 90˚ pulse length used was 2.5 µs and the repetition delay 2 s. The CP-MAS spectra have been acquired with a CP contact pulse length of 1 ms and 2048 transients, using SPINAL64 decoupling during acquisition. The temperature was varied in eight linearly spaced steps in the range

256-364 K using a BSVT temperature control and a BCU-II cooling unit. The spectra were externally referenced to the CH_3-signal of solid L-Alanine (1.34 ppm for ^{1}H and 20.5 ppm for ^{13}C).

The experiments listed below were performed:

- ^{1}H MAS (Magic angle-spinning) and ^{13}C CP-MAS (Cross-polarisation magic angle-spinning) variable-temperature (VT) studies.
- ^{13}C INEPT MAS (Insensitive Nuclei Enhanced by Polarisation Transfer Experiment), which is our case $^{1}H \rightarrow {}^{13}C$ transfer, using a 145 Hz J coupling.
- 2D ^{1}H MAS-^{13}C INEPT MAS heteronuclear correlation.

Differential scanning calorimetry (DSC)

Calorimetric studies of copolymers were performed in aluminium standard 40µl crucibles without pin (ME-26763) with a Mettler DSC822e thermal analyser at the heating rate of 10 K/min using about 5 mg of sample, nitrogen as a purge gas (100 mL/min) and liquid nitrogen for the cooling system. The equipment was previously calibrated with indium (429.7 K) and zinc (692.6 K) pearls.

Polarised optical microscopy (POM)

Clearing temperatures and liquid crystal (LC) mesophases were investigated by polarised optical microscopy (POM); textures of the samples were observed with an Axiolab Zeiss optical microscope equipped with a Linkam TP92 hot stage.

4.3. Results and discussion

Solid-state NMR methods under fast magic-angle spinning (MAS), INEPT MAS and 2D ^{1}H MAS-^{13}C INEPT MAS were used to study the structure and dynamics of the synthesised side chain liquid crystal polymers (SCLCP), which consist of a polymer backbone with benzoyl and dendritic side groups (TAP) that self-assemble into a columnar structure.

4.3.1. Liquid-crystalline polyamines study

Polyamines bearing benzoyl and the tapered 3,4,5-tris[4-(n-dodecan-1-yloxy)benzyloxy]benzoate group (TAP) were synthesised by chemical modification of poly[2-(aziridin-1-yl)ethanol] (PAZE) as described in a previous work by following a two-step pathway. [20] The resulting degrees of modification and the thermal transitions of the obtained copolyamines are reported in **Table 4.1**.

Table 4.1. Modification degrees, melting points and clearing temperatures of the studied copolymers.

Copolymer	Benzoyl modification degree (%) [a]	Tapered modification degree (%) [a]	Total modification degree (%) [a]	T_m (K) [b]	T_c (K) [b]
PA1.1	9	85	94	335	321 [c]
PA3	25	75	100	260	373-377
PA4	33	43	76	259	354-359

[a] Modification degree determined by using ^{13}C solution NMR.
[b] Determined by DSC second scan heating and POM.
[c] Monotropic liquid crystal.

The modification degrees were calculated based on solution NMR spectroscopy data. As an example, **Table 4.2** reports ^{1}H and ^{13}C NMR solution spectrum data of PA4 performed at room temperature in deuterated chloroform ($CDCl_3$). Quantification was carried out from the ^{13}C NMR by comparing the areas of the carbon of methylene c and c'' in the modified monomeric units at 62.3 ppm and the carbon of methylene c' in the unmodified monomeric unit at 59.3 ppm.

All synthesised polyamines exhibited a LC mesophase. The DSC analysis of these copolymers put into evidence two endotherms. For all samples except PA1.1, the first one could be related to the melting and the second one to the clearing point. As we expected, on increasing the content of the mesogenic TAP group, the clearing points and enthalpies of the copolymers also increased similarly to what was reported for columnar copolyethers and copolyamines modified only with TAP. [16, 18] On the other hand, in any copolymer of this family a T_g was not observed by DSC.

Table 4.2. NMR data and structure of the PA4 copolymer in $CDCl_3$.

^{1}H NMR		^{13}C NMR	
Signal (ppm)	**Assignment**	**Signal (ppm)**	**Assignment**
12	0-8	**12**	14.0
3-11	1.2-1.4	**11**	22.6
2	1.7	**3**	26.0
a, a', a'', b, b', b''	2.5-2.8	**2, 4-9**	29.1-29.6
c'	3.6	**10**	31.8
1	3.8	**a, a', a'', b, b', b''**	52.0-57.0
c, c''	4.3	**c'**	59.3
e''	4.8	**c, c''**	62.3
Ar	6.5-7.9	**1**	67.8
		e'' lateral	70.8
		e'' central	74.6
		II'	108.8
		VII'	114.0
		I'	124.8
		I-IV, V', VI'	128.3-133.0
		IV'	142.4
		III'	152.5
		VIII'	158.6
		COO	165.9-166.2

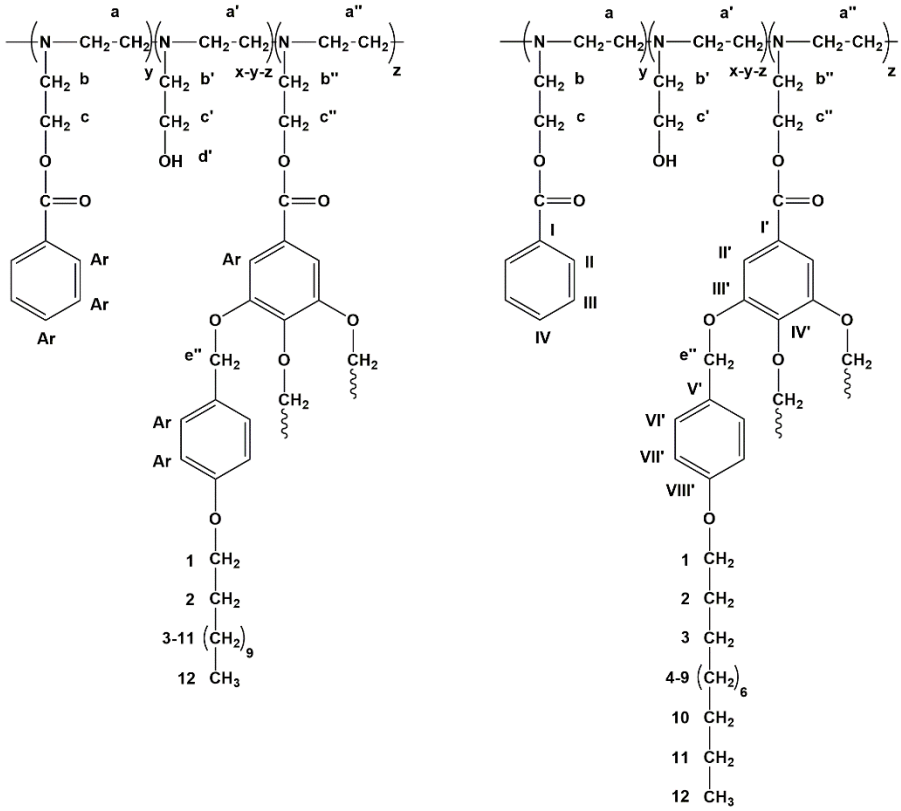

Structural features of PA1.1: 2D ^{1}H MAS-^{13}C INEPT MAS correlation spectrum

In order to assign all the signals in NMR spectra, we recorded 2D ^{1}H-^{13}C INEPT MAS correlation spectrum of polymer PA1.1 (**Figure 4.2**). It allows the resonances of the carbons and their attached protons to be assigned for the different CH_n groups of PA1.1 copolyamine. In this spectrum, three regions can be distinguished: the aromatic, the –OCH_2– and the aliphatic region. No signals of the copolymer backbone were observed, due to insufficient motional averaging of anisotropic NMR interaction at these sites supporting a strongly reduced molecular mobility of the polymer backbone.

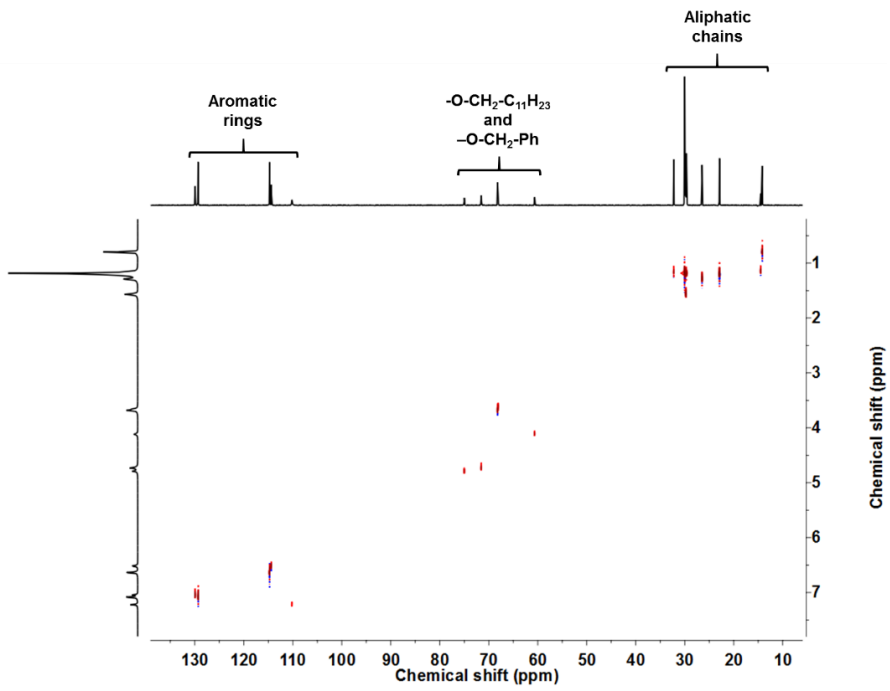

Figure 4.2. 2D ^{1}H-^{13}C INEPT MAS NMR correlation spectrum of PA1.1 copolymer.

In the aromatic region of the ^{13}C INEPT MAS spectrum five peaks are observed between 110 and 131 ppm, which are assigned to the aromatic carbons attached to a proton of the dendron units and also to the benzoyl units, as indicated in **Table 4.2**.

In the $–OCH_2–$ region, different types of groups can be distinguished, corresponding to the molecular structure of PA1.1 (depicted in **Figure 4.1**): $–OCH_2R$ groups in the dodecyl chain (with R = $–C_{11}H_{23}$), $–OCH_2Ph–$ between the phenyl rings, and a $–CH_2(COO)–$ group that links the dendron to the polymer backbone. On the basis of symmetry considerations, the $–OCH_2Ph–$ groups in the 4-position of the phenyl ring can be expected to exhibit different NMR signals from those in the 3- and 5- positions, as we can observe in the 2D spectrum, where the signals of all $–OCH_2Ph–$ groups present a similar

chemical shift in the ^{1}H MAS spectrum, but in the case of ^{1}H-^{13}C INEPT MAS correlation spectrum it is possible to distinguish the signals corresponding to the central and lateral –OCH_2Ph– units (**Table 4.2**).

The third spectral region of interest corresponds to the aliphatic chain of the TAP groups. This region include the signals between 0.8 and 1.6 ppm in the ^{1}H MAS spectrum which are correlated to the carbon signals between 14 and 33 ppm in the ^{13}C INEPT.

Mobility of liquid-crystalline polyamines

All the samples from **Table 4.1** were analysed using solid state NMR techniques. However, with the observed behaviour referring to different calorimetric features for all the copolymers, we can divide them in two different groups: one group includes only the sample PA1.1 and the second group includes the rest of the samples. In the second group, PA3 is the only copolymer which is completely modified with prevalence of TAP over benzoyl (0.75 : 0.25 respectively). On the other hand, PA4 was not completely modified and contains a fairly similar amount of the three possible repeating units: benzoyl, free hydroxyl groups and TAP (0.33 : 0.24 : 0.43 respectively), linked to the polyamine main chain. For this reason, the copolymers PA1.1, PA3 and PA4 were selected in order to study these three different cases.

The comparison of ^{1}H MAS NMR, ^{13}C CP-MAS NMR and ^{13}C INEPT MAS spectra at different temperatures (VT NMR experiments) will allow us to distinguish mobile and rigid moieties of these copolyamines, while the combination of VT NMR and DSC analysis will permit to identify which specific groups are involved in thermal transitions observed in these copolymers.

a) Mobility of PA1.1 copolyamine

Table 4.3 summarizes the transitions observed by DSC, ^{1}H MAS and ^{13}C CP-MAS NMR analysis. As we mentioned in our previous study, [20] to improve the separation of the two endotherms that appear overlapped in the DSC, the copolymer was annealed for 2 h at temperatures slightly below the first peak maximum (312-315 K). Then, we repeated the DSC analysis again after cooling the sample (**Figure 4.3**). In this case, two sharp endotherms were obtained: the first one could be related to the melting transition of crystalline part, while the second one can be attributed to the clearing of a monotropic LC mesophase that grew during the annealing process as shown in **Table 4.3**.

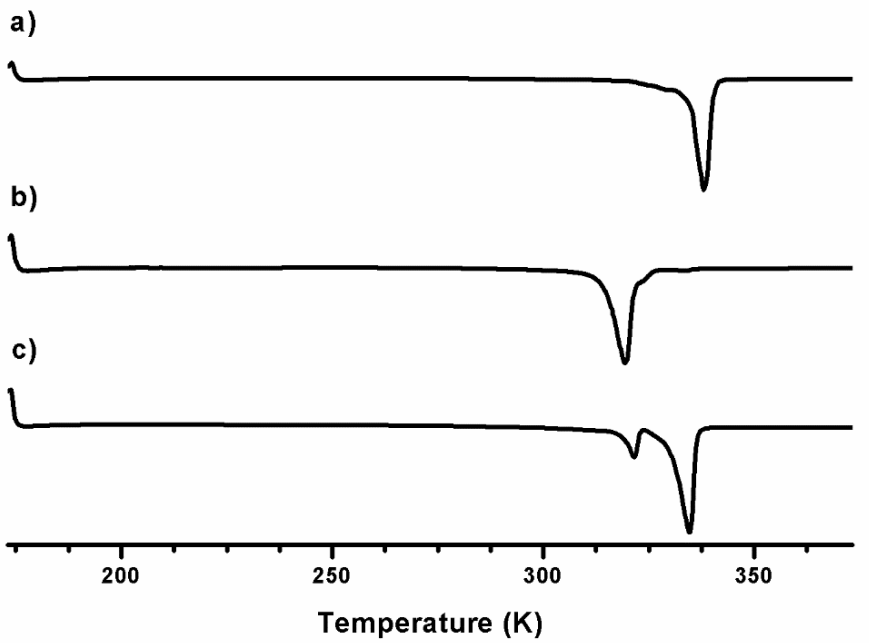

Figure 4.3. DSC thermographs of PA1.1 copolymer: a) First heating scan, b) Second heating scan, c) Heating scan after annealing the sample at 40˚C on cooling during 2 h.

Table 4.3. Transitions observed by DSC, ^{1}H MAS and ^{13}C CP-MAS NMR analysis for PA1.1 copolymer.

DSC (K) [a]	^{1}H and ^{13}C CP-MAS NMR (K) [b]	Chemical shifts (ppm) of ^{1}H MAS NMR [c]	Chemical shifts (ppm) of ^{13}C CP-MAS NMR [c]	Observations
321	318-333	-	-	melting
335	318-333	0.0-7.2	all peaks vanish	clearing

[a] Temperature of the peak maximum (referred to scan c in **Figure 4.3)**.
[b] Temperature at which transitions are observed.
[c] Chemical shifts of the groups involved in the transition.

VT ^{1}H MAS and ^{13}C CP-MAS experiments were performed in order to elucidate the nature of dynamic processes for PA1.1 copolymer.

The recorded VT ^{1}H MAS spectra of sample PA 1.1 are shown in **Figure 4.4**. Well resolved ^{1}H MAS NMR spectra are obtained at temperatures higher than the clearing temperature, indicating a fully isotropic liquid phase of the copolyamine at these temperatures.

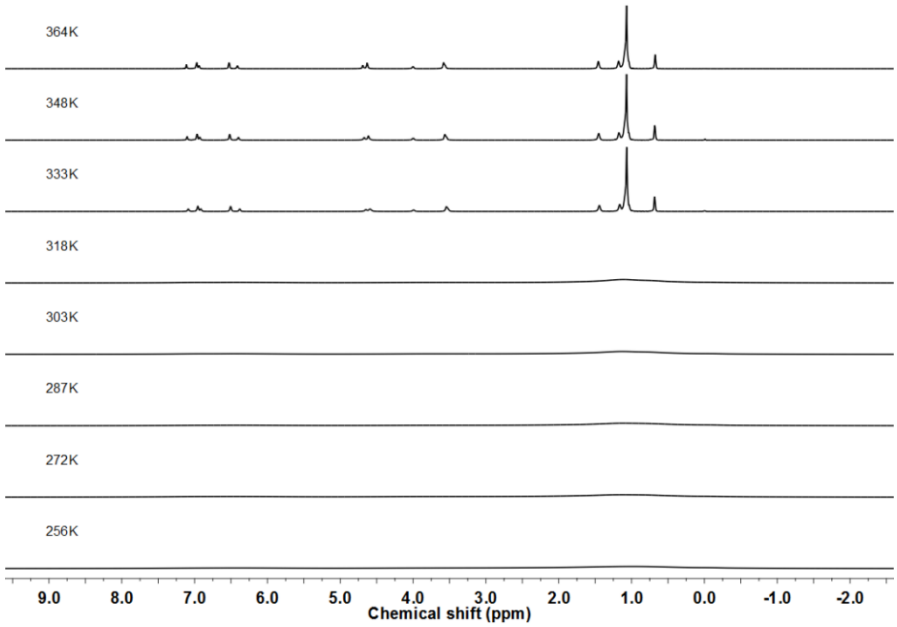

Figure 4.4. ^{1}H MAS NMR spectra of PA1.1 copolymer (850 MHz ^{1}H Larmor frequency, 25 kHz MAS frequency, between 256 and 364 K).

Figure 4.5 shows a magnification of the region between -2 and 9 ppm of the PA1.1 copolymer in the ^{1}H MAS spectra from 256 to 318 K. Due to the rigid nature of the sample at low temperatures, the proton resonances are broad and have a low intensity in this temperature range.

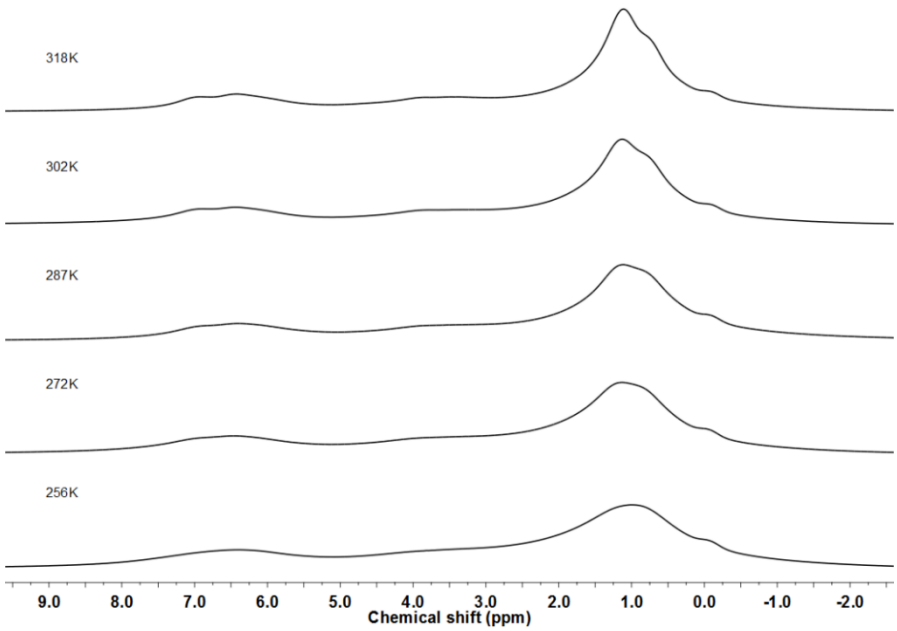

Figure 4.5. ^{1}H MAS NMR spectra of PA1.1 copolymer (850 MHz ^{1}H Larmor frequency, 25 kHz MAS frequency, between 256 and 318 K).

For this copolyamine, the observed thermal transitions (melting and clearing) appear close to each other. Within this narrow temperature interval, a highly mobile LC phase, as it is often observed in NMR studies of low molecular liquid-crystalline compounds and which requires molecular motions with correlation times shorter than 10 µs, cannot fully develop below the clearing temperature. Nevertheless, the onset of molecular motion in the LC phase is reflected in the slightly improved spectral resolution at 318 K.

Another evidence that the melting and the clearing of the PA1.1 copolymer occur between 318 and 333 K is found in the VT ^{13}C CP-MAS NMR spectra (**Figure 4.6**). Using this experiment, all peaks vanish from the spectra at temperatures higher than 333 K, which confirms that this copolyamine is in an isotropic liquid phase. Thus, these spectra are in

agreement with the previously shown results obtained by ^{1}H MAS NMR (**Figure 4.4**).

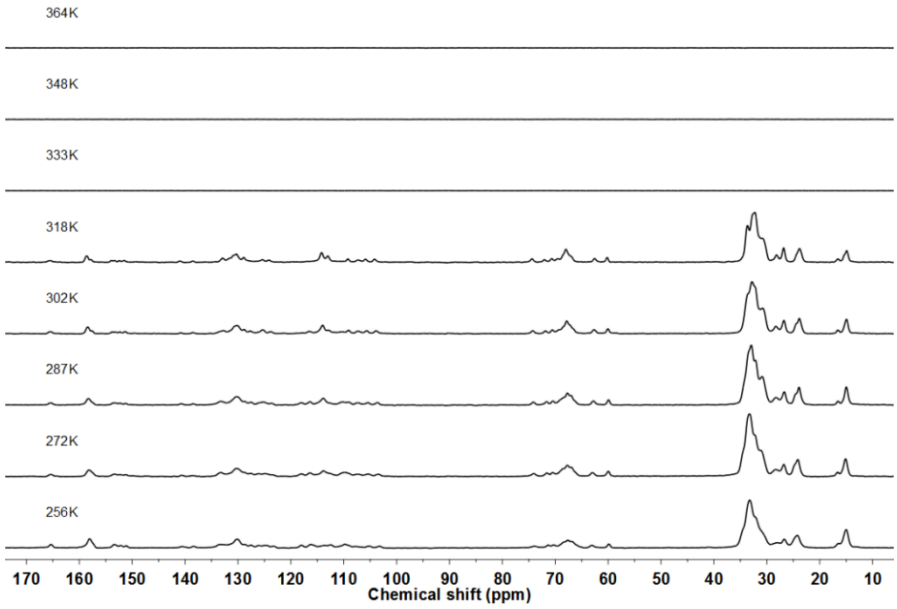

Figure 4.6. ^{13}C CP-MAS NMR spectra of PA1.1 copolymer isolated after precipitation (first heating run, 850 MHz, 25 kHz MAS frequency, between 256 and 364 K).

Additionally, in the temperature range from 256 to 318 K some changes are highlighted:

- In the aliphatic region, there are two peaks with different intensities around 14 ppm, which corresponds to the end methyl group ($–CH_3$) of the aliphatic chain of the pendant TAP dendrons. To explain why this signal splits in two different peaks we need to refresh the structure of the dendron. As we can see in **Figure 4.1**, the dendrons contain three aliphatic chains, one in the center

surrounded by two more chains (lateral aliphatic chains). We suggest that the central chains present a different packing than the lateral chains in the dendrons. Another remarkable thing is that between 30-35 ppm is possible to see how, when increasing the temperature, the aliphatic chains change their conformation basically from a predominant *anti* conformation at 256 K (around 33 ppm) to an intermediate conformation between *gauche* and *anti* conformation seen at 318 K (around 31 ppm). [22]

- In solution NMR the signals of the polymer backbone have been observed between 40 and 60 ppm. In solid state NMR measurements, however, the signals of the polymer backbone could not be observed, which might be either due to molecular reorientations on an unfavourable timescale and thus interfering with the line narrowing techniques of solid state NMR, or due to a broad spread of possible conformations leading to an extreme broadening of the weak backbone signals, so that these signals occur only as baseline distortions in the solid state NMR spectrum.
- In the aromatic region, most of the carbon signals split in more than one peak. The different packing arrangements inside TAP moieties of the copolymer are responsible for additional splittings of carbon NMR signals beyond the number of chemically distinct sites of phenyl rings in every TAP group. As an example, in **Figure 4.7** two different peaks for the carbon assigned as IV' and three or four signals for the carbon assigned as III' can be seen. (**Table 4.2**).

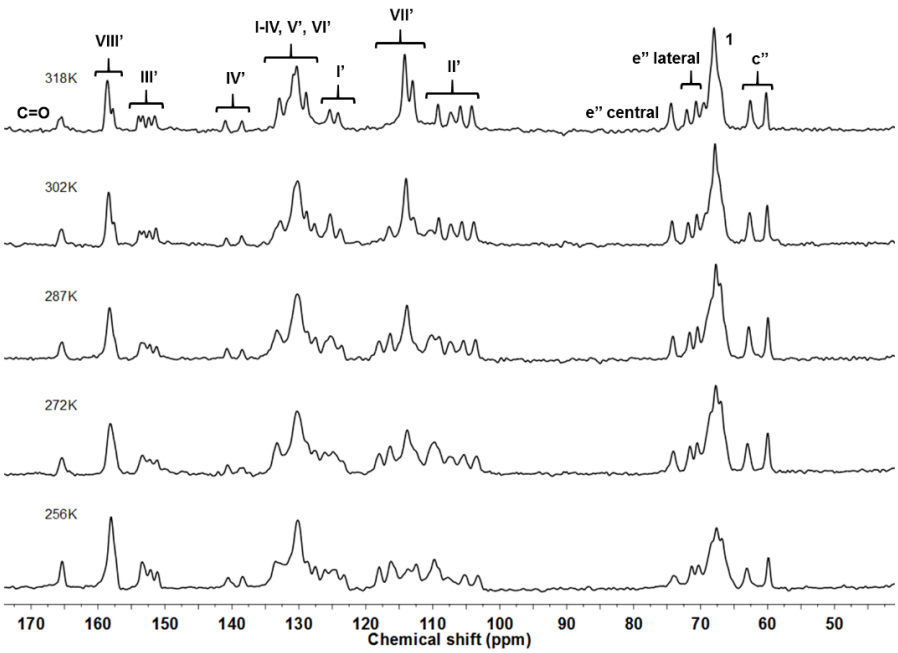

Figure 4.7. ^{13}C CP-MAS NMR spectra of PA1.1 copolymer isolated after precipitation (first heating run, 850 MHz, 25 kHz MAS frequency, between 256 and 318 K).

Usually, the NMR experiments were recorded after the purification of the copolymers (first heating). To purify these copolymers, a precipitation process was used. However, as shown in **Figure 4.3**, the DSC trace recorded after the isolation of the PA1.1 copolymer by precipitation (curve a) differs substantially from the DSC results obtained in the second heating run, in which the copolymer was melted and cooled to solid state prior to the acquisition of curve b. [20] Analogous to DSC, also a second acquisition of ^{1}H and ^{13}C CP-MAS experiments were performed after cooling the molten copolymer to the solid state.

In ^{1}H MAS NMR, no differences were detected between the spectra recorded during the first and the second heating. But when the ^{13}C CP-MAS spectra are compared, some differences can be highlighted:

- In **Figure 4.8**, between 256 and 302 K, every carbon signal appear as a single broad peak as opposed to what was observed in **Figure 4.7**, in which spectra most of carbon signals appear splited in more than one peak.
- At 318 K, is appreciable the most obvious difference between the spectrum acquired in the first and the second heating run. At this temperature, a weak intensity of the remaining peaks in the second heating if compared with the spectra obtained in the first heating is detected. We can assume that the copolymer is melted because the temperature used to acquire this spectrum is truly close to the melting temperature of the copolymer (**Figure 4.3**, curve b).
- Therefore, the peaks in the spectrum acquired at 318 K are attributed mainly to the remaining LC mesophase of the copolymer, which is less stable than the crystalline phase. These remaining signals are splited in the same number of peaks as in the spectrum obtained during the first heating as an evidence that confirms still the presence of the LC mesophase. As an example, in both spectra acquired at 318 K it is possible to distinguish four signals for the carbon assigned as II' and two signals for the carbon assigned as VII'.

As commented, in this particular sample the results of the experiments differ if the DSC or NMR experiments were done with the solution crystallised copolymer or if the analysis were done with the melt crystallised copolymer. With this behaviour, it is evident that the properties of PA1.1 copolymer strongly depends on the processing.

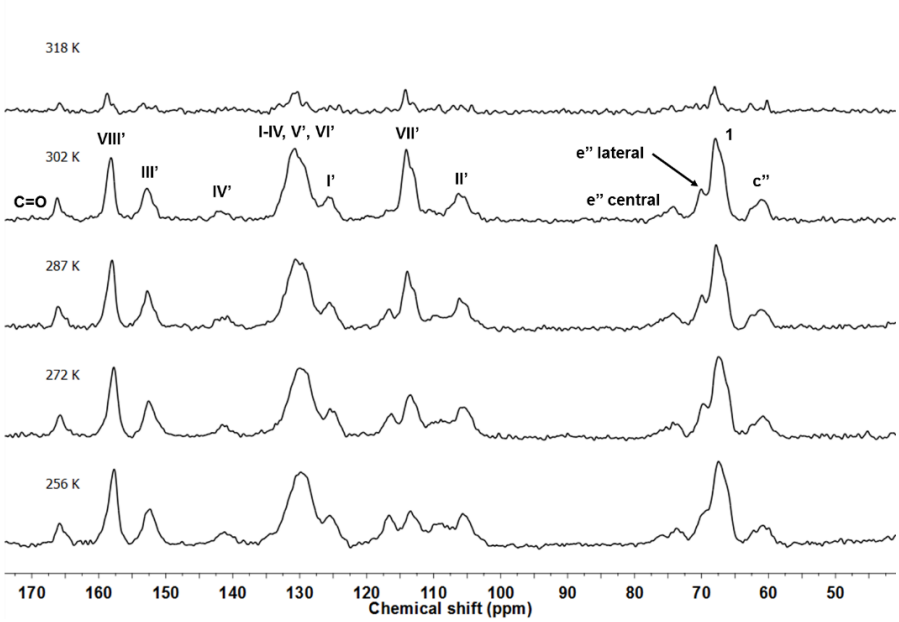

Figure 4.8. ^{13}C CP-MAS NMR spectra of crystallised PA1.1 copolymer after cooling from the molten state (second heating run, 850 MHz, 25 kHz MAS frequency, between 256 and 318 K).

a.1) Temperature and solvent dependent phase studies with Polarised Optical Microscope (POM)

In order to analyse the influence of the LC mesophase on the local molecular packing by solid-state deuterium NMR [23], we previously carried out a temperature and solvent dependent phase study using POM. This study was performed to check if the addition of the solvent (benzene was selected for this study) affects the formation of the LC mesophase of the PA1.1 copolymer.

For this experiment, solutions of this copolymer with different concentrations were analysed using benzene as a solvent (10, 20, 50, 70 and 80 wt%). However, when we performed the thermal study to isolate the LC

mesophase of the PA1.1 in a benzene solution, as we did before with this copolymer but without using any solvent, we observed the predominance of the crystalline phase of this copolymer in solution. These fact demonstrates that in order to observe the LC behaviour of the PA1.1 copolymer in solution and thus avoiding the problem that the two thermal transitions (melting and clearing) are very close in temperature, the use of another solvent instead of benzene is needed. Moreover, the substitution of the solvent can vary the required molecular correlation times necessary to detect the characteristic LC behaviour of the copolymer. Finding the ideal solvent for this study, however, will be a demanding task requiring substantial time and chemical resource, and therefore has not been followed in this work.

b) Mobility of PA3 copolyamine

Using the same methodology as used for the sample PA1.1, VT ^{1}H MAS and ^{13}C CP-MAS experiments were performed in order to understand the nature of dynamic processes in the case of PA3 copolymer. Furthermore, VT ^{13}C INEPT MAS was acquired to complement the information obtained about molecular dynamics with the ^{13}C CP-MAS. [24, 25] The comparison of the ^{13}C MAS spectra acquired with CP and INEPT ^{1}H-^{13}C polarisation transfer is a convenient way of obtaining site-resolved qualitative information about molecular segment dynamics.

Table 4.4 summarizes the transitions observed by DSC, ^{1}H MAS and ^{13}C CP-MAS NMR analysis. DSC analysis of PA3 copolymer put into evidence two endotherms at 260 and 376 K, which were assigned to the melting and the clearing transitions, respectively, by the aid of DSC and POM.

Table 4.4. Transitions observed by DSC, ^{1}H MAS and ^{13}C CP-MAS NMR analysis for PA3 copolymer.

DSC (K) [a]	^{1}H and ^{13}C CP-MAS NMR (K) [b]	Chemical shifts (ppm) of ^{1}H MAS NMR [c]	Chemical shifts (ppm) of ^{13}C CP-MAS NMR [c]	Observations
260	256-272	0.0-8.0	14.0-166.0	melting
376	Not reached [d]	-	-	clearing

[a] Temperature of the peak maximum.
[b] Temperature at which transitions are observed.
[c] Chemical shifts of the groups involved in the transition.
[d] Clearing temperature not reached using the selected VT range.

Figure 4.9 shows the ^{1}H MAS NMR spectra between -2 and 9 ppm of the PA3 copolymer from 256 to 364 K. As we can see, the sample is very rigid at 256 K, but at temperatures higher than the melting point (260 K), the proton spectra exhibits a remarkable line narrowing with the increasing temperature.

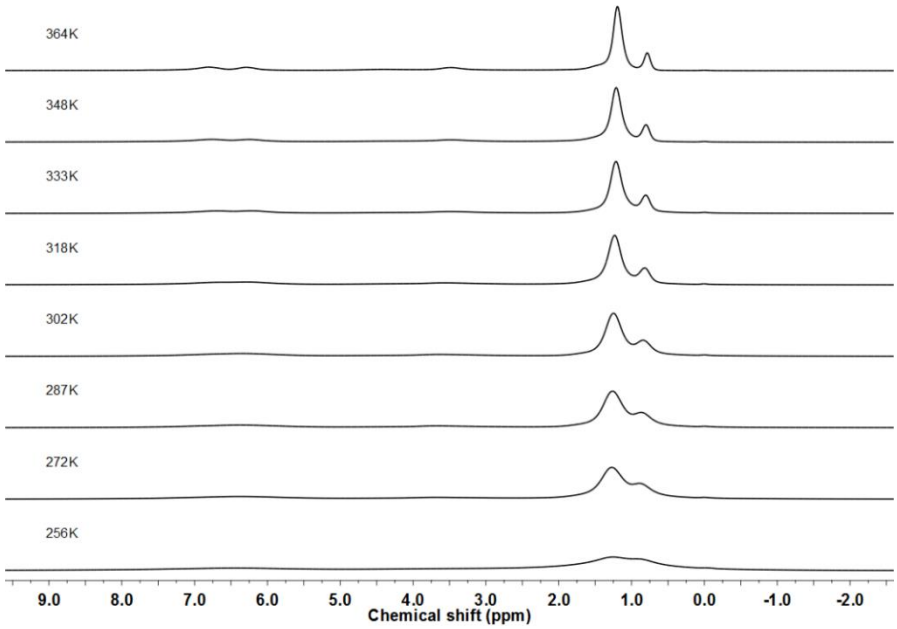

Figure 4.9. ^{1}H MAS NMR spectra of PA3 copolymer (850 MHz ^{1}H Larmor frequency, 25 kHz MAS frequency, between 256 and 364 K).

Comparing to PA1.1 copolyamine, the rest of the synthesised copolyamines are more mobile than this copolymer at temperatures between 272 and 318 K. We can find evidences of this behaviour in ^{1}H MAS and ^{13}C CP-MAS spectra performed at 256 and 272 K. The ^{1}H MAS spectra shows very broad peaks in the case of polymer PA3 at 256 K, while when this spectra was performed at 272 K, the peaks start getting defined. In a similar way, the peaks in the ^{13}C CP-MAS NMR spectrum at 256 K are very broad when we compared with the peaks of the same spectrum performed at 272 K. This information is in agreement with the observed transition at 260 K by DSC and confirms that the PA3 copolymer melts in this temperature range.

In ^{13}C CP-MAS spectra, at temperature below the melting point the peaks are very broad. For this copolymer, with the performed VT solid state NMR study is not possible to reach the clearing temperature. The presence of some peaks in the ^{13}C CP-MAS spectra acquired at 364 K indicates that the clearing point was not reached at this temperature. Furthermore, several changes were detected in **Figure 4.10** between 256 and 364 K:

- In the aliphatic region, the intensity of the signal around 14 ppm, which corresponds to the methyl group of the aliphatic chains, starts to decrease at a temperature higher than the melting point (260 K). This fact indicates as well that the aliphatic region of the dendron contributes to the melting of the polymer.
- Moreover, at 256 K a carbon peak centred at 33 ppm is observed. This signal corresponds to the carbons 2 and 4-9 of the TAP chains being in all-*anti* conformation. When we increase the temperature to 272 K, this signal moves upfield in the spectrum (around 30 ppm). The movement of this chemical shift can be caused by the changes in the conformation from a predominant *anti* conformation at low temperatures to a more random conformation of the aliphatic chains of TAP groups with stronger *gauche* contributions.
- In **Figure 4.11**, where a magnification of the ^{13}C CP-MAS spectra between 256 and 287 K is presented, we can observe a broad halo in the region between 40 and 65 ppm in ^{13}C CP-MAS spectra, which can be assigned to the main chain of the polymer. At low temperatures, the structure of the inner part of the polymer is completely rigid, and the final irregular conformation of the copolymers was determined by the attached benzoyl and TAP groups (**Figure 4.12**). As a result, this irregular conformation gives a very broad distribution in the ^{13}C CP-MAS spectra. When the temperature increase, the intensity of this shadow decreases considerable, which shows that the polymer main chain gains some mobility at higher temperatures than the melting point.

- In the region between 65 and 80 ppm, we can observe how the intensity of the peaks decreases between 256 and 364 K. However, the appearance of the signal at 68.7 ppm attributed to the –O**CH$_2$**–($C_{11}H_{23}$) groups at 364 K demonstrates that even at this temperature this part of the molecule has a certain rigidity, indicating that the –O**CH$_2$**–($C_{11}H_{23}$) groups contribute to the clearing.
- Similarly than in other regions, we observe a homogeneous decay in intensity of the aromatic peaks in the ^{13}C MAS spectrum between 256 and 364 K. Finally, when the experiment was performed at the highest temperature, there is no evidence of peaks in this region.

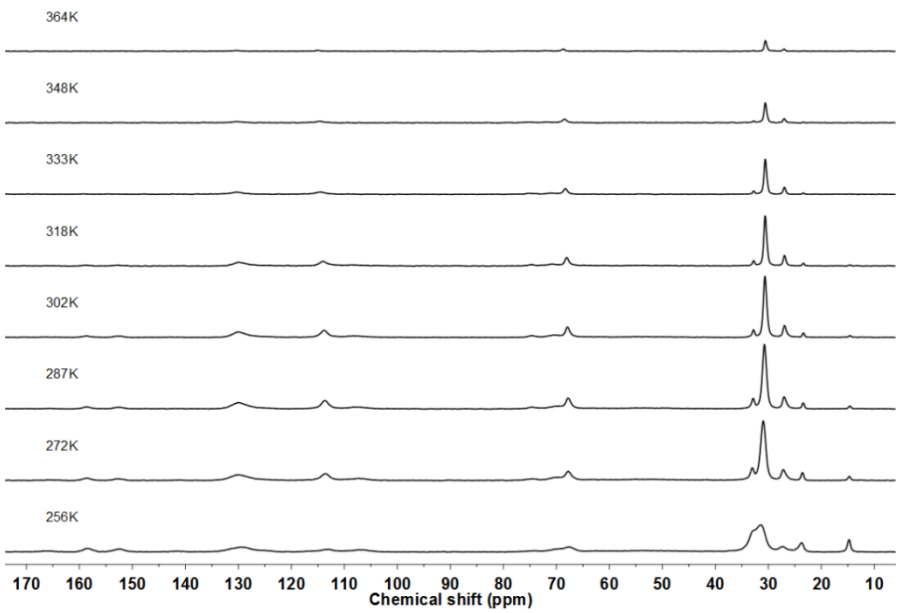

Figure 4.10. ^{13}C CP-MAS NMR spectra of PA3 copolymer (850 MHz, 25 kHz MAS frequency, between 256 and 364 K).

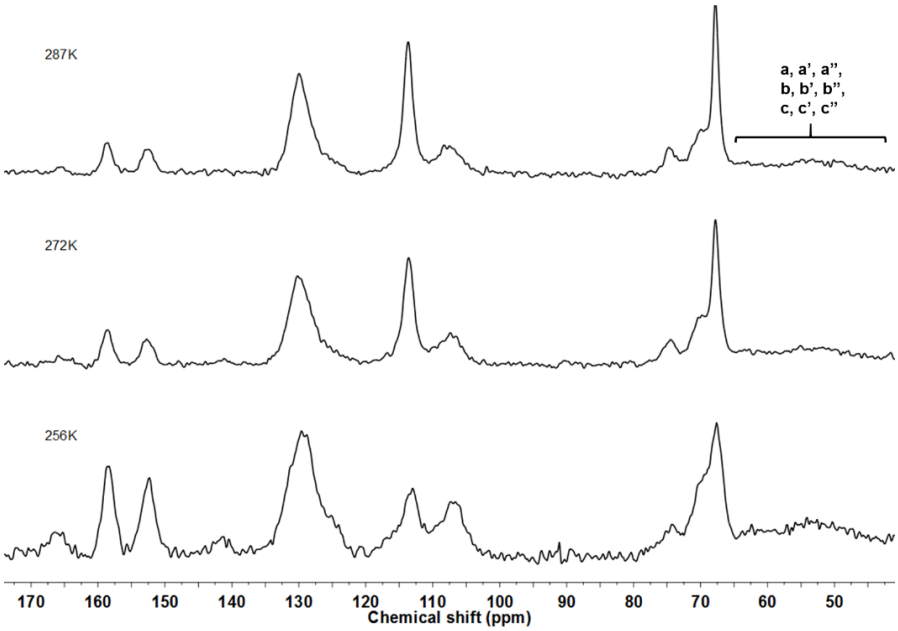

Figure 4.11. ^{13}C CP-MAS NMR spectra of PA3 copolymer (850 MHz, 25 kHz MAS frequency, between 256 and 287 K).

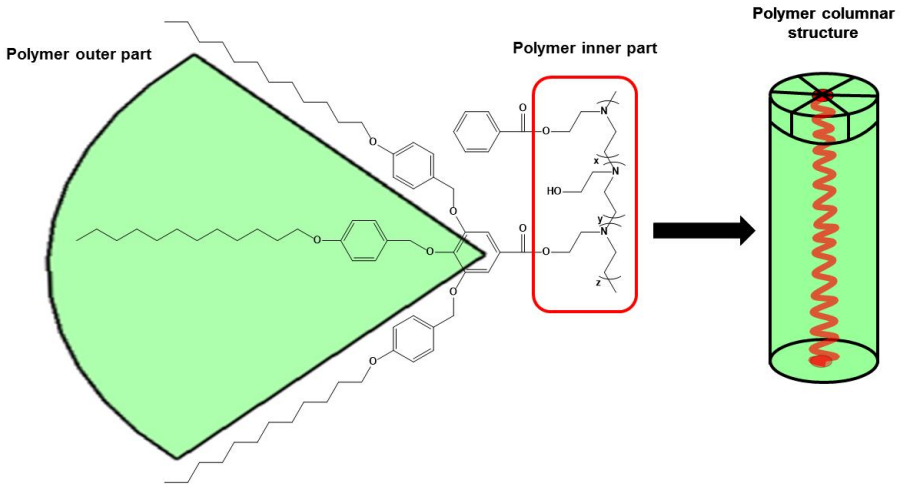

Figure 4.12. General chemical structure of dendronised copolyamines that self-assemble into a columnar structure.

c) Mobility of PA4 copolyamine

In the same way as for PA3, the PA4 copolymer was studied using the VT ^{1}H MAS and ^{13}C CP-MAS experiments.

Table 4.5 summarizes the transitions observed by DSC, ^{1}H MAS and ^{13}C CP-MAS NMR analysis. DSC analysis of PA4 copolymer put into evidence two peaks at 259 and 354 K, which were assigned to melting and clearing, respectively, by the aid of DSC and POM.

Table 4.5. Transitions observed by DSC, ^{1}H MAS and ^{13}C CP-MAS NMR analysis for PA4 copolymer.

DSC (K) [a]	^{1}H and ^{13}C CP-MAS NMR (K) [b]	Chemical shifts (ppm) of ^{1}H MAS NMR [c]	Chemical shifts (ppm) of ^{13}C CP-MAS NMR [c]	Observations
259 354	256-272 350-370	0.0-8.0 0.7-1.7; 2.0-5.3; 6.4-7.7	14.0-166.0 26-31; 68; 114.5; 130.0 (peaks that vanish)	melting clearing

[a] Temperature of the peak maximum.
[b] Temperature at which transitions are observed.
[c] Chemical shifts of the groups involved in the transition.

Figure 4.13 shows the VT ^{1}H MAS NMR spectra between -2 and 9 ppm of the PA4 copolymer. As similar as PA3, the PA4 copolyamine presents a rigid structure at 256 K, but the proton spectrum exhibits a gradual line narrowing with increasing the temperature between 272 and 364 K.

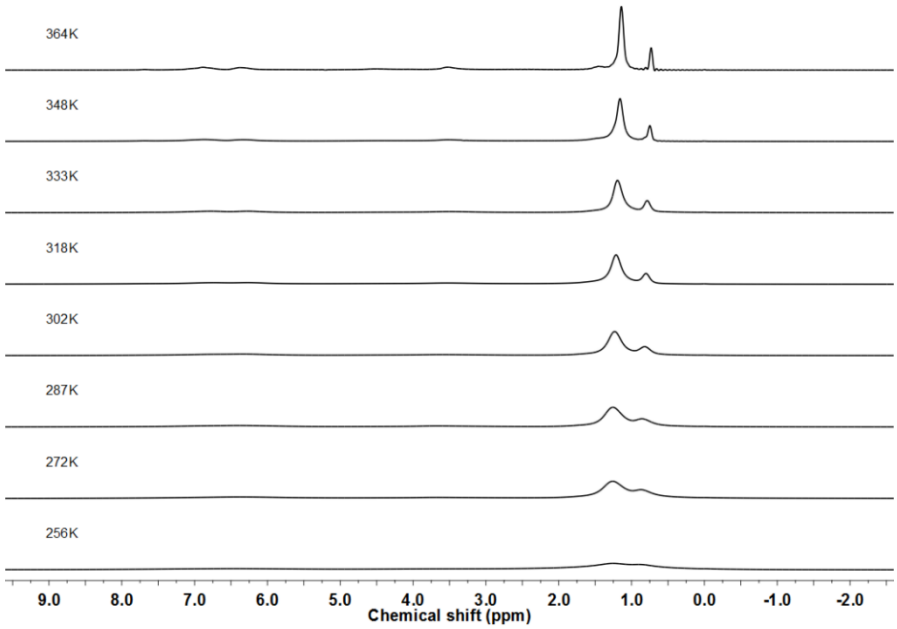

Figure 4.13. ^{1}H MAS NMR spectra of PA4 copolymer (850 MHz ^{1}H Larmor frequency, 25 kHz MAS frequency, between 256 and 364 K).

As we expected, at temperatures below the melting point the peaks are very broad in the ^{13}C CP-MAS spectra. For PA4 copolymer, the clearing takes place between 348 and 364 K because all the peaks have almost vanished at the spectrum performed at 364 K (At this temperature only a tiny signal of the methylene units related to the aliphatic chain of TAP is still observable). Furthermore, several changes were observed in **Figure 4.14** between 256 and 364 K:

- In the aliphatic region, the intensity of the signal around 14 ppm, which corresponds to the methyl group of the aliphatic chains, starts to decrease at a temperature higher than the melting point (259 K). Similarly to the sample PA3, the aliphatic region of the dendron contributes to the melting of the copolymer.

- Moreover, at 256 K a carbon signal is observed at a chemical shift of 32 ppm, which can be assigned to the carbons 2 and 4-9 of the TAP chains in a mainly *anti* conformation. At a higher temperatures than the melting point this signal moves upfield in the spectrum (around 30 ppm), where the aliphatic chains shows a random conformation with predominant *gauche* contributions.
- Another remarkable thing is the observation of a broad halo in the ^{13}C CP-MAS spectra between 40 and 65 ppm (256-287 K), which can be assigned to the main chain of the polymer. Between 256 and 287 K the structure of the inner part of the polymer is completely rigid, and the final irregular conformation of the copolymers was determined by the attached benzoyl and TAP groups. As a result, this irregular conformation gives a very broad distribution in the ^{13}C CP-MAS spectra. When the temperature increases, the intensity of this shadow decreases considerable, which shows that the polymer main chain gain some mobility at higher temperatures than the melting point.
- Furthermore, in the region between 65 and 80 ppm and the region comprising the aromatic signals all the peaks vanish at 364 K. This evidence indicates that both $–OCH_2–$ groups and aromatic moieties contribute to the clearing because at temperature higher than the clearing these moieties are completely mobile.

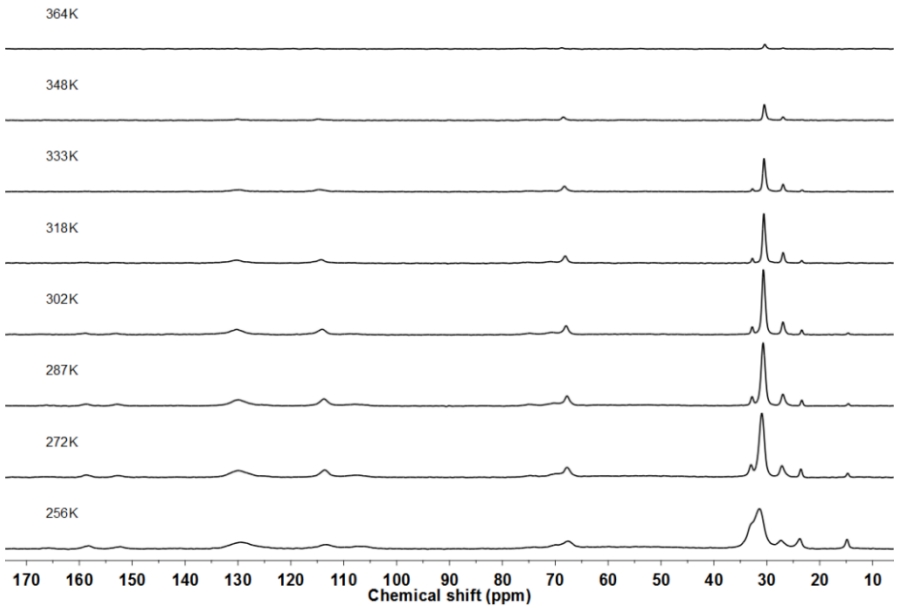

Figure 4.14. ^{13}C CP-MAS NMR spectra of PA4 copolymer (850 MHz, 25 kHz MAS frequency, between 256 and 364 K).

However, as we can see in **Table 4.1**, the clearing temperatures for most of these samples (except for PA1.1) were detected in the range between 347 and 378 K by DSC and POM. In this way, to evaluate the behaviour around the clearing temperature of these copolyamines by using VT solid state NMR, we performed the VT ^{1}H MAS, ^{13}CP-MAS experiments in another range of temperature (310 to 390 K). The PA4 copolymer was selected for this analysis. Also, VT ^{13}C INEPT MAS was acquired to complement the information obtained about molecular dynamics with the ^{13}C CP-MAS.

Figure 4.15 shows a magnification of the VT ^{1}H MAS NMR spectra between 2 and 9 ppm of the PA4 copolymer from 310 to 390 K. At temperatures below the clearing (354 K), the proton resonances appear as broad signals, but when we increase the temperature, the peaks experience a continuous line narrowing in the spectra. As we expected, the ^{1}H MAS

spectrum at 390 K appears well resolved. Moreover, at higher temperatures than the clearing it is possible to distinguish a peak at 7.7 ppm, which is attributed to the protons in *ortho*- position of the benzoyl units attached to the copolymer. In the region between 3 and 5.5 ppm we could see four peaks: two peaks centred at 5.3 and 4.6 which are attributed to the –O**CH$_2$**Ph– in the central and lateral positions of the dendrons; and two more peaks centred at 4.1 and 3.6 ppm which are assigned to the –O**CH$_2$**C$_{11}$H$_{23}$ groups in the dodecyl chain. Furthermore, at higher temperatures than the clearing point, for this copolymer we observe a broad peak centred at 2.6 ppm which could be assigned to the copolymer main chain.

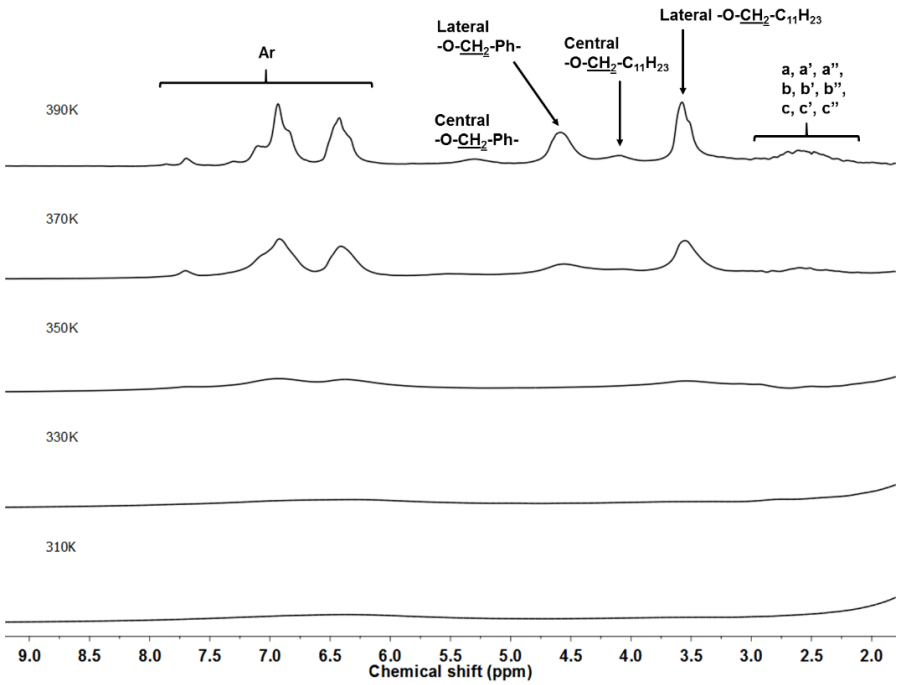

Figure 4.15. ^{1}H MAS NMR spectra of PA4 copolymer (500 MHz ^{1}H Larmor frequency, 10 kHz MAS frequency, between 310 and 390 K).

The VT ^{13}C CP-MAS confirms that the clearing temperature was reached between 350 and 370 K. In **Figure 4.16** it is possible to observe how all the peaks vanish in the spectra at temperatures above the clearing temperature (354 K), besides a tiny signal of the methylene units of the aliphatic chain of TAP can be observed at 370 K.

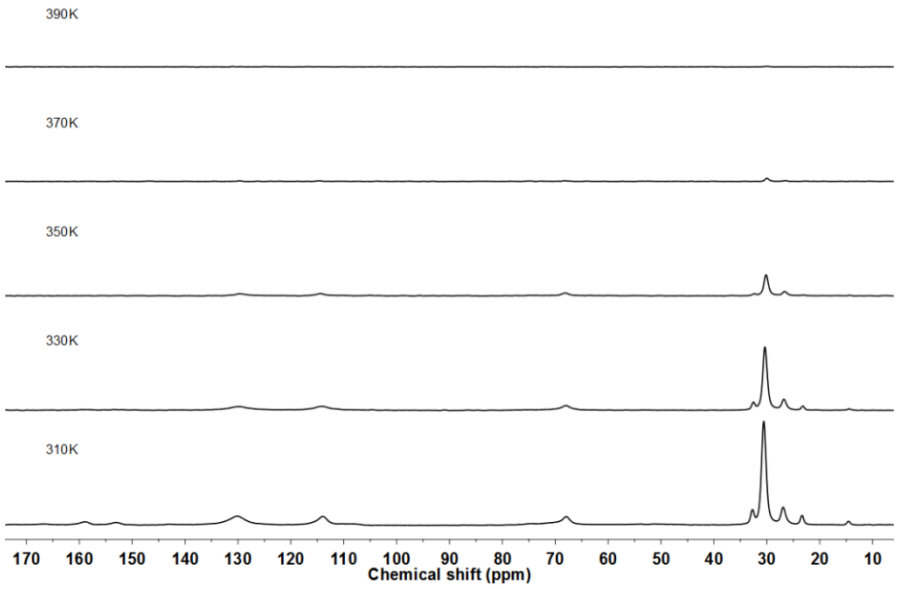

Figure 4.16. ^{13}C CP-MAS NMR spectra of PA4 copolymer (500 MHz, 10 kHz MAS frequency, between 310 and 390 K).

On the other hand, to evaluate the mobile regions of PA4, VT ^{13}C INEPT MAS experiment was carried out. The resulting spectra are presented in **Figure 4.17**. At 330 K, only peaks in the aliphatic region appear, which demonstrate that the aliphatic chains gain some mobility at temperatures below the isotropisation temperature (354 K). It is evident that the intensity of the peak that appears around 14 ppm, which corresponds to

the methyl group of the long aliphatic chains of the TAP, is higher than the other peaks of the aliphatic region in the spectra. This points out that the terminal $–CH_3$ groups are more mobile than the rest of the aliphatic chain at 330 K. This fact was in agreement with the intensity decrease of the peak which corresponds to C_{12} at 14 ppm in the ^{13}C CP-MAS spectra in the same range of temperature. All these evidences confirms that the melting transition affects the outer part of the dendrons.

Between 330 and 350 K, the carbons C_{12}, C_{11}, $C_{4\text{-}9}$ and C_2 of the side alkyl chains (14, 23, 30 and 33 ppm) are quite mobile. In contrast, the spectrum at 390 K displays intense signals in all the regions of the spectrum (aliphatic, $–OCH_2–$ and the aromatic regions of the copolymer structure), suggesting that these moieties are completely mobile at temperatures above the clearing. Moreover, at temperature slightly above the clearing (370 K), the signal intensities are still biased by restricted mobility at some sites, while the signal intensities at 390 K are almost quantitative and reflect the stoichiometry of the different moieties comprised in PA4 copolymer.

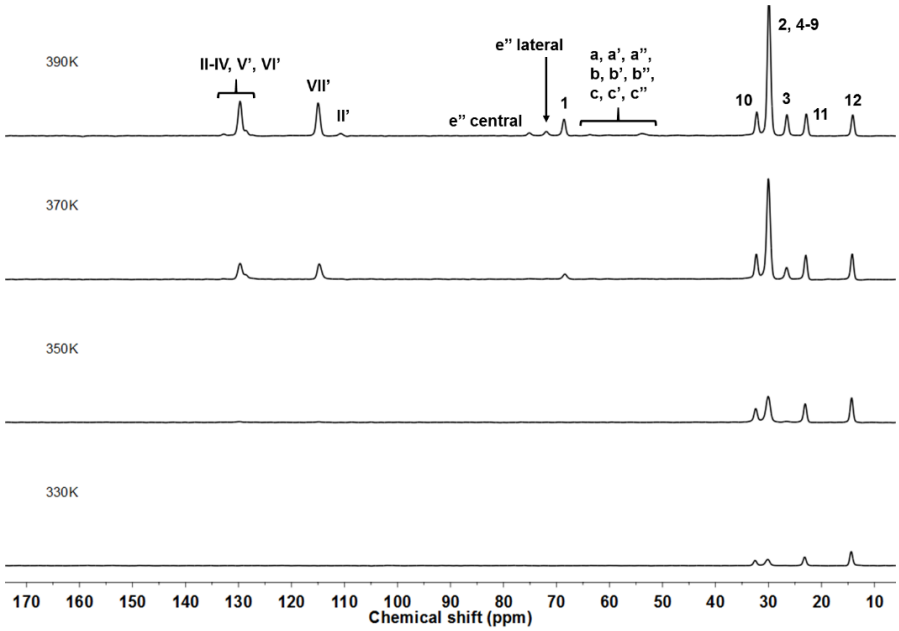

Figure 4.17. ^{13}C INEPT MAS NMR spectra of PA4 copolymer (500 MHz, 10 kHz MAS frequency, between 310 and 390 K).

In fact, all moieties of PA4 copolymer are involved in the clearing transition due to the substantial increase on mobility above the clearing deduced from the different spectra acquired of this copolymer.

4.4. Conclusions

Solid state NMR techniques (^{1}H MAS NMR, ^{13}C CP-MAS NMR and ^{13}C INEPT MAS VT studies) were used in combination with DSC analysis to elucidate the nature of the different thermal transitions of a previously synthesised family of copolyamines.

Moreover, the use of 2D ^{1}H MAS-^{13}C INEPT MAS technique helped us to confirm the chemical structure of PA1.1 copolymer.

Using VT NMR experiments, PA1.1 copolymer shows a different behaviour when compared with the other samples analysed. The first noticeable difference is that with the selected VT range was not possible to discern between the melting and the clearing transitions for the PA1.1 copolymer in the first heating run. Nonetheless, the observed differences in the spectra of the PA1.1 copolymer in the first and second heating run gives information about the different behaviour of that sample depending on the pre-treatment performed on the material: when PA1.1 copolymer was isolated after precipitation, the growth of the crystalline phase is more favoured; while the analysis of the melt crystallised copolymer detects almost exclusively the LC behaviour and the crystallisation is not observed.

Furthermore, the second heating run provides strong evidences that this copolymer tends to crystallise because in the ^{13}C CP-MAS spectra the signals which are attributed to the LC phase have a very weak intensity in comparison with the peaks attributed to the crystalline phase.

For the copolymers PA3 and PA4, this study confirms that the observed transition between 256 and 272 K refers to melting as we checked before by means of DSC. At higher temperature than the melting point, the methyl group at the end of the aliphatic chains of TAP units gains some mobility, indicating that the melting involves mainly the outer part of the dendrons grafted to the copolymer.

For most of the copolyamines of this family it was not possible to achieve the clearing temperature with the accessible VT range (256-364 K). The presence of some peaks in the ^{13}C CP-MAS spectrum obtained at 364 K for PA3 indicates that some parts of this copolymer are still rigid at this temperature.

In order to evaluate the clearing temperature, ^{1}H MAS, ^{13}C CP-MAS and ^{13}C INEPT MAS were performed selecting another range of temperatures (310-390 K) in the case of the PA4 copolymer. For this sample, the comparison of VT ^{13}C CP-MAS NMR and ^{13}C INEPT MAS gives information

about which moieties are rigid or mobile at temperatures below and above the clearing.

Differently than the supramolecular systems studied by Rapp, the inner and the outer phenyl rings of the dendron show a similar mobility inside these copolymers. Conversely, the dendritic aliphatic branches exhibit a mobility gradient from the inner to the outer part. In this way, the outer part of the aliphatic branches is obviously more affected by the first observed transition in the studied polymers: the melting point.

In conclusion, the usage of solid state NMR techniques provides useful information about the local structure of dendronised polymers, likewise about the dynamics of different molecular building blocks in these complex systems.

4.5. References

1. Lehn J-M. Supramolecular Polymer Chemistry - Scopus and Perspectives, in Supramolecular Polymers. London: Taylor & Francis Group, 2005. pp. 3-28.

2. Brunsveld L, Folmer BJB, Meijer EW, and Sijbesma RP. Chem. Rev. 2001;101(12):4071-4098.

3. Fenniri H, Deng B-L, and Ribbe AE. J. Am. Chem. Soc. 2002;124(37):11064-11072.

4. Steed JW and Atwood JL. Concepts, in Supramolecular chemistry. Chichester: John Wiley & Sons Ltd., 2009. pp. 1-48.

5. Bhattacharya A. Nature 2010;463(7281):605-606.

6. Friebolin H. The Physical Basis of NMR Spectroscopy, in Basic One- and Two-Dimensional NMR Spectroscopy. Weinheim: Wiley-VCH Verlag GmbH & Co. KGaA, 2010. pp. 1-42.

7. Emsley L. J. Am. Chem. Soc. 2013;135(22):8089-8091.

8. Scheler U. Solid Polymers, in Solid-State NMR Spectroscopy Principles and Applications. Oxford: Blackwell Science Ltd, 2007. pp. 483-511.

9. Schmidt-Rohr K and Spiess HW. Multidimensional Solid-State NMR and Polymers. London: Harcourt Brace & Company, 1994.

10. Andrew ER, Bradbury A, and Eades RG. Nature 1958;182(4650):1659-1659.

11. Lowe IJ. Phys. Rev. Lett. 1959;2(7):285-287.

12. Hansen MR, Graf R, and Spiess HW. Acc. Chem. Res. 2013;46(9):1996-2007.

13. Graf R, Hansen MR, Hinderberger D, Muennemann K, and Spiess HW. Phys. Chem. Chem. Phys. 2014;16(21):9700-9712.

14. Hansen MR, Graf R, and Spiess HW. Chem. Rev. 2016;116(3):1272-1308.

15. Rapp A, Schnell I, Sebastiani D, Brown SP, Percec V, and Spiess HW. J. Am. Chem. Soc. 2003;125(43):13284-13297.

16. Ronda JC, Reina JA, and Giamberini M. J. Polym. Sci., Part A: Polym. Chem. 2004;42(2):326-340.

17. Bhosale SV, Rasool MA, Reina JA, and Giamberini M. Polym. Eng. Sci. 2013;53(1):159-167.

18. Šakalytė A, Reina JA, and Giamberini M. Polymer 2013;54(19):5133-5140.

19. Montané X, Bhosale SV, Reina JA, and Giamberini M. Polymer 2015;66:100-109.

20. Montané X, Bogdanowicz KA, Colace G, Reina JA, Cerruti P, and Giamberini M. Submitted 2016.

21. Šakalytė A, Reina JA, Giamberini M, and Lederer A. Polym. Eng. Sci. 2014;54(3):579-591.

22. Schmidt-Rohr K and Spiess HW. Macromolecules 1991;24(19):5288-5293.

23. Spiess HW. Colloid. Polym. Sci. 1983;261(3):193-209.

24. Nowacka A, Bongartz NA, Ollila OHS, Nylander T, and Topgaard D. J. Magn. Reson. 2013;230:165-175.

25. Warschawski DE and Devaux PF. J. Magn. Reson. 2000;145(2):367-372.

Chapter 5

Columnar liquid-crystalline polyglycidol derivatives: a novel alternative for proton-conducting membranes

Xavier Montané, Suryakant Vilasrao Bhosale, José Antonio Reina, Marta Giamberini*

*- Polymer 2015;66:100-109

5.1. Introduction

Most research in the field of proton conductivity has been devoted by the materials science community in the last thirty years, mainly for the development of new proton-conducting materials to be used in electrochemical cells (e.g. fuel cells, batteries, sensors). In this field, perfluorosulfonic acid (PFSA) membranes, such as Nafion® (marketed by DuPont), represent the benchmark materials for their proton-conducting properties. [1] However, these materials exhibit serious drawbacks, such as the need of controlling water management, relative affinity of methanol and water in direct methanol fuel cells (DMFCs), mechanical, thermal and oxidative stability, high cost and environmental inadaptability. For this reason, more than 200 patents and papers have been recently published on the preparation of new proton-conducting membranes. [2-5] An alternative approach is to design materials containing ion transport channels, in which the channels localize the permeation path and simultaneously protect the transport process against the environment, like an ion-transporting molecular cable. [6-9]

Percec and coworkers have comprehensively investigated the self-organisation of supramolecular monodendrons and styrene-, methacrylate-, or oxazoline-based polymers for the design of ion-active nanostructured supramolecular systems. [10-14]

Columnar structures were also obtained for liquid-crystalline block copolymers based on dendronised polymers from poly(ethyleneglycol), polystyrene or polymethacrylate (PMA). [15-17] In this case, the combination of dendrimer structure with the characteristic microphase separation of traditional linear block copolymers, gives rise to macromolecular architectures which can find several applications such as optical storage materials or membranes. Successful perpendicular or parallel orientation of cylindrical nanodomains has recently been obtained for a liquid-crystalline block copolymer based on poly(ethylene oxide) and PMA-bearing

azobenzene mesogen side chains, by air-anchoring or surface effect, respectively. [18]

In our previous studies, [19-21] we reported the chemical modification of poly(epichlorohydrin) (PECH) and poly(epichlorohydrin-co-ethylene oxide) [P(ECH-co-EO)] with tapered mesogenic groups to yield high-molecular-weight polyethers with different degrees of modification. As we reported, these polymers self-assemble into a columnar structure, due to an exo-recognition of the side-chain dendrons. In the resulting structure, the polyether main chain forms a channel in the inner part of the columns, while the hydrophobic side-chain dendrons lie in the outer part. The presence of the polar ether linkages in the inner channel favours the interaction with proton and other cations, in the same way as crown ethers would do. [22] For this reason, the inner polyether chain could work as an ion channel. Satisfactory orientation of the polymer was achieved by sandwiching the polymer solution between a water layer and a wet glass layer to induce unfavourable surface interactions between the outer, hydrophobic portion of the columns and their surroundings. The presence of oriented channels in the polymeric membrane resulted in remarkable proton permeability, around $2 \cdot 10^{-6}$ $cm^2 \cdot s^{-1}$, comparable to that of Nafion® N117. [23] However, the procedure used to prepare the oriented membranes had poor reproducibility.

Another drawback which could be exhibited by polyethers obtained out of modified PECH and [P(ECH-co-EO)], lies in the presence of remaining chlorine atoms in the modified polymers, which can lead to long-term development of radical reactions that could alter polymer structure and accelerate its degradation. Polyols like linear polyglycidol (LPG) can be other suitable polyether candidates which can be modified with 3,4,5-tris[4-(n-dodecan-1-yloxy)benzyloxy]benzoic acid (TAP) in order to obtain liquid-crystalline columnar polyethers, which do not contain chlorine. In this paper, we investigated the modification of LPG using carbodiimide mediated Steglich esterification between free hydroxyl groups of the linear polyglycidol and carboxylic groups of the dendron under different conditions. The use of

a lower molecular weight precursor polymer, could lead to systems that can be more easily oriented: therefore, chemical modification was performed on a relatively low molecular weight LPG. In this way, we also intended to test the performances of a lower molecular weight modified polyether as far as orientation and transport are concerned. Modified LPGs were subsequently studied in terms of liquid-crystalline behaviour. It was found that modified LPGs are showing different mesophases like lamellar columnar, rectangular columnar (distorted hexagonal) and hexagonal columnar depending on the degree of modification, the higher the number of dendrons, the more ordered the mesophase. Finally, we prepared oriented membranes based on selected copolymers, having three different modification degrees. In this case, membrane orientation was achieved by means of a simpler and reproducible thermal treatment on fluorinated ethylene propylene sheet support. The obtained membranes exhibited promising proton permeabilities, in one case comparable to that of Nafion® and negligible water uptake. Therefore, transport can be attributed to the presence of the oriented channels.

5.2. Experimental

5.2.1. Materials

All the chemicals were purchased from Sigma–Aldrich, while all solvents were purchased from Scharlab. *p*-toluenesulfonic acid monohydrate (TsOH, 98.5%), potassium *tert*-butoxide (1 M solution in THF), 4-dimethylaminopyridine (DMAP, ≥98.0%) and *N,N'*-dicyclohexyl-carbodiimide (DCC, ≥99.0%) were used as received. Glycidol (96%) was distilled under reduced pressure and stored over molecular sieves at 2-5˚C. Diglyme [bis(2-methoxyethyl) ether] was first shaken with a weakly acidic ion-exchange resin (Amberlite IR-120) to remove the amine-like odour. After filtered the solution, it was distilled at reduced pressure from CaH_2. [24] *N,N*-dimethylformamide (DMF, 99%) were predried using powder molecular sieves before distilling under vacuum. Linde type 4 Å and powder molecular

sieves were previously activated by heating them in an oven at 220˚C for 48 h, and then left to cool and kept under argon atmosphere in a well-dried flask.

3,4,5-tris[4-(n-dodecan-1-yloxy)benzyloxy]benzoic acid (TAP) was synthesised as previously reported. [25] Yield: 93%.

Synthesis of linear polyglycidol (LPG)

1-ethoxyethyl glycidyl ether was polymerized according to Schmitz et al. [26] Linear polyglycidol was prepared by subsequent removal of the acetal protecting groups of protected linear polyglycidol under acidic hydrolysis conditions (**Scheme S5.1**). Yield: 78%. Degree of polymerization (DP) = 20.

^{1}H NMR (DMSO-d_6, TMS, δ, ppm): = 7.3-7.1 (m), 4.5 (s), 3.7-3.3 (m), 2.6 (t), 1.7 (m).

^{13}C NMR (DMSO-d_6, TMS, δ, ppm): 142.0-125.9, 81.1, 73.0-69.4, 64.8, 61.1, 31.8, 31.2.

Modification of linear polyglycidol

The linear polyglycidol was successfully modified with TAP using carbodiimide mediated Steglich esterification [27] between the free hydroxyl groups of the linear polyglycidol and carboxylic group of TAP (**Scheme 5.1**):

In a three necked round bottom flask, a solution of TAP (2.00 g, 2.01 mmol) was prepared by dissolving into dry DMF (5 mL). Stoichiometric amounts of DMAP and DCC at 0˚C were allowed to stir for 30 min in an Ar atmosphere. The necessary amount of linear polyglycidol was dissolved into dry DMF (5 ml) and added dropwise to the above reaction mixture. The

reaction mixture was allowed to stir for 2 days (7 days in the case of LPG6 attempt) at room temperature under Ar atmosphere. Afterwards, the reaction mixture was precipitated in 500 mL of methanol. Precipitated product was dissolved into THF and re-precipitated in 500 mL methanol. This precipitation was repeated for 5 times, in order to remove DMAP, DCC, free acid and other impurities. After precipitation, the modified polymer was collected and dried at 40˚C *in vacuo* for 48 hours.

Different degrees of modifications and corresponding yields are given in **Table 5.1**.

Membranes preparation

Membranes were prepared by immersion precipitation process, in which a homogeneous polymer solution in THF (30% w/w) was cast on a FEP (fluorinated ethylene propylene) sheet support and immersed in a bath of Milli-Q water. The solvent diffused into the precipitation bath, while the non-solvent (water) diffused into the cast film. After a time in which the solvent and the non-solvent were exchanged, the polymer solution (wet film) became thermodynamically unstable and demixing took place. Finally, a solid polymer membrane was formed with an asymmetric structure. Afterwards, the membrane was dried overnight at room temperature and subsequently used for baking process. The polymer membrane along with FEP sheet was mounted on a hot stage (Linkam TP92) and it was heated above the clearing temperature; then it was allowed to cool slowly (0.5˚C/min) down to room temperature. After the baking process, the membrane was kept at room temperature for approximately 1 hour and then it was separated from the FEP sheet and obtained as an intact, uniform membrane with thickness around 300 µm. The thickness of the membranes was measured using a micrometer with a sensitivity of 2 µm. The measurements were carried out at various points, and the membranes were found to have constant thickness.

Membranes were in their rubbery state at room temperature (**Table 5.3**) and they flowed above their clearing temperature.

5.2.2. Characterisation and measurements

Nuclear magnetic resonance (NMR) spectroscopy

^{1}H NMR and ^{13}C NMR spectra were recorded at 400 and 100.4 MHz, respectively, on a Varian Gemini 400 spectrometer with proton noise decoupling for ^{13}C NMR. The central peak of the solvent was taken as the reference, and the chemical shifts were given in parts per million from TMS (Tetramethylsilane). The ^{13}C NMR spectra of the polymers were recorded at 30˚C, with a flip angle of 45˚, and the number of transients ranged from 20,000 to 40,000 with 10-20% (w/v) sample solutions in DMSO-d_6, $CDCl_3$ or 1,1,2,2-tetrachloroethane-d_2.

Differential scanning calorimetry (DSC)

Thermal transitions were detected with a Mettler–Toledo differential scanning calorimeter mod. 822 in dynamic mode at a heating or cooling rate of 10˚C/min. Nitrogen was used as the purge gas. The calorimeter was calibrated with an indium standard (heat flow calibration) and an indium–lead–zinc standard (temperature calibration).

Polarised optical microscopy (POM)

Clearing temperatures and liquid-crystalline mesophases were investigated by polarised optical microscopy (POM); textures of the samples were observed with an Axiolab Zeiss optical microscope equipped with a Linkam TP92 hot stage.

Density measurements (ρ)

Densities were determined by gas pycnometry using Micrometritics AccuPyc 1330 machine at 30˚C.

Size-exclusion chromatography (SEC)

Average molecular weights were determined in THF by size-exclusion chromatography (SEC); analyses were carried out with an Agilent 1200 series system with PLgel 3 µm MIXED-E, PLgel 5 µm MIXED-D, and PLgel 20 µm MIXED-A columns in series, and equipped with an Agilent 1100 series refractive-index detector. Calibration curves were based on polystyrene standards having low polydispersities. THF was used as an eluent at a flow rate of 1.0 mL/min, the sample concentrations were 5-10 mg/mL, and injection volumes of 100 µL were used.

X-ray diffraction (XRD)

For X-ray experiments, two different diffractometers were used depending on the 2θ range investigated:

For low 2θ range: XRD measurements were performed with a Bruker-AXS D8-Discover diffractometer equipped with parallel incident beam (Göbel mirror), vertical θ-θ goniometer, XYZ motorized stage and with a GADDS (General Area Detector Diffraction System). Samples were placed directly on to a low background Si(510) sample holder for reflection analysis. An X-ray collimator system close-to-the-sample allows to analyse areas of 500 µm. The X-ray diffractometer was operated at 40 kV and 40 mA to generate $Cu_{k\alpha}$ radiation. The GADDS detector was a HI-STAR (multiwire proportional counter of 30x30 cm with a 1024x1024 pixel) placed at 30 cm from the sample. The X-ray beam hit the sample at 0.5˚ of incidence. The collected

frame (2D XRD pattern) covers a 2θ range from 0.9 up to 9.2˚. The diffracted X-ray beam travels through a He beam path (SAXS attachment) to reduce the air scattering at low angles. The direct X-ray beam is stopped by a beam stop placed directly on the detector face. The exposition time was of 300 s per frame. The resulting frames were both radially integrated to obtain a 2θ diffractogram and 2θ integrated to obtain an azimuthal intensity plot. In the case of membranes, XRD experiments were performed on both sides and no differences could be detected.

For medium 2θ range: XRD measurements were performed with a Siemens D5000 diffractometer (Bragg-Brentano parafocusing geometry and vertical θ-θ goniometer) fitted with a curved graphite diffracted-beam monochromator, incident and diffracted-beam Soller slits, a 0.06˚ receiving slit and scintillation counter as a detector. Samples were placed directly on to a low background Si(510) sample holder for reflection analysis. The X-ray diffractometer was operated at 40 kV and 30 mA to generate $Cu_{K\alpha}$ radiation. The angular 2θ diffraction range was between 1 and 40˚. The data were collected with an angular step of 0.03˚ at 6 s per step.

Contact angle measurements (CA)

Contact angles of water drops on a membrane surface were measured with a Kruss contact angle instrument (Hamburg, Germany) equipped with a motorized pipet (Matrix Technology, Nashua, NH) and deionized water as the probe liquid. The contact angle was measured immediately after putting the water drop (3 μL) on the membrane surface. Measurements were repeated using different areas of the membrane. For each test reported, at least three drops of water were used.

Swelling experiments

Swelling experiments were performed by soaking the membranes at room temperature in Milli-Q water and monitoring the change in membrane weight versus time for 24 h.

Proton transport experiments

Transport experiments were carried out using a Teflon test cell that comprised two compartments, separated by the tested membrane, containing the feed and stripping solutions, respectively. The feed and stripping volumes were 200 ml and the effective membrane area was 0.86 cm^2. For the proton transport experiments, the initial feed solution was 0.1 M HCl aqueous solution and the stripping solution was 0.1 M NaCl aqueous solution. The pH of the stripping solution was measured every 30 s by a Crison MM 40 Multimeter. Prior to the proton transport experiments, membranes were conditioned in 0.1 M NaCl aqueous solution for 15 min.

Under steady-state conditions, proton flux was calculated by Fick's First Law:

$$J = \frac{P\Delta C}{l} \cdot 10^{-3} \qquad (1)$$

where *l* (cm) is the membrane thickness and ΔC is the difference in concentration ($mol \cdot l^{-1}$) between the initial feed solution (C_0) and the final stripping solution. In our experimental conditions, C_0 was much greater than the final stripping concentration, so we considered $\Delta C \sim C_0$.

P is the proton permeability ($cm^2 \cdot s^{-1}$), defined as:

$$P = DS \qquad (2)$$

where *D* is the proton diffusion coefficient and *S* is the sorption equilibrium parameter.

The flux is related to the permeability coefficient *p* ($cm \cdot s^{-1}$), as:

$$J = pC_0 \quad (3)$$

$$P = pl \quad (4)$$

The permeability coefficient, can be described by the following equation: [28]

$$-\ln\frac{C_f}{C_0} = \frac{Ap}{V_f}t \quad (5)$$

where C_0 ($mol \cdot l^{-1}$) is the initial concentration of the feed solution and C_f ($mol \cdot l^{-1}$) is the feed concentration calculated from the stripping solution at time t (s):

$$C_f = C_0 - C_s \quad (6)$$

V_f is the feed volume (mL) and *A* is the actual membrane area (cm^2).

We calculated the proton permeabilities in accordance with the above equations. Data were fitted according to equation (5) in the time range $1.2 \cdot 10^3$-$7.0 \cdot 10^4$ s, depending on the system under investigation.

5.3. Results and discussion

5.3.1. Synthesis of linear polyglycidol (LPG)

As explained in the experimental part, 1-ethoxyethyl glycidyl ether was first synthesised from glycidol according to Fitton et al.; [29] then,

1-ethoxyethyl glycidyl ether was polymerized according to Schmitz et al. [26]. Finally, LPG was prepared by subsequent removal of the acetal protecting groups.

The structure of the obtained linear polyglycidol was confirmed by ^{1}H and ^{13}C NMR techniques as shown in **Figure S5.1** and **Figure S5.2,** respectively. The presence of the aromatic ring as a head group, allowed calculating the degree of polymerization (DP) from ^{1}H NMR spectra, by comparing the integrated areas of the peaks coming from aromatic, aliphatic and alcoholic protons as shown in **Figure S5.1**. DP resulted equal to 20.

5.3.2. Modification of linear polyglycidol

The Steglich esterification represents one of the most versatile esterification methods, which take advantages of *N,N'*-diciclohexyl-carbodiimide (DCC) as a promoter. [27] Although stoichiometric dosage of this reagent, or more, is necessary, this procedure enjoys various advantages. The reaction usually proceeds at room temperature, and the conditions are so mild that substrates with various functional groups can be employed. The reaction is not sensitive to steric hindrance of the reactants, allowing production of esters of tertiary alcohols. As such, a wide range of applications have been achieved in the field of natural products, peptides, nucleotides, etc. however, unfortunately this procedure has some drawbacks: yields are not always high, and undesirable *N*-acylureas are occasionally formed. These drawbacks can be overcome by addition of strong acids such as *p*-toluenesulfonic acid. [30] Alternatively, addition of a catalytic amount of *p*-aminopyridines is more effective. [31, 32]

In this way, we applied Steglich esterification in chemical modification of LPG (**Scheme 5.1**).

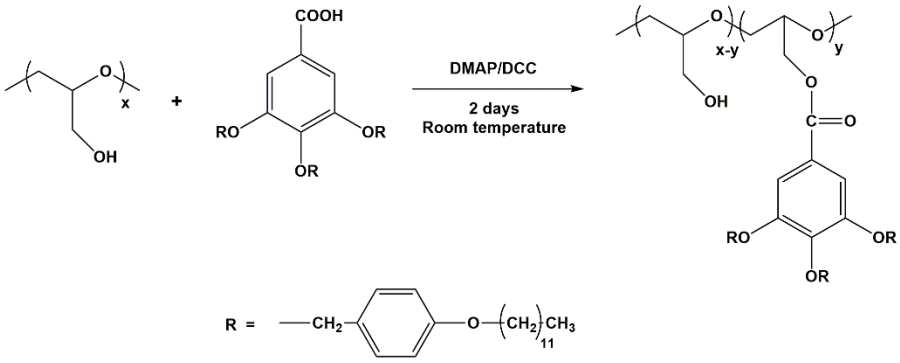

Scheme 5.1. Chemical modification of linear polyglycidol.

In case of LPG, we studied this chemical modification under different reaction conditions, which are given in **Table 5.1** along with and their corresponding degree of modification and product yields.

Table 5.1. Chemical modification conditions, modification degrees and yields obtained in the modification of LPG.

	Copolymer	RCOOH (mmol) [a]	–OH/ RCOOH	Time (days)	T (°C)	Modification degree (%) [b]	Yield (%)
c	LPG1	2	1:0.3	2	25	8	61
	LPG2	2	1:0.5	2	25	23	70
	LPG3	2	1:0.7	2	25	27	68
	LPG4	2	1:1	2	25	39	81
	LPG5	2	1:1.25	2	25	43	87
d	LPG6	2	1:1	7	25	42	79
	LPG7	2	1:1	2	40	40	75
	LPG8	2	1:1	2	80	11	65

[a] Stoichiometric amounts of DMAP and DCC in each case.
[b] Average value determined by ^{1}H NMR.
[c] Series 1.
[d] Series 2.

In most cases this esterification was carried out at room temperature, since the side product *N*-acylurea formation is less likely at lower temperatures; in other words, high temperatures favour the formation of side products and are therefore expected to reduce modification degrees correspondingly.

We considered products LPG1 to LPG5 as series 1 and from LPG6 to LPG8 as series 2. In case of series 1, only the –OH/ROOH molar ratio was varied, while there was no change in reaction time and temperature. It can be seen that in this case the degree of modification increased on increasing the molar ratio; finally, we got 43% degree of modification in case of LPG5.

In case of series 2, we studied the effect of increase in reaction time and temperature on degree of modification. However, the degree of modification could not be increased with increasing reaction time up to 7 days, as it can be seen in case of LPG6. As far as reaction temperature is concerned, an increase up to 40˚C did not affect the reaction since a degree of modification of 40% was reached in the case of LPG7; on the other hand, the degree of modification was significantly decreased up to 11% when the reaction was performed at 80˚C, as in the case of LPG8.

Therefore, we supposed a modification plateau of 43%, which could not be further increased by raising reaction time and temperature. Reaction yield could not be improved beyond 87% (LPG5); however, one should take into account that, in order to get rid of DMAP and DCC, several precipitations were required which caused loss of product and inevitably turned into low product yield.

The structure of the copolymers was characterised by NMR spectroscopy. **Figure 5.1** reports the ^{1}H NMR spectrum in $CDCl_3$ of modified LPG1 as an example.

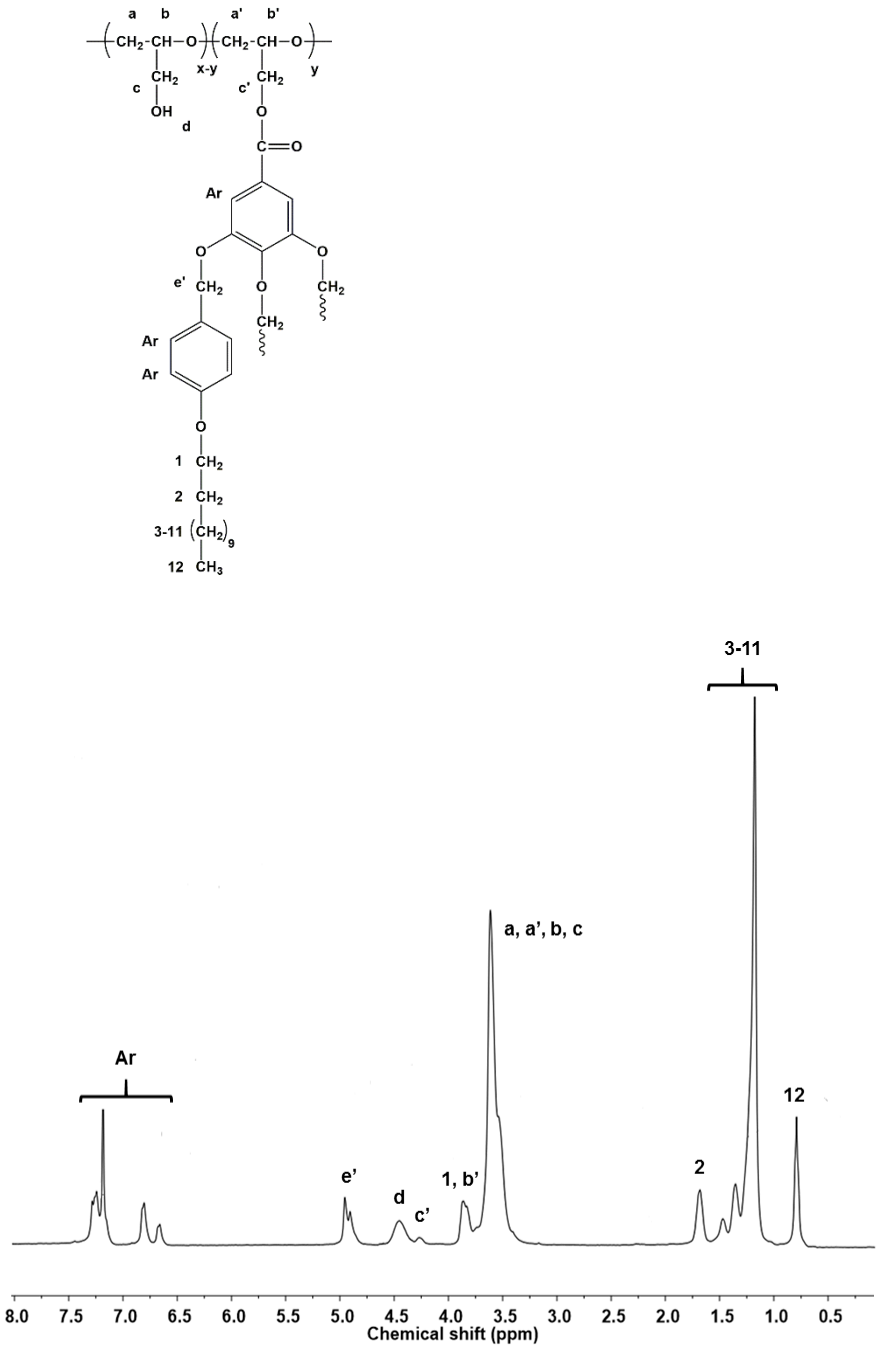

Figure 5.1. ^{1}H NMR spectrum of modified LPG1 in $CDCl_3$.

All ^{1}H NMR spectra are characterised by broad signals in three regions. The aromatic region shows three signals at 7.2, 6.8, and 6.7 ppm. Considering the relative integration areas and by comparison with the spectrum of 3,4,5-tris[4-(n-dodecan-1-yloxy)benzyloxy]benzoic acid, the signal at 7.2 (8 H) can be assigned to the protons of the benzoyl group plus the aromatic protons *ortho* to the benzylic carbon $–CH_2O–$. The signals at 6.8 and 6.6 ppm (4 H + 2 H) correspond to the aromatic protons *meta* to the benzylic carbon $–CH_2O–$ of the lateral and central alkyloxybenzyloxy substituents respectively. The characteristic signals, corresponding to most protons of the dodecyloxy alkyl chains in the dendron, can be observed in the high-field region at 1.7, 1.4, 1.3, 1.2, and 0.8 ppm. In the region between 5 and 3.4 ppm five signals can be observed: the two signals at 4.4 and 4.3 ppm correspond to the methylenic protons c' in the modified monomeric unit; in this region, also signals coming from the free –OH groups are overlapped. The signal at 3.9 ppm corresponds to the methylene attached to the oxygen in the alkyl chains of the mesogenic unit and to methinic proton b'. The broad signal between 3.8 and 3.4 ppm corresponds to the methylenic and methinic protons a, a', b, and c in the modified and unmodified monomeric units. Finally, the signal centered at 4.9 ppm can be assigned to the benzylic methylenes of the dodecyloxybenzyloxy substituent.

Figure 5.2 shows the ^{13}C NMR spectrum in 1,1,2,2-tetrachloroethane-d_2 of modified LPG1 with the corresponding assignments.

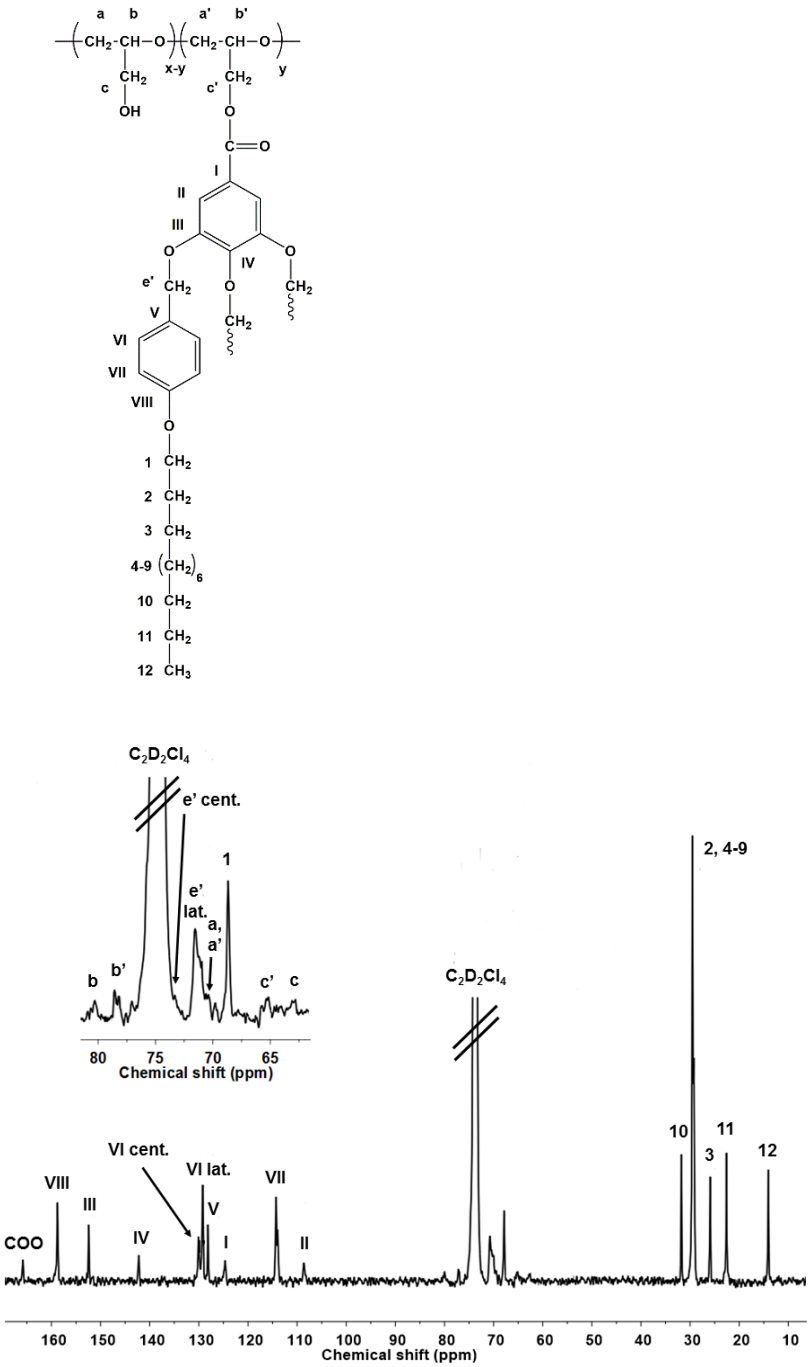

Figure 5.2. ^{13}C NMR spectrum of modified LPG1 in 1,1,2,2-tetrachloroethane-d_2.

The aromatic carbons and the carbonyl carbon appear between 166 and 108 ppm, whereas carbons 2-12 of the aliphatic alkyl chains appear in the region between 32 and 14 ppm. The carbons of the backbone appear in the central region of the spectrum. The methine and side methylenic carbons of the modified and unmodified monomeric units appear at different chemical shifts. Thus, b and b' appear at 80.6 and 77.4 ppm, while c and c' appear at 62.2 and 64.4 ppm respectively. The carbons a and a' appear overlapped at 69.5 ppm. Carbon 1 of the alkyl chains appears as a sharp peak at 67.8 ppm. The chemical shifts of the benzylic methylenes depend on their relative position in the benzoyl ring: those in position 3 and 5 appear at 71.1 ppm, whereas the same carbon in position 4 appears overlapped with peaks coming from 1,1,2,2-tetrachloroethane-d_2.

The degree of modification of modified polymer was calculated by ^{1}H NMR spectra by comparing the areas of the aromatic peaks between 7.4 and 6.6 ppm and the benzylic proton signal at 4.9 ppm with the broad signal between 3.8 and 3.4 ppm.

Molecular weights and polydispersities of LPG derivatives determined by SEC are reported in **Table 5.2**. Molecular weights increased with modification degree. In general terms, density values (**Table 5.2**) did not exhibit appreciable variation; slightly higher values were found in the case of LPG5, LPG6 and LPG7, which also showed higher polydispersities.

Table 5.2. Average molecular weights and densities of the modified LPG.

Polymer	Modification degree (%)	$M_n \cdot 10^{-3}$ [a]	$M_w \cdot 10^{-3}$ [a]	M_w/M_n [a]	ρ (g/cm^3) [b]
LPG [c]	-	1.48 [d]	-	-	1.02
LPG1	8	2.70	3.19	1.18	1.07
LPG2	23	4.79	6.57	1.37	1.07
LPG3	27	5.16	7.34	1.42	1.08
LPG4	39	7.36	10.87	1.47	1.08
LPG5	43	7.62	12.76	1.62	1.17
LPG6	42	7.52	11.46	1.52	1.17
LPG7	40	7.11	10.93	1.53	1.17
LPG8	11	2.93	3.57	1.21	1.07

[a] Determined by SEC.
[b] Determined at 30°C. Error: ± 3%.
[c] Unmodified linear polyglycidol.
[d] Calculated from ^{1}H NMR.

5.3.3. Mesomorphic characterisation of modified linear polyglycidol

Mesomorphic phases were investigated by Differential Scanning Calorimetry (DSC), Polarised Optical Microscopy (POM) and confirmed by X-ray diffraction (XRD). **Table 5.3** shows the clearing temperatures ranges and the glass transition temperatures of the whole LPG series.

Table 5.3. Clearing temperature ranges and glass transition temperatures of the modified LPG.

Polymer	Modification degree (%)	T_g (˚C) [a]	T_c (˚C) [b]
LPG	-	-10	32-35
LPG1	8	-10	32-35
LPG2	23	-30	71-75
LPG3	27	-32	79-84
LPG4	39	-27	97-101
LPG5	43	-16	116-120
LPG6	42	-21	95-98
LPG7	40	-13	95-99
LPG8	11	-20	49-52

[a] Determined by DSC second heating scan.
[b] Determined by DSC second heating scan and POM.

The liquid-crystalline textures of LPG samples were observed by POM after annealing the samples for two hours at a temperature slightly lower than their respective clearing temperatures, in order to favour the growth of the liquid-crystalline domains. POM images of both series are shown in **Figure 5.3**.

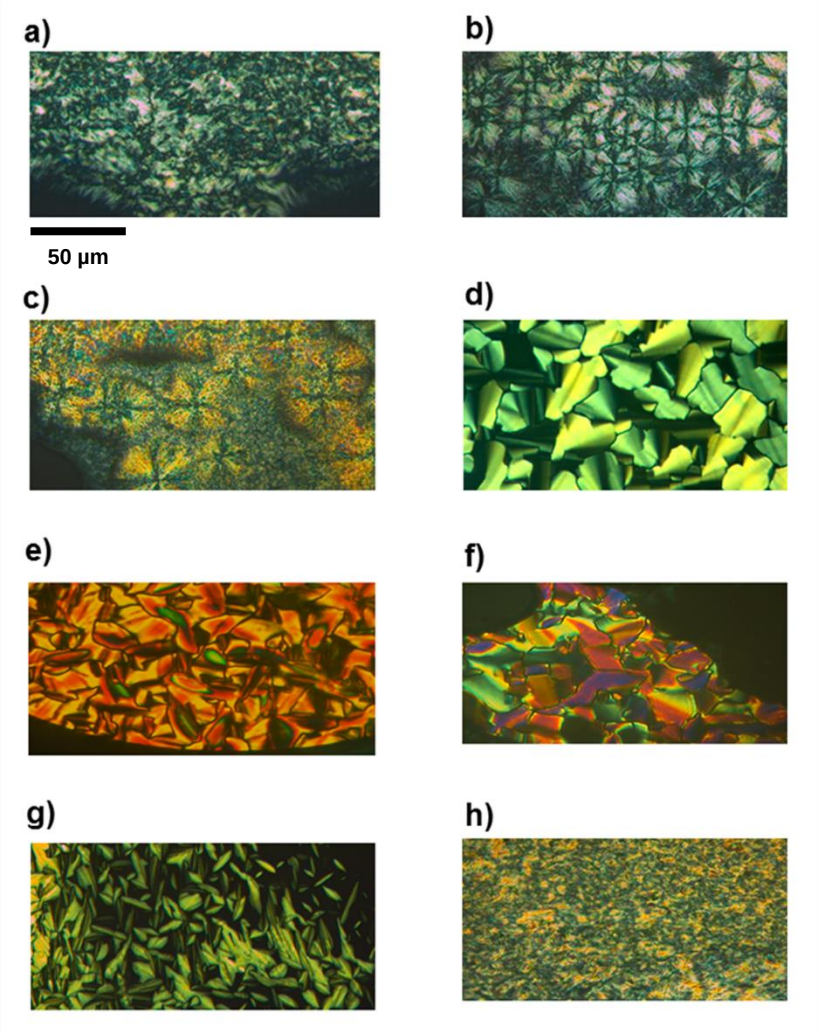

Figure 5.3. Optical micrographics between crossed polars of (sample, modification degree, test temperature: a) LPG1, 8%, 30˚C; b) LPG2, 23%, 69˚C; c) LPG3, 27%, 79˚C; d) LPG4, 39%, 97˚C; e) LPG5, 43%, 116˚C; f) LPG6, 42%, 94˚C; g) LPG7, 40%, 93˚C; and h) LPG8, 11%, 47˚C.

A typical broken fan-shaped texture could be seen in case of LPG2-LPG7 samples, whose modification degrees ranged between 20 and 40%

approximately. At variance, LPG1 and LPG8, with modification degrees around 10%, exhibited a texture which resembled smectic bâtonnets.

In order to assign their mesophases, LPG1, LPG2, LPG3 and LPG4 were studied by XRD. LPG5-LPG7 have modification degrees quite close to LPG4 and, in the case of LPG6 and LPG7, the clearing range was also similar to LPG4. Therefore, we considered reasonable to extend the results from XRD experiments on LPG4 also to LPG5-LPG7. In case of LPG8, similar texture to LPG1 was observed by POM, but the glass transition temperature and the clearing temperature range resulted quite different, so we decided to characterise it as well. Summing up, only samples from LPG1 to LPG4 and LPG8 were analysed by XRD. The results from XRD are summarized in **Table 5.4**.

Table 5.4. X-ray diffraction data of LPG copolymers at room temperature.

Copolymer	Modification degree (%)	d_{exp} (Å)	hkl	Mesophase [a]	Lattice constants (Å)
LPG1	8	42.0	100	Col_L	a= 42.0
		4.4 (b) [c]	001		
LPG8	11	40.1	100	Col_r	a=40.1
		25.0	010		b= 25.0
		13.8	020		
		4.3 (b) [c]	001		
LPG8 OM [b]	11	40.3	100	Col_r	a=40.3
		26.0	010		b= 26.0
		13.1	020		
		4.3 (b) [c]	001		
LPG2	23	41.1	100	Col_r	a=41.1
		27.3	010		b= 27.3
		13.5	020		
		4.4 (b) [c]	001		
LPG2 OM [b]	23	40.0	100	Col_L	a= 40.0
		4.4 (b) [c]	001		
LPG3	27	41.0	100	Col_h	a=b=47.3
		23.8	110		
		4.4 (b) [c]	001		
LPG4	39	46.4	100	Col_h	a=b=53.6
		26.3	110		
		23.5	200		
		4.6 (b) [c]	001		
LPG4 OM [b]	39	36.5	100	Col_h	a=b=42.1
		21.8	110		
		18.1	200		
		4.6 (b) [c]	001		
		31.4	100	Col_r	a=31.4
		25.6	010		b= 25.6
		15.5	200		
		13.1	020		
		4.6 (b) [c]	001		

[a] Col_L: lamellar columnar, Col_r : rectangular columnar, Col_h : hexagonal columnar.
[b] Oriented membrane obtained by immersion precipitation + baking process.
[c] (b): broad halo.

The intensity vs. 2θ graph of LPG1 copolymer is shown in **Figure S5.3**. Only two signals are evident, a sharp reflection at 2θ = 2.1˚, corresponding to a d-spacing of 42.0 Å, and a broad halo at 2θ around 20˚, giving a d-spacing of 4.4 Å. This pattern is compatible with a smectic as well as with a lamellar columnar mesophase (Col_L); however, the characterisation previously performed on the systems obtained out of PECH and [P(ECH-co-EO)] [18] suggested the existence of Col_L mesophase, the sharp reflection corresponding to the interlamellar distance, while the halo to the distance between adjacent dendrons.

XRD patterns of samples LPG2 and LPG3 are shown in **Figure S5.4** and **Figure S5.5**, respectively. In the case of LPG2, we could observe three sharp reflections at 2θ = 2.1˚, 3.2˚ and 6.5˚, corresponding to d = 41.1 Å, 27.3 Å and 13.5 Å respectively, and a diffuse halo centered round 2θ = 20˚, giving d = 4.4 Å. On the other hand, LPG3 showed two sharp reflections at 2θ = 2.1˚ and 3.7˚, corresponding to d = 41.0 Å and 23.8 Å respectively, and a diffuse halo centered round 2θ = 20˚, giving d = 4.4 Å. This last diffraction pattern, which exhibited d-spacings of the sharp reflections in the ratio of 1:1/√3 and a diffuse halo at high angle region, confirmed the presence of a hexagonal columnar mesophase (Col_h), where the first two sharp reflections correspond to the planes (100) and (110) respectively, while the broad halo is related to (001). Similar conclusions could be drawn from the XRD pattern of sample LPG4, since it showed three sharp reflections corresponding to d = 46.4 Å, 26.3 Å and 23.5 Å respectively, and a diffuse halo centered round d = 4.6 Å. The d-spacings of the sharp reflections were in the ratio 1:1/√3:1/2, confirming the presence of a hexagonal columnar mesophase (Col_h). The XRD pattern of LPG4 is reported in **Figure S5.6**.

At variance, the X-ray diffraction pattern of polymer LPG2 was in agreement with the less-symmetrical rectangular columnar mesophase (Col_r). In this case, the sharp reflections at 41.1, 27.3 and 13.5 Å could be assigned to (100), (010) and (020) planes, respectively. It must be noted, that the occurrence of a rectangular columnar mesophase is also compatible with

the broken fan shaped texture as observed by POM (**Figure 5.3b**). Also in the case of LPG8, whose modification degree was 11%, XRD pattern was compatible with a rectangular columnar mesophase (**Table 5.4**). As we have explained, on increasing the modification degree, the LC phase of the modified copolymers changed from lamellar columnar to hexagonal columnar, through an intermediate, less symmetric rectangular columnar. This can be ascribed to the self-assembling of the dendrons (**Figure 5.4**): in the case of low modification degrees (LPG1), the π-π interaction between the aromatic rings, as well as the inter-digitation of peripheral aliphatic chains is only able to drive the system to lamellar packing (**Figure 5.4a**) while, when the modification degree is higher (LPG3 to LPG7), the increased symmetry of the system can induce the assembling of the columns into a hexagonal packing (**Figure 5.4c**). In the case of intermediate modification degree (LPG2 and LPG8), columnar organisation is not perfectly hexagonal yet and the elliptical shape of the column cross-section gives rise to a rectangular columnar mesophase (**Figure 5.4b**).

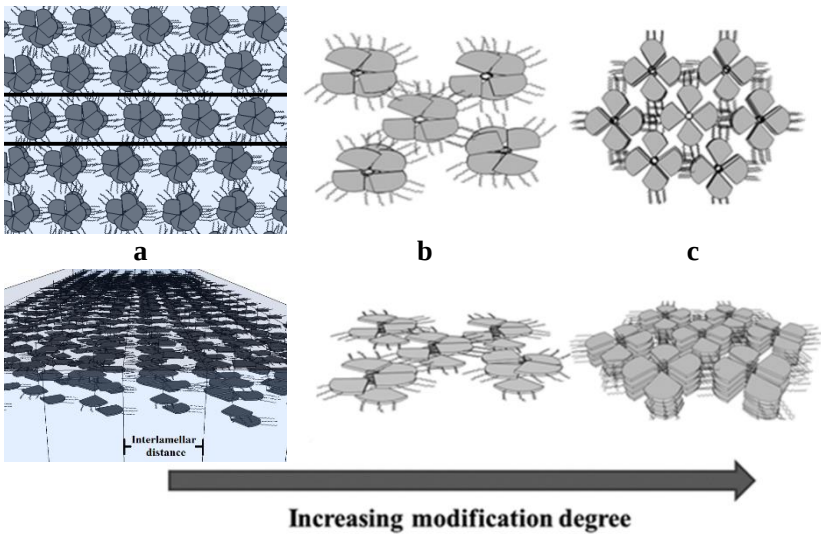

Figure 5.4. Schematic representation of the self-assembling of LPG copolymers on increasing the modification degree; a: lamellar columnar; b: rectangular columnar; c: hexagonal columnar. Top: top views; bottom: side views.

In all cases, the organisation of the copolymers into columns can be supposed to lead to the formation of biomimetic ion channels, where the polyether main chain arranges in the inner part of the column.

5.3.4. Membrane preparation and assessment

In order to assess the potential of the synthesised copolymers as proton-conducting materials, we prepared oriented membranes out of selected samples. LPG8, LPG2 and LPG4 were selected as representative of three different increasing modification degrees. In order to get efficient transport, the columns which are expected to work as ion channels should be oriented homeotropically, that is, perpendicularly to the membrane surface.

According to the studies done by Percec et al., [11, 18] it was demonstrated that columnar self-assembling polymers containing tapered groups can be homeotropically oriented when the system is allowed to self-organise during slow cooling on a hydrophobic substrate from the melt into the liquid crystal phases. The dendrons were found to be the structure-directing moieties of the columnar architectures, and π-π stacking of aromatic units produces the driving forces responsible for this homeotropic orientation.

Therefore, as mentioned in the experimental part, membranes were first prepared by immersion precipitation process. Then, with the described baking process, we obtained satisfactorily oriented membranes in the homeotropic direction. Previously, the baking process was successfully applied to the preparation of homeotropically oriented membranes based on chemically modified PECH and [P(ECH-co-EO)]. [18]

As an example, **Figure 5.5** shows the XRD image of a LPG4 membrane after baking process. The diffraction at $2\theta = 2.4^{\circ}$, which corresponds to $d_{100} = 36.5$ Å and to $a = b = 42.1$ Å, exhibits orientation in the equatorial plane, which indicates that columns are oriented perpendicularly to the membrane surface to some extent.

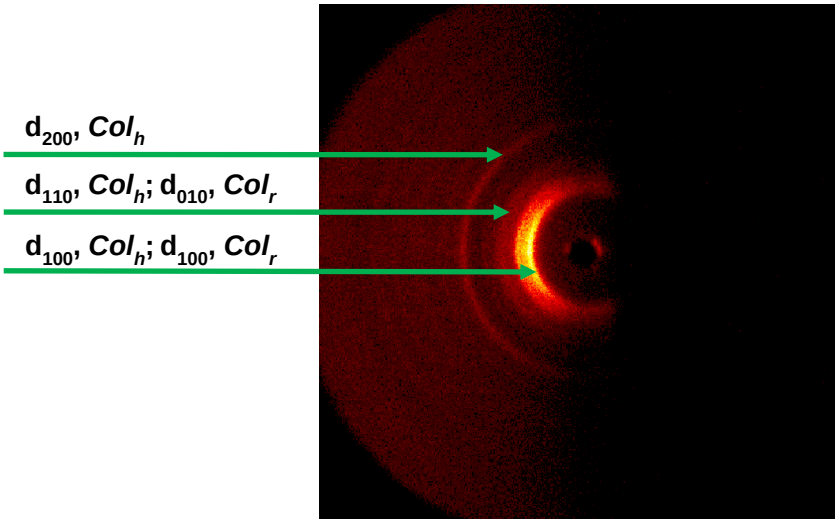

Figure 5.5. XRD pattern of LPG4 oriented membrane at room temperature recorded in reflection mode.

As it can be seen in **Table 5.4**, in some cases surface interactions, which are responsible for the orientation process, seem to alter the ordering of LPG copolymers. As a matter of fact, in one case a different mesophase was observed (LPG2), while in another one, coexistence with a new mesophase was put into evidence. (LPG4).

The obtained membranes were also investigated in terms of water contact angle measurement by considering FEP side and air-side, that is, the part which was directly in contact with the FEP support during the baking process, and the other one, on opposite side. The values of contact angles on FEP side are reported in **Table 5.5**.

Table 5.5. Water contact angles and proton permeabilities of LPG-based oriented membranes.

Polymer	Water contact angle (˚) [a]	Permeability ($cm^2 \cdot s^{-1}$)
LPG2	116.4 ± 0.8	$(3.8 \pm 0.1) \cdot 10^{-7}$
LPG4	112.3 ± 0.3	$(1.0 \pm 0.3) \cdot 10^{-7}$
LPG8	115.8 ± 1.5	$(2.2 \pm 0.5) \cdot 10^{-6}$
Nafion® N117	94.0 ± 0.9	$(2.59 \pm 0.05) \cdot 10^{-6}$

[a] Determined on FEP side.

In our case, both sides were found hydrophobic, having similar contact angles. This evidence confirmed that the membranes were homogeneously oriented. Surface hydrophobicity can be ascribed to dominating exposition of tapered groups which represents the hydrophobic part of the polymer: that is, in case of homeotropic orientation, the membrane surface is hydrophobic because of maximum area occupied by well oriented hydrophobic tapered groups.

Proton transport tests were performed on the membranes obtained with LPG2, LPG4 and LPG8 respectively. Calculated permeability values are reported in **Table 5.5**. The value found for Nafion® N117 $(2.59 \pm 0.05) \cdot 10^{-6}$ $cm^2 \cdot s^{-1}$ was used as a reference standard in the evaluation of proton permeability of the other materials. Permeabilities of LPG copolymers are comparable to Nafion®, while no permeability at all was detected for the samples not previously submitted to the baking process; in the case of LPG8, the calculated value resulted very close to Nafion®, being $(2.2 \pm 0.5) \cdot 10^{-6}$ $cm^2 \cdot s^{-1}$. Plots according to equation (5) for Nafion® N117 and LPG8 are reported in **Figure 5.6**.

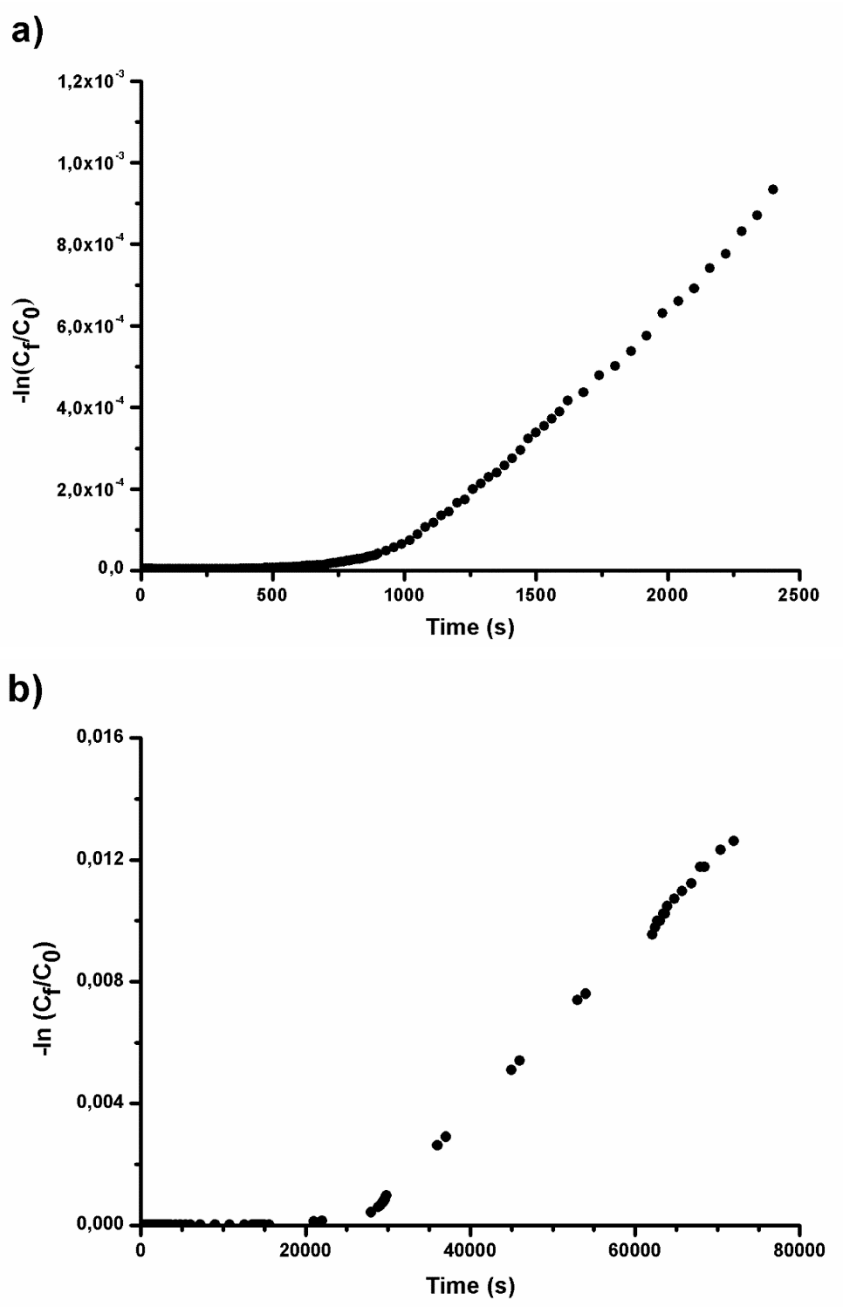

Figure 5.6. Plot of $-\ln(C_f/C_0)$ versus time for Nafion® N117 membrane (a) and for LPG8 membrane (b) during a proton transport test.

In both cases, the plot exhibits two different regions: the first one, which was much shorter for Nafion® N117 (**Figure 5.6a**), corresponds to proton absorption and diffusion across the membrane; once the membranes were saturated by protons, the mechanism became hopping-dominated. One has to keep into account that LPG8 membrane is thicker with respect to Nafion® N117 membrane; moreover, proton transport through LPG8 membrane determines some changes in polymer conformation and an increase in its orientation, as it will be shown hereinafter: this could justify the longer time needed for proton diffusion across the membrane. From the slope of the second region, which was quite similar for both materials, we calculated proton permeability.

LPG8 corresponds to a low modification degree (11%) which, in turn, represents high hydroxyl group content and, consequently, is expected to be one of the most hydrophilic copolymers in the series. Therefore, in order to test whether in this case such a remarkable proton transport could be due to the presence of water, in analogy to Nafion®, a swelling test was performed. Surprisingly, water uptake resulted as low as 3.1%. This suggests that water is not crucial for proton transport which occurs instead due to the presence of oriented channels in the membrane. Therefore, alike to modified PECH, these polyglycidol derivatives could be also suitable candidates for the preparation of proton transporting membranes.

In the case of LPG8, it is noteworthy that the XRD pattern of the membrane after transport experiment showed higher degree of order when compared to the fresh oriented membrane. In fact, for the azimuthal scan of the peak at $2\theta = 2.1^{\circ}$, we could observe a decrease of calculated FWHM (Full Width at Half Maximum) from $186 \pm 6^{\circ}$ to $67.2 \pm 0.9^{\circ}$. In fact, before transport experiments (**Figure S5.7**), the columns are only slightly homeotropically oriented, while, after transport experiments (**Figure S5.8**), the peak corresponding to the homeotropically oriented columns is sharper (although some perpendicularly oriented columns can also be evidenced). Thus, transport is able to induce a change in the degree of order of LPG8; this could

be favoured by higher chain mobility of this copolymer, which exhibits the lowest modification degree with respect to the other copolymers of the series.

5.4. Conclusions

We prepared linear polyglycidol with a polymerization degree equal to 20, and subsequently modified it with the dendron 3,4,5-tris[4-(n-dodecan-1-yloxy)benzyloxy]benzoic acid by Steglich esterification with *N,N'*-dicyclohexylcarbodiimide. In this way, we prepared a family of self-assembling liquid-crystalline copolyethers whose modification degrees ranged between 8 and 43%, depending on the –OH/RCOOH molar ratio. On the other hand, the modification degree could not be further improved on increasing reaction time and temperature. The whole copolymer family exhibited liquid-crystalline behaviour and the higher the modification degree, the higher the clearing range. It was found that mesophase self-assembling depended on the amount of dendrons introduced: in the case of the lowest modification degree (8%), the copolymer exhibited lamellar columnar packing; in the case of intermediate degrees, the mesophase turned into rectangular columnar while, for the highest modification degrees, hexagonal columnar mesophase was observed. Due to the columnar organisation of the copolymers, the polyether backbone is expected to assume a helical conformation, suitable for cation transport through the channel mechanism. Polymer membranes were prepared by immersion precipitation on a fluorinated ethylene propylene (FEP) support. By means of the baking process, we obtained an effective homeotropic orientation of the polymeric columns in the membranes, as confirmed by XRD analysis. Oriented membranes were found to be hydrophobic on both sides of the membrane as shown by their contact angles. The presence of oriented ion channels in the polymeric membranes resulted in remarkable proton permeability, similar to Nafion®. Besides, the studied membranes exhibited negligible water uptake

after soaking in Milli-Q water at room temperature for 24 hours; therefore, in this case membrane hydration does not seem critical for ion transport.

5.5. Acknowledgements

Financial support from CTQ2013-46825-R (Ministerio de Economía y Competitividad) is gratefully acknowledged. The authors are also grateful to Dr. Francesc Guirado for help with the XRD experiments.

5.6. Supporting information

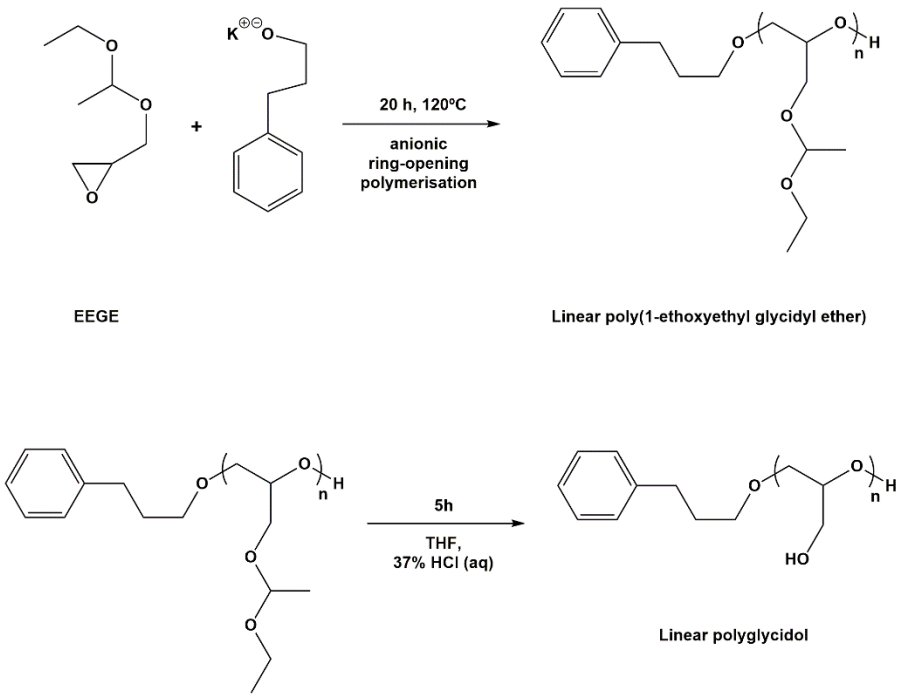

Scheme S5.1. Synthesis of linear polyglycidol.

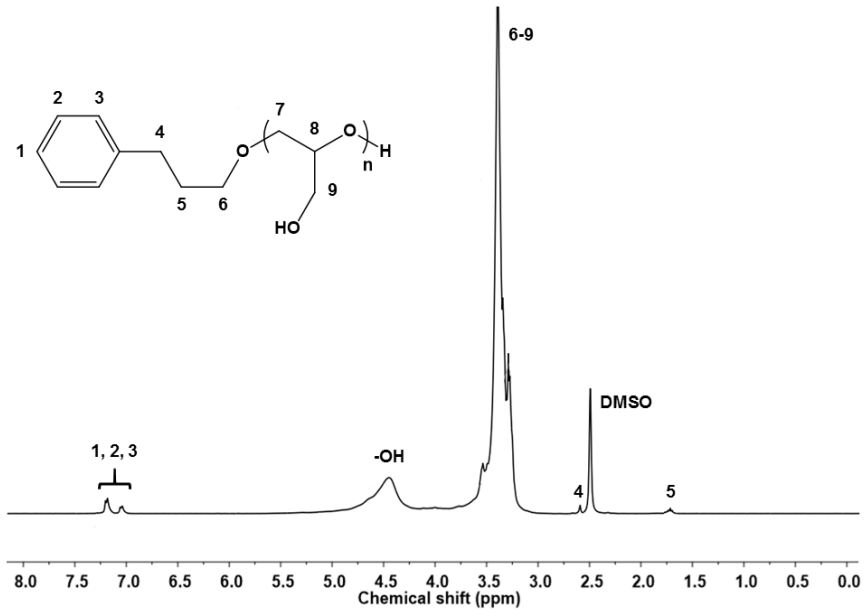

Figure S5.1. ^{1}H NMR spectrum of linear polyglycidol in DMSO-d_6.

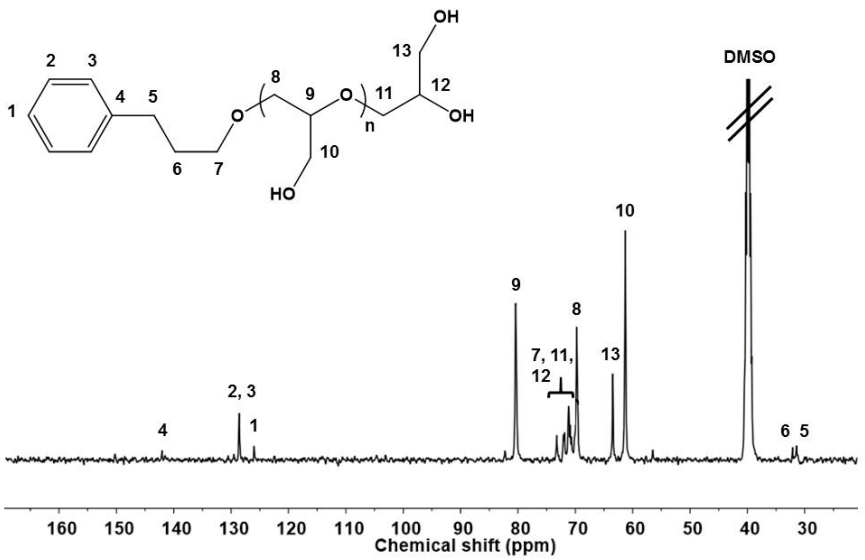

Figure S5.2. ^{13}C NMR spectrum of linear polyglycidol in DMSO-d_6.

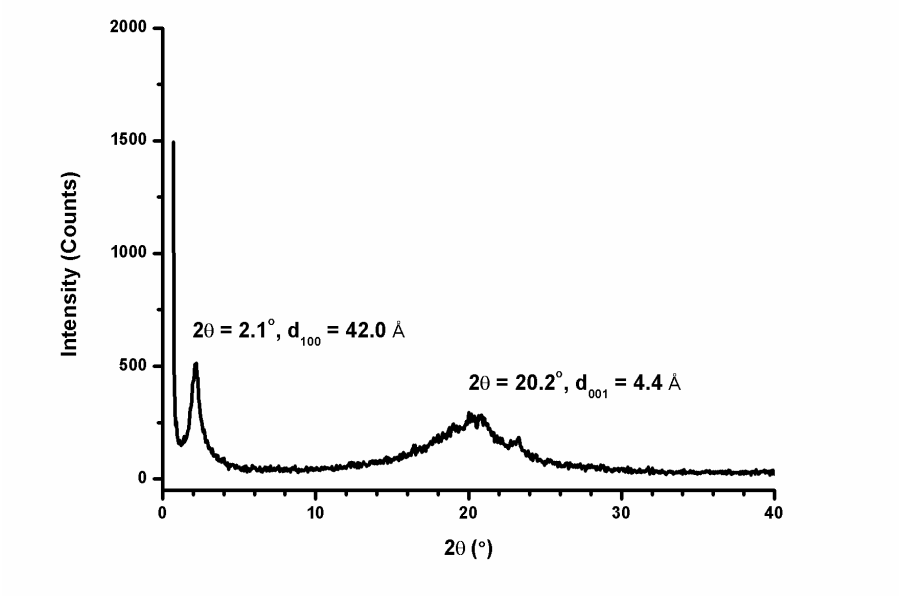

Figure S5.3. XRD pattern of LPG1 at room temperature.

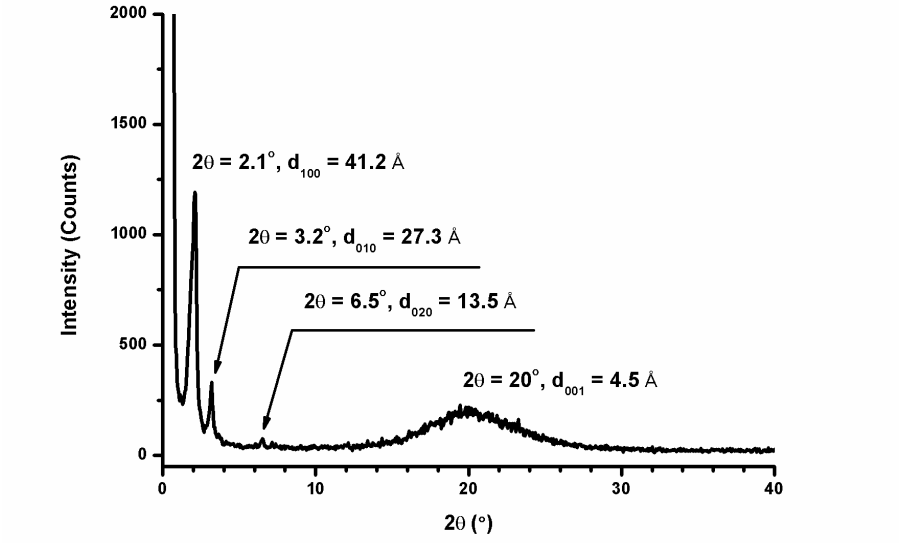

Figure S5.4. XRD pattern of LPG2 at room temperature.

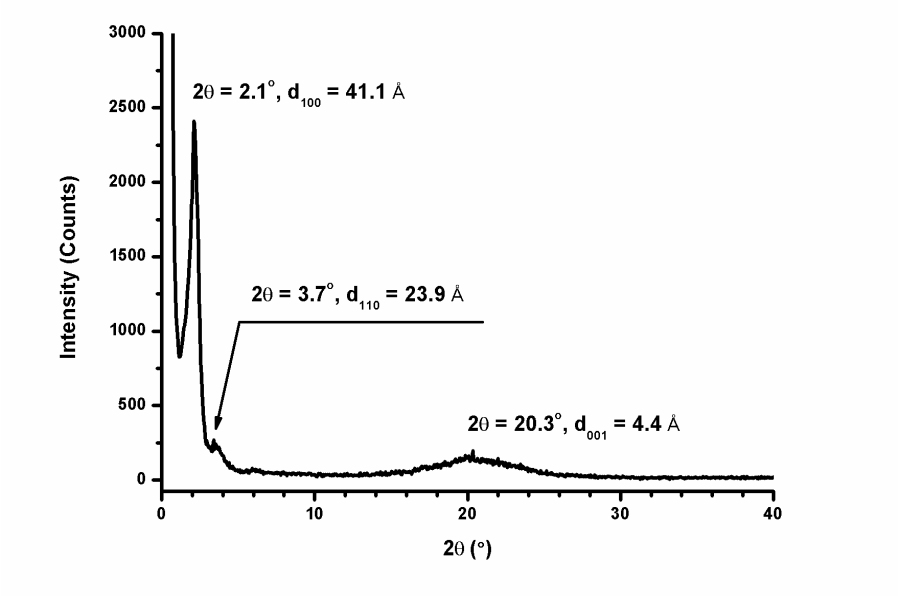

Figure S5.5. XRD pattern of LPG3 at room temperature.

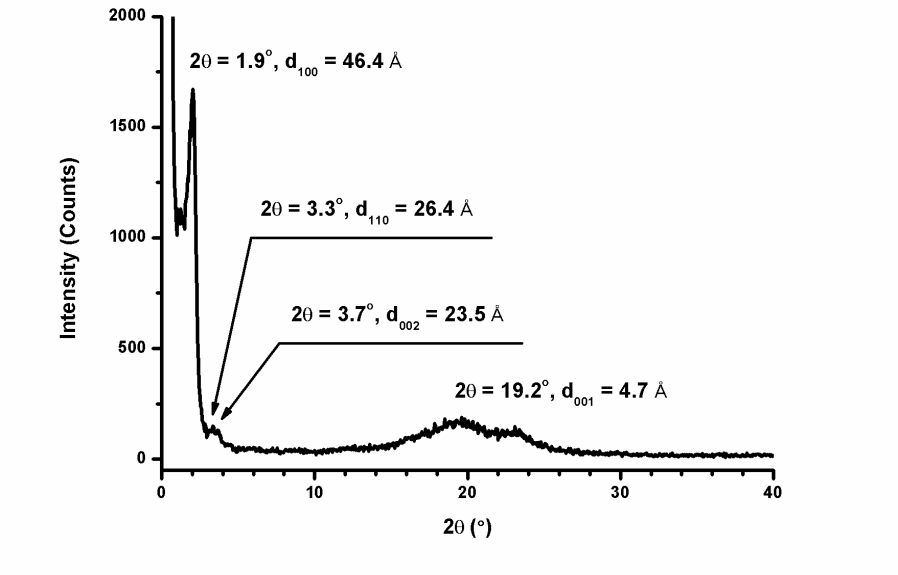

Figure S5.6. XRD pattern of LPG4 at room temperature.

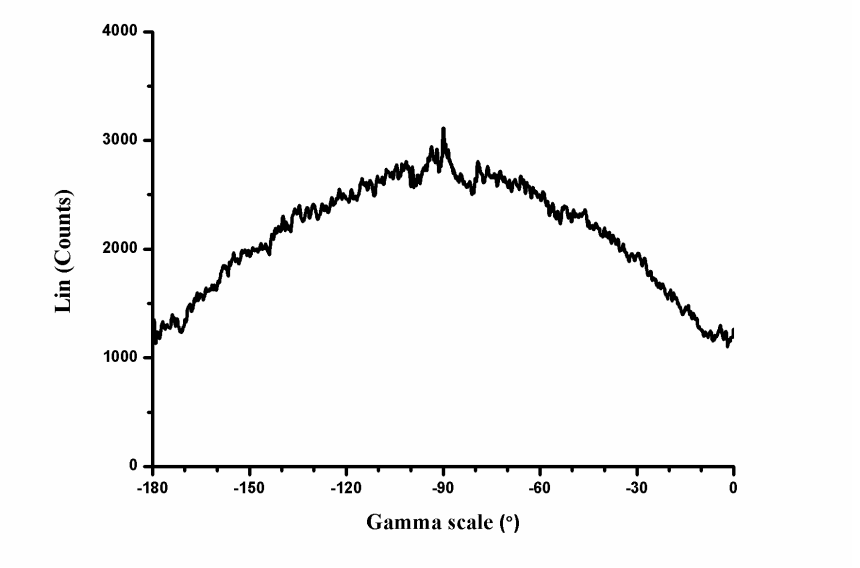

Figure S5.7. XRD azimuthal intensity plot of LPG8 membrane before permeability test at room temperature (2θ = 2.097˚).

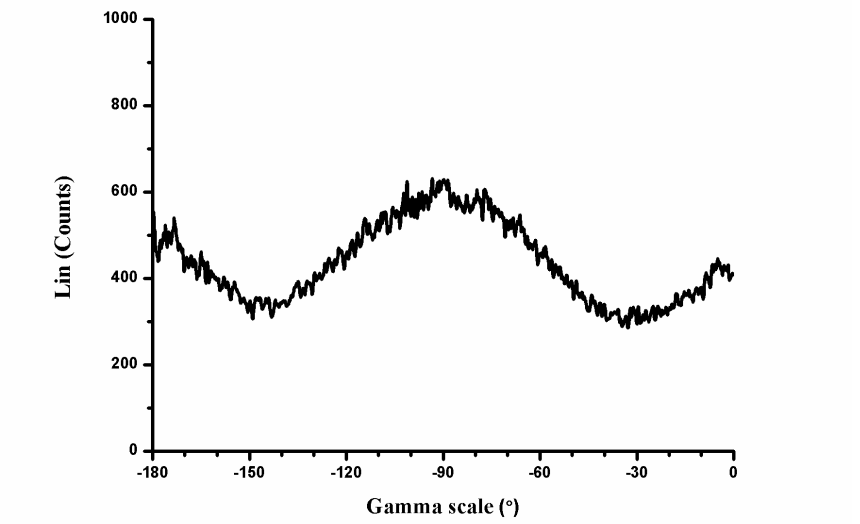

Figure S5.8. XRD azimuthal intensity plot of LPG8 membrane after permeability test at room temperature (2θ = 2.211˚).

5.7. References

1. Mauritz KA and Moore RB. Chem. Rev. 2004;104:4535-4585

2. Wilhelm FG, Pünt IGM, van der Vegt NFA, Strathmann H, and Wessling M. J. Membr. Sci. 2002;199(1–2):167-176.

3. Miyatake K, Chikashige Y, Higuchi E, and Watanabe M. J. Am. Chem. Soc. 2007;129(13):3879-3887.

4. Li Y, Jin R, Wang Z, Cui Z, Xing W, and Gao L. J. Polym. Sci., Part A: Polym. Chem. 2007;45(2):222-231.

5. Alberti G, Costantino U, Casciola M, Ferroni S, Massinelli L, and Staiti P. Solid State Ionics 2001;145(1–4):249-255.

6. Percec V, Johansson G, Heck J, Ungarb G, and Battyb SV. J. Chem. Soc., Perkin Trans. 1 1993(13):1411-1420.

7. Beginn U, Zipp G, and Möller M. Adv. Mater. 2000;12(7):510-513.

8. Yoshio M, Kagata T, Hoshino K, Mukai T, Ohno H, and Kato T. J. Am. Chem. Soc. 2006;128(16):5570-5577.

9. Jiménez-García L, Kaltbeitzel A, Pisula W, Gutmann JS, Klapper M, and Müllen K. Angew. Chem., Int. Ed. 2009;48(52):9951-9953.

10. Percec V, Ahn CH, Ungar G, Yeardley DJP, Moller M, and Sheiko SS. Nature 1998;391(6663):161-164.

11. Percec V, Glodde M, Bera TK, Miura Y, Shiyanovskaya I, Singer KD, Balagurusamy VSK, Heiney PA, Schnell I, Rapp A, Spiess HW, Hudson SD, and Duan H. Nature 2002;417(6905):384-387.

12. Percec V, Schlueter D, Ungar G, Cheng SZD, and Zhang A. Macromolecules 1998;31(6):1745-1762.

13. Percec V, Cho W-D, Ungar G, and Yeardley DJP. J. Am. Chem. Soc. 2001;123(7):1302-1315.

14. Percec V, Imam MR, Peterca M, and Leowanawat P. J. Am. Chem. Soc. 2012;134(9):4408-4420.

15. Shi Z, Chen D, Lu H, Wu B, Ma J, Cheng R, Fang J, and Chen X. Soft Matter 2012;8(22):6174-6184.

16. Chuang W-T, Lo T-Y, Huang Y-C, Su C-J, Jeng US, Sheu H-S, and Ho R-M. Macromolecules 2014;47(17):6047-6054.

17. Yi Z, Liu X, Jiao Q, Chen E, Chen Y, and Xi F. J. Polym. Sci., Part A: Polym. Chem. 2008;46(12):4205-4217.

18. Komura M, Yoshitake A, Komiyama H, and Iyoda T. Macromolecules 2015;48(3):672-678.

19. Ronda JC, Reina JA, Cádiz V, Giamberini M, and Nicolais L. J. Polym. Sci., Part A: Polym. Chem. 2003;41(19):2918-2929.

20. Ronda JC, Reina JA, and Giamberini M. J. Polym. Sci., Part A: Polym. Chem. 2004;42(2):326-340.

21. Bhosale SV, Rasool MA, Reina JA, and Giamberini M. Polym. Eng. Sci. 2013;53(1):159-167.

22. Dulyea LM, Fyles TM, and Robertson GD. J. Membr. Sci. 1987;34:87-108.

23. Tylkowski B, Castelao N, Giamberini M, Garcia-Valls R, Reina JA, and Gumí T. Mater. Sci. Eng. C 2012;32(2):105-111.

24. Perrin DD and Armarego WLF. Purification of Laboratory Chemicals, 6th ed. Oxford: Pergamon Press, 2009. pp. 127-128.

25. Šakalytė A, Reina JA, and Giamberini M. Polymer 2013;54(19):5133-5140.

26. Schmitz C, Keul H, and Möller M. Eur. Polym. J. 2009;45(9):2529-2539.

27. Otera J. Reaction of Alcohos with Carboxylic Acids and their Derivatives, in Esterification: Methods, Reactions, and Applications. Weinheim: Wiley-VCH GmbH & Co. KGaA, 2003. pp. 21-24.

28. Mulder J. Transport in membranes, in Basic Principles of Membrane Technology, 2nd ed. Dordrecht: Kluwer Academic Publishers, 1996. pp. 210-279.

29. Fitton AO, Hill J, Jane DE, and Millar R. Synthesis 1987;1987(12):1140-1142.

30. Neises B and Steglich W. Angew. Chem., Int. Ed. Engl. 1978;17(7):522-524.

31. Hassner A and Alexanian V. Tetrahedron Lett. 1978;19(46):4475-4478.

32. Ivanov VT and Mikhaleva II. Main-Chain-Modified Peptides, in Methods of Organic Chemistry (Houben - Weyl): Synthesis of Peptides and Peptidomimetics, vol. E 22 c. Stuttgart: Thieme Publishers, 2003. pp. 277-280.

Chapter 6

Improvement of the synthesis of linear polyglycidol to obtain a higher molecular weight polymer: a future alternative for proton-conducting membranes

6.1. Introduction

In the last decades, glycidol derived polymers have attracted the interest of different research groups due to the low price of glycidol (≈\$0.3 g^{-1}), the large number of possible architectures shown by these polymers (linear, star-shaped, arborescent-branched) and their high functionality and biocompatibility. All these properties make glycidol derived polymers promising candidates for their future application in biomedical, technological and other fields. [1-3]

To obtain linear polyglycidol (LPG), the hydroxyl group of glycidol must be protected by a suitable group (acetal) and then the polymerisation can be performed under anionic conditions. 1-ethoxyethyl glycidyl ether (EEGE) has been used as a protected monomer. Once linear poly(1-ethoxyethyl glycidyl ether) is obtained, it can be easily deprotected by hydrolysis under mild acidic conditions to lead LPG. [4, 5]

In a previous chapter, [6] we reported the synthesis of LPG (with a polymerisation degree, DP = 20) and its subsequent chemical modification using the dendron 3,4,5-tris-[4-(n-dodecan-1-yloxy)benzyloxy]benzoic acid (TAP) to obtain liquid-crystalline polyethers that self-assemble into a columnar structure. As we reported, an exo-recognition of the side-chain dendrons allows the self-assembly process, resulting in a supramolecular structure in which the polyether main chain forms a channel in the inner part of the columns, while the hydrophobic side-chain dendrons lie in the outer part. The presence of the polar ether linkages in the inner channel favours the interaction with proton and other cations, in the same way as crown ethers would do. [7]

The resulting polymers can be used as ion transport channels when they are casted as membranes and oriented. The presence of oriented channels in these polymeric membranes resulted in a remarkable proton permeability, similar to that shown by Nafion®. [6] However, despite oriented

membranes were successfully prepared, it must be noted that they are brittle and exhibit poor mechanical properties.

Thus, to improve the mechanical properties of these membranes, an attempt of the synthesis of a higher molecular weight LPG was performed. The properties of the two LPG with different degree of polymerisation were compared.

6.2. Experimental

6.2.1. Materials

All the chemicals were purchased from Sigma–Aldrich, while all solvents were purchased from Scharlab. *p*-toluenesulfonic acid monohydrate (TsOH*,* 98.5%), potassium *tert*-butoxide (1 M solution in THF) and 3-phenyl-1-propanol (98%) were used as received. Glycidol (96%) was distilled at reduced pressure and stored over 4 Å molecular sieves at 2-5˚C. Diglyme [bis(2-methoxyethyl) ether] was first shaken with a weakly acidic ion-exchange resin (Amberlite IR-120) to remove the amine-like odour. After filtered the solution, it was distilled at reduced pressure from CaH_2. [8] Linde type 4 Å molecular sieves were previously activated by heating them in an oven at 220˚C for 48 h, and then left to cool and kept under argon atmosphere in a well-dried flask.

EEGE was synthesised following the method described by Fitton et al. [9] To a magnetically stirred solution of glycidol (40.0 g, 0.540 mol) in ethyl vinyl ether (200 mL, 2.1 mol), TsOH (1.0 g, 5.8 mmol) was added portionwise, while keeping the temperature below 40˚C. The mixture is stirred for 3 h and saturated aqueous $NaHCO_3$ (100 mL) is then added. The organic layer is separated, dried and evaporated under reduced pressure. Distillation of the residue gives EEGE as a colourless liquid. The structure of EEGE was confirmed by ^1H NMR (**Figure 6.1** and **Figure 6.2**). Yield: 76%.

^{1}H NMR ($CDCl_3$, TMS, δ, ppm): 4.7 (m), 3.8-3.6 (m), 3.5-3.3 (m), 3.1 (m), 2.8-2.6 (m), 1.3 (m), 1.2 (m).

^{13}C NMR ($CDCl_3$, TMS, δ, ppm): 99.7, 65.8-65.1, 61.0, 50.9, 44.7, 19.8, 15.3.

6.2.2. Synthesis of linear polyglycidol (LPG)

For the synthesis of the two linear polyglycidols, the same general method was followed, [10] even though different 3-phenyl-1-propanol : potassium *tert*-butoxide ratios were used.

LPG-A. In a 50 mL round-bottomed flask, 3-phenyl-1-propanol (0.27 g, 2.0 mmol) was dissolved in 7 mL of diglyme, and then potassium *tert*-butoxide (0.20 mL of a 1 M solution in THF, 0.2 mmol) was added. The formed *tert*-butyl alcohol was removed under vacuum. 1-ethoxyethyl glycidyl ether (6.98 g, 47.7 mmol) was added and the mixture was magnetically stirred for 20 h at 120˚C. The solvent was then removed at 80˚C under vacuum and linear poly(glycidol acetal) was obtained as a viscous liquid. The obtained poly(glycydol acetal) was dissolved in tetrahydrofuran (700 mL), and aqueous 37% HCl (41.2 g) was added. After 5 h, the linear polyglycidol was precipitated as an oil. The solvent was removed by decantation and the polyglycidol was dried under vacuum at 80˚C. Yield: 80%. DP = 28.

LPG-B. LPG-B was prepared in the same manner, but using 0.027 g (0.2 mmol) of 3-phenyl-1-propanol. Yield: 79%. DP = 289.

^{1}H NMR (DMSO-d_6, TMS, δ, ppm): 7.3-7.1 (m), 4.4 (s), 3.6-3.3 (m), 2.6 (t), 1.8 (m).

^{13}C NMR (DMSO-d_6, TMS, δ, ppm): 141.9-125.9, 80.1, 72.7-69.4, 63.1, 60.9, 31.8, 31.2.

6.2.3. Characterisation and measurements

Nuclear magnetic resonance (NMR) spectroscopy

^{1}H NMR and ^{13}C NMR spectra were recorded at 400 and 100.4 MHz, respectively, on a Varian Gemini 400 spectrometer with proton noise decoupling for ^{13}C NMR. The central peak of the solvent was taken as the reference, and the chemical shifts were given in parts per million from TMS (Tetramethylsilane). The ^{13}C NMR spectra of the polymers were recorded at 30˚C, with a flip angle of 45˚, and the number of transients ranged from 20,000 to 40,000 with 10-20% (w/v) sample solutions in $CDCl_3$ or DMSO-d_6.

Differential scanning calorimetry (DSC)

Glass transition temperatures were determined with a Mettler–Toledo differential scanning calorimeter mod. 822 in dynamic mode at a heating rate of 10˚C/min. Nitrogen was used as the purge gas. The calorimeter was calibrated with an indium standard (heat flow calibration) and an indium–lead–zinc standard (temperature calibration).

Thermogravimetric analysis (TGA)

Thermal stability studies were carried out in ALU OXIDE crucibles of 70 µL (ME-24123) with a Mettler TGA/SDTA851e/LF/1100 device at temperatures ranging from 30 to 600˚C with a heating rate of 10˚C/min using around 10 mg of sample in a nitrogen atmosphere (100 mL/min). The equipment was previously calibrated with indium (156.6˚C) and aluminium (660.3˚C) pearls.

6.3. Results and discussion

In order to access to well-defined linear polyols derived from glycidol, hydroxyl functions of that monomer had to be protected. [5] In an opposed way, the unprotected glycidol monomer leads to a highly branched structure in the polymer product. Altough *tert*-butyl glycidyl ether (*t*BuGE) is a good candidate used to protect glycidol due to its commercial availability, [11] EEGE is most frequently used for the preparation of linear polyglycidol owing to the ease of the monomer protection step and the facile removal of the acetal protecting group under mild acidic conditions. [12]

As explained in the experimental part and shown in **Scheme 6.1**, 1-ethoxyethyl glycidyl ether (EEGE) was synthesised by the reaction of glycidol and ethyl vinyl ether according to Fitton et al. [9] In this nucleophilic addition catalysed by *p*-toluensulfonic acid, the hydroxyl groups of glycidol are protected forming acetal groups.

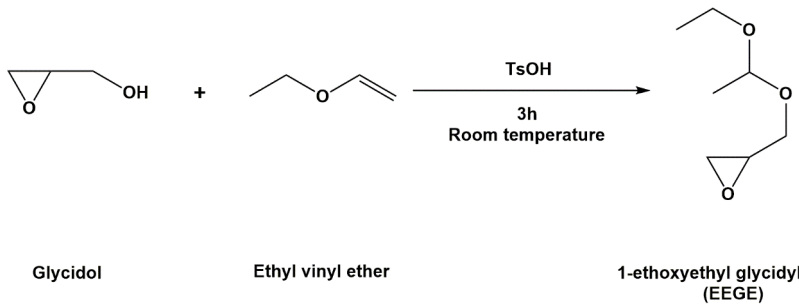

Scheme 6.1. Synthesis of 1-ethoxyethyl glycidyl ether.

The colourless liquid was isolated by distillation with a yield of 76 %. The structure of 1-ethoxyethyl glycidyl ether was confirmed by ^{1}H and ^{13}C NMR spectra as shown in **Figure 6.1** and **Figure 6.2,** respectively. Both spectra exhibit the expected peaks of the desired product.

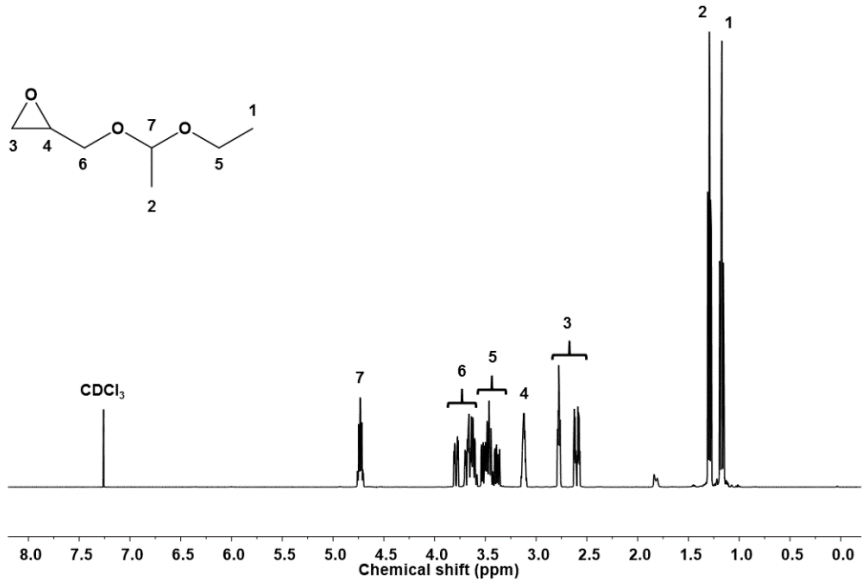

Figure 6.1. ^{1}H NMR spectrum of EEGE in $CDCl_3$.

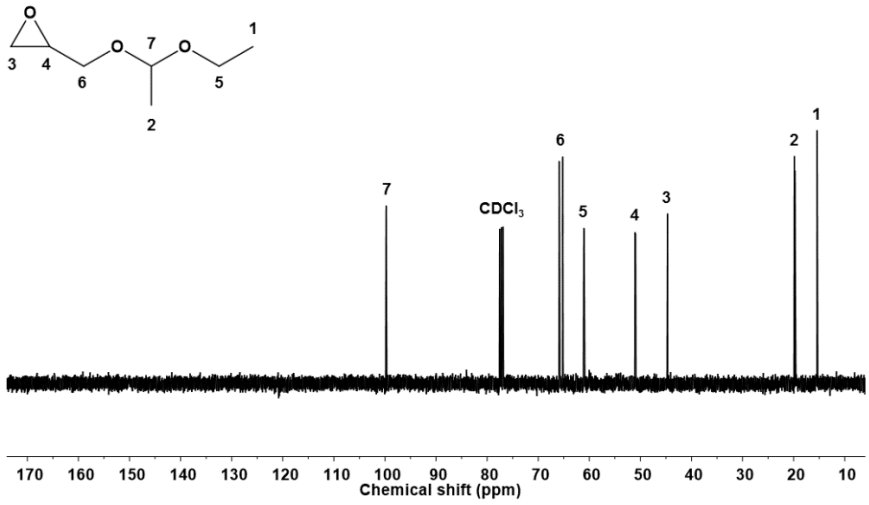

Figure 6.2. ^{13}C NMR spectrum of EEGE in $CDCl_3$.

Then, EEGE was polymerised through a “living” anionic mechanism using the same procedure described by Schmitz et al. [10] In this procedure, the selected initiator is potassium 3-phenyl-1-propoxide, which is obtained from the proton-exchange reaction between potassium *tert*-butoxide and 3-phenyl-1-propanol. Finally, linear polyglycidol LPG-A was prepared by subsequent removal of the acetal protecting groups through acidic hydrolysis (**Scheme 6.2**).

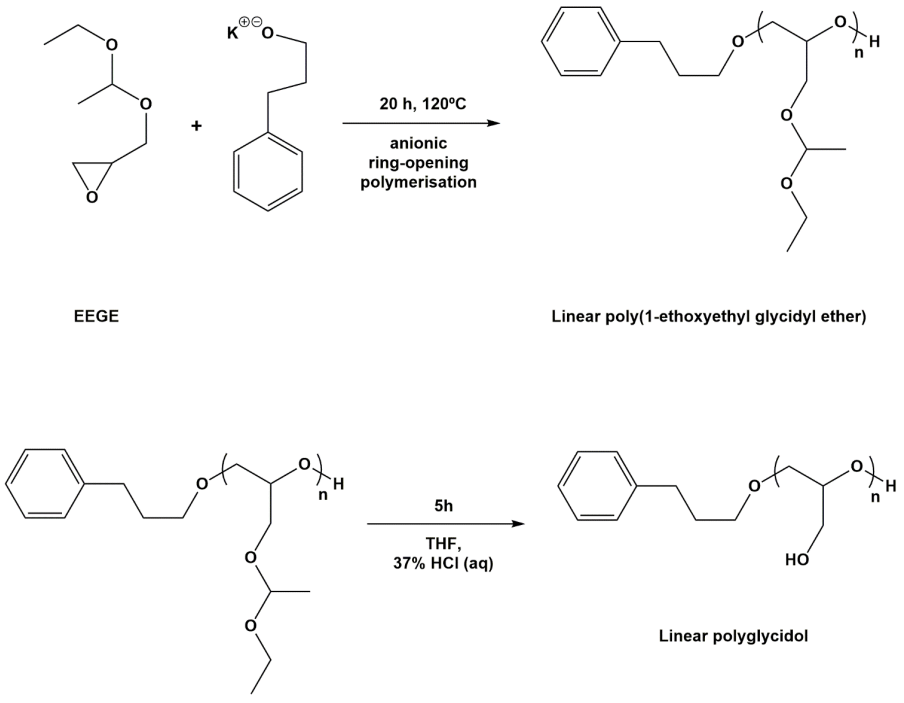

Scheme 6.2. Synthesis of linear polyglycidol.

The structure of the obtained linear polyglycidol was confirmed by ^{1}H and ^{13}C NMR spectra as shown in **Figure 6.3** and **Figure 6.4,** respectively. In **Figure 6.3**, the presence of the aromatic ring as a head group, allowed

calculating the degree of polymerisation from ^{1}H NMR spectrum, by comparing the integrated areas of the peaks coming from aromatic and the aliphatic region between 3.3 and 3.6 ppm. In this case, the calculated degree of polymerisation was 28. Furthermore, in the aliphatic region two more peaks were detected at 2.6 and 1.8 ppm which correspond to the signals assigned as 4 and 5 of the head group, respectively. Finally, we also could observe a peak at 5.1 ppm due to the proton of the hydroxyl groups.

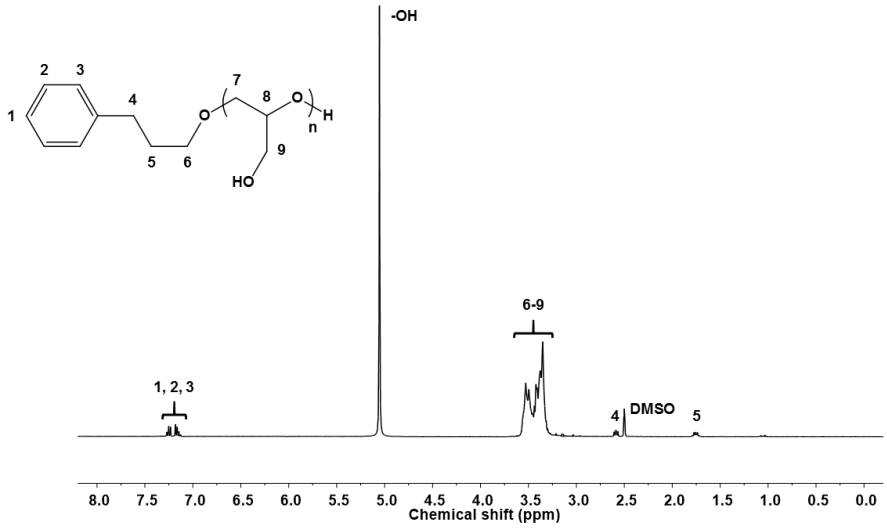

Figure 6.3. ^{1}H NMR spectrum of LPG-A in DMSO-d_6.

In the ^{13}C NMR spectrum of LPG-A, it is also possible to observe the signals attributed to the carbons of the aromatic ring of the head group between 125 and 142 ppm. Moreover, the methylene groups assigned as 5 and 6 of the head group appear at 31.2 and 31.8 ppm, respectively. The other signals, which are attributed to carbons linked to oxygen, appear between 61 and 81 ppm in the spectrum.

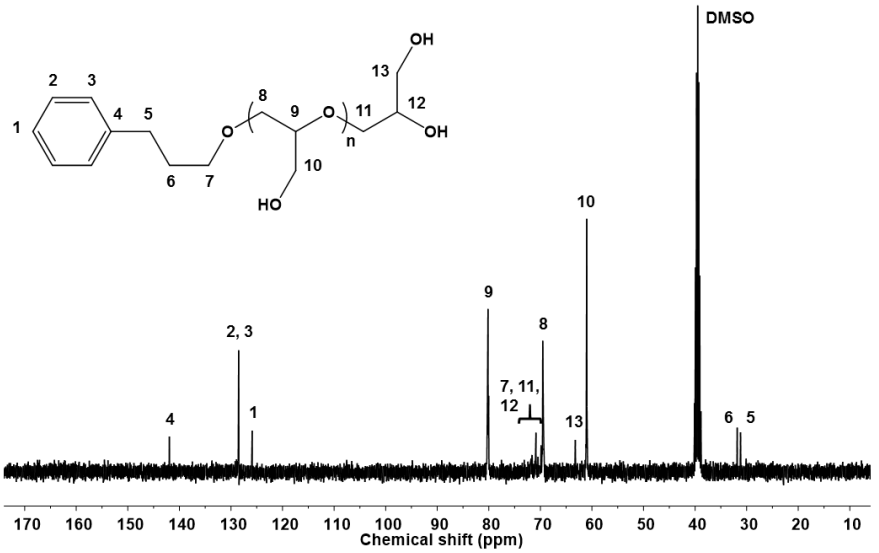

Figure 6.4. ^{13}C NMR spectrum of LPG-A in DMSO-d_6.

As mentioned above, in this anionic ring-opening polymerisation, the initiator (potassium 3-phenyl-1-propoxide) was obtained from potassium *tert*-butoxide through a proton-exchange reaction (**Scheme 6.3**). So, in principle, one could expect that the degree of polymerisation were related to the ratio between the monomer and potassium *tert*-butoxide (47.7 : 0.2, respectively).

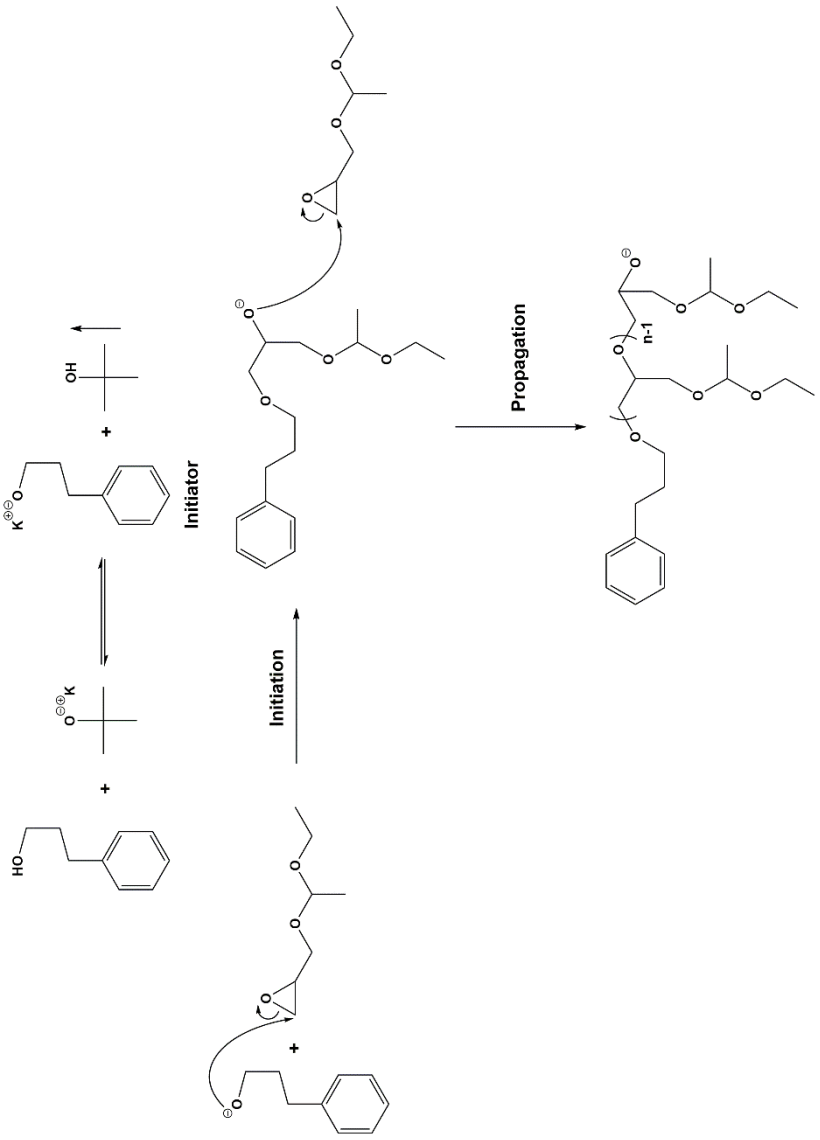

Scheme 6.3. Mechanism of the anionic ring-opening polymerisation of EEGE.

However, the obtained LPG-A has a lower DP than expected (only 28 repeating units in front of 239 units expected). To explain this fact, we need to take into account all the chemical species present in the system. For the formation of the initiator, an excess of 3-phenyl-1-propanol was added with respect to potassium *tert*-butoxide (10 : 1, respectively). During the anionic polymerisation, this excess of 3-phenyl-1-propanol could be involved in a chain-transfer reaction (**Scheme 6.4**), which in turn would stop the growth of the propagation species, so leading to a decrease of the length of the obtained polymer chains. In fact, the degree of polymerisation will be then determined by the ratio between the monomer and 3-phenyl-1-propanol (47.7 : 2, respectively), which lead to an expected DP value of 24, closely in agreement with the obtained one.

It must be noted that in all works where LPG was prepared by using this procedure, [11, 13, 14] an excess of 3-phenyl-1-propanol was added. In spite of this, in none of these papers is mentioned the expected chain-transfer reaction.

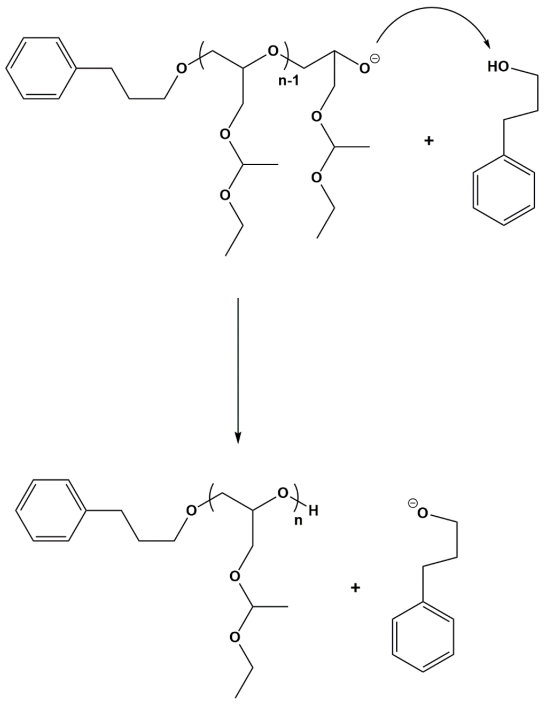

Scheme 6.4. Chain-transfer reaction presumably taking place on the polymerisation of EEGE.

Once the origin of the problem of the low molecular weight of LPG was detected, the polymerisation of EEGE was repeated, but changing the ratio of 3-phenyl-1-propanol vs. potassium *tert*-butoxide in order to improve the degree of polymerisation. In this case, the same amount of both compounds was used (ratio EEGE : 3-phenyl-1-propanol : potassium *tert*-butoxide; 47.7 : 0.2 : 0.2, respectively). Therefore, no excess of 3-phenyl-1-propanol was added.

The structure of the obtained linear polyglycidol (LPG-B) was confirmed by ^{1}H and ^{13}C NMR spectra. Both NMR spectra are shown in **Figure 6.5** and **Figure 6.6,** respectively. In **Figure 6.5**, by comparison of the integration of the signal due to the aromatic protons and the peak of the

aliphatic region between 3.3 and 3.6 ppm, the degree of polymerisation was calculated to be 289, not far away from the expected DP = 239. In this spectrum, the peak attributed to the proton of the hydroxyl groups moves towards 4.4 ppm.

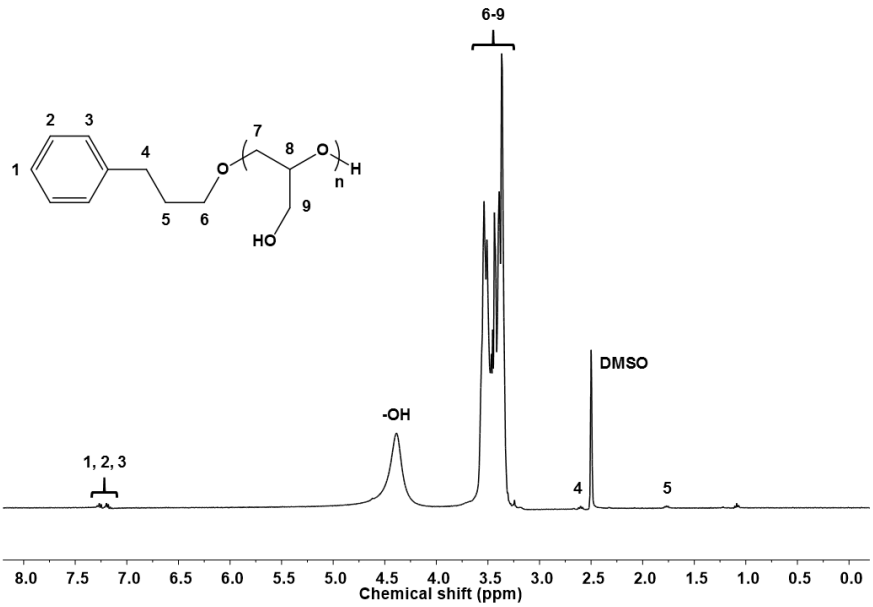

Figure 6.5. ^{1}H NMR spectrum of LPG-B in DMSO-d_6.

In the ^{13}C NMR spectrum, it can be observed that the peaks assigned to the head and tail group are very weak in comparison with the signals attributed to the main chain. This observation was in agreement with the higher molecular weight of the LPG-B.

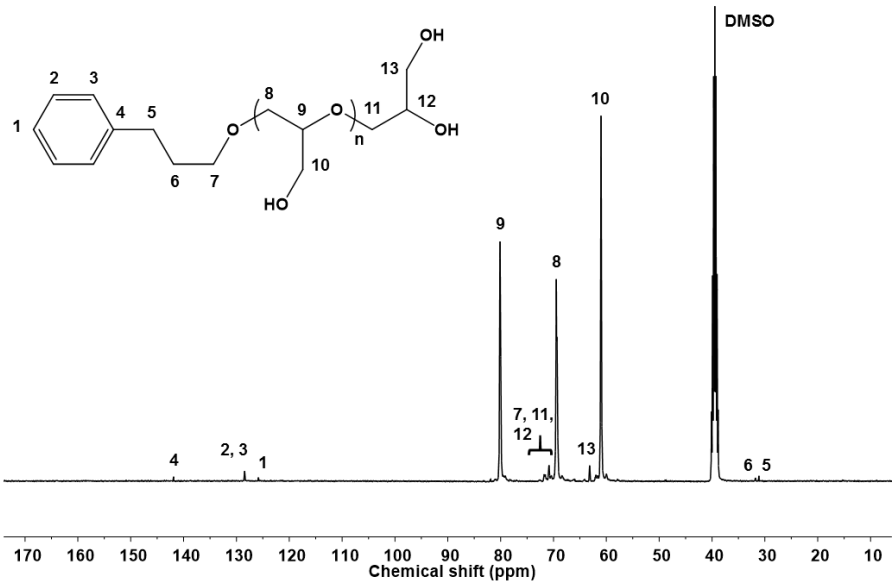

Figure 6.6. ^{13}C NMR spectrum of LPG-B in DMSO-d_6.

Monomer conversions were determined by comparing the ^{1}H NMR spectrum of EEGE with the ^{1}H NMR spectrum of crude protected linear polyglycidol. In both cases, the conversion of the monomer resulted to be almost complete. In fact, when the "living" polymerisation of EEGE takes place, the peaks of the epoxy ring (which appear between 2.6 and 3.1 ppm in **Figure 6.1**) disappear in the ^{1}H NMR spectrum of the crude polymer (**Figure 6.7**), confirming that all monomer reacts to obtain protected LPG.

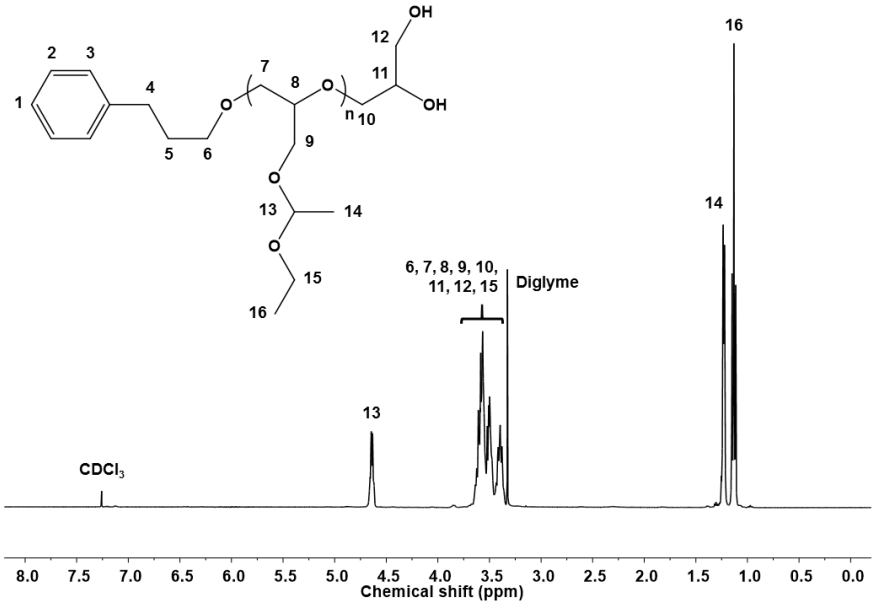

Figure 6.7. ^{1}H NMR spectrum of protected LPG-B in $CDCl_3$.

In **Table 6.1** the yields and degrees of polymerisation of both LPG synthesised are listed.

Table 6.1. Yields and degrees of polymerisation of both LPG synthesised.

Polymer	Yield (%)	DP
LPG-A	80	28
LPG-B	79	289

As the molecular weight of the two prepared LPG is markedly different, their thermal properties are expected also to differ. The results of the thermal characterisation performed for both LPG are shown in **Table 6.2**.

The glass transition temperature (T_g) shows, as expected, a small increase from -15 to -11˚C on increasing the degree of polymerisation from 28 to 289.

Referred to TGA analysis, linear polyglycidols degrade in a single mass loss step. As observed in **Table 6.2**, on increasing the degree of polymerisation, the onset in TGA curve is increased from 285 to 345˚C. Thus, the higher polymerisation degree seems to lead to a more stable polyglycidol.

Table 6.2. Thermal properties of both LPG synthesised.

Polymer	T_g (˚C)	Onset TGA curve (5% mass loss) (˚C)	Temperature of the maximum rate of weight loss (˚C)
LPG-A	-15	285	372
LPG-B	-11	345	395

As already mentioned, LPG could be used as a precursor for the synthesis of liquid-crystalline polymers that self-assemble into columns, which could be used as ion channels. The presence of longer polyether chains could lead to a more effective ion transport. Moreover, the use of a polymer with a higher degree of polymerisation would presumably lead to membranes with improved mechanical properties. The better thermal properties exhibited by LPG-B in front of LPG-A in terms of thermal degradation confirms these hypothesis.

6.4. Conclusions

The anionic ring-opening polymerisation of 1-ethoxyethyl glycidyl ether was re-examined to increase the degree of polymerisation of the final

LPG. The occurrence of a chain-transfer reaction between the growing chain and the 3-phenyl-1-propanol excess limits the DP of the synthesised LPG. Hence, the use of a stoichiometric amount of 3-phenyl-1-propanol vs. potassium *tert*-butoxide as an initiator system allows the real "living" polymerisation to occur, so leading to a higher DP.

6.5. References

1. Keul H and Möller M. J. Polym. Sci., Part A: Polym. Chem. 2009;47(13):3209-3231.

2. Zhang H and Grinstaff MW. Macromol. Rapid Commun. 2014;35(22):1906-1924.

3. Thomas A, Müller SS, and Frey H. Biomacromolecules 2014;15(6):1935-1954.

4. Taton D, Leborgne A, Sepulchre M, and Spassky N. Macromol. Chem. Phys. 1994;195(1):139-148.

5. Dworak A, Panchev I, Trzebicka B, and Walach W. Polym. Bull. 1998;40(4):461-468.

6. Montané X, Bhosale SV, Reina JA, and Giamberini M. Polymer 2015;66:100-109.

7. Dulyea LM, Fyles TM, and David Robertson G. J. Membr. Sci. 1987;34(1):87-108.

8. Perrin DD and Armarego WLF. Purification of Laboratory Chemicals, 6th ed. Oxford: Pergamon Press, 2009. pp. 127-128.

9. Fitton AO, Hill J, Jane DE, and Millar R. Synthesis 1987;1987(12):1140-1142.

10. Schmitz C, Keul H, and Möller M. Eur. Polym. J. 2009;45(9):2529-2539.

11. Erberich M, Keul H, and Möller M. Macromolecules 2007;40(9):3070-3079.

12. Gervais M, Brocas A-L, Cendejas G, Deffieux A, and Carlotti S. Macromol. Symp. 2011;308(1):101-111.

13. Hans M, Gasteier P, Keul H, and Moeller M. Macromolecules 2006;39(9):3184-3193.

14. Hans M, Keul H, and Moeller M. Polymer 2009;50(5):1103-1108.

Chapter 7

General conclusions and future work

7.1. General conclusions

The conclusions of this research are summarized as follows:

- The synthesis of a family of LC polyamines by chemical modification of poly[2-(aziridin-1-yl)ethanol] (PAZE) polymer with benzoyl chloride and afterwards with 3,4,5-tris[4-(n-dodecan-1-yloxy)benzyloxy]benzoic acid (TAP) dendron was achieved at different extents (PAn copolyamines) with the purpose to avoid the observed tendency to crystallise of PAZE modified only with TAP, reported in previous studies.

- All the obtained PAn copolyamines exhibit a LC columnar mesophase. Moreover, they are not crystalline at room temperature and exhibit liquid crystal behaviour in a wider temperature range than the LC polyamines obtained by modification of PAZE with TAP only.

- Oriented membranes based on selected LC polyamines were successfully prepared under thermal treatment. The perpendicular orientation of the copolymer columns to the membrane surface was confirmed by means of XRD. The achieved homeotropical orientation of the columns allows the use of these membranes in proton transport devices.

- Linear sweep voltammetry experiments in chloride solution revealed damage of the self-supported PAn based membranes probably caused by the presence of gaseous chlorine, as confirmed by different techniques: SEM, TEM and ^{1}H NMR spectroscopy.

- The assessment of ionic transport across these oriented membranes was carried out in order to evaluate the possible application as proton transport materials. In this manner, a

comparison of the results obtained in linear sweep voltammetry experiments for PAn based membranes vs. hybrid membranes prepared with PAZE modified only with TAP and an inorganic support was carried out. Despite the chemical degradation in the presence of gaseous chlorine that PAn based membranes suffer, and their lower selectivity, they can be more easily prepared, are cheaper, show a better homeotropical orientation, exhibits a LC phase with a higher thermal stability and have improved mechanical properties in comparison with the hybrid systems. Therefore, these series of interesting advantages make these membranes useful, for instance, in applications where higher temperature regimes are required.

- The LC copolyamines were studied by using NMR techniques and DSC in order to interpret the chemical structure and the dynamics of the thermal transitions detected.

- VT solid state NMR studies confirms that the observed transition between 256 and 272 K for PA3 (TAP : 75%, Benzoyl : 25%) and PA4 (TAP : 43%, Benzoyl : 33%, –OH : 24%) copolymers is attributed to the melting of a part of TAP moieties. The mobility gained by the outer part of the dendron at temperatures higher than the melting corroborates this fact.

- A study of the chemical structure and the particular behaviour of PA1.1 (TAP : 85%, Benzoyl : 9%, –OH : 6%) copolymer was performed by using solid state NMR experiments. This copolymer exhibited high tendency to crystallise, similarly than previously modified PAZE only with TAP. For this specific sample, as observed during the first heating run performed on the precipitated copolymer, the growth of the crystalline phase is more favoured. Nevertheless, when a second heating run was performed after melting PA1.1 copolyamine, the LC behaviour was almost

exclusively detected while crystallisation was not observed, suggesting that this copolymer shows different behaviour depending on the pre-treatment performed on the material.

- Liquid crystalline columnar copolyethers were prepared by chemical modification of previously synthesised linear polyglycidol with TAP mesogenic group. Copolyethers with different modification degree ranging from 8 to 43% were obtained depending on the polyether/TAP ratio used.

- All copolymers exhibit liquid-crystalline columnar mesophases ranging from lamellar columnar in the case of the lowest modification degree (8%) to hexagonal columnar for the highest modification degree with TAP (27-43%). Copolyethers with an intermediate modification degree (11-23%) exhibit rectangular columnar mesophase.

- Homeotropically oriented membranes based on selected LC polyethers were successfully prepared under the same thermal treatment used for the preparation of PAn based membranes. The presence of ion channels capable to transport protons through the membrane resulted in a proton permeability similar to Nafion®.

- Both in the case of polyamines and polyethers, the membranes were found to be hydrophobic on both sides and exhibited negligible water uptake after soaking in Milli-Q water at room temperature for a period of 24 hours. Thus, membrane hydration does not seem critical for ion transport.

- With the aim to prepare LC copolyethers with improved mechanical properties, the anionic ring-opening polymerisation of linear polyglycidol was re-investigated. A chain-transfer reaction between the growing chain and 3-phenyl-1-propanol excess limits the degree of polymerisation of the linear polyether. Thus, the usage of

a stoichiometric amount of 3-phenyl-1-propanol vs. potassium *tert*-butoxide as an initiator system allows the real "living" polymerisation to occur, obtaining linear polyglycidol with higher degree of polymerisation.

7.2. Future work

- For the copolyamine PA1.1, a deeper study by polarised optical microscope with an appropriate solvent should be carried out. The presence of a suitable solvent may separate the detected thermal transitions. Furthermore, the substitution of the solvent can vary the required molecular correlation times necessary to detect the characteristic LC behaviour of the copolymer by solid state NMR.

- Linear polyglycidol with higher molecular weight can be chemically modified with TAP in order to obtain LC copolyethers able to prepare tougher membranes.

Appendices

Appendix A

Index of figures, schemes and tables

Index of figures

Index of schemes

Index of tables

Appendix B

List of publications, meeting contributions and abroad research stay

List of publications

Directly related with the thesis:

Title: Columnar liquid-crystalline polyglycidol derivatives: A novel alternative for proton-conducting membranes

Authors: X. Montané, S. Vilasrao Bhosale, J. A. Reina, M. Giamberini.

Ref.: Polymer, Vol. 66, pp. 100-109, 2015.

Title: Advances in the design of self-supported ion-conducting membranes – new family of columnar liquid-crystalline polyamines. Part 1: copolymer synthesis and membrane preparation

Authors: X. Montané, K. A. Bogdanowicz, G. Colace, J. A. Reina, P. Cerruti, M. Giamberini.

Ref.: Polymer, submitted.

Title: Advances in the design of self-supported ion-conducting membranes – new family of columnar liquid-crystalline polyamines. Part 2: ion transport characterisation and comparison to hybrid membranes

Authors: X. Montané, K. A. Bogdanowicz, G. Colace, J. A. Reina, P. Cerruti, M. Giamberini.

Ref.: Polymer, submitted.

Meeting contributions

Authors: X. Montané, S. V. Bhosale, J. A. Reina, M. Giamberini.

Poster Presentation: Columnar liquid crystalline polyglycidol derivatives: new alternative for proton conducting membranes.

XIII Meeting of the Group of Polymers (GEP) on the Spanish Royal Chemistry and Royal Physics Societies, September 2014, Girona, Spain.

Authors: X. Montané, S. Vilasrao Bhosale, J. A. Reina, M. Giamberini.

Poster Presentation: Columnar liquid crystalline polyglycidol derivatives: new alternatives for biomimetic proton-conducting membranes.

Fourth International Conference on Multifunctional, Hybrid and Nanomaterials (HYMA 2015), March 2015, Sitges, Spain.

Authors: X. Montané, J. A. Reina, M. Giamberini.

Poster Presentation: Columnar liquid crystalline polyamines containing side dendrons: advances in the construction of proton-conducting membranes.

European Polymer Federation Congress, June 2015, Dresden, Germany.

Authors: X. Montané, J. A. Reina, M. Giamberini.

Oral Presentation: Columnar liquid crystalline polyamines containing side dendrons: advances in the design of proton-conducting membranes.

First French-Spanish Joint Congress for Young Researchers in Polymers (JIP-JEPO 2015), September 2015, San Sebastián, Spain.

Abroad research stay

Organisation: Max Planck Institute for Polymer Research
Department: Department of molecular electronics
Supervisor: Dr. Robert Graf
City: Mainz **Country:** Germany
Length: 3 months (February-April, 2016)

Appendix C

Columnar liquid crystalline polyglycidol derivatives: A novel alternative for proton-conducting membranes

Polymer 66 (2015) 100–109

Contents lists available at ScienceDirect

Polymer

journal homepage: www.elsevier.com/locate/polymer

Columnar liquid crystalline polyglycidol derivatives: A novel alternative for proton-conducting membranes

Xavier Montané [a], Suryakant Vilasrao Bhosale [a], José Antonio Reina [a], Marta Giamberini [b, *]

[a] Departament de Química Analítica i Química Orgànica, Universitat Rovira i Virgili, Carrer Marcel.li Domingo s/n, Campus Sescelades, 43007 Tarragona, Spain
[b] Departament de Enginyeria Química, Universitat Rovira i Virgili, Av. Països Catalans, 26 Campus Sescelades, 43007 Tarragona, Spain

ARTICLE INFO

Article history:
Received 28 January 2015
Received in revised form
25 March 2015
Accepted 26 March 2015
Available online 15 April 2015

Keywords:
Polyglicydol
Liquid-crystalline polymers (LCP)
Biomimetic

ABSTRACT

A family of self-assembling LC columnar polyethers were prepared by chemical modification of linear polyglycidol with a polymerization degree equal to 20, with the dendron 3,4,5-tris[4-(n-dodecan-1-yloxy)benzyloxy]benzoic acid by Steglich esterification. The modification degrees of the resulting LC polyethers ranged between 8 and 43%. All the obtained copolymers exhibited LC behavior and the higher the modification degree, the higher the clearing range, as expected. Mesophase self-assembling depended on the amount of dendrons introduced: in the case of modification degree ranging around 10%, the copolymers exhibited lamellar columnar structure, while for the highest modification degrees, hexagonal columnar mesophase resulted; in the case of intermediate degree of modification, the copolymers exhibited a rectangular columnar mesophase. Oriented membranes could be prepared from modified polyglycidol with different modification degrees and showed promising proton permeability values. Therefore, these materials are proposed as interesting candidates for proton transport materials.

1. Introduction

Most research in the field of proton conductivity has been devoted by the materials science community in the last thirty years, mainly for the development of new proton-conducting materials to be used in electrochemical cells (e.g. fuel cells, batteries, sensors). In this field, perfluorosulfonic acid (PFSA) membranes, such as Nafion® (marketed by DuPont), represent the benchmark materials for their proton-conducting properties [1]. However, these materials exhibit serious drawbacks, such as the need of controlling water management, relative affinity of methanol and water in direct methanol fuel cells (DMFCs), mechanical, thermal and oxidative stability, high cost and environmental inadaptability. For this reason, more than 200 patents and papers have been recently published on the preparation of new proton-conducting membranes [2–5]. An alternative approach is to design materials containing ion transport channels, in which the channels localize the permeation path and simultaneously protect the transport process against the environment, like an ion-transporting molecular cable [6–9].

Percec and coworkers have comprehensively investigated the self-organization of supramolecular monodendrons and styrene-, methacrylate-, or oxazoline-based polymers for the design of ion-active nanostructured supramolecular systems [10–14].

Columnar structures were also obtained for liquid crystalline block copolymers based on dendronized polymers from poly(-ethyleneglycol), polystyrene or polymethacrylate (PMA) [15–17]. In this case, the combination of dendrimer structure with the characteristic microphase separation of traditional linear block copolymers, gives rise to macromolecular architectures which can find several applications such as optical storage materials or membranes. Successful perpendicular or parallel orientation of cylindrical nanodomains has recently been obtained for a liquid crystalline block copolymer based on poly(ethylene oxide) and PMA-bearing azobenzene mesogen side chains, by air-anchoring or surface effect, respectively [18].

In our previous studies [19–21], we reported the chemical modification of poly(epichlorohydrin) (PECH) and poly(epichlorohydrin-co-ethylene oxide) [P(ECH-co-EO)] with tapered mesogenic groups to yield high-molecular-weight polyethers with different degrees of

* Corresponding author.
E-mail address: marta.giamberini@urv.cat (M. Giamberini).

http://dx.doi.org/10.1016/j.polymer.2015.03.071
0032-3861/

modification. As we reported, these polymers self-assemble into a columnar structure, due to an exo-recognition of the side-chain dendrons. In the resulting structure, the polyether main chain forms a channel in the inner part of the columns, while the hydrophobic side-chain dendrons lie in the outer part. The presence of the polar ether linkages in the inner channel favors the interaction with proton and other cations, in the same way as crown ethers would do [22]. For this reason, the inner polyether chain could work as an ion channel. Satisfactory orientation of the polymer was achieved by sandwiching the polymer solution between a water layer and a wet glass layer to induce unfavorable surface interactions between the outer, hydrophobic portion of the columns and their surroundings. The presence of oriented channels in the polymeric membrane resulted in remarkable proton permeability, around $2 \cdot 10^{-6}$ cm^2 s^{-1}, comparable to that of Nafion® N117 [23]. However, the procedure used to prepare the oriented membranes had poor reproducibility.

Another drawback which could be exhibited by polyethers obtained out of modified PECH and [P(ECH-co-EO)], lies in the presence of remaining chlorine atoms in the modified polymers, which can lead to long-term development of radical reactions that could alter polymer structure and accelerate its degradation. Polyols like linear polyglycidol (LPG) can be other suitable polyether candidates which can be modified with 3,4,5-tris[4-(n-dodecan-1-yloxy)benzyloxy]benzoic acid in order to obtain liquid crystalline columnar polyethers, which do not contain chlorine. In this paper, we investigated the modification of LPG using carbodiimide mediated Steglich esterification between free hydroxyl groups of the linear polyglycidol and carboxylic groups of the dendron under different conditions. The use of a lower molecular weight precursor polymer could lead to systems that can be more easily oriented: therefore, chemical modification was performed on a relatively low molecular weight LPG. In this way, we also intended to test the performances of a lower molecular weight modified polyether as far as orientation and transport are concerned. Modified LPGs were subsequently studied in terms of liquid crystalline behavior. It was found that modified LPGs are showing different mesophases like lamellar columnar, rectangular columnar (distorted hexagonal) and hexagonal columnar depending on the degree of modification, the higher the number of dendrons, the more ordered the mesophase. Finally, we prepared oriented membranes based on selected copolymers, having three different modification degrees. In this case, membrane orientation was achieved by means of a simpler and reproducible thermal treatment on fluorinated ethylene propylene sheet support. The obtained membranes exhibited promising proton permeabilities, in one case comparable to that of Nafion® and negligible water uptake. Therefore, transport can be attributed to the presence of the oriented channels.

2. Experimental

2.1. Materials

All the chemicals were purchased from Sigma–Aldrich, while all solvents were purchased from Scharlab. Diglyme (bis(2-methoxyethyl) ether), *p*-toluenesulfonic acid monohydrate (*TsOH*, 98.5%), potassium tert-butoxide (1 M solution in THF), *N*,*N*′-dicyclohexylcarbodiimide (DCC, 99%), 4-dimethylaminopyridine (DMAP, ≥99%), trimethylolpropane (TMP) (97%) and potassium methylate solution (25% v/v in methanol) were used as received. Glycidol (96%) was distilled under reduced pressure and stored over molecular sieves at 2–5 °C. Dimethylformamide (DMF, 99%) and dioxane were dried before use.

3,4,5-Tris[4-(n-dodecan-1-yloxy)benzyloxy]benzoic acid (compound **D**) was synthesized as previously reported [24]. Yield: 93%.

2.1.1. Synthesis of linear polyglycidol (LPG) (Scheme S1)

Linear poly[(1-ethoxyethyl)glycidyl ether] was prepared from (1-ethoxyethyl)glycidyl ether according to Schmitz et al. [25]. Linear polyglycidol was prepared by subsequent removal of the acetal protecting groups of [linear (1-ethoxyethyl)glycidyl ether] under acidic hydrolysis conditions. Yield: 78%. Degree of polymerization (DP) = 20.

^{1}H NMR (^{d}DMSO, TMS, δ, ppm): = 7.3–7.1 (m, 3H), 4.5 (s, 1H), 3.7–3.3 (m, 7H), 2.6 (t, 2H), 1.7 (q, 2H).

^{13}C NMR (^{d}DMSO, TMS, δ, ppm): 145–125 (Aryl), 81.1 ($CH_2\underline{C}HOCH_2$), 74–70 ($ArCH_2CH_2\underline{C}H_2$, $CH_2O\underline{C}H_2CH$, $OCH_2\underline{C}HOH$), 64.8 ($CH\underline{C}H_2OH$), 61.1 ($OCH_2CHO\underline{C}H_2OH$), 32–31 ($ArCH_2\underline{C}H_2$, $Ar\underline{C}H_2CH_2$).

2.1.2. Modification of linear polyglycidol (Scheme 1)

The linear polyglycidol was successfully modified by compound **D** using carbodiimide mediated Steglich esterification [26] between the free hydroxyl groups of the linear polyglycidol and carboxylic group of D:

In three necked round bottom flask, solution of **D** (2 g, 2 mmol) was prepared by dissolving into dry DMF (5 ml). Stoichiometric amounts of DCC and DMAP at 0 °C were allowed to stir for 30 min in an Ar atmosphere. The necessary amount of linear polyglycidol was dissolved into dry DMF (5 ml) and added dropwise to the above reaction mixture. The reaction mixture was allowed to stir for 2 days at room temperature under Ar atmosphere. Afterward, the reaction mixture was precipitated in 500 ml of methanol. Precipitated product was dissolved into THF and re-precipitated in 500 ml methanol. This precipitation was repeated for 5 times, in order to remove DCC, DMAP, free acid and other impurities. After precipitation, the modified polymer was collected and dried at 40 °C *in vacuo* for 48 h.

Different degrees of modifications and corresponding yields are given in Table 1.

2.1.3. Membranes preparation

Membranes were prepared by immersion precipitation process, in which a homogeneous polymer solution in THF (30% w/w) was cast on a FEP (fluorinated ethylene propylene) sheet support and immersed in a bath of Milli-Q water. The solvent diffused into the precipitation bath, while the non-solvent (water) diffused into the cast film. After a time in which the solvent and the non-solvent were exchanged, the polymer solution (wet film) became thermodynamically unstable and demixing took place. Finally, a solid polymer membrane was formed with an asymmetric structure. Afterward, the membrane was dried overnight at room temperature and subsequently used for baking process. The polymer membrane along with FEP sheet was mounted on a hot stage (Linkam TP92) and it was heated above the clearing temperature; then it was allowed to cool slowly (0.5 °C/min) down to room temperature. After the baking process, the membrane was kept at room temperature for approximately 1 h and then it was separated from the FEP sheet and obtained as an intact, uniform membrane with thickness around 300 μm. Membranes were in their rubbery state at room temperature (see Table 3) and they flowed above their clearing temperature.

2.2. Characterization and measurements

^{1}H NMR and ^{13}C NMR spectra were recorded at 400 and 100.4 MHz, respectively, on a Varian Gemini 400 spectrometer with proton noise decoupling for ^{13}C NMR. The ^{13}C NMR spectra of the polymers were recorded at 30 °C, with a flip angle of 45°, and the number of transients ranged from 20,000 to 40,000 with 10–20% (w/v) sample solutions in $CDCl_3$. The central peak of $CDCl_3$ was

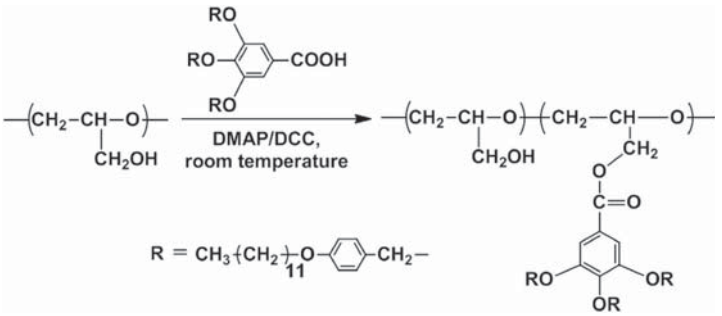

Scheme 1. Chemical modification of linear polyglycidol.

taken as the reference, and the chemical shifts were given in parts per million from TMS (tetramethylsilane) with the appropriate shift conversions.

Thermal transitions were detected with a Mettler-Toledo differential scanning calorimeter mod. 822 in dynamic mode at a heating or cooling rate of 10 °C/min. Nitrogen was used as the purge gas. The calorimeter was calibrated with an indium standard (heat flow calibration) and an indium–lead–zinc standard (temperature calibration).

Clearing temperatures and liquid crystalline mesophases were investigated by polarized optical microscopy (POM); textures of the samples were observed with an Axiolab Zeiss optical microscope equipped with a Linkam TP92 hot stage.

Densities were determined by gas pycnometry using Micrometritics AccuPyc 1330 machine at 30 °C.

Average molecular weights were determined in THF by size exclusion chromatography (SEC); analyses were carried out with an Agilent 1200 series system with PLgel 3 μm MIXED-E, PLgel 5 μm MIXED-D, and PLgel 20 μm MIXED-A columns in series, and equipped with an Agilent 1100 series refractive-index detector. Calibration curves were based on polystyrene standards having low polydispersities. THF was used as an eluant at a flow rate of 1.0 ml/min, the sample concentrations were 5–10 mg/ml, and injection volumes of 100 μl were used.

For X-ray experiments, two different diffractometers were used depending on the 2θ range investigated:

For low 2θ range: XRD measurements were performed with a Bruker-AXS D8-Discover diffractometer equipped with parallel incident beam (Göbel mirror), vertical θ–θ goniometer, *XYZ* motorized stage and with a GADDS (General Area Detector Diffraction System). Samples were placed directly on to a low background Si(510) sample holder for reflection analysis. An X-ray collimator system close-to-the-sample allows to analyze areas of 500 μm. The X-ray diffractometer was operated at 40 kV and 40 mA to generate $Cu_{k\alpha}$ radiation. The GADDS detector was a HI-STAR (multiwire proportional counter of 30 × 30 cm with a 1024 × 1024 pixel) placed at 30 cm from the sample. The X-ray beam hit the sample at 0.5° of incidence. The collected frame (2D XRD pattern) covers a range from 0.9 up to 9.2° 2θ. The diffracted X-ray beam travels through a He beam path (SAXS attachment) to reduce the air scattering at low angles. The direct X-ray beam is stopped by a beam stop placed directly on the detector face. The exposition time was of 300 s per frame. The resulting frames were both radially integrated to obtain a 2θ diffractogram and 2θ integrated to obtain an azimuthal intensity plot.

For medium 2θ range: XRD measurements were performed with a Siemens D5000 diffractometer (Bragg–Brentano parafocusing geometry and vertical θ–θ goniometer) fitted with a curved

Table 1
Modification degrees and yields obtained in modification of LPG.

	Sample	RCOOH (mmol) [a]	–OH/RCOOH	Time (days)	T (°C)	Modification degree (%) [b]	Yield (%)
c	**LPG1**	2	1:0.3	2	25	8	61
c	**LPG2**	2	1:0.5	2	25	23	70
c	**LPG3**	2	1:0.7	2	25	27	68
c	**LPG4**	2	1:1	2	25	39	81
c	**LPG5**	2	1:1.25	2	25	43	87
d	**LPG6**	2	1:1	7	25	42	79
d	**LPG7**	2	1:1	2	40	40	75
d	**LPG8**	2	1:1	2	80	11	65

[a] Stoichiometric amounts of DCC and DMAP in each case
[b] Average value determined by ^{1}H NMR
[c] Series 1
[d] Series 2

graphite diffracted-beam monochromator, incident and diffracted-beam Soller slits, a 0.06° receiving slit and scintillation counter as a detector. Samples were placed directly on to a low background Si(510) sample holder for reflection analysis. The X-ray diffractometer was operated at 40 kV and 30 mA to generate CuK_α radiation. The angular 2θ diffraction range was between 1 and 40°. The data were collected with an angular step of 0.03° at 6 s per step. In the case of membranes, XRD experiments were performed on both sides and no differences could be detected.

The thickness of the membranes was measured using a micrometer with a sensitivity of 2 μm. The measurements were carried out at various points, and the membranes were found to have constant thickness.

Contact angles of water drops on a membrane surface were measured with a Kruss contact angle instrument (Hamburg, Germany) equipped with a motorized pipette (Matrix Technology, Nashua, NH) and deionized water as the probe liquid. The contact angle was measured immediately after putting the water drop (3 μl) on the membrane surface. Measurements were repeated using different areas of the membrane. For each test reported, at least three drops of water were used.

Swelling experiments were performed by soaking the membranes at room temperature in milli-Q water and monitoring the change in membrane weight versus time for 24 h.

Transport experiments were carried out using a Teflon test cell that comprised two compartments, separated by the tested membrane, containing the feed and stripping solutions, respectively. The feed and stripping volumes were 200 ml and the effective membrane area was 0.86 cm^2. For the proton transport experiments, the initial feed solution was 0.1 M HCl aqueous solution and the stripping solution was 0.1 M NaCl aqueous solution. The pH of the stripping solution was measured every 30 s by a Crison MM 40 Multimeter. Prior to the proton transport experiments, membranes were conditioned in 0.1 M NaCl aqueous solution for 15 min.

Under steady-state conditions, proton flux was calculated by Fick's first law:

$$J = \frac{P\Delta C}{l}\cdot 10^{-3} \tag{1}$$

where l (cm) is the membrane thickness and ΔC is the difference in concentration (mol l^{-1}) between the initial feed solution (C_0) and the final stripping solution. In our experimental conditions, C_0 was much greater than the final stripping concentration, so we considered $\Delta C \sim C_0$.

P is the proton permeability ($cm^2\ s^{-1}$), defined as:

$$P = DS \tag{2}$$

where D is the proton diffusion coefficient and S is the sorption equilibrium parameter.

The flux is related to the permeability coefficient p (cm s^{-1}), defined as:

$$J = pC_0 \tag{3}$$

$$P = pl \tag{4}$$

The permeability coefficient, can be described by the following equation: [27]

$$-\ln\frac{C_f}{C_0} = \frac{Ap}{V_f}t \tag{5}$$

where C_0 (mol l^{-1}) is the initial concentration of the feed solution and C_f (mol l^{-1}) is the feed concentration calculated from the stripping solution at time t (s):

$$C_f = C_0 - C_s \tag{6}$$

V_f is the feed volume (ml) and A is the actual membrane area (cm^2).

We calculated the proton permeabilities in accordance with the above equations. Data were fitted according to equation (5) in the time range (1.2–500) × 10^3 s, depending on the system under investigation.

3. Results and discussion

3.1. Synthesis of linear polyglycidol (LPG)

As explained in the experimental part and shown in Scheme S1, (1-ethoxyethyl)glycidyl ether was first synthesized from glycidol according to Fitton et al. [28]; then, linear poly[(1-ethoxyethyl) glycidyl ether] was prepared from (1-ethoxyethyl)glycidyl ether according to Schmitz et al. [25]. Finally, LPG was prepared by subsequent removal of the acetal protecting groups.

The structure of the obtained linear polyglycidol was confirmed by ^1H and ^{13}C NMR techniques as shown in Figs. S1 and S2, respectively. The presence of the aromatic ring as a head group, allowed calculating the degree of polymerization (DP) from ^1H NMR spectra, by comparing the integrated areas of the peaks coming from aromatic, aliphatic and alcoholic protons as shown in Fig. S1. DP resulted equal to 20.

3.2. Modification of LPG

The Steglich esterification represents one of the most versatile esterification methods, which take advantages of *N,N′*-dicyclohexylcarbodiimide (DCC) as a promoter [26]. Although stoichiometric dosage of this reagent, or more, is necessary, this procedure enjoys various advantages. The reaction usually proceeds at room temperature, and the conditions are so mild that substrates with various functional groups can be employed. The reaction is not sensitive to steric hindrance of the reactants, allowing production of esters of tertiary alcohols. As such, a wide range of applications has been achieved in the field of natural products, peptides, nucleotides, etc. however, unfortunately this procedure has some drawbacks: yields are not always high, and undesirable N-acylureas are occasionally formed. These drawbacks can be overcome by addition of strong acids such as p-toluenesulfonic acid [29]. Alternatively, addition of a catalytic amount of p-aminopyridines is more effective [30,31].

In this way, we applied Steglich esterification in chemical modification of LPG (Scheme 1).

In case of LPG, we studied this chemical modification under different reaction conditions, which are given in Table 1 along with and their corresponding degree of modification and product yields.

In most cases this esterification was carried out at room temperature, since the side product N-acylurea formation is less likely at lower temperatures; in other words, high temperatures favor the formation of side products and are therefore expected to reduce modification degrees correspondingly.

We considered products LPG1 to LPG5 as series 1 and from LPG6 to LPG8 as series 2. In case of series 1, only the −OH/ROOH molar ratio was varied, while there was no change in reaction time and temperature. It can be seen that in this case the degree of modification increased on increasing the molar ratio; finally, we got 43% degree of modification in case of LPG5.

In case of series 2, we studied the effect of increase in reaction time and temperature on degree of modification. However, the degree of modification could not be increased with increasing reaction time up to 7 days, as it can be seen in case of LPG6. As far as reaction temperature is concerned, an increase up to 40 °C did not affect the reaction since a degree of modification of 40% was reached in the case of LPG7; on the other hand, the degree of modification was significantly decreased up to 11% when the reaction was performed at 80 °C, as in the case of LPG8.

Therefore, we supposed a modification plateau of 43%, which could not be further increased by raising reaction time and temperature. Reaction yield could not be improved beyond 87% (LPG5); however, one should take into account that, in order to get rid of DMAP and DCC, several precipitations were required which caused loss of product and inevitably turned into low product yield.

The structure of the copolymers was characterized by NMR spectroscopy. Fig. 1 reports the ^{1}H NMR spectrum in $CDCl_3$ of modified LPG1 as an example.

All ^{1}H NMR spectra are characterized by broad signals in three regions. The aromatic region shows three signals at 7.2, 6.8, and 6.7 ppm. Considering the relative integration areas and by comparison with the spectrum of methyl 3,4,5-tris(n-dodecan-1-yloxy) benzoate, the signal at 7.2 (8H) can be assigned to the protons of the benzoate group plus the aromatic protons ortho to the benzylic carbon $-CH_2O-$. The signals at 6.8 and 6.6 ppm (4H + 2H) correspond to the aromatic protons meta to the benzylic carbon $-CH_2O-$ of the lateral and central alkyloxybenzyloxy substituents, respectively. The characteristic signals, corresponding to most protons of the dodecyloxy alkyl chains in the dendron, can be observed in the high-field region at 1.7, 1.4, 1.3, 1.2, and 0.8 ppm. In the region between 5 and 3.4 ppm five signals can be observed: the two signals at 4.4 and 4.3 ppm correspond to the methylenic protons c′ in the modified monomeric unit; in this region, also signals coming from the free −OH groups are overlapped. The signal at 3.9 ppm corresponds to the methylene attached to the oxygen in the alkyl chains of the mesogenic unit and to methinic proton b′. The broad signal between 3.8 and 3.4 ppm corresponds to the methylenic and methinic protons a, a′, b, and c in the modified and unmodified monomeric units. Finally, the signal centered at 4.9 ppm can be assigned to the benzylic methylenes of the dodecyloxybenzyloxy substituent.

Fig. 2 shows the ^{13}C NMR spectrum in 1,1,2,2-tetrachloroethane-d2 of modified LPG1 with the corresponding assignments.

The aromatic carbons and the carbonyl carbon appear between 166 and 108 ppm, whereas carbons 2–12 of the aliphatic alkyl chains appear in the region between 32 and 14 ppm. The carbons of the backbone appear in the central region of the spectrum. The methine and side methylenic carbons of the modified and unmodified monomeric units appear at different chemical shifts. Thus, b and b′ appear at 80.6 and 77.4 ppm, while c and c′ appear at 62.2 and 64.4 ppm, respectively. The carbons a and a' appear overlapped at 69.5 ppm. Carbon 1 of the alkyl chains appears as a sharp peak at 67.8 ppm. The chemical shifts of the benzylic methylenes depend on their relative position in the benzoate ring: those in positions 3 and 5 appear at 71.1 ppm, whereas the same carbon in position 4 appears overlapped with peaks coming from 1,1,2,2-tetrachloroethane-d2.

The degree of modification of modified polymer was calculated by ^{1}H NMR spectra by comparing the areas of the aromatic peaks between 7.4 and 6.6 ppm and the benzylic proton signal at 4.9 ppm with the broad signal between 3.8 and 3.4 ppm.

Molecular weights and polydispersities of LPG derivatives determined by SEC are reported in Table 2. Molecular weights increased with modification degree. In general terms, density values (Table 2) did not exhibit appreciable variation; slightly higher values were found in the case of LPG5, LPG6 and LPG7, which also showed higher polydispersities.

3.3. Mesomorphic characterization of modified LPG

Mesomorphic phases were investigated by Differential Scanning Calorimetry (DSC), Polarized Optical Microscopy (POM) and confirmed by X-ray diffraction (XRD). Table 3 shows the clearing temperatures ranges and the glass transition temperatures of the whole LPG series.

The liquid crystalline textures of LPG samples were observed by POM after annealing the samples for 2 h at a temperature slightly lower than their respective clearing temperatures, in order to favor

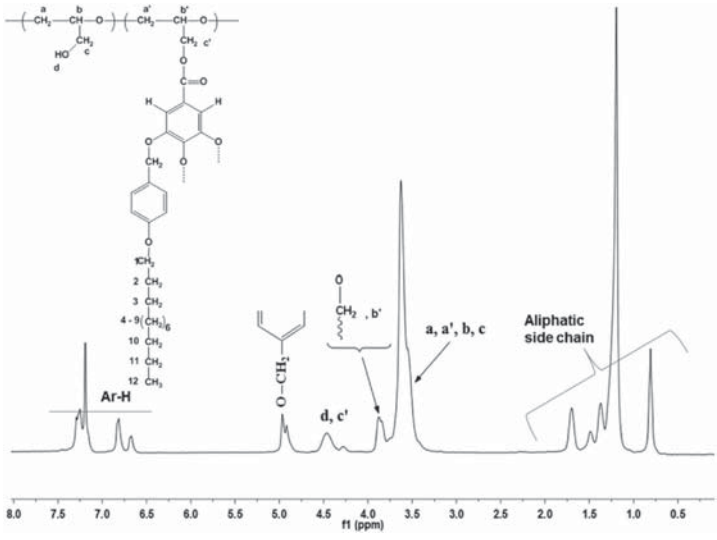

Fig. 1. ^{1}H NMR spectrum of modified LPG1 in $CDCl_3$.

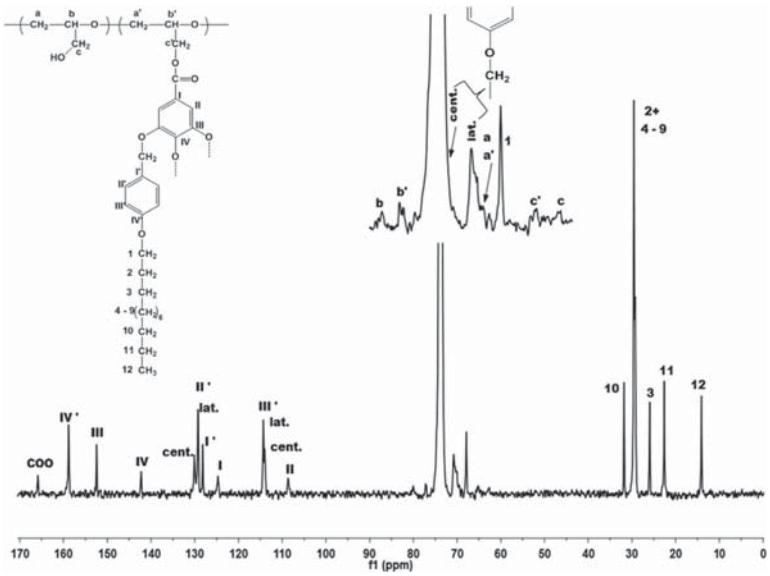

Fig. 2. ^{13}C NMR spectrum of modified LPG1 in 1,1,2,2-tetrachloroethane-d2.

the growth of the liquid crystalline domains. POM images of both series are shown in Fig. 3.

A typical broken fan-shaped texture could be seen in case of LPG2–LPG7 samples, whose modification degrees ranged between 20 and 40% approximately. At variance, LPG1 and LPG8, with modification degrees around 10%, exhibited a texture which resembled smectic bâtonnets.

In order to assign their mesophases, LPG1, LPG2, LPG3 and LPG4 were studied by XRD. LPG5–LPG7 have modification degrees quite close to LPG4 and, in the case of LPG6 and LPG7, the clearing range was also similar to LPG4. Therefore, we considered reasonable to extend the results from XRD experiments on LPG4 also to LPG5–LPG7. In case of LPG8, similar texture to LPG1 was observed by POM, but the glass transition temperature and the clearing temperature range resulted quite different, so we decided to characterize it as well. Summing up, only samples from LPG1 to LPG4 and LPG8 were analyzed by XRD. The results from XRD are summarized in Table 4.

The intensity vs. 2θ graph of LPG1 copolymer is shown in Fig. S3. Only two signals are evident, a sharp reflection at $2\theta = 2.1°$, corresponding to a d-spacing of 42.0 Å, and broad halo at 2θ around 20°, giving a d-spacing of 4.4 Å. This pattern is compatible with a smectic as well as with a lamellar columnar mesophase (Col_L); however, the characterization previously performed on the systems obtained out of PECH and [P(ECH-co-EO)] [18] suggested the existence of Col_L mesophase, the sharp reflection corresponding to the interlamellar distance, while the halo to the distance between adjacent dendrons.

XRD patterns of samples LPG2 and LPG3 are shown in Figs. S4 and S5, respectively. In the case of LPG2, we could observe three sharp reflections at $2\theta = 2.1°$, 3.2° and 6.5°, corresponding to $d = 41.1$ Å, 27.3 Å and 13.5 Å, respectively, and a diffuse halo centered round $2\theta = 20°$, giving $d = 4.4$ Å. On the other hand, LPG3 showed two sharp reflections at $2\theta = 2.1°$ and 3.7°, corresponding to $d = 41.0$ Å and 23.8 Å Å, respectively, and a diffuse halo centered round $2\theta = 20°$, giving d = 4.4 Å. This last diffraction pattern, which exhibited d-spacings of the sharp reflections in the ratio of $1:1/\sqrt{3}$ and a diffuse halo at high angle region, confirmed the presence of a hexagonal columnar mesophase (Col_h), where the first two sharp reflections correspond to the planes (100) and (110), respectively, while the broad halo is related to (001). Similar conclusions could be drawn from the XRD pattern of sample LPG4, since it showed three sharp reflections corresponding to $d = 46.4$ Å, 26.3 Å and 23.5 Å, respectively, and a diffuse halo centered round $d = 4.6$ Å.

Table 2
Average molecular weights and densities of the modified LPG.

Sample	Modification degree (%)	$M_n \cdot 10^{-3}$ [b]	$M_w \cdot 10^{-3}$ [b]	M_w/M_n [b]	ρ (g/cm^3) [c]
LPG1	8	2.70	3.19	1.18	1.07
LPG2	23	4.79	6.57	1.37	1.07
LPG3	27	5.16	7.34	1.42	1.08
LPG4	39	7.36	10.87	1.47	1.08
LPG5	43	7.62	12.76	1.62	1.17
LPG6	42	7.52	11.46	1.52	1.17
LPG7	40	7.11	10.93	1.53	1.17
LPG8	11	2.93	3.57	1.21	1.07
LPG [a]	–	1.48 [d]	–	–	1.02

[a] Unmodified linear polyglycidol.
[b] Determined by SEC.
[c] Determined at 30 °C. Error: ±3%.
[d] Calculated from ^{1}H NMR.

Table 3
Clearing temperature ranges and glass transition temperatures of the modified LPG.

Sample	Modification (%)	T_g (°C) [a]	T_c (°C) [b]
LPG	–	−10	–
LPG1	8	−10	32–35
LPG2	23	−30	71–75
LPG3	27	−32	79–84
LPG4	39	−27	97–101
LPG5	43	−16	116–120
LPG6	42	−21	95–98
LPG7	40	−13	95–99
LPG8	11	−20	49–52

[a] Determined by DSC second heating scan.
[b] Determined by DSC second heating scan and POM.

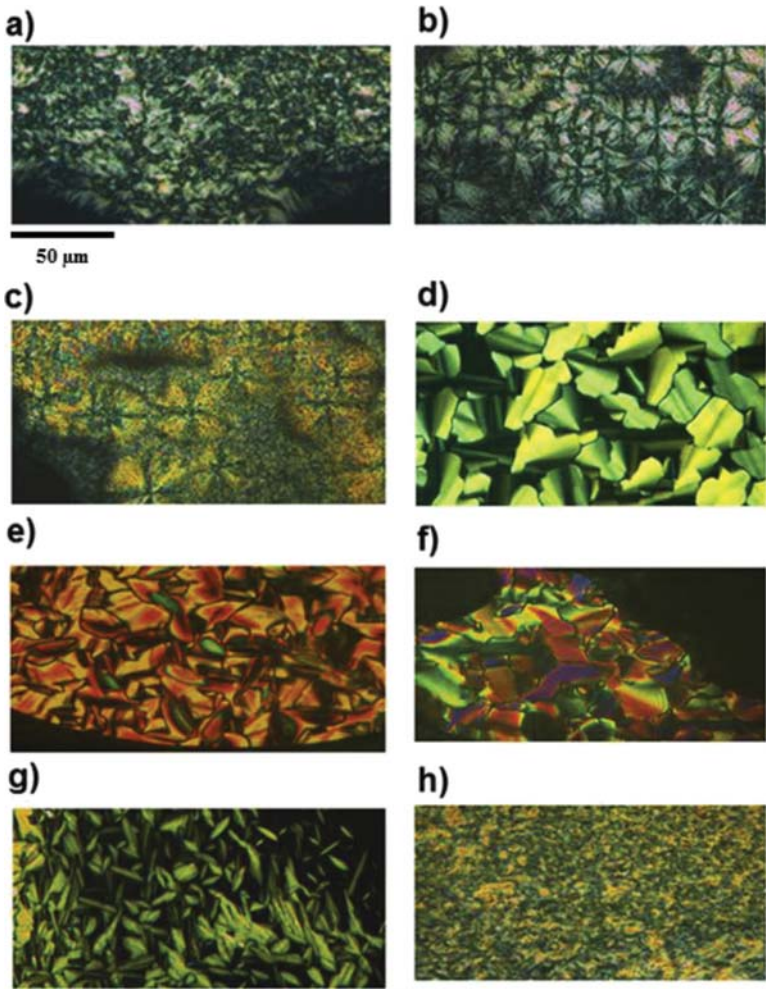

Fig. 3. Optical micrographics between crossed polars of (sample, modification degree, test temperature): a) LPG1, 8%, 30 °C; b) LPG2, 23%, 69 °C; c) LPG3, 27%, 79 °C; d) LPG4, 39%, 97 °C; e) LPG5, 43%, 116 °C; f) LPG6, 42%, 94 °C; g) LPG7, 40%, 93 °C; and h) LPG8, 11%, 47 °C.

The *d*-spacings of the sharp reflections were in the ratio $1:1/\sqrt{3}:1/2$, confirming the presence of a hexagonal columnar mesophase (Col_h). The XRD pattern of LPG4 is reported in Fig. S6.

At variance, the X-ray diffraction pattern of polymer LPG2 was in agreement with the less-symmetrical rectangular columnar mesophase (Col_r). In this case, the sharp reflections at 41.1, 27.3 and 13.5 Å could be assigned to (100), (010) and (020) planes, respectively. It must be noted, that the occurrence of a rectangular columnar mesophase is also compatible with the broken fan shaped texture as observed by POM (Fig. 3b). Also in the case of LPG8, whose modification degree was 11%, XRD pattern was compatible with a rectangular columnar mesophase (Table 4). As we have explained, on increasing the modification degree, the LC phase of the modified copolymers changed from lamellar columnar to hexagonal columnar, through an intermediate, less symmetric rectangular columnar. This can be ascribed to the self-assembling of the dendrons (Fig. 4): in the case of low modification degrees (LPG1), the $\pi-\pi$ interaction between the aromatic rings, as well as the inter-digitation of peripheral aliphatic chains is only able to drive the system to lamellar packing (Fig. 4a) while, when the modification degree is higher (LPG3–LPG7), the increased symmetry of the system can induce the assembling of the columns into a hexagonal packing (Fig. 4c). In the case of intermediate modification degree (LPG2 and LPG8), columnar organization is not perfectly hexagonal yet and the elliptical shape of the column cross-section gives rise to a rectangular columnar mesophase (Fig. 4b).

In all cases, the organization of the copolymers into columns can be supposed to lead to the formation of biomimetic ion channels, where the polyether main chain arranges in the inner part of the column.

3.4. Membrane preparation and assessment

In order to assess the potential of the synthesized copolymers as proton-conducting materials, we prepared oriented membranes

Table 4
X-ray diffraction data of LPG copolymers at room temperature.

Sample	Modification degree (%)	d_{exp} (Å)	*hkl*	Mesophase[b]	Lattice constants (Å)
LPG1	8	42.0	100	Col_L	$a = 42.0$
		4.4 (b)[a]	001		
LPG8	11	40.1	100	Col_r	$a = 40.1$
		25.0	010		$b = 25.0$
		13.8	020		
		4.3 (b)[a]	001		
LPG8OM[c]	11	40.3	100	Col_r	$a = 40.3$
		26.0	010		$b = 26.0$
		13.1	020		
		4.3 (b)[a]	001		
LPG2	23	41.1	100	Col_r	$a = 41.1$
		27.3	010		$b = 27.3$
		13.5	020		
		4.4 (b)[a]	001		
LPG2 OM[c]	23	40.0	100	Col_L	$a = 40.0$
		4.4 (b)[a]	001		
LPG3	27	41.0	100	Col_h	$a = b = 47.3$
		23.8	110		
		4.4 (b)[a]	001		
LPG4	39	46.4	100	Col_h	a = b = 53.6
		26.3	110		
		23.5	200		
		4.6 (b)[a]	001		
LPG4 OM[c]	39	36.5	100	Col_h	$a = b = 42.1$
		21.8	110		
		18.1	200		
		4.6 (b)[a]	001		
		31.4	100	Col_r	$a = 31.4$
		25.6	010		$b = 25.6$
		15.5	200		
		13.1	020		
		4.6 (b)[a]	001		

[a] (b): broad halo.
[b] Col_L: lamellar columnar, Col_r: rectangular columnar, Col_h: hexagonal columnar.
[c] Oriented membrane obtained by immersion precipitation + baking process.

out of selected samples. LPG8, LPG2 and LPG4 were selected as representative of three different increasing modification degrees. In order to get efficient transport, the columns which are expected to work as ion channels should be oriented homeotropically, that is, perpendicularly to the membrane surface.

According to the studies done by Percec et al. [11,18], it was demonstrated that columnar self-assembling polymers containing tapered groups can be homeotropically oriented when the system is allowed to self-organize during slow cooling on a hydrophobic substrate from the melt into the liquid crystal phases. The dendrons were found to be the structure-directing moieties of the columnar architectures, and π–π stacking of aromatic units produces the driving forces responsible for this homeotropic orientation.

Therefore, as mentioned in the experimental part, membranes were first prepared by immersion precipitation process. Then, with the described baking process, we obtained satisfactorily oriented membranes in the homeotropic direction. Previously, the baking process was successfully applied to the preparation of homeotropically oriented membranes based on chemically modified PECH and [P(ECH-co-EO)] [18].

As an example, Fig. 5 shows the XRD image of a LPG4 membrane after baking process. The diffraction at $2\theta = 2.4°$, which corresponds to $d_{100} = 36.5$ Å and to $a = b = 42.1$ Å, exhibits orientation in the equatorial plane, which indicates that columns are oriented perpendicularly to the membrane surface to some extent.

As it can be seen in Table 4, in some cases surface interactions, which are responsible for the orientation process, seem to alter the ordering of LPG copolymers. As a matter of fact, in one case a different mesophase was observed (LPG2), while in another one, coexistence with a new mesophase was put into evidence (LPG4).

The obtained membranes were also investigated in terms of water contact angle measurement by considering FEP side and air-side, that is, the part which was directly in contact with the FEP support during the baking process, and the other one, on opposite side. The values of contact angles on FEP side are reported in Table 5.

In our case, both sides were found hydrophobic, having similar contact angles. This evidence confirmed that the membranes were homogeneously oriented. Surface hydrophobicity can be ascribed to dominating exposition of tapered groups which represents the hydrophobic part of the polymer: that is, in case of homeotropic orientation, the membrane surface is hydrophobic because of maximum area occupied by well oriented hydrophobic tapered groups.

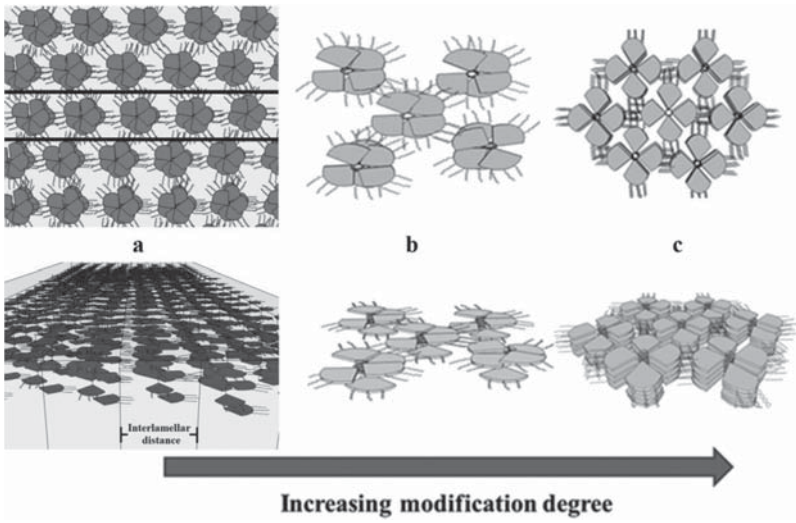

Fig. 4. Schematic representation of the self-assembling of LPG copolymers on increasing the modification degree; a: lamellar columnar; b: rectangular columnar; c: hexagonal columnar. Top: top views; bottom: side views.

Proton transport tests were performed on the membrane obtained with LPG8, LPG2 and LPG4. Calculated permeability values are reported in Table 5. The value found for Nafion® N117 ($2.59 \cdot 10^{-6}$ cm^2 s^{-1}) was used as a reference standard in the evaluation of proton permeability of the other materials. Permeabilities of LPG copolymers are comparable to Nafion®, while no permeability at all was detected for the samples not previously submitted to the baking process; in the case of LPG8, the calculated value resulted very close to Nafion®, being 2.2 (± 0.5)$\cdot 10^{-6}$ cm^2 s^{-1}. Plots according to equation (5) for Nafion® N117 and LPG8 are reported in Fig. 6.

In both cases, the plot exhibits two different regions: the first one, which was much shorter for Nafion® N117 (Fig. 6a), corresponds to proton absorption and diffusion across the membrane; once the membranes were saturated by protons, the mechanism became hopping-dominated. One has to keep into account that LPG8 membrane is thicker, with respect to Nafion® N117 membrane; moreover, proton transport through LPG8 membrane determines some changes in polymer conformation and an increase in its orientation, as it will be shown hereinafter: this could justify the longer time needed for proton diffusion across the membrane. From the slope of the second region, which was quite similar for both materials, we calculated proton permeability.

LPG8 corresponds to a low modification degree (11%) which, in turn, represents high hydroxyl group content and, consequently, is expected to be one of the most hydrophilic copolymers in the series. Therefore, in order to test whether in this case such a remarkable proton transport could be due to the presence of water, in analogy to Nafion®, a swelling test was performed. Surprisingly, water uptake resulted as low as 3.1%. This suggests that water is not crucial for proton transport which occurs instead due to the presence of oriented channels in the membrane. Therefore, alike to modified PECH, these polyglycidol derivatives could be also suitable candidates for the preparation of proton transporting membranes.

In the case of LPG8, it is noteworthy that the XRD pattern of the membrane after transport experiment showed higher degree of order when compared to the fresh oriented membrane. In fact, for the azimuthal scan of the peak at $2\theta = 2.1°$, we could observe a decrease of calculated FWHM (Full Width at Half Maximum) from $186 \pm 6°$ to $67.2 \pm 0.9°$. In fact, before transport experiments (Fig. S7), the columns are only slightly homeotropically oriented, while, after transport experiments (Fig. S8), the peak corresponding to the homeotropically oriented columns is sharper (although some perpendicularly oriented columns can also be evidenced). Thus, transport is able to induce a change in the degree of order of LPG8;

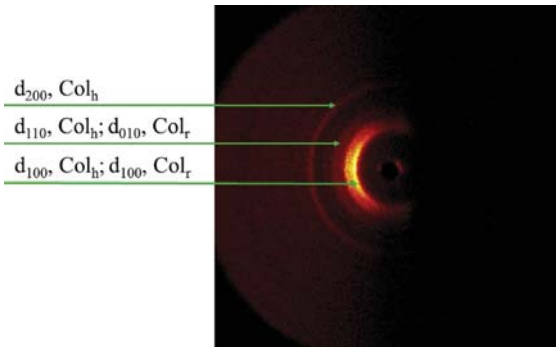

Fig. 5. XRD pattern of LPG4 oriented membrane at room temperature recorded in reflection mode.

Table 5
Water contact angles and proton permeabilities of LPG-based oriented membranes.

Sample	Water contact angle[a] (°)	Permeability (cm^2 s^{-1})
LPG8	115.8 ± 1.5	2.2 (±0.5)·10^{-6}
LPG2	116.4 ± 0.8	3.8 (±0.1)·10^{-7}
LPG4	112.3 ± 0.3	1.0 (±0.3)·10^{-7}
Nafion® N117	94.0 ± 0.9	2.59 (±0.05)·10^{-6}

[a] Determined on FEP side.

this could be favored by higher chain mobility of this copolymer, which exhibits the lowest modification degree with respect to the other copolymers of the series.

4. Conclusions

We prepared linear polyglycidol with a polymerization degree equal to 20, and subsequently modified it with the dendron 3,4,5-tris[4-(n-dodecan-1-yloxy)benzyloxy]benzoic acid by Steglich esterification with *N,N'*-dicyclohexylcarbodiimide. In this way, we prepared a family of self-assembling LC copolyethers whose modification degrees ranged between 8 and 43%, depending on the −OH/RCOOH molar ratio. On the other hand, the modification degree could not be further improved on increasing reaction time and temperature. The whole copolymer family exhibited LC behavior

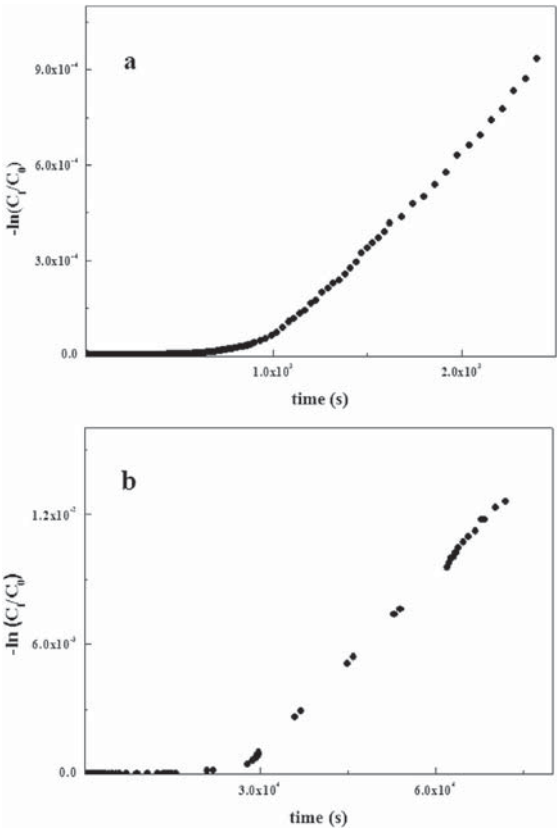

Fig. 6. Plot of $-\ln(C_t/C_0)$ versus time for Nafion® N117 (a) and for polymer LPG8 (b) during a proton transport test.

and the higher the modification degree, the higher the clearing range. It was found that mesophase self-assembling depended on the amount of dendrons introduced: in the case of the lowest modification degree (8%), the copolymer exhibited lamellar columnar packing; in the case of intermediate degrees, the mesophase turned into rectangular columnar while, for the highest modification degrees, hexagonal columnar mesophase was observed. Due to the columnar organization of the copolymers, the polyether backbone is expected to assume a helical conformation, suitable for cation transport through the channel mechanism. Polymer membranes were prepared by immersion precipitation on a fluorinated ethylene propylene (FEP) support. By means of the baking process, we obtained an effective homeotropic orientation of the polymeric columns in the membranes, as confirmed by XRD analysis. Oriented membranes were found to be hydrophobic on both sides of the membrane as shown by their contact angles. The presence of oriented ion channels in the polymeric membranes resulted in remarkable proton permeability, similar to Nafion®. Besides, the studied membranes exhibited negligible water uptake after soaking in milli-Q water at room temperature for 24 h; therefore, in this case membrane hydration does not seem critical for ion transport.

Acknowledgements

Financial support from CTQ2013-46825-R (Ministerio de Economía y Competitividad) is gratefully acknowledged. The authors are also grateful to Dr. Francesc Guirado for help with the XRD experiments.

Appendix A. Supplementary data

Supplementary data related to this article can be found at http://dx.doi.org/10.1016/j.polymer.2015.03.071.

References

[1] Mauritz KA, Moore RB. Chem Rev 2004;104:4535–85.
[2] Wilhelm FG, Pünt IGM, van der Vegt NFA, Strathmann H, Wessling M. J Membr Sci 2002;199(1–2):167–76.
[3] Miyatake K, Chikashige Y, Higuchi E, Watanabe M. J Am Chem Soc 2007;129(13):3879–87.
[4] Li Y, Jin R, Wang Z, Cui Z, Xing W, Gao L. J Polym Sci Part A Polym Chem 2007;45(2):222–31.
[5] Alberti G, Costantino U, Casciola M, Ferroni S, Massinelli L, Staiti P. Solid State Ionics 2001;145(1–4):249–55.
[6] Percec V, Johansson G, Heck J, Ungarb G, Battyb SV. J Chem Soc Perkin Trans 1 1993;0(13):1411–20.
[7] Beginn U, Zipp G, Möller M. Adv Mater 2000;12:510–3.
[8] Yoshio M, Kagata T, Hoshino K, Mukai T, Ohno H, Kato T. J Am Chem Soc 2006;128(16):5570–7.
[9] Jiménez-García L, Kaltbeitzel A, Pisula W, Gutmann JS, Klapper M, Müllen K. Angew Chem Int Ed 2009;48:9951–3.
[10] Percec V, Ahn CH, Ungar G, Yeardley DJP, Moller M, Sheiko SS. Nature 1998;391(6663):161–4.
[11] Percec V, Glodde M, Bera TK, Miura Y, Shiyanovskaya I, Singer KD, et al. Nature 2002;417(6905):384–7.
[12] Percec V, Schlueter D, Ungar G, Cheng SZD, Zhang A. Macromolecules 1998;31(6):1745–62.
[13] Percec V, Cho W-D, Ungar G, Yeardley DJP. J Am Chem Soc 2001;123(7):1302–15.
[14] Percec V, Imam MR, Peterca M, Leowanawat P. J Am Chem Soc 2012;134(9):4408–20.
[15] Shi Z, Chen D, Lu H, Wu B, Ma J, Cheng R, et al. Soft Matter 2012;8:6174–84.
[16] Chuang W-T, Lo T-Y, Huang Y-C, Su C-J, Jeng U-S. Macromolecules 2014;47:6047–54.
[17] Yi Z, Liu X, Jiao Q, Chen E, Chen Y, Xi F. J Polym Sci Part A Polym Chem 2008;46:4205–17.
[18] Komura M, Yoshitake A, Komiyama H, Iyoda T. Macromolecules 2015;48(3):672–8.
[19] Ronda JC, Reina JA, Cádiz V, Giamberini M, Nicolais L. J Polym Sci Part A Polym Chem 2003;41(19):2918–29.
[20] Ronda JC, Reina JA, Giamberini M. J Polym Sci Part A Polym Chem 2004;42(2):326–40.
[21] Bhosale SV, A.Rasool M, Reina JA, Giamberini M. Polym Eng Sci 2013;53(1):159–67.
[22] Dulyea LM, Fyles TM, Robertson GD. J Membr Sci 1987;34:87–108.
[23] Tylkowski B, Castelao N, Giamberini M, Garcia-Valls R, Reina JA, Gumí T. Mater Sci Eng C 2012;32(2):105–11.
[24] Šakalytė A, Reina JA, Giamberini M. Polymer 2013;54(19):5133–40.
[25] Schmitz C, Keul H, Möller M. Eur Polym J 2009;45(9):2529–39.
[26] Otera J, Nishikido J. Esterification: methods, reactions, and applications. John Wiley & Sons; 2010.
[27] Mulder M. Basic principles of membrane technology. 2nd ed. The Netherlands: Kluwer Academic Publishers; 2003.
[28] Fitton AO, Hill J, Jane DE, Millar R. Synthesis 1987;1987(12):1140–2.
[29] Neises B, Steglich W. Angew Chem Int Ed Engl 1978;17(7):522–4.
[30] Hassner A, Alexanian V. Tetrahedron Lett 1978;19(46):4475–8.
[31] Goodman LM, Toniolo C, Felix A. Houben-Weyl methods in organic chemistry. 4th ed. Thieme Publishers; 2003.